THE BINDING OF ALZHEIMER'S AMYLOID BETA PEPTIDES WITH A CANDIDATE DRUG MOLECULE, 12-CROWN-4, AND A BIOLOGICAL MEMBRANE: INSIGHT FROM MOLECULAR DYNAMICS SIMULATIONS

NIKHIL AGRAWAL

214584572

A thesis submitted to the School of Health Science, University of KwaZulu-Natal, Westville campus, in fulfilment of the Doctor of Philosophy in Pharmaceutical Chemistry

Supervisor

Dr. Adam A Skelton

University of KwaZulu-Natal, Durban

2018

THE BINDING OF ALZHEIMER'S AMYLOID BETA PEPTIDES WITH A CANDIDATE DRUG MOLECULE, 12-CROWN-4, AND A BIOLOGICAL MEMBRANE: INSIGHT FROM MOLECULAR DYNAMICS SIMULATIONS

NIKHIL AGRAWAL

214584572

A thesis submitted to the School of Pharmacy and Pharmacology, College of Health Science, University of KwaZulu-Natal, Westville, for the degree of Ph.D. in Pharmaceutical Chemistry.

This is the thesis in which the chapters are written as a set of discrete research publications, with an overall introduction and final summary. Typically these chapters will have been published in internationally recognized, peer-reviewed journals.

This is to certify that the contents of this thesis are the original research work of **Mr. Nikhil Agrawal**

As the candidate's supervisor, I have approved this thesis for submission.

Supervisor:

Signed: ----------

Name: Dr. Adam A. Skelton

Date: 30/05/2018

ABSTRACT

Alzheimer's disease is the most common form of dementia and is considered to be caused by the conformational change of Aβ monomers, from their native monomeric states, to form Aβ oligomers/fibrils and affects the structure and function of neural cells leading to synaptic dysfunction. Recent experimental data elucidated that 12- crown-4 ether molecule can inhibit Aβ aggregation, reduce toxicity and disrupt the Aβ fibril structure, but the mechanism remains elusive. Various experimental studies have revealed that Aβ aggregate and fibrils interact with biological membranes, which lead to neuronal toxicity, especially cholesterol-rich DPPC membrane; however, the mechanism of interaction remains unknown. To this end, I have performed several microseconds of all-atom molecular dynamics simulations of Aβ40 and Aβ42 monomers, and Aβ40 trimer, in presence and absence of 12-crown-4 ether and coarse-grained simulations of the $A\beta_{9\text{-}40}$ hexamer with the cholesterol-rich DPPC bilayer.

Simulations of Aβ40 and Aβ42 monomers with 12-crown-4 shows that the molecule is highly specific toward positively charged Lys residues and the region around Val24-Lys28 is most prevalent for turn formation. Simulations data of Aβ fibrils trimer with 12-crown-4 simulations reveals that it spontaneously, inserted into the hydrophobic core and opened the "U-shaped" topology of Aβ fibrils trimer and also disrupted Lys28-Asp23 salt bridge. Aβ fibrils hexamer with cholesterol-rich DPPC bilayer simulations reveals that Aβ fibrils hexamer spontaneously inserted to the mixed bilayer and hydrophobic residues played a key role in its binding, especially central hydrophobic cluster region (Lys16, Leu17, Val18, Phe19 and Phe20).

Results of Aβ monomers and Aβ fibrils trimer with 12-crown-4 ether reveals key pharmacophore features required in molecules to specifically bind with Aβ peptides. Data of Aβ fibrils hexamer reveals key pharmacophore features of Aβ protein to bind with the mixed lipid bilayer. The pharmacophore features identified in all the three studies will not only help in designing new candidate drug molecules, which are specific to Aβ peptides but could also be used to design new imaging probe molecules, which could be used for labeling Aβ peptides.

DECLARATION 1 – PLAGIARISM

I, **Nikhil Agrawal** declare that

1. The research reported in this thesis, except where otherwise indicated, and is my original research.

2. This thesis has not been submitted for any degree or examination at any other university.

3. This thesis does not contain other persons' data, pictures, graphs or other information, unless specifically acknowledged as being sourced from other persons.

4. This thesis does not contain other persons' writing, unless specifically acknowledged as being sourced from other researchers. Where other written sources have been quoted, then: Their words have been re-written but the general information attributed to them has been referenced. Where their exact words have been used, then their writing has been placed in italics and inside quotation marks, and referenced.

5. This thesis does not contain text, graphics or tables copied and pasted from the Internet, unless specifically acknowledged, and the source being detailed in the thesis and in the References sections.

A detail contribution to publications that form part and/or include research presented in this thesis is stated (include publications submitted, accepted, in *press* and published).

29/05/2018

Signature with Date

DECLARATION 2 – PUBLICATIONS

1. **Agrawal, Nikhil**, and Adam A. Skelton. "Binding of 12-crown-4 with Alzheimer's Aβ40 and Aβ42 monomers and its effect on their conformation: insight from molecular dynamics simulations." ACS Molecular pharmaceutics,15, 289-299. (2017). (Published)
DOI: 10.1021/acs.molpharmaceut.7b00966 (**Impact factor: 4.44)**

Contribution:

Nikhil Agrawal: Design the study, performed the experiment, analysis of the data, and drafted the manuscript.

Adam A. Skelton: Supervisor

2. Agrawal, Nikhil, and Adam A. Skelton. "12-Crown-4 Ether Disrupts the Patient Brain-Derived Amyloid-β-Fibril Trimer: Insight from All-Atom Molecular Dynamics Simulations." ACS chemical neuroscience 7.10 (2016): 1433-1441. (Published)
DOI: 10.1021/acschemneuro.6b00185 **(Impact factor: 4.348)**

Contribution:

Nikhil Agrawal: Design the study, performed the experiment, analysis of the data, and drafted the manuscript.

Adam A. Skelton: Supervisor

3. **Agrawal, Nikhil** and Adam A. Skelton "Binding of Alzheimer's Amyloid βeta9-40 Fibrils with Cholesterol rich DPPC Bilayer: Insight from Coarse Grained Molecular Dynamics Simulations" ACS Journal of Physical Chemistry B. (Submitted) Manuscript ID: jp-2018-01102x **(Impact factor: 3.177)**

Contribution:

Nikhil Agrawal: Design the study, performed the experiment, analysis of the data, drafted the manuscript.

Adam A. Skelton: Supervisor

RESEARCH OUTPUT

A. PUBLICATIONS

1. **Agrawal, Nikhil**, and Adam A. Skelton. "Binding of 12-crown-4 with Alzheimer's Aβ40 and Aβ42 monomers and its effect on their conformation: insight from molecular dynamics simulations." ACS Molecular pharmaceutics,15, 289-299. (2017).
DOI: 10.1021/acs.molpharmaceut.7b00966 (**Impact factor: 4.44)**

2. Agrawal, Nikhil, and Adam A. Skelton. "12-Crown-4 Ether Disrupts the Patient Brain-Derived Amyloid-β-Fibril Trimer: Insight from All-Atom Molecular Dynamics Simulations." ACS chemical neuroscience 7.10 (2016): 1433-1441. **DOI:** 10.1021/acschemneuro.6b00185 **(Impact factor: 4.348)**

3. Agrawal, Nikhil and Adam A. Skelton "Binding of Alzheimer's Amyloid $\beta eta_{9\text{-}40}$ Fibrils with Cholesterol rich DPPC Bilayer: Insight from Coarse Grained Molecular Dynamics Simulations" "ACS Journal of Physical Chemistry B. Manuscript ID: jp-2018-01102x **(Impact factor: 3.177)**

B. CONFRENCES

1. Nikhil Agrawal, Adam A. Skelton, "12-Crown-4 Ether Disrupts the Patient Brain-Derived Amyloid-β-Fibril Trimer: Insight from All-Atom Molecular Dynamics Simulations", the Frank Warren 2106, 4-8 December 2016, University of Rhodes, Grahamstown, South Africa (Poster Presentation).

2. **Nikhil Agrawal**, Adam A. Skelton," Amyloid-β fibrils remodeling by an organic molecule: Insight from all-atomic Molecular Dynamics Simulations", Theory and Applications of Computational Chemistry 2016, 28Aug-2Sept, 2016, University of Washington, Seattle, United States of America (Poster Presentation)

ACKNOWLEDGMENTS

I would like to thank my supervisor Dr. Adam A. Skelton for his guidance and support, Dr. Adam is not only my supervisor, but also my scientific friend who usually has great ideas and insightful discussions on my research. I am grateful that I became more confident and wiser under his guidance.

I would like to thank present and past members of my lab for providing moral support and sharing enjoyable moments. Specifically, I would like to thank post-doctoral fellows Dr. Sukesh Kalva , Dr. Deepali Sharma, Dr. Khalid Ahmed and Dr. Nashiour Rahman.

I give my sincerest thanks to Dr. Lipi Thukral, (my project supervisor during my job at CSIR-Institute of Genomics and Integrative Biology, New Delhi, India). Dr. Shakti Shai (my master's thesis supervisor at Gautam Buddha University, Greater Noida, India) and Dr. Parul Tewatia, for inspiring me and instilling me a love for Molecular dynamics simulations at a crucial age.

I thank my parents (Mr. Rahul Agrawal, Mrs. Geeta Agrawal) and my brother, Mr. Mukul Bindal for their support and encouragement. I would like to thank my friends, Mr. Nikhil Khurana, Dr. Saumitra Misra, and Dr. Balakumar Chandrasekaran with whom I have shared a quality time during my Ph.D.

Last but not least, I want to thank National Research Foundation for providing me DST-innovation doctoral fellowship and conference travel grants. I would also like to thank, college of Health Science for funding and infrastructure support and Centre of High-Performance Computing, Cape Town and "HIPPO" supercomputing facilities for providing computer resources.

ABBREVIATIONS

Aβ40	Amyloid beta peptide 40 amino acids in length
Aβ42	Amyloid beta peptide 42 amino acids in length
Aβ40 fibrils trimer	Amyloid beta 40 amino acids long three peptides
Aβ9-40 fibrils hexamer	Amyloid beta fibrils 32 amino acids long six peptide
ACDPFF	Classical Drude Polarizable Force Fields for Linear and Cyclic Ethers
AD	Alzheimer's Disease
AFM	Atomic Force Microscopy
APP	Amyloid Precursor Protein
BBB	Blood-Brain Barrier
CHC	Central Hydrophobic Core of Aβ
CARS	Coherent Anti-Stokes Raman Scattering
CHARMM	Chemistry at Harvard Macromolecular Mechanics
CG	Coarse-Grained
COM	Centre of Mass
Cryo-EM	Cryogenic electron microscopy
ET	Electron Tomography
DPPC	Dipalmitoyl Phosphatidylcholine
DSSP	Dictionary of Secondary Structure of Proteins
H-BONDS	Hydrogen Bonds
GROMACS	Groningen Machine for Chemical Simulations
LINCS	Linear Constraint Solver
MD	Molecular Dynamics
MM-PBSA	Molecular Mechanic-Poisson Boltzmann Surface Area
NMR	Nuclear magnetic resonance
NPT	Isothermalisobaric ensemble
ns	Nano seconds
NSAID	Nonsteroidal anti-in ammatory drugs
NVT	Canonical ensemble
PiB	Pittsburgh compound B
PiB-C	Pittsburgh compound B conjugate with

	12-crown-4 ether
PDB	Protein data bank
PET	positron emission tomography
PME	Particle-Mesh Ewald
RMSD	Root-mean-square deviation
Rg	Radius of Gyration
TEM	Transmission electron microscopy
TIP3P	Transferable intermolecular potential 3 point
VdW	van der Waals
μs	Micro seconds

TABLE OF CONTENTS

LIST OF FIGURES

LIST OF TABLES

CHAPTER 1

1. Introduction

1.1 Overview of Alzheimer's disease (AD)

Alzheimer's disease (AD) is the most common form of dementia, affecting around 40 million people around the world and global annual estimated for 2018 is the US $1 trillion[1-3]. More than 2.2 million South African are living with Alzheimer's[4]. AD leads to a slow and progressive decline in cognitive domains, most commonly involving episodic memory and executive functions which cause occupational or social impairment[5]. Despite intense research for decades still, there is no complete understanding of the disease etiology. However, the possible cause of AD could be categorized into three groups; these are (1) cellular (2) genetic and (3) molecular imbalances[6, 7]. Misfolding and aggregation of Amyloid-β (Aβ) peptides[8], belongs to the molecular imbalance group.

1.2 Amyloid Cascade Hypothesis

The amyloid cascade hypothesis proposed by Hardy and Higgins in 1992[9] and since then it has played a crucial role in explaining the etiology and pathogenesis of Alzheimer's disease (AD) and dominated research for the past twenty years[10]. It suggests that accumulation of Aβ peptides in the brain is the early event in AD, which leads to the formation of senile plaques (SPs) and further neurofibrillary tangles (NFTs), causing neuronal cell death, and ultimately dementia. The various experimental studies have supported this hypothesis[11].

1.2.1 Production of Aβ peptides

The term amyloid was conied by Rudolph Virchow, in 1854 to represent tissue abnormality that exhibited a positive iodine staining reaction[12]. Aβ peptides are cleavage products of the transmembrane amyloid precursor protein (APP), which is cleaved by enzyme complexes α, β, and γ-secretases[13]. (Figure: 1.1) APP cleaved by α-secretase produce N-terminal ectodomain (sAPPα) and 83-amino acid C-terminal membrane fragment (C83), which is sequentially cleaved by γ-secretase to generate non-pathogenic P3 peptide and APP intracellular domain (AICD); this pathway termed as "non-amyloidogenic pathway." When APP is cleaved by β-secretase instead of α-secretase, it produces N-terminal ectodomain (sAPPβ) and 99-amino acid C terminal membrane fragment (C99), which is sequentially cleaved by γ-secretase to produce pathogenic Aβ peptide and AICD; this pathway termed as "Amyloidogenic pathway"[14, 15] (Figure: 1.1). Since γ-secretase lacks the ability to cleave Aβ peptide accurately, this results in a variable length of Aβ peptides; the most common variants are Aβ1-40 and Aβ1-42[16].

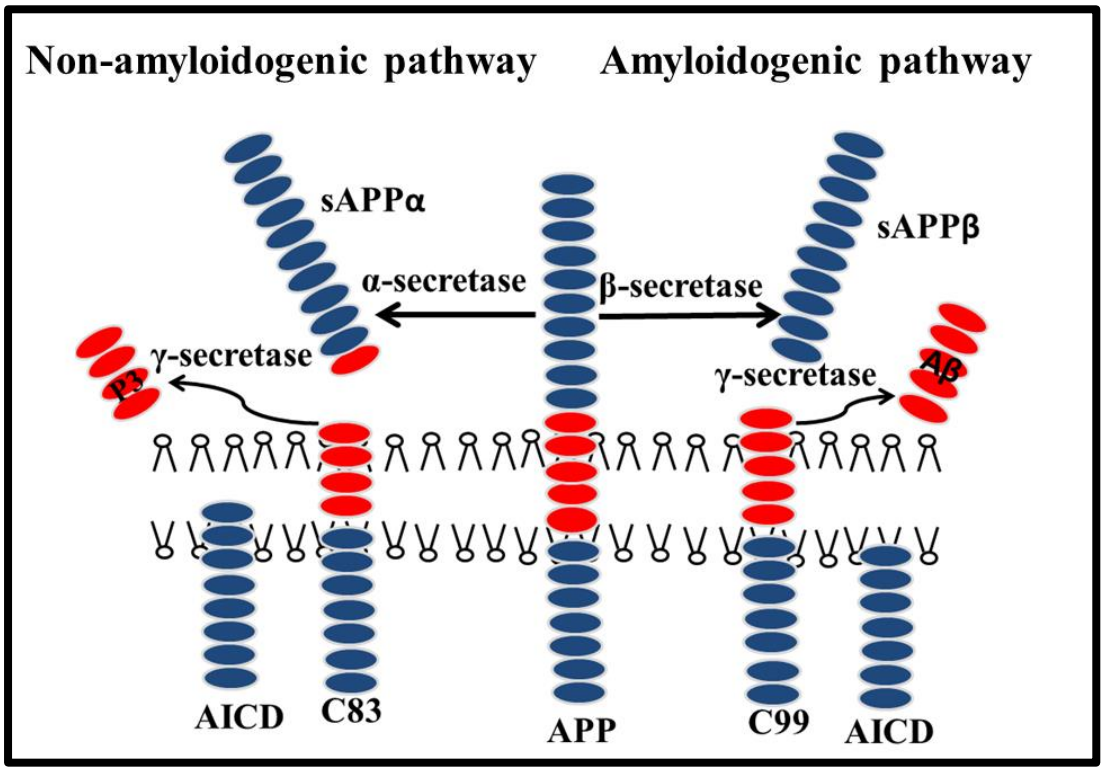

Figure: 1.1 Shows non-amyloidogenic and Amyloidogenic pathways of APP cleavage. Aβ region of protein has been shown in red and other part has been shown in blue.

1.3 Amino acids sequence of Aβ peptides

The amino acids sequence of Aβ peptide was discovered in 1984 from extracellular deposits and amyloid plaques[17]. The Aβ1-40 peptide contains 17 hydrophobic, 11 polar and 12 charged residues, Aβ1-42 peptide includes 2 additional hydrophobic residues at C-terminal residues,(Figure: 1.2) which make Aβ1-42 peptide more toxic and aggregation prone[18].

- **Aβ1-40**
  DAEFRHDSGYEVHHQKLVFFAEDVGSNK
  GAIIGLMVGGVV

- **Aβ1-42**
  DAEFRHDSGYEVHHQKLVFFAEDVGSNK
  GAIIGLMVGGVVIA

Figure: 1.2 Shows the amino acids sequence of Aβ1-40 and Aβ1-42 peptides. Negatively charged residues has

been shown in red, positively charged residues has been shown in green, polar residues has been shown in black and nonpolar residues has been shown in light blue color.

1.4 Structure of Aβ1-40 and Aβ1-42 Monomers

The Aβ monomer is an intrinsically disordered peptide (IDP) in the water environment, meaning that instead of single dominant folded conformations, Aβ peptide populates a large number of different conformation, which makes problematic to crystallize their structures[19, 20]. The knowledge of Aβ monomers structures has been majorly driven from NMR and MD simulations. In the membrane-mimicking environment, Aβ1-40 and Aβ1-42 monomers predominantly remain an α-helical conformation. The Aβ1-40 monomer region, Asp1-His14 remains unstructured, and the region between residues, Gln15 to Val36 adopts a α-helical conformation with a turn around Gly25-Asn27[21] (Figure: 1.3B). Aβ1-42 monomer contains two α-helix regions: i) helixI (Ser8-Val24) and helixII (Lys28-Val38) and a turn region around (Gly25-Lys28)[22, 23] (Figure: 1.3C). Aβ1-40 monomer structure in complete aqueous environment reveals that the region between His13-Asp23 forms a 3_{10}-helix and the N- and C-terminal remains unstructured[24] (Figure: 1.3A). The Aβ1-42 monomer structure in 70% aqueous environment reveales that the region between Try10-Asp23 remained in α-helix conformation and the region between Leu34-Gly38 contains a certain degree of helical structure and the Gly25-Lys28 region forms a turn[25] (Figure: 1.3D). All the structure mentioned above of Aβ monomers has been resolved in different *in-vivo* environments by representing a range of 100% water to micelle-like membrane environment. In Table: 1.1 we have summarized structures and their environment.

PDB id	**In vivo environment**
2LFM[24] (Aβ1-40 monomer)	100% water
1BA4[21] (Aβ1-40 monomer)	Water-micelle like environment
1IYT [22] (Aβ1-42 monomer)	20% water
1Z0Q[25] (Aβ1-42 monomer)	70% water

Table: 1.1 Aβ1-40/42 in different *in vivo* environments.

These structures could be further categorized by their α-helix content; as the water content increases there is a loss of α-helix content observed in these structures. The Aβ peptide present in the micelle-like environment has the highest α-helix content, and the one in 100% water environment has the lowest α-helix content. The pattern of α-helix in decreasing order follows as 1BA4> 1Z0Q>1IYT>2LFM.

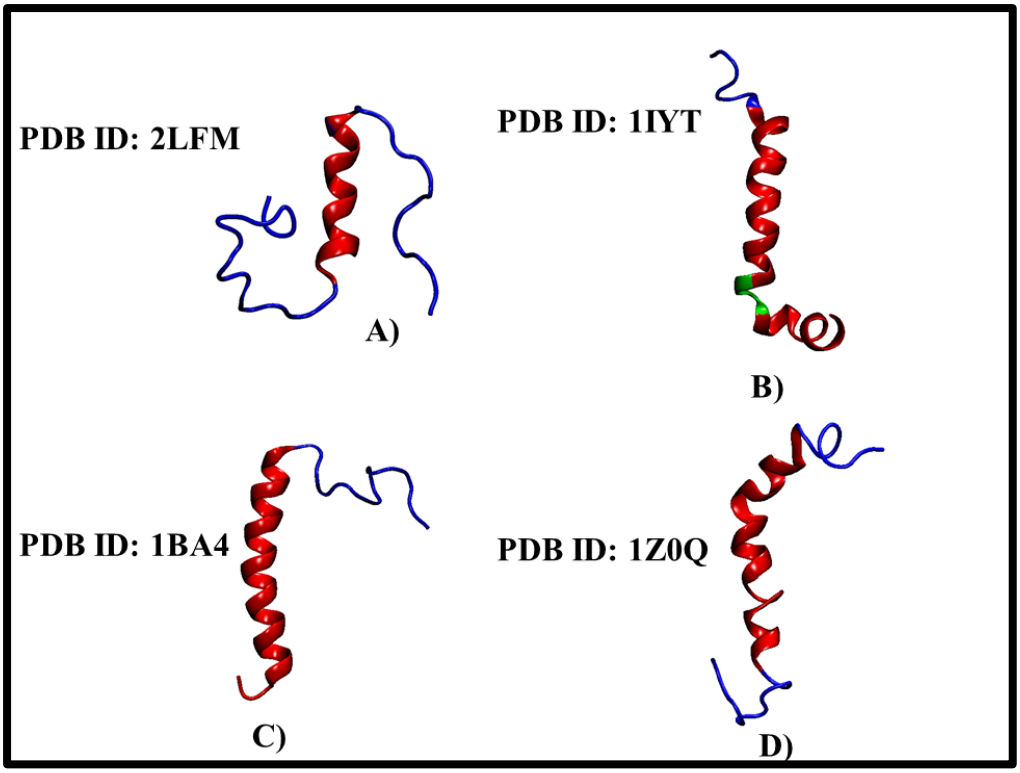

Figure: 1..3 A) Shows Aβ40 monomer structure (PDB ID: 2LFM). B) Shows Aβ42 monomer structure (PDB ID: 1IYT). B) Shows Aβ40 monomer structure (PDB ID: 1BA4). D) Shows Aβ42 monomer structure (PDB ID: 1Z0Q). The monomers have been shown in cartoon represen representation, and α-helix region has shown in red color, and unstructured region has been shown in blue color and turns region has been shown in green.

MD simulations of Aβ monomers in aqueous and membrane environment have provided crucial information about these peptides. Luttmann *et. al.*[26] performed MD simulation of full-length Aβ monomers in aqueous environment their data revealed that Ala21-Gly33 forms a turn region and residue between Asp1-Tyr10 are highly flexible. Agrawal *et. al.*[27] performed MD simulation of Aβ1-40 and Aβ1-42 monomers in an explicit water environment and their data revealed that a gain of water molecules around Lys28 and a loss of water molecules around Val24 play a key role in turn formation. Valerio[28] *et al.* performed MD simulation study of Aβ1-40 and their results showed that hydrophobicity, flexibility, and mobility of N-terminal region is important for obtaining misfolded structure. Miyashita[29] *et al.* performed the replica-exchange simulation of Aβ1-40 and Aβ1-42 in membrane environment and their results showed that the C-terminal region of both peptides favors membrane environment and N-terminal region favors aqueous region and forms a coil.

1.5 Different shapes of Aβ fibrils

Aβ fibrils are non-crystalline and insoluble in water, which makes them incompatible with solution NMR and x-ray crystallography[30]. However, techniques like x-ray diffraction[31] solid-state NMR (SS-NMR)[32], transmission electron microscopy (TEM)[33], cryo-electron microscopy (cryo-EM)[34], atomic force microscopy (AFM)[35], and MD simulation[36] have provided valuable information about Aβ fibrils.

X-ray diffraction studies helped to establish that Aβ fibril forms "cross-β-sheet" structures[37-39], in which Aβ peptides assemble into β-sheets with β-strands oriented perpendicular to the long axis of the fibril and stabilized by H-bonds. β-sheet structures of Aβ fibrils were further confirmed by binding of β-sheet specific dyes such as thioflavin-T and Congo red[40, 41]. SS-NMR studies have revealed that Aβ fibrils contain two β-sheets, and these β-sheets are connected by a turn region, which gives Aβ fibrils a dual-sheet motif or "U-shaped" topology (Figure: 1.4A). The region between two β-sheet contains a hydrophobic core, which is completely devoid of water molecules[42, 43]. There are several factors, which play an important role in the stability of these fibrils and these are the following: i) hydrogen bonding between the backbone amide groups of two nearby chains. ii) VdW interactions between top and bottom β-sheets in the hydrophobic core region. iii) enhancement in the entropy of water molecules that are expelled from the interior of two β-sheets, and iv) salt-bridge between Asp23-Lys28[44, 45]. Recent studies have revealed that "S-shaped" structure of Aβ1-42 fibrils, which contains three β-sheets, β1 (12–18), β2 (24–33), and β3 (36–40) in which Lys28 formed a salt bridge with the Ala42 carboxyl terminus[46-48] (Figure: 1.4B). . Rodriguez[49] *et al.* performed MD simulations of "S-shaped" Aβ1-42 fibrils in water with 150mM NaCl and their data showed that monomer is not stable in its "S-shaped" structure. However, a dimer of Aβ1-42 peptides showed stability and retained its S-shaped conformation.

Cryo-EM has provided a new finding in this field; a recently resolved structure using cryo-EM revealed that Aβ fibril structures obtained an "L-S" shape (Figure: 1.4C). In the "L-S" shaped structure the N-terminus is "L-shaped," and the C-terminus is "S-shaped." There are three hydrophobic clusters present in the structure i) Ala2, Val36, Phe4, and Leu34, ii) Leu17, Ile31, and Phe19 and iii) Ala30, Ile32, Met35, and Val40), which helps the structure to be stabilized[50]. Nakayama[51] *et al.* using high-speed AFM revealed the fibril formation and elongation of Aβ1–42 and their data showed two different growth modes of Aβ1-42; the first one produces straight fibrils and the second one produces spiral fibrils. TEM studies have revealed that as Aβ fibrils are straight, unbranched filaments that are approximate,10 nm in size, which often exceeds up to 1 μm[52]. MD simulation studies have provided important insights about the structural stability of Aβ protofibrils/fibrils, e.g., Masman *et al.*[53] performed MD simulation of Aβ1-42 fibrils; their data suggested that the hydrophobic core region is crucial in stabilizing the Aβ aggregates. Lemkul *et. al.*[54] performed MD simulations of Aβ protofibrils and their results revealed that a finite level of hydration around the Asp23-Lys28 salt bridge is crucial for protofibril stability. Their data further showed that interaction between Ile32 and the aliphatic portion of the Lys28 side chain regulates the level of hydration in the core of the protofibril.

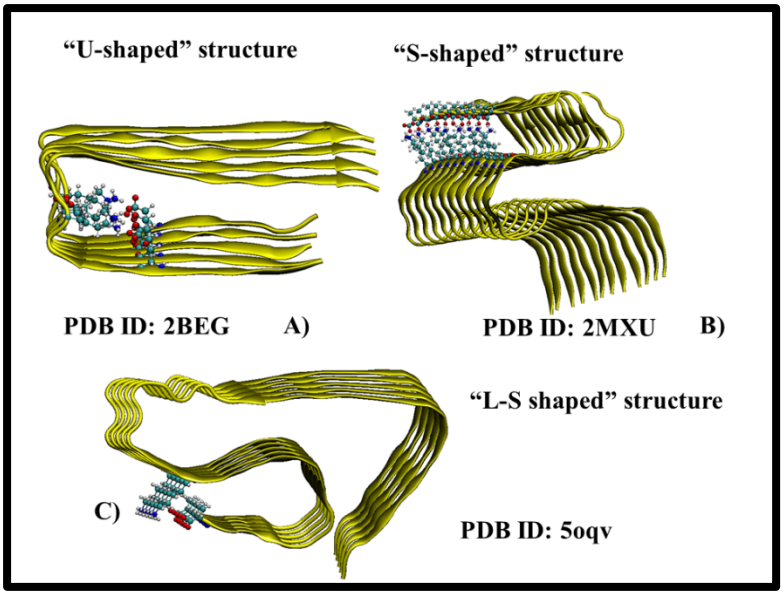

Figure 1.4 A) Shows Aβ17-42 fibrils "U-shaped" structure PDB id: 2BEG[55]. B) Shows "S-shaped" structure of Aβ1-42 fibrils PDB id: 2MXU[46]. C) Shows "L-S" Shaped Aβ1-42 fibrils PDB id: 5OQV[50]. Structure of Aβ fibrils has shown in new cartoon representation and salt--bridge formed by them in CPK representation.

1.5.1 Arrangement of Aβ fibrils in two-symmetry and three-fold symmetry

In the two-fold symmetry, Aβ fibril structures contain two symmetric strands that form separate β-sheets in a double-layered, cross-β motif. The two protofilaments aggregate in the fibril growth direction and have a helical symmetry along the axis (Figure: 1.5A-E). In the three-fold symmetry, Aβ fibrils contain three β-strands that form separate β-sheets in a triangular cross-β motif arrangement and same as two-fold symmetry structure. These three protofibrils can aggregate in the fibril growth direction and also have a helical symmetry along the axis[56] (Figure: 1.5E). In two-fold symmetry packing of "U-shaped" (Figure: 1.5A), Aβ fibrils Met35 interacts along and across the fibril axis and stabilize the two-fold symmetry structure. Wu[57] *et al.* performed MD simulations of "U-shaped" $A\beta_{9-40}$ fibrils in two-fold symmetry in six different possibilities, their results revealed that in all the possibilities hydrophobic residues stabilized the interface between two units. Colvin[47] *et al.* determined Aβ1-42 fibrils structure in two-fold symmetry. In this structure, each β-strand in "S-shaped" (Figure: 1.5B) and arranged in such a manner that generates two hydrophobic cores, and interchain contacts of two units formed between residues Met35 and either Leu17 or Gln15. These factors mentioned above help to stabilize "S-shaped" Aβ fibrils in the two-fold symmetry (Figure: 1.5B). Wang[58] *et al.* performed MD simulations of "S-shaped" structure of Aβ1-42 fibrils in the two-fold symmetry in two different arrangement, PSA (packing between β1-β1) and PSB (packing between β3-β3). In PSA, packing Lys16 of one unit formed a salt-bridge with Glu22/Asp23 of another unit and stabilized the two-fold symmetry structure. In PSB packing, the Val40 side chain formed contact with Gly38 of another unit to stabilize the structure in two-fold symmetry. "LS-shaped structure of Aβ1-42 fibrils in two-fold symmetry revealed that β-strands of different units

formed salt-bridges between Asp1 and Lys28, which help to stabilize the structure in the two-fold symmetry[50]. Schmidt[34] *et al.* study showed Aβ1-42 fibril in "tilde-shaped" conformation arranged in two-fold symmetry, in which the C-terminal region of the peptide is surrounded by the N-terminal region. This arrangment leads to the formation of a hydrophoic core region between C and N-terminal (Figure: 1.5D). Wälti[48] *et al.* resolved the atomic-resolution structure of Aβ1-42 fibril arragned in two-fold symmetry, in which residues 15-42 form a double-horseshoe–like cross–β-sheet with maximally buried hydrophobic side chains. Residues 1–14 are partially ordered and in a β-strand conformation. Miller[59] *et al.* performed MD simulations of "U-shaped" $A\beta_{1-40}$ fibrils in three-fold symmetry and their results showed that Met35 formed interactions along the fibril axis and Ile31-Val39 of different cross-β units formed interactions. Their data further showed Aβ1 –40 triangular structure has a large cavity along the fibril axis and the N—terminal help to stabilize the structure in three-fold symmetry by interacting C-terminal domains of other units. Dong[60] *et al.* performed MD simulation of "U-shaped" $A\beta_{40}$ fibrils in two-fold and three-fold symmetries and their results suggested that packing of "U-shaped" $A\beta_{40}$ fibrils in the two-fold symmetry are more stable in comparison to the packing of "U-shaped" $A\beta_{40}$ fibrils in the three-fold symmetry.

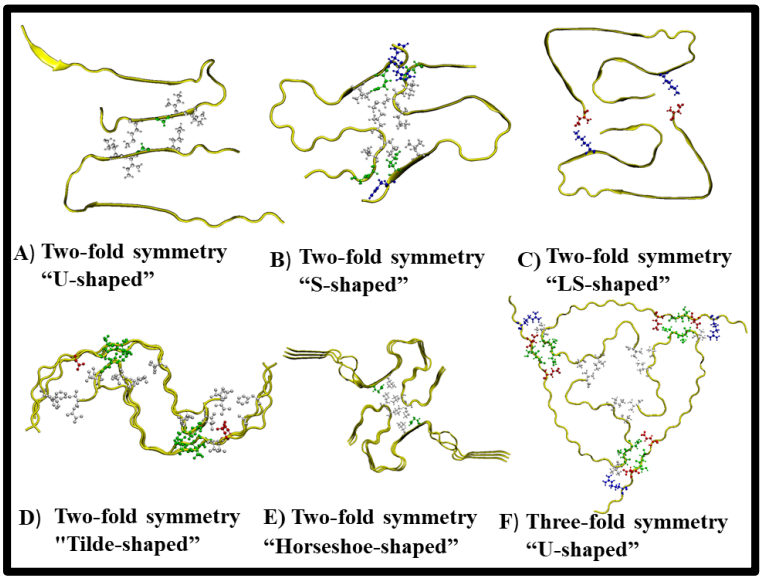

Figure: 1.2 A) Shows "U-shaped" Aβ9-40 fibrils (PDB ID: 2LMN[42]) in two-fold symmetry. B) Shows "S-shaped" Aβ1-42 fibrils (PDB ID: 5KK3[47]) in two-fold symmetry. C) Shows "LS-shaped" (PDB ID: 5OQV[50]) Aβ1-42 fibrils in two-fold symmetry. D) Shows "Tilde-shaped" (PD ID: 5AEF[34]) Aβ1-42 fibril in two-fold symmetry. E) Shows "Horseshoe-shaped" Aβ1-42 fibril in two-fold symmetry (PDB ID: 2NAO[48]). F) Shows "U-shaped" Aβ1-40 fibrils (PDB ID: 2M4J[61]) in the three-fold symmetry. All the fibrils have shown in new-cartoon representation, and contact residues have been shown CPK. Hydrophobic residues have been shown in white, polar residues have been shown in green, negatively charged residues have been shown in red, and positively charged residues have been shown in blue.

1.5.2 Polymorphism in Aβ fibrils and its implications

Now its very evident that the structure of Aβ fibril does not depend on the amino acids sequence[62], as we have mentioned in the previous section that Aβ peptides can arrange in the different shapes and symmetries. The polymorphism in Aβ fibril structures suggests that multiple interaction sites present within each Aβ molecule, give rise to differences in fiber morphologies and physicochemical properties on the surface of the fibers that may be correlated with different levels of cellular toxicity[42, 63, 64].

1.5.3 Elongation of Aβ fibrils

Elongation of Aβ fibrils is a very complex process and studies have suggested that it takes place by the inclusion of structured/unstructured monomers at the fibril tips[65]. This process is termed as "dock and lock" mechanism. In the first step (docking) of this process, a monomer “docks” to the Aβ fibrils surface and in the second step (locking) the monomer undergoes conformation rearrangements to form the native contacts present in Aβ fibrils[66]. A MD simulation study by Schwierz[67] *et al.* has revealed that solvent entropy is the major driving force in the elongation process. Their data further showed that the “docking” stage (Figure: 1.6 A, B) is fast as interactions are mediated by transient non-native hydrogen bonds and the “locking” stage (Figure: 1.6 C) is very slow due to the formation of long-lived non-native hydrogen bonds. Bacci[68] *et al.* performed MD simulation of Aβ42 pentamer to study the elonagtion process and their data revealed that in the both “docking” and “locking” steps, hydrophobic interaction plays a key role.

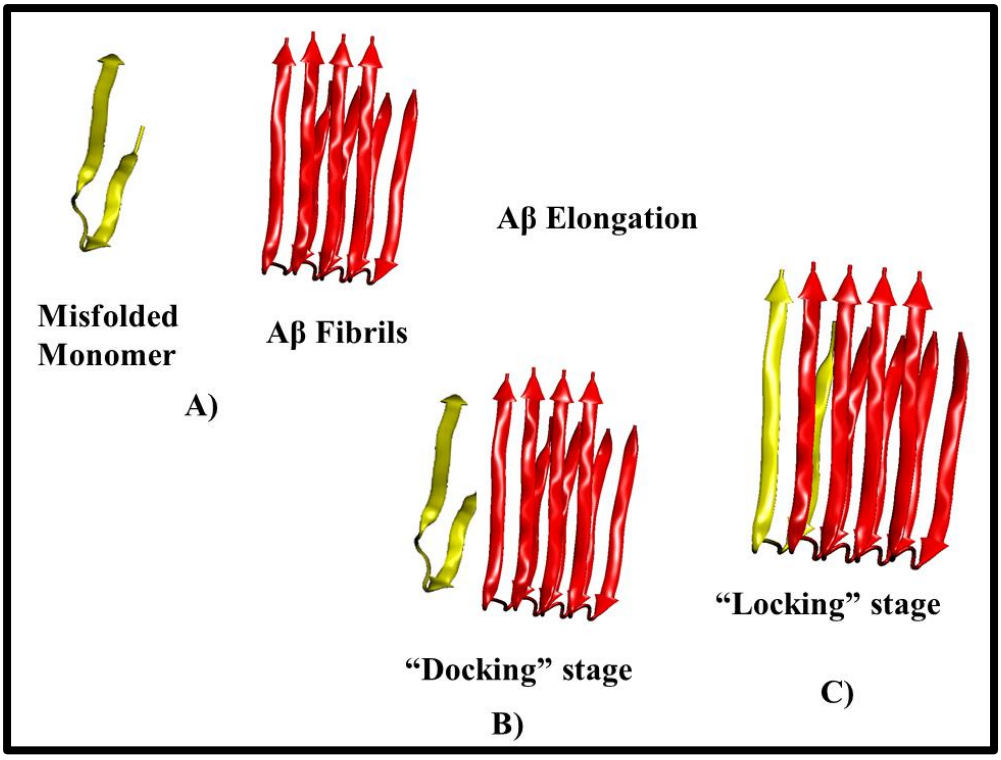

Figure:1.6 A) Shows misfolded Aβ monomer and Aβ fibrils B) "Docking" stage of monomer association with Aβ fibrils C) Shows "Locking" stage of Aβ monomer association with Aβ fibrils.

1.6 Aβ aggregates/Fibrils interaction with Membranes

Studies have suggested that Aβ aggregate/fibrils form a nonspecific association with cell membranes (Figure: 1.7), which perturbs the structural properties of both of them[69]. Kremer[70] *et al.* experimental study suggested that aggregated Aβ decreases the fluidity of membranes. Lindberg[71] *et al.* work revealed that charged lipid membranes which represent the outer cell membranes can significantly increase autocatalytic steps in the self-assembly of $A\beta_{1-42}$ into fibrils. Xiang[72] *et al.* performed MD simulation of $A\beta_{11-42}$ aggregate/fibrils with membranes and their data revealed that Aβ peptides larger than two peptides could lead to the lipid deformation and water channel formation. Scala[73] *et al.* study revealed the molecular mechanism of pore formation in the membrane by the Aβ oligomer aggregates; they showed cholesterol and ganglioside interact with amyloid proteins, which leads to the creation of pores in the membranes. Martins[74] *et al.* study showed that lipids can revert Aβ fibrils into neurotoxic protofibrils.

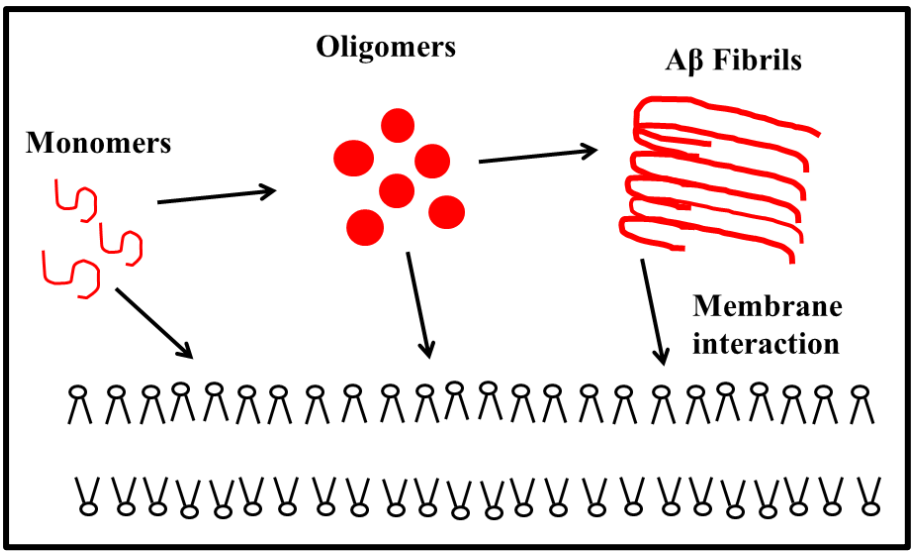

Figure: 1. 7 Shows different stages of Aβ peptides from monomers to fibrils (at any stage, they can interact with the biological membrane).

1.7 Inhibitors of Aβ Proteins Toxicity

Misfolding and aggregation of Aβ monomers is the first step in a multi-step pathway to form neurotoxic soluble oligomers and mature Aβ fibrils. Toxicity of an independent Aβ monomers is still debatable as some studies suggest that they are toxic[75] and other labeled them as nontoxic[76]. However, there is a consensus in the scientific community regarding the toxicity of Aβ oligomers[77, 78] . Aβ fibrils are also neurotoxic as they can interact with the cell membranes[74, 79]. Inhibition of misfolding and aggregation of Aβ peptides and remodeling the Aβ fibril morphology could significantly reduce its cytotoxicity[80,61].

In past decades, several Aβ peptide inhibitors have been discovered and many of them failed in the preclinical stage; some of them failed in advanced clinical stage (Phase III). Below we discuss the molecule and antibodies which went into clinical phases II and III. To best of our knowledge these are the antibodies, which has enterted in to clinical phase III.

1.7.1 Tramiprosate (Alzhemed®)

Homotaurine is an amino sulfonate compound (Figure: 1.8A), which is extracted from marine red algae[81]. These compounds were chemically synthesized and introduced into clinical use as tramiprosate by Neurochem, Inc[82]. In vitro studies have shown that Alzhemed (Figure: 8A) preferentially binds to soluble Aβ peptides, inhibits their aggregation and fibrillogenesis and reduces Aβ neurotoxicity. Martineau[83] *et al.* suggested that Homotaurine binds with Aβ peptides using its sulfonate head group. It has also been shown that Tramiprosate could reduce ~30% Aβ plaque level in the brain[84]. The clinical phase III study of Tramiprosate was carried out in the United States in 1052 patients with AD to test the efficacy, tolerance, and safety of the Tramiprosate, but unfortunately, Tramiprosate failed to show efficacy[85].

1.7.2 Solanezumab

Solanezumab is an anti-Aβ peptide monoclonal antibody developed by Eli Lilly. Crespi[86] *et al.* resolved the crystal structure of Solanezumab complex with Aβ peptide and their results showed that Solanezumab recognized the mid-region residues, 16-26, of Aβ peptide. Their results further revealed that Aβ16-26 forms extensive contacts and hydrogen bonds to the Solanezumab and Aβ binds to the Solanezumab in an unstructured conformation (Figure: 1.8B). The rationale to use Solanezumab as an anti-Aβ peptide was that it could remove small, toxic, soluble Aβ peptides, which may lead to the reduction in synaptic toxicity. The clinical phase I and II studies showed that Solanezumab was tolerated in both healthy and AD patients without any side effects[87, 88]. However, Solanezumab failed to demonstrate efficacy in the clinical phase III[89].

1.7. 3 Bapineuzumab (humanized 3D6)

Bapineuzumab is an anti-Aβ monoclonal antibody developed by Pfizer and Johnson & Johnson. The rationale to use Bapineuzumab as an anti-Aβ antibody was that it could clear excess Aβ peptides. Feinberg[90] *et al.* resolved the crystal structure of Bapineuzumab complex with Aβ peptide and their results showed that Bapineuzumab antibody specifically recognized Aβ residue 1-5 with a strong preference for an exposed Asp residue at the N-terminus. Their results further revealed that Aβ1-5 bound in 3_{10}-helix conformation with Bapineuzumab. In another study Miles[91] *et al.* also resolved the crystal structure of Bapineuzumab complex with Aβ. Their results revealed that Bapineuzumab binds to the N-terminal end of the Aβ (residues 1-6) in a helical conformation (Figure: 1.8C). The clinical phase I and II studies showed that Bapineuzumab was well-tolerated in patients with mild to moderate AD. However, Bapineuzumab also failed in phase III clinical trial, when it was unable to protect patients from cognitive and functional decline[92, 93].

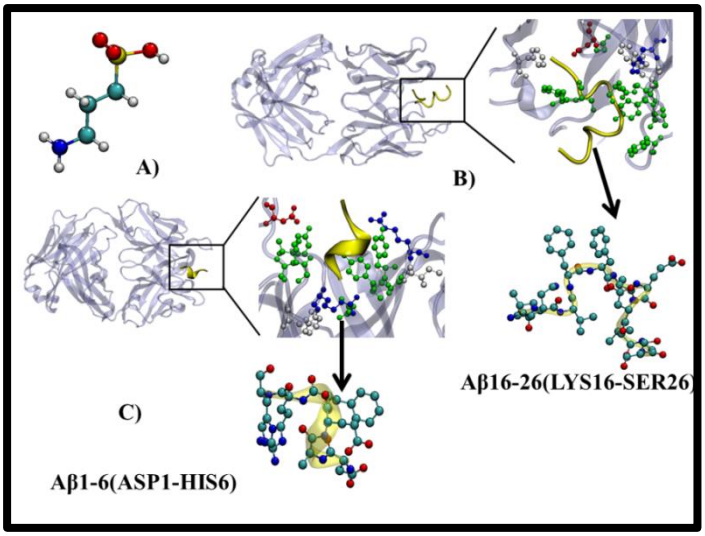

Figure: 1.8 A) Shows the structure of Homotaurine (PubChem CID: 1646). B) Shows $A\beta_{16-26}$ bound with Solanezumab (PDB id:4XXD[86]). C) Shows $A\beta_{1-6}$ bound with Bapineuzumab (PDB id: 4HIX[91]).

The failures of above-mentioned candidate drug molecule/antibodies at clinical stages (II and III) has driven the research to explore the new strategies for developing drugs for AD. Tian[94] *et al.* proposed a new approach to attenuate the aggregation of Aβ peptide through a non-covalent modification at its surface and reasoned that crown ethers could be exploited to "neutralize" positive charges of the amino groups of Aβ peptide through the formation of hydrogen bonds.

1.8 Crown ethers

Crown ethers are small cyclic polyethers, first synthesized by 1987 Nobel Prize winner in chemistry Charles J. Pedersen[95, 96]. Crown ether molecules have been widely applied in biological chemistry, probe chemistry,[97, 98], and ion channles[99, 100]. Morrison[101] *et al.* used crown ethers as permeability enhancers for ocular drug delivery. Lee[102] *et al.* performed an experimental and MD simulations study to reveal that crown ethers could modify protein surface behavior dramatically by stabilizing either intra- or intermolecular interactions. Banik[103] *et al.* used crown ethers for inhibition of fibrillar assemblies of l-Phenylalanine. Angelinia[104] *et al.* complexed crown ethers with lipid, and applied as potential DNA vectors. There is no crown ether based molecule that has entered into clinical trials for the Alzheimer's disease until now; however, a 12-crown-4 fused quinazoline drug name Icotinib is in the market as an inhibitor of epidermal growth factor receptor tyrosine kinase (EGFR-TK)[105.] Even though the 12-crown-4 may not be a viable drug, the molecule is small, cheap (sigma sells it in 80 euro/5grams purity 98%) and easy to manage,which makes 12-crown-4 suitable for the lab and useful for simulations. Understanding the 12-crown-4 binding mechanism to Aβ proteins will generate the knowledge, which could be utilized to design new more potential drug molecules.

1.9 Aim and objectives

The aim of this thesis is to carry out MD simulations to reveal the molecular mechanism of 12-crown-4 binding to Aβ40, Aβ42 monomers, Aβ40 fibril trimer and $A\beta_{9-40}$ fibrils hexamer binding to cholesterol-rich DPPC bilayer.

The following objectives of this work were:

1) Role of water in turn formation or early stage misfolding of Aβ1-40 and Aβ1-42 monomers.

2) Identify the region of 12-crown-4 binding and its impact on Aβ1-40 and Aβ1-42 monomers conformations.

3) Effect of 12-crown-4 binding on conformation entropy of Aβ monomer.

4) Decipher the binding modes of 12-crown-4 on Aβ40 fibril trimer and effects of binding on its conformations.

5) Reveal the mechanism of $A\beta_{9-40}$ hexamer fibrils binding with cholesterol-rich DPPC bilayer.

1.10 Overview of thesis

This thesis will take the following form

Chapter-2: will discuss the basics of molecular dynamics (MD) simulations.

Chapter-3: (Published work- this chapter is presented in the required format of the journal and the final accepted version)

This chapter deals with a research paper entitled "Binding of 12-Crown-4 with Alzheimer's Aβ40 and Aβ42 Monomers and Its Effect on Their Conformation: Insight from Molecular Dynamics Simulations"; which was published in ACS Molecular Pharmaceutics[27]. This chapter describes the role of water in the turn formation in Aβ40 and Aβ42 monomers and binding of 12-crown-4 with these monomers using all-atom MD simulations.

Chapter-4: (Published work- this chapter is presented in the required format of the journal and the final accepted version)

This chapter deals with a research paper entitled "12-Crown-4 Ether Disrupts the Patient Brain-Derived Amyloid-β-Fibril Trimer: Insight from All-Atom Molecular Dynamics Simulations"; which was published in ACS chemical neuroscience[45]. This chapter describes binding modes of 12-crown-4, on patient brained derived Aβ40 fibril using all-atom MD simulations.

Chapter-5: (Submitted work – this chapter is presented in the required format of the journal and is the final version of the submitted manuscript)

This chapter deals with a research work entitled "Binding of Alzheimer's Amyloid βeta_{9-40} Fibrils with Cholesterol-rich DPPC Bilayer: Insight from Coarse Grained Molecular Dynamics Simulations"; which has been submitted to ACS Journal of Physical Chemistry B. This chapter describes the binding of $A\beta_{9-40}$ fibril hexamer binding with cholesterol-rich DPPC bilayer using coarse-grained MD simulations.

Chapter-6: deals with concluding remarks.

1.11 References:

[1] Uflacker, A., and Doraiswamy, P. M. (2017) Alzheimer's Disease: An Overview of Recent Developments and a Look to the Future, *Focus 15*, 13-17.

[2] Association, A. s. (2016) 2016 Alzheimer's disease facts and figures, *Alzheimer's & Dementia 12*, 459-509.

[3] Wimo, A., Guerchet, M., Ali, G.-C., Wu, Y.-T., Prina, A. M., Winblad, B., Jönsson, L., Liu, Z., and Prince, M. (2017) The worldwide costs of dementia 2015 and comparisons with 2010, *Alzheimer's & Dementia 13*, 1-7.

[4] Dirk, N. (2015) 2.2 million S Africans have Alzheimer's, *2018*.

[5] Tarawneh, R., and Holtzman, D. M. (2012) The clinical problem of symptomatic Alzheimer disease and mild cognitive impairment, *Cold Spring Harbor perspectives in medicine 2*, a006148.

[6] Herrup, K. (2015) The case for rejecting the amyloid cascade hypothesis, *Nature neuroscience*, 794-799.

[7] Bali, J., Halima, S. B., Felmy, B., Goodger, Z., Zurbriggen, S., and Rajendran, L. (2010) Cellular basis of Alzheimer's disease, *Annals of Indian Academy of Neurology 13*, S89.

[8] Hardy, J., and Selkoe, D. J. (2002) The amyloid hypothesis of Alzheimer's disease: progress and problems on the road to therapeutics, *science 297*, 353-356.

[9] Hardy, J. A., and Higgins, G. A. (1992) Alzheimer's disease: the amyloid cascade hypothesis, *Science 256*, 184.

[10] Karran, E., Mercken, M., and De Strooper, B. (2011) The amyloid cascade hypothesis for Alzheimer's disease: an appraisal for the development of therapeutics, *Nature reviews Drug discovery 10*, 698-712.

[11] Reitz, C. (2012) Alzheimer's disease and the amyloid cascade hypothesis: a critical review, *International journal of Alzheimer's disease 2012*.

[12] Sipe, J. D., and Cohen, A. S. (2000) History of the amyloid fibril, *Journal of structural biology 130*, 88-98.

[13] O'Brien, R. J., and Wong, P. C. (2011) Amyloid precursor protein processing and Alzheimer's disease, *Annual review of neuroscience 34*, 185-204.

[14] Del Prete, D., Checler, F., and Chami, M. (2014) Ryanodine receptors: physiological function and deregulation in Alzheimer disease, *Molecular neurodegeneration 9*, 21.

[15] Spies, P. E., Verbeek, M. M., van Groen, T., and Claassen, J. (2012) Reviewing reasons for the decreased CSF Abeta42 concentration in Alzheimer disease, *Front Biosci 17*, 2024-2034.

[16] Bergström, P., Agholme, L., Nazir, F. H., Satir, T. M., Toombs, J., Wellington, H., Strandberg, J., Bontell, T. O., Kvartsberg, H., and Holmström, M. (2016) Amyloid precursor protein

expression and processing are differentially regulated during cortical neuron differentiation, *Scientific reports 6*.

[17] Glenner, G., and Wong, C. (1988) Alzheimer's disease: initial report of the purification and characterization of a novel cerebrovascular amyloid protein, *Alzheimer Disease & Associated Disorders 2*, 134.

[18] Yoshiike, Y., Chui, D.-H., Akagi, T., Tanaka, N., and Takashima, A. (2003) Specific compositions of amyloid-β peptides as the determinant of toxic β-aggregation, *Journal of Biological Chemistry 278*, 23648-23655.

[19] Uversky, V. N. (2009) Intrinsic disorder in proteins associated with neurodegenerative diseases, In *Protein folding and misfolding: neurodegenerative diseases*, pp 21-75, Springer.

[20] Ball, K. A., Phillips, A. H., Nerenberg, P. S., Fawzi, N. L., Wemmer, D. E., and Head-Gordon, T. (2011) Homogeneous and heterogeneous tertiary structure ensembles of amyloid-β peptides, *Biochemistry 50*, 7612-7628.

[21] Coles, M., Bicknell, W., Watson, A. A., Fairlie, D. P., and Craik, D. J. (1998) Solution Structure of Amyloid β-Peptide (1− 40) in a Water− Micelle Environment. Is the Membrane-Spanning Domain Where We Think It Is?, *Biochemistry 37*, 11064-11077.

[22] Crescenzi, O., Tomaselli, S., Guerrini, R., Salvadori, S., D'Ursi, A. M., Temussi, P. A., and Picone, D. (2002) Solution structure of the Alzheimer amyloid β-peptide (1–42) in an apolar microenvironment, *The FEBS Journal 269*, 5642-5648.

[23] Janek, K., Rothemund, S., Gast, K., Beyermann, M., Zipper, J., Fabian, H., Bienert, M., and Krause, E. (2001) Study of the conformational transition of Aβ (1− 42) using d-amino acid replacement analogues, *Biochemistry 40*, 5457-5463.

[24] Vivekanandan, S., Brender, J. R., Lee, S. Y., and Ramamoorthy, A. (2011) A partially folded structure of amyloid-beta (1–40) in an aqueous environment, *Biochemical and biophysical research communications 411*, 312-316.

[25] Tomaselli, S., Esposito, V., Vangone, P., van Nuland, N. A., Bonvin, A. M., Guerrini, R., Tancredi, T., Temussi, P. A., and Picone, D. (2006) The α-to-β Conformational Transition of Alzheimer's Aβ-(1–42) Peptide in Aqueous Media is Reversible: A Step by Step Conformational Analysis Suggests the Location of β Conformation Seeding, *ChemBioChem 7*, 257-267.

[26] Luttmann, E., and Fels, G. (2006) All-atom molecular dynamics studies of the full-length β-amyloid peptides, *Chemical physics 323*, 138-147.

[27] Agrawal, N., and Skelton, A. A. (2017) Binding of 12-crown-4 with Alzheimer's Aβ40 and Aβ42 monomers and its effect on their conformation: insight from molecular dynamics simulations, *Molecular pharmaceutics* 15, 289-299.

[28] Valerio, M., Colosimo, A., Conti, F., Giuliani, A., Grottesi, A., Manetti, C., and Zbilut, J. P. (2005) Early events in protein aggregation: molecular flexibility and hydrophobicity/charge

interaction in amyloid peptides as studied by molecular dynamics simulations, *Proteins: Structure, Function, and Bioinformatics 58*, 110-118.

[29] Miyashita, N., Straub, J. E., and Thirumalai, D. (2009) Structures of β-Amyloid Peptide 1− 40, 1− 42, and 1− 55□ the 672− 726 Fragment of APP□ in a Membrane Environment with Implications for Interactions with γ-Secretase, *Journal of the American Chemical Society 131*, 17843-17852.

[30] Roychaudhuri, R., Yang, M., Hoshi, M. M., and Teplow, D. B. (2009) Amyloid β-protein assembly and Alzheimer disease, *Journal of Biological Chemistry 284*, 4749-4753.

[31] Morris, K. L., and Serpell, L. C. (2012) X-ray fibre diffraction studies of amyloid fibrils, *Amyloid Proteins: Methods and Protocols*, 121-135.

[32] Scheidt, H. A., Morgado, I., Rothemund, S., and Huster, D. (2012) Dynamics of amyloid β fibrils revealed by solid-state NMR, *Journal of Biological Chemistry 287*, 2017-2021.

[33] Anderson, V. L., and Webb, W. W. (2011) Transmission electron microscopy characterization of fluorescently labelled amyloid β 1-40 and α-synuclein aggregates, *BMC biotechnology 11*, 125.

[34] Schmidt, M., Rohou, A., Lasker, K., Yadav, J. K., Schiene-Fischer, C., Fändrich, M., and Grigorieff, N. (2015) Peptide dimer structure in an Aβ (1–42) fibril visualized with cryo-EM, *Proceedings of the National Academy of Sciences 112*, 11858-11863.

[35] Parbhu, A., Lin, H., Thimm, J., and Lal, R. (2002) Imaging real-time aggregation of amyloid beta protein (1–42) by atomic force microscopy, *Peptides 23*, 1265-1270.

[36] Buchete, N.-V., and Hummer, G. (2007) Structure and dynamics of parallel β-sheets, hydrophobic core, and loops in Alzheimer's Aβ fibrils, *Biophysical journal 92*, 3032-3039.

[37] Inouye, H., Fraser, P. E., and Kirschner, D. A. (1993) Structure of beta-crystallite assemblies formed by Alzheimer beta-amyloid protein analogues: analysis by x-ray diffraction, *Biophysical journal 64*, 502-519.

[38] Sunde, M., Serpell, L. C., Bartlam, M., Fraser, P. E., Pepys, M. B., and Blake, C. C. (1997) Common core structure of amyloid fibrils by synchrotron X-ray diffraction, *Journal of molecular biology 273*, 729-739.

[39] Kirschner, D. A., Abraham, C., and Selkoe, D. J. (1986) X-ray diffraction from intraneuronal paired helical filaments and extraneuronal amyloid fibers in Alzheimer disease indicates cross-beta conformation, *Proceedings of the National Academy of Sciences 83*, 503-507.

[40] Nilsson, M. R. (2004) Techniques to study amyloid fibril formation in vitro, *Methods 34*, 151-160.

[41] Nasica-Labouze, J., Nguyen, P. H., Sterpone, F., Berthoumieu, O., Buchete, N.-V., Coté, S. b., De Simone, A., Doig, A. J., Faller, P., and Garcia, A. (2015) Amyloid β protein and Alzheimer's disease: When computer simulations complement experimental studies, *Chemical reviews 115*, 3518-3563.

[42] Paravastu, A. K., Leapman, R. D., Yau, W.-M., and Tycko, R. (2008) Molecular structural basis for polymorphism in Alzheimer's β-amyloid fibrils, *Proceedings of the National Academy of Sciences 105*, 18349-18354.

[43] Petkova, A. T., Ishii, Y., Balbach, J. J., Antzutkin, O. N., Leapman, R. D., Delaglio, F., and Tycko, R. (2002) A structural model for Alzheimer's β-amyloid fibrils based on experimental constraints from solid state NMR, *Proceedings of the National Academy of Sciences 99*, 16742-16747.

[44] Riek, R., and Eisenberg, D. S. (2016) The activities of amyloids from a structural perspective, *Nature 539*, 227-235.

[45] Agrawal, N., and Skelton, A. A. (2016) 12-Crown-4 Ether Disrupts the Patient Brain-Derived Amyloid-β-Fibril Trimer: Insight from All-Atom Molecular Dynamics Simulations, *ACS chemical neuroscience 7*, 1433-1441.

[46] Xiao, Y., Ma, B., McElheny, D., Parthasarathy, S., Long, F., Hoshi, M., Nussinov, R., and Ishii, Y. (2015) A [beta](1-42) fibril structure illuminates self-recognition and replication of amyloid in Alzheimer's disease, *Nature structural & molecular biology 22*, 499-505.

[47] Colvin, M. T., Silvers, R., Ni, Q. Z., Can, T. V., Sergeyev, I., Rosay, M., Donovan, K. J., Michael, B., Wall, J., and Linse, S. (2016) Atomic resolution structure of monomorphic Aβ42 amyloid fibrils, *Journal of the American Chemical Society 138*, 9663-9674.

[48] Wälti, M. A., Ravotti, F., Arai, H., Glabe, C. G., Wall, J. S., Böckmann, A., Güntert, P., Meier, B. H., and Riek, R. (2016) Atomic-resolution structure of a disease-relevant Aβ (1–42) amyloid fibril, *Proceedings of the National Academy of Sciences 113*, E4976-E4984.

[49] Rodriguez, R. A., Chen, L. Y., Plascencia-Villa, G., and Perry, G. (2017) Elongation affinity, activation barrier, and stability of Aβ42 oligomers/fibrils in physiological saline, *Biochemical and biophysical research communications 487*, 444-449.

[50] Gremer, L., Schölzel, D., Schenk, C., Reinartz, E., Labahn, J., Ravelli, R. B., Tusche, M., Lopez-Iglesias, C., Hoyer, W., and Heise, H. (2017) Fibril structure of amyloid-β (1–42) by cryo–electron microscopy, *Science 358*, 116-119.

[51] Watanabe-Nakayama, T., Ono, K., Itami, M., Takahashi, R., Teplow, D. B., and Yamada, M. (2016) High-speed atomic force microscopy reveals structural dynamics of amyloid β1–42 aggregates, *Proceedings of the National Academy of Sciences 113*, 5835-5840.

[52] Hayden, E. Y., and Teplow, D. B. (2013) Biophysical Characterization of AB Assembly, *Alzheimer's Disease: Insights Into Low Molecular Weight and Cytotoxic Aggregates from in Vitro and Computer Experiments: Molecular Basis of Amyloid-beta Protein Aggregation and Fibril Formation 7*, 83.

[53] Masman, M. F., Eisel, U. L., Csizmadia, I. G., Penke, B., Enriz, R. D., Marrink, S. J., and Luiten, P. G. (2009) In silico study of full-length amyloid β 1− 42 tri-and penta-oligomers in solution, *The Journal of Physical Chemistry B 113*, 11710-11719.

[54] Lemkul, J. A., and Bevan, D. R. (2010) Assessing the stability of Alzheimer's amyloid protofibrils using molecular dynamics, *The Journal of Physical Chemistry B 114*, 1652-1660.

[55] Lührs, T., Ritter, C., Adrian, M., Riek-Loher, D., Bohrmann, B., Döbeli, H., Schubert, D., and Riek, R. (2005) 3D structure of Alzheimer's amyloid-β (1–42) fibrils, *Proceedings of the National Academy of Sciences of the United States of America 102*, 17342-17347.

[56] Xu, Z., Paparcone, R., and Buehler, M. J. (2010) Alzheimer's Aβ (1-40) Amyloid Fibrils Feature Size-Dependent Mechanical Properties, *Biophysical journal 98*, 2053-2062.

[57] Wu, C., Bowers, M. T., and Shea, J.-E. (2010) Molecular structures of quiescently grown and brain-derived polymorphic fibrils of the Alzheimer amyloid Aβ9-40 peptide: a comparison to agitated fibrils, *PLoS computational biology 6*, e1000693.

[58] Xi, W., Wang, W., Abbott, G., and Hansmann, U. H. (2016) Stability of a Recently Found Triple-β-Stranded Aβ1–42 Fibril Motif, *The Journal of Physical Chemistry B 120*, 4548-4557.

[59] Miller, Y., Ma, B., and Nussinov, R. (2011) The unique Alzheimer's β-amyloid triangular fibril has a cavity along the fibril axis under physiological conditions, *Journal of the American Chemical Society 133*, 2742-2748.

[60] Dong, M., Paul, T. J., Hoffmann, Z., Chan, K., Hu, D., Ai, H., and Prabhakar, R. (2016) Structural and Material Properties of Amyloid Aβ40/42 Fibrils, *ChemPhysChem 17*, 2558-2566.

[61] Lu, J.-X., Qiang, W., Yau, W.-M., Schwieters, C. D., Meredith, S. C., and Tycko, R. (2013) Molecular structure of β-amyloid fibrils in Alzheimer's disease brain tissue, *Cell 154*, 1257-1268.

[62] Tycko, R. (2014) Physical and structural basis for polymorphism in amyloid fibrils, *Protein Science 23*, 1528-1539.

[63] Elkins, M. R., Wang, T., Nick, M., Jo, H., Lemmin, T., Prusiner, S. B., DeGrado, W. F., Stohr, J., and Hong, M. (2016) Structural polymorphism of Alzheimer's β-amyloid fibrils as controlled by an E22 Switch: a solid-state NMR study, *Journal of the American Chemical Society 138*, 9840-9852.

[64] Colletier, J.-P., Laganowsky, A., Landau, M., Zhao, M., Soriaga, A. B., Goldschmidt, L., Flot, D., Cascio, D., Sawaya, M. R., and Eisenberg, D. (2011) Molecular basis for amyloid-β polymorphism, *Proceedings of the National Academy of Sciences 108*, 16938-16943.

[65] Young, L. J., Schierle, G. S. K., and Kaminski, C. F. (2017) Imaging Aβ (1–42) fibril elongation reveals strongly polarised growth and growth incompetent states, *Physical Chemistry Chemical Physics 19*, 27987-27996.

[66] Esler, W. P., Stimson, E. R., Jennings, J. M., Vinters, H. V., Ghilardi, J. R., Lee, J. P., Mantyh, P. W., and Maggio, J. E. (2000) Alzheimer's disease amyloid propagation by a template-dependent dock-lock mechanism, *Biochemistry 39*, 6288-6295.

[67] Schwierz, N., Frost, C. V., Geissler, P. L., and Zacharias, M. (2016) Dynamics of Seeded Aβ40-Fibril Growth from Atomistic Molecular Dynamics Simulations: Kinetic Trapping and Reduced Water Mobility in the Locking Step, *Journal of the American Chemical Society 138*, 527-539.

[68] Bacci, M., Vymětal, J. í., Mihajlovic, M., Caflisch, A., and Vitalis, A. (2017) Amyloid β Fibril Elongation by Monomers Involves Disorder at the Tip, *Journal of chemical theory and computation 13*, 5117-5130.

[69] Williams, T. L., and Serpell, L. C. (2011) Membrane and surface interactions of Alzheimer's Aβ peptide–insights into the mechanism of cytotoxicity, *The FEBS journal 278*, 3905-3917.

[70] Kremer, J. J., Pallitto, M. M., Sklansky, D. J., and Murphy, R. M. (2000) Correlation of β-amyloid aggregate size and hydrophobicity with decreased bilayer fluidity of model membranes, *Biochemistry 39*, 10309-10318.

[71] Lindberg, D. J., Wesén, E., Björkeroth, J., Rocha, S., and Esbjörner, E. K. (2017) Lipid membranes catalyse the fibril formation of the amyloid-β (1–42) peptide through lipid-fibril interactions that reinforce secondary pathways, *Biochimica et Biophysica Acta (BBA)-Biomembranes*.

[72] Xiang, N., Lyu, Y., Zhu, X., and Narsimhan, G. (2018) Investigation of the interaction of amyloid β peptide (11–42) oligomers with a 1-palmitoyl-2-oleoyl-sn-glycero-3-phosphocholine (POPC) membrane using molecular dynamics simulation, *Physical Chemistry Chemical Physics*.

[73] Di Scala, C., Yahi, N., Boutemeur, S., Flores, A., Rodriguez, L., Chahinian, H., and Fantini, J. (2016) Common molecular mechanism of amyloid pore formation by Alzheimer's β-amyloid peptide and α-synuclein, *Scientific reports 6*, 28781.

[74] Martins, I. C., Kuperstein, I., Wilkinson, H., Maes, E., Vanbrabant, M., Jonckheere, W., Van Gelder, P., Hartmann, D., D'Hooge, R., and De Strooper, B. (2008) Lipids revert inert Aβ amyloid fibrils to neurotoxic protofibrils that affect learning in mice, *The EMBO journal 27*, 224-233.

[75] Stroud, J. C., Liu, C., Teng, P. K., and Eisenberg, D. (2012) Toxic fibrillar oligomers of amyloid-β have cross-β structure, *Proceedings of the National Academy of Sciences 109*, 7717-7722.

[76] Zhang-Haagen, B., Biehl, R., Nagel-Steger, L., Radulescu, A., Richter, D., and Willbold, D. (2016) Monomeric amyloid beta peptide in hexafluoroisopropanol detected by small angle neutron scattering, *PloS one 11*, e0150267.

[77] Larson, M. E., and Lesné, S. E. (2012) Soluble Aβ oligomer production and toxicity, *Journal of neurochemistry 120*, 125-139.

[78] Benilova, I., Karran, E., and De Strooper, B. (2012) The toxic A [beta] oligomer and Alzheimer's disease: an emperor in need of clothes, *Nature neuroscience 15*, 349-357.

[79] Wyss-Coray, T., and Rogers, J. (2012) Inflammation in Alzheimer disease—a brief review of the basic science and clinical literature, *Cold Spring Harbor perspectives in medicine 2*, a006346.

[80] Ghosh, A., Pradhan, N., Bera, S., Datta, A., Krishnamoorthy, J., Jana, N. R., and Bhunia, A. (2017) Inhibition and Degradation of Amyloid Beta (Aβ40) Fibrillation by Designed Small Peptide: A Combined Spectroscopy, Microscopy, and Cell Toxicity Study, *ACS chemical neuroscience 8*, 718-722.

[81] Caltagirone, C., Ferrannini, L., Marchionni, N., Nappi, G., Scapagnini, G., and Trabucchi, M. (2012) The potential protective effect of tramiprosate (homotaurine) against Alzheimer's disease: a review, *Aging clinical and experimental research 24*, 580-587.

[82] Wood, S., and Vargas, G. (2015) Translational Approaches in Alzheimer's Disease, *Translational Medicine: Tools And Techniques*, 157.

[83] Martineau, E., De Guzman, J. M., Rodionova, L., Kong, X., Mayer, P. M., and Aman, A. M. (2010) Investigation of the noncovalent interactions between anti-amyloid agents and amyloid β peptides by ESI-MS, *Journal of the American Society for Mass Spectrometry 21*, 1506-1514.

[84] Gervais, F., Paquette, J., Morissette, C., Krzywkowski, P., Yu, M., Azzi, M., Lacombe, D., Kong, X., Aman, A., and Laurin, J. (2007) Targeting soluble Aβ peptide with Tramiprosate for the treatment of brain amyloidosis, *Neurobiology of aging 28*, 537-547.

[85] Watson, R. R. (2015) *Foods and Dietary Supplements in the Prevention and Treatment of Disease in Older Adults*, Academic Press.

[86] Crespi, G. A., Hermans, S. J., Parker, M. W., and Miles, L. A. (2015) Molecular basis for mid-region amyloid-β capture by leading Alzheimer's disease immunotherapies, *Scientific reports 5*, 9649.

[87] Siemers, E. R., Friedrich, S., Dean, R. A., Gonzales, C. R., Farlow, M. R., Paul, S. M., and DeMattos, R. B. (2010) Safety and changes in plasma and cerebrospinal fluid amyloid β after a single administration of an amyloid β monoclonal antibody in subjects with Alzheimer disease, *Clinical neuropharmacology 33*, 67-73.

[88] Farlow, M., Arnold, S. E., Van Dyck, C. H., Aisen, P. S., Snider, B. J., Porsteinsson, A. P., Friedrich, S., Dean, R. A., Gonzales, C., and Sethuraman, G. (2012) Safety and biomarker effects of solanezumab in patients with Alzheimer's disease, *Alzheimer's & Dementia 8*, 261-271.

[89] Sacks, C. A., Avorn, J., and Kesselheim, A. S. (2017) The Failure of Solanezumab-How the Fda Saved Taxpayers Billions, *The New England journal of medicine 376*, 1706-1708.

[90] Feinberg, H., Saldanha, J. W., Diep, L., Goel, A., Widom, A., Veldman, G. M., Weis, W. I., Schenk, D., and Basi, G. S. (2014) Crystal structure reveals conservation of amyloid-β conformation recognized by 3D6 following humanization to bapineuzumab, *Alzheimer's research & therapy 6*, 31.

[91] Miles, L. A., Crespi, G. A., Doughty, L., and Parker, M. W. (2013) Bapineuzumab captures the N-terminus of the Alzheimer's disease amyloid-beta peptide in a helical conformation, *Scientific reports 3*, 1302.

[92] Vandenberghe, R.; Rinne, J. O.; Boada, M.; Katayama, S.; Scheltens, P.; Vellas, B.; Tuchman, M.; Gass, A.; Fiebach, J. B.; Hill, D., Bapineuzumab for mild to moderate Alzheimer's disease in two global, randomized, phase 3 trials. *Alzheimer's research & therapy* **2016,** *8* (1), 18.

[93] Fagan, T. (2012) Bapineuzumab phase 3: target engagement, but no benefit, In *Alzheimer Research Forum online http://www. alzforum. org/new/detail. asp*.

[94] Tian, Y., Zhang, X., Li, Y., Shoup, T. M., Teng, X., Elmaleh, D. R., Moore, A., and Ran, C. (2014) Crown ethers attenuate aggregation of amyloid beta of Alzheimer's disease, *Chemical Communications 50*, 15792-15795.

[95] Pedersen, C. J. (1967) Cyclic polyethers and their complexes with metal salts, *Journal of the American Chemical Society 89*, 7017-7036.

[96] Pedersen, C. J. (1972) Macrocyclic Polyethers: Dibenzo-18-crown-6 Polyether and Dicyclohexyl-18-crown-6 Polyether, *Organic Syntheses*, 66-66.

[97] Li, J., Yim, D., Jang, W.-D., and Yoon, J. (2017) Recent progress in the design and applications of fluorescence probes containing crown ethers, *Chemical Society Reviews 46*, 2437-2458.

[98] Gokel, G. W., Leevy, W. M., and Weber, M. E. (2004) Crown ethers: sensors for ions and molecular scaffolds for materials and biological models, *Chemical reviews 104*, 2723-2750.

[99] Skelton, A., Agrawal, N., and Fried, J. (2015) Quantum mechanical calculations of the interactions between diazacrowns and the sodium cation: an insight into Na+ complexation in diazacrown-based synthetic ion channels, *RSC Advances 5*, 55033-55047.

[100] Cazacu, A., Tong, C., van der Lee, A., Fyles, T. M., and Barboiu, M. (2006) Columnar self-assembled ureido crown ethers: an example of ion-channel organization in lipid bilayers, *Journal of the American Chemical Society 128*, 9541-9548.

[101] Morrison, P. W., Porfiryeva, N. N., Chahal, S., Salakhov, I. A., Lacourt, C., Semina, I. I., Moustafine, R. I., and Khutoryanskiy, V. V. (2017) Crown Ethers: novel permeability enhancers for ocular drug delivery?, *Molecular Pharmaceutics 14*, 3528-3538.

[102] Lee, C. C., Maestre-Reyna, M., Hsu, K. C., Wang, H. C., Liu, C. I., Jeng, W. Y., Lin, L. L., Wood, R., Chou, C. C., and Yang, J. M. (2014) Crowning proteins: modulating the protein surface properties using crown ethers, *Angewandte Chemie International Edition 53*, 13054-13058.

[103] Banik, D., Dutta, R., Banerjee, P., Kundu, S., and Sarkar, N. (2016) Inhibition of Fibrillar Assemblies of l-Phenylalanine by Crown Ethers: A Potential Approach toward Phenylketonuria, *The Journal of Physical Chemistry B 120*, 7662-7670.

[104] Angelini, G., Pisani, M., Mobbili, G., Marini, M., and Gasbarri, C. (2013) Neutral liposomes containing crown ether-lipids as potential DNA vectors, *Biochimica et Biophysica Acta (BBA)-Biomembranes 1828*, 2506-2512.

[105] "About Us". Beta Pharma. Retrieved 31 October 2017.

CHAPTER 2

2. Molecular Dynamics Simulations

"If we were to name the most powerful assumption of all, which leads one on and on in an attempt to understand life, it is that all things are made of atoms, and that everything that living things do can be understood in terms of the jigglings and wigglings of atoms".

-----Richard Feynman, recipient of the 1965 Nobel Prize in Physics

2.1 Introduction

The MD simulations were originated within the theoretical physics community during the 1950's; the earliest reported simulation was performed by Alder and Wainwright in 1957[1]. The first protein simulation was performed in 1976[2, 3] and now, MD simulations are routinely used in the field of biophysics[4], pharmaceutical chemistry[5] and material sciences[6]. MD simulations have been very successful in studying the protein folding/misfolding[7, 8] protein dynamics[9], protein-ligand binding and impact of the ligand on protein dynamics[10]. MD techniques are also widely used in the refinement of structures determined by X-ray crystallography[11], NMR[12], and Cryo-EM[13]. There are various dynamics processes that take place in proteins, which could range from femtoseconds to hours[14, 15] and depending on the process needed to be studied, different level of approximation can employed. Figure: 2.1 shows time dependent events in protein dynamics.

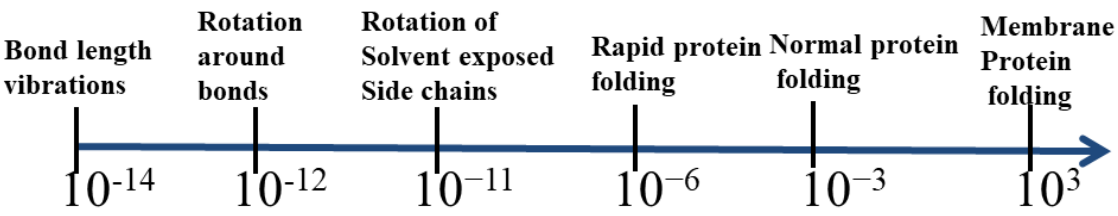

Figure: 2.1 Shows the time-dependent in protein dynamics.

2.2 Theory

MD simulation is a computational technique used to understand the time-dependent behaviour of biomolecules, their kinetics and thermodynamics. MD simulation is based on Newton's second law of motion; where the forces are obtained as gradients of the potential energy. Integration of the equation of motion produces a trajectory containing positions, velocity and accelerations of atoms along the time. Enhancement of computational hardware and algorithms has helped researchers to simulate solvated protein systems at microsecond timescale.

Newton's equation of motion is given by

$$F_i = m_i\, a_i \tag{2.1}$$

Where F_i is the force exerted on particle i, m_i is the mass of particle i and a_i is the acceleration of particle i.

$$\frac{d^2 r_i}{dt^2} = \frac{F_i}{m_i} \tag{2.2}$$

$$\frac{dr_i}{dt^2} = a_i \tag{2.3}$$

$$\frac{dv_i}{dt} = \frac{F_i}{m_i} \tag{2.4}$$

Force is the derivative of potential with respect to position that can be calculated analytically. We then need to integrate the force to obtain the velocities and the positions in the next time step. Various algorithms are available for integrating the equations of motion. Many of these are finite difference methods in which the integration is partitioned into small steps, each separated in time by a specific period Δt because the continuous potentials describing atomic interaction preclude an analytical solution[14].

2.2.1 Verlet algorithm

Verlet integration is a numerical method used to integrate Newton's equations of motion. It is frequently used to calculate trajectories of particles in molecular dynamics simulation.

$$r(t+\delta t) = r(t) + v(t)\delta t + \frac{1}{2}a(t)\delta t^2 \tag{2.5}$$

Where, **r** is positions of atoms**, t** is time, **v** is velocities of atoms and **a** is accelerations of atoms.

$$r(t-\delta t) = r(t) - v(t)\delta t + \frac{1}{2}a(t)\delta t^2 \tag{2.6}$$

The addition of the above two equations, produces:

$$r(t+\delta t) = 2r(t) - r(t-\delta t)\delta t + a(t)\delta t^2 \tag{2.7}$$

2.2.2 Velocity Verlet algorithm

This algorithm generates positions, velocities and accelerations at time t. There is no compromise on precision.

$$r(t+\delta t) = r(t) + v(t)\delta t + \frac{1}{2}a(t)\delta t^2 \qquad (2.8)$$

$$v(t+\delta t) = v(t) + \frac{1}{2}\,[a(t) + a(t+\delta t)]\,\delta t \qquad (2.9)$$

2.2.3 Leapfrog algorithm

The leapfrog algorithm uses the positions at time *t* and the velocities at time $t - (\Delta t/2)$ for the update of both positions and velocities.

$$r(t+\Delta t) = r(t) + v\,(t + \tfrac{1}{2}\,\Delta t)\Delta t \qquad (2.10)$$

$$v\,(t + \tfrac{1}{2}\,\Delta t) = v\,(t - \tfrac{1}{2}\,\Delta t) + a(t)\Delta t \qquad (2.11)$$

Velocities at time t can be approximated by the following expression:

$$v\,(t) = \frac{1}{2}\left[v\left(t - \frac{1}{2}\Delta t\right) + v\left(t + \frac{1}{2}\Delta t\right)\right] \qquad (2.12)$$

2.3 Force fields

The term "force field" refers to the mathematical expression and associated parameters that describe the energy of the system as a function of its atomic coordinates[16, 17]

$$V(r) = \overbrace{\underbrace{\frac{1}{2}\sum k_b\,(b - b_0)^2}_{\text{bonds}} + \underbrace{\frac{1}{2}\sum k_\theta\,(\theta - b_\theta)^2}_{\text{angles}} + \underbrace{\frac{1}{2}\sum k_\emptyset\left(1 + cos(n\emptyset - \delta)\right)^2}_{\text{dihedrals}} +}^{\text{Bonded}} \overbrace{\sum\left[\frac{A}{r^{12}} - \frac{C}{r^6} + \frac{q_1\,q_2}{\epsilon_r}\right]}^{\text{Non-bonded}} \qquad (2.13)$$

Bonded forces emerge through bonds and angles are modeled using simple virtual springs, and dihedral angles are modeled using a sinusoidal function that approximates the energy differences between eclipsed and staggered conformations. Non-bonded forces emerge due to van der Waals interactions, modeled using the Lennard-Jones 6-12 potential and charged (electrostatic) interactions, modeled using Coulomb's law[18].

2.4 Type of force field

There are three types of force fields:

2.4.1) All atoms: parameters provided for every single atom within the system,e.g., OPLS-AA[19], AMBER[20] and CHARMM[21].

2.4.2) United atoms: parameters provided for all atoms except non-polar hydrogen, e.g., GROMOS[22].

2.4.3) Coarse grained: an abstract representation of molecules by grouping several atoms into "super-atoms."e.g. ,MARTINI[23] .

2.5 Ensembles: An ensemble is a collection of all possible systems that have differing microscopic states but belong to a single macroscopic or thermodynamic state. Various different formal ensembles with differing characteristics exist. The most widely simulated are as follows:

2.5.1 The canonical ensemble (NVT): This is the collection of all systems whose thermodynamic state is characterized by a fixed number of atoms, *N*, fixed volume, *V*, and fixed temperature, *T*.

2.5.2 The isobaric-isothermal ensemble (NPT): An ensemble with a fixed number of atoms, *N*, fixed pressure, *P*, and fixed temperature, *T*.

2.6 References:

[1] Alder, B., and Wainwright, T. (1957) Phase transition for a hard sphere system, *The Journal of chemical physics 27*, 1208-1209.

[2] McCammon, J. (1976) Molecular dynamics study of the bovine pancreatic trypsin inhibitor, *Models for Protein Dynamics*, 137.

[3] McCammon, J. A., Gelin, B. R., and Karplus, M. (1977) Dynamics of folded proteins, *Nature 267*, 585-590.

[4] Klepeis, J. L., Lindorff-Larsen, K., Dror, R. O., and Shaw, D. E. (2009) Long-timescale molecular dynamics simulations of protein structure and function, *Current opinion in structural biology 19*, 120-127.

[5] De Vivo, M., Masetti, M., Bottegoni, G., and Cavalli, A. (2016) Role of molecular dynamics and related methods in drug discovery, *Journal of medicinal chemistry 59*, 4035-4061.

[6] Rickman, J., and LeSar, R. (2002) Free-energy calculations in materials research, *Annual Review of Materials Research 32*, 195-217.

[7] Freddolino, P. L., Harrison, C. B., Liu, Y., and Schulten, K. (2010) Challenges in protein-folding simulations, *Nature physics 6*, 751-758.

[8] Naeem, A., Khan, T., and Fazili, N. (2015) Protein Folding and Misfolding: A Perspective from Theory, *Journal of Glycomics & Lipidomics 5*, 1.

[9] Salsbury, F. R. (2010) Molecular dynamics simulations of protein dynamics and their relevance to drug discovery, *Current opinion in pharmacology 10*, 738-744.

[10] Dutta Dubey, K., Kumar Tiwari, R., and Prasad Ojha, R. (2013) Recent Advances in Protein−Ligand Interactions: Molecular Dynamics Simulations and Binding Free Energy, *Current computer-aided drug design 9*, 518-531.

[11] Kohn, J. E., Afonine, P. V., Ruscio, J. Z., Adams, P. D., and Head-Gordon, T. (2010) Evidence of functional protein dynamics from X-ray crystallographic ensembles, *PLoS computational biology 6*, e1000911.

[12] Fisette, O., Lagüe, P., Gagné, S., and Morin, S. (2012) Synergistic applications of MD and NMR for the study of biological systems, *BioMed Research International 2012*.

[13] Chan, K. Y., Trabuco, L. G., Schreiner, E., and Schulten, K. (2012) Cryo-Electron Microscopy Modeling by the Molecular Dynamics Flexible Fitting Method, *Biopolymers 97*, 678-686.

[14] Adcock, S. A., and McCammon, J. A. (2006) Molecular dynamics: survey of methods for simulating the activity of proteins, *Chemical reviews 106*, 1589-1615.

[15] Lindahl, E. R. (2008) Molecular dynamics simulations, *Molecular modeling of proteins*, 3-23.

[16] González, M. (2011) Force fields and molecular dynamics simulations, *École thématique de la Société Française de la Neutronique 12*, 169-200.

[17] Guvench, O., and MacKerell, A. D. (2008) Comparison of protein force fields for molecular dynamics simulations, *Molecular modeling of proteins*, 63-88.

[18] Durrant, J. D., and McCammon, J. A. (2011) Molecular dynamics simulations and drug discovery, *BMC biology 9*, 71.

[19] Jorgensen, W. L., Maxwell, D. S., and Tirado-Rives, J. (1996) Development and testing of the OPLS all-atom force field on conformational energetics and properties of organic liquids, *J. Am. Chem. Soc 118*, 11225-11236.

[20] Duan, Y., Wu, C., Chowdhury, S., Lee, M. C., Xiong, G., Zhang, W., Yang, R., Cieplak, P., Luo, R., and Lee, T. (2003) A point-charge force field for molecular mechanics simulations of proteins based on condensed-phase quantum mechanical calculations, *Journal of computational chemistry 24*, 1999-2012.

[21] Huang, J., and MacKerell, A. D. (2013) CHARMM36 all-atom additive protein force field: Validation based on comparison to NMR data, *Journal of computational chemistry 34*, 2135-2145.

[22] Schmid, N., Eichenberger, A. P., Choutko, A., Riniker, S., Winger, M., Mark, A. E., and van Gunsteren, W. F. (2011) Definition and testing of the GROMOS force-field versions 54A7 and 54B7, *European biophysics journal 40*, 843.

[23] Marrink, S. J., Risselada, H. J., Yefimov, S., Tieleman, D. P., and De Vries, A. H. (2007) The MARTINI force field: coarse grained model for biomolecular simulations, *The journal of physical chemistry B 111*, 7812-7824.

CHAPTER 3

Published Article

Binding of 12-crown-4 with Alzheimer's Aβ40 and Aβ42 monomers and its effect on their conformation: insight from molecular dynamics simulations

Nikhil Agrawal[1]*, Adam A. Skelton[1]*

[1]College of Health Sciences, Discipline of Pharmaceutical Sciences, University of KwaZulu-Natal, South Africa

*corresponding authors: nikhil.08oct@gmail.com, skelton@ukzn.ac.za

3.1 Abstract

Alzheimer's disease is the most common form of dementia and is considered to be caused by the conformational change of Aβ monomers, from their native monomeric states, to form Aβ oligomers/aggregates in the brain. Turn formation in Aβ monomer has been suggested to be the nucleation step for Aβ misfolding. In the present work, we have performed a series of all-atom molecular dynamics simulations, a total time of 11.4 μs, to elucidate factor that contributes for early stage misfolding of Aβ40 and Aβ42 monomers and reveals the binding modes of 12-crown-4 on Aβ40 and Aβ42 monomer and effect of its binding on structural stability. Our simulation data revealed that the region around Val24-Lys28 is most prevalent for turn formation and a gain of water molecules around Lys28 sidechains occurs at the same time as a significant gain in conformational entropy of the sidechain. The initiation steps lead a greater number of water molecules available and enhancement of the conformational entropy of the backbone atoms; this leads to greater probability of breaking Lys28 backbone intra-peptide H-bonds, and consequently turns formation.

Simulations of Aβ40 and Aβ42 monomers with 12-crown-4 showed that the molecule is highly specific towards positively charged Lys16, Lys28 residues, and N-terminal Asp1. Lys16 and Asp1 have been previously reported to make Aβ peptide toxic. Our secondary structure analysis revealed that in the absence of 12-crown-4 there was a β-sheet formed in the Aβ40 peptide. In case of Aβ42 monomer, in the absence of 12-crown-4, we observed that the second helix region converted into a coil and turn; however, in the presence of 12-crown-4 it remained stable.

Observed pharmacophore features of, 12-crown-4 will not only help in designing new candidate drug molecules, which are specific to Aβ peptides but could also be used to design new imaging probe molecules, which could be used for labeling Aβ peptide

Keywords: Alzheimer, Amyloid βeta, crown ethers, MD simulations

3.2 Introduction:

Alzheimer's disease (AD) is the most prevalent form of neurodegenerative disease, affecting around 40 million people worldwide[1,2]. Since its first description by a psychiatrist and neuropathologist Alois Alzheimer, in 1907, there is still no known cure for this illness, majorly due to lack of complete understanding of the disease etiology[3, 4, 5]. The most widely accepted amyloid cascade hypothesis suggests that Amyloid-β (Aβ) peptide misfolding and aggregation is the principal culprit for AD[6]. The Aβ peptide is produced from the amyloid precursor protein (APP) by the proteolytic activities of β and γ-secretase. Since γ-secretase is unable to cleave Aβ peptide precisely, this results in a variable length of Aβ peptides; the most common isoforms being Aβ40 and Aβ42[7].

NMR and MD simulations studies have suggested that Aβ monomer misfolding is nucleated by the formation of a turn around Val24-Lys28 and these studies have further highlighted various important factors that contribute to the turn formation and stabilization of misfolded Aβ monomer; these factors are 1) The intrinsic, conformational properties of the Val-Gly-Ser-Asn and Gly-Ser-Asn-Lys sequences to form the turn[8]. 2) The long range electrostatic interactions between Lys28 and Glu22 or Asp23[9, 10]. 3) Hydrophobic interactions between Val24 and Lys28 sidechains [8, 9, 11, 12] 4) Hydrogen bond formation between the negatively charged Asp23 side chain with the backbone atoms of the turn region residues, Gly25, Ser26, Asn27, and Lys28[9].

Various MD simulation studies of Aβ peptide, in an explicit water environment, have suggested the importance of the displacement of water molecules around the hydrophobic and hydrophilic region in Aβ misfolding and aggregation. Khatua *et. al.*[13] revealed that water molecules around the hydrophobic region are relatively weakly bound and expected to be easily displaced during the hydrophobic collapse. In another study Melquiond *et.al.*[14] it was revealed that water molecule expulsion took place in the hydrophilic region between residue 22 and residue 28 to form the aggregates/fibrils. Tarus *et. al.*[12] revealed that an early event in the oligomerization process is the expulsion of water molecules that facilitate the turn formation around residues 24-27. It has been suggested that intra-peptide H-Bonds play a key role in stabilizing the folded forms of proteins and H-bond cooperativity plays an important role in stabilization of a α-helix[15,16]. It is widely appreciated that hydrated water molecules, around proteins, form H-bond networks and play a crucial role in dynamics and stabilization of protein structure[17]. The presence of hydrated water molecules around the backbone causes lengthening of intra-peptide H-bonds within the backbone, thus loosening the structure[18].

To investigate the inhibition of the Aβ peptide misfolding and aggregation by a candidate drug molecule, several studies have been performed. Hernández-Rodríguez *et. al.*[19] performed an *in-silico* and *in-vitro* study of galanthamine with Aβ42 their results revealed that galanthamine binds with Lys28, which helped the Aβ42 monomer to remain in an unfolded conformation . Sinha *et. al.*[20],

by a mass spectrometry and solution-state NMR study, revealed that a "molecular tweezer", CLR01, specifically binds with Lys16 and Lys28 at the monomer stage which resulted in the formation of nontoxic structures of Aβ. Sinha *et. al.*[21] revealed, by a mutational study, that substitution of Lys16 for Ala significantly reduced Aβ toxicity. All these studies have highlighted the importance of Lys16 and Lys28 in the conversion of Aβ monomers to Aβ aggregates/fibrils and their toxicity.

The Conformational entropy of proteins is a proxy measure of its conformational dynamics, which is directly related to a number of conformation obtained by it[22,23]. It has been suggested that loss of backbone and sidechain conformational entropy plays an important role in protein stability[23, 24]. Conformational entropy significantly contributes to binding affinity and specific association between a protein and its ligand[25] and it has been revealed that binding of a ligand with a protein leads to the loss of conformation entropy of both ligand and protein binding residue[26,27]. A candidate molecule that can bind strongly to key residues should be able to counteract conformational entropy losses upon binding, and, therefore, could play an important role in the stability of the protein.

Crown ethers are small cyclic polyethers, first discovered by Nobel Prize winner Charles Pedersen more than 50 years ago. Due to their strong binding affinities to various metal ions and primary amines, members of the crown ether family have been widely applied in biological chemistry and probe chemistry [28, 29,30,31]. Oukhatar *et. al.*[32] used crown ethers to design molecular magnetic resonance imaging (MRI) sensing probe for neurotransmitters. Gawley *et. al.*[33] used crown ethers to design visible fluorescence chemosensors for Saxitoxin (a potent neurotoxin). In another study, Işık *et .al.*[34] used crown ethers to design an intracellular fluorescent probe for Glutathione (GSH), that worked satisfactorily inside the human breast adenocarcinoma cells, and highlighted GSH distribution in the cytosol. All these aforementioned studies revealed that crown ethers can be used for imaging probes.

A recent study by Tian *et. al.*[35] showed the testing of 12-crown-4 and 12-crown-4 conjugated with Pittsburgh compound B (PiB) a positron emission tomography (PET) tracer and targeting agent widely used for Aβ imaging. It was shown that 12-crown-4 ether and 12-crown-4 conjugated Pittsburgh compound B (PiB-C) inhibits the Aβ40 aggregation. It was revealed that the aggregation of Aβ40 was significantly reduced by 12-crown-4 and PiB-C. Furthermore, a dot blot experiment showed that in the presence of 12-crown-4 and PiB-C, a significantly lower number of fibrillar/prefibrillar structures were formed than in its absence or with PiB (PiB without conjugation). To investigate whether 12-crown-4 can reduce the Aβ42 toxicity, the authors treated SH-SY5Y neuronal cells with Aβ42 in the absence and presence of 12-crown-4, PiB and PiB-C; their data revealed that 12-crown-4 and PiBC could significantly reduce the toxicity of Aβ42. Two-photon microscopic imaging data revealed that PiB-C could readily penetrate the blood -brain barrier (BBB) and efficiently label Aβ. Overall the data of the aforementioned study suggested that 12-crown-4 and PiB-C could efficiently inhibit the aggregation of Aβ monomers into protofibrils/fibrils. The authors

hypothesized that hydrogen bonds between crown ethers and positively charged amino acids of Aβ such as Arg5, Lys16, Lys28, His13 and His14 inhibited/modified its aggregation. An experimental and computational study by Lee *et. al.* [36] revealed that crown ethers can modify protein surface behaviour dramatically by forming intra- or intermolecular interactions and they proposed that crown ethers can be used to modulate protein oligomerization/aggregation. In our previous study, we performed MD simulation of 12-crown-4 with Aβ40 fibrils trimer[37] and revealed three binding modes of 12-crown-4 on Aβ40 fibrils trimer. In the first binding mode, 12-crown-4 ether entered into the hydrophobic core and opened the "U-shaped" topology of Aβ40 fibril trimer, which is important for its cytotoxicity[38]. In the second binding mode, 12-crown-4 interacted with Lys28 breaking the salt-bridge formed between Asp23-Lys28, which plays an important role in aggregate/fibril stability[39]. Lastly, 12-crown-4 specifically interacted with Lys16, which is important for toxicity[20].

In the present study, we aim to find a molecular basis for the early steps misfolding of Aβ peptides and effect of 12-crown-4 ether on Aβ40 and Aβ42 monomers misfolding, To fulfill this aim we have performed 29 all-atom molecular dynamics (MD) simulations, with a total simulation time of 11.4μs, in the presence and absence of 12-crown-4; these methods allow us to study the Aβ40 and Aβ42 monomers conformation dynamics and monitor the interaction between the 12-crown-4 and the Aβ40 and Aβ42 monomers. The MD study will allow us to answer the following questions: 1) How does turn-formation take place in Aβ monomers? 2) What is the role of water solvation around turn-region residues in turn-formation? 3) Which region does 12-crown-4 bind to? 4) What is the impact of 12-crown-4 binding on Aβ40 and Aβ42 monomers? 5) How does 12-crown-4 binding with Aβ40 residues affect its conformational entropy and what are the implications of such entropy changes?

3.3 Methods

3.3.1 Structure and Force field for Aβ40 Monomer

In the present molecular dynamics study, NMR derived Aβ40 monomer (PDB id: 1BA4) and Aβ42 monomer (PDB id :1IYT) structures have been used (Figure: 3.1A, B). The Aβ40 monomer structure contains 1-14 unstructured region; the rest of the peptide adopts α-helical conformation [40]. The Aβ42 monomer structure contains two helical regions first one from residues 8–25 and the second one from 28–38, both regions connected by a regular a β-turn[41]. In this study we have used Charmm36 force field[42] for Aβ40 and Aβ42 monomer; a recent study Siwy *et.al.*[43] performed a comparative MD simulation study of $A\beta_{10-40}$ using four different protein force fields and two water models (standard TIP3P and modified TIP3P). Their data revealed that J-coupling and residual dipolar coupling constants of the Charmm36 force field, with standard TIP3P water model, was in the close agreement with experimental values. Thus, Charmm36 produces an accurate representation of the $A\beta_{10-40}$ conformational ensemble.

3.3.2 Structure and force field parameters for 12-crown-4 ether: The structure of 12-crown-4 ether was taken from PubChem compound library (CID: 9269) [44] and is shown in Figure: 3.1C. The 12-crown-4 is a cyclic tetramer of ethylene oxide; its chemical formula is $C_8H_{16}O_4$[45]. 12-crown-4 ether force field parameters were derived from the Charmm Additive and Classical Drude Polarizable Force Fields for Linear and Cyclic Ethers (ACDPFF) [46]. ACDPFF is force field for linear and cyclic ether molecules and the same force field parameters for 12-crown-4 ether were used in our previous MD simulation work[37]. Aβ40/42 peptides are generated through a serial cleavage of amyloid precursor protein (APP) by β- and γ-secretase enzymes[7,47]. After cleavage, Aβ40/42 peptides are independent peptides, not associated with APP and contain their own N and C-terminals. In the present work, in the case of Aβ40, we have treated ASP-1 as an N-terminal residue and VAL-40 as a C-terminal. In the case of Aβ42, we have treated ASP-1 as an N-terminal residue and ALA-42 as a C-terminal residue.

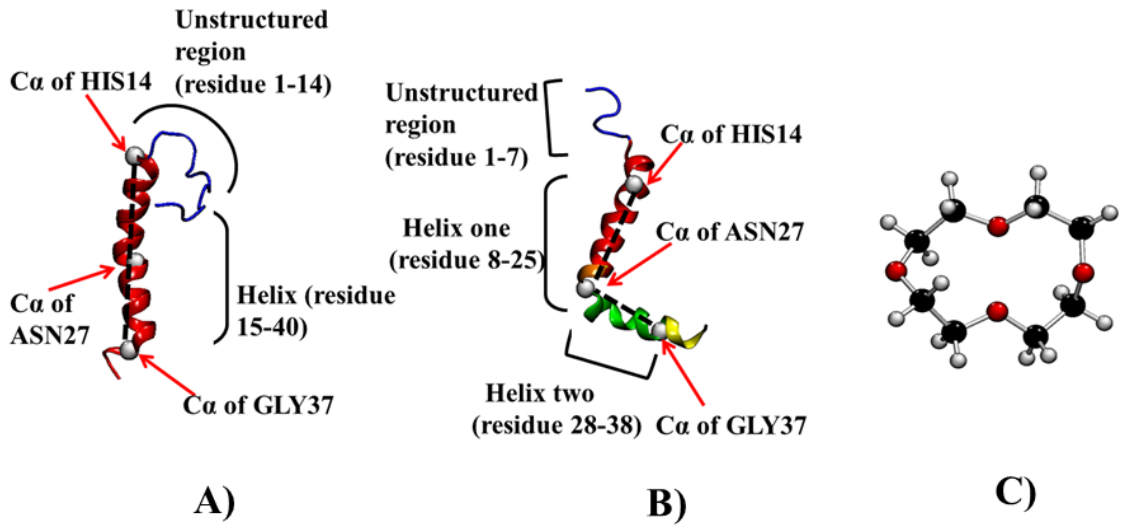

Figure: 3.1A) shows the initial structure of Aβ40 Monomer in cartoon representation. The unstructured region (residue 1 to 14) has been shown in blue colour, helix region (residue 15 to 40) has been shown in red colour, B) shows the structure of Aβ42 Monomer in cartoon representation. The unstructured region (residue 1 to 7) has been shown in blue colour; helix one region (residue 8 to 25) has been shown in red colour and helix two regions (residue 28 to 38) has been shown in green colour. Cα atoms of His14, Asn27, and Gly37 used in angle calculation have been represented in VdW representation for both peptides in white colour. C) shows the structure of 12-crown-4 in cpk representation,

3.3.3 Simulation Protocol: The system, in the presence of the 12-crown-4, contains one Aβ40 monomer, two 12-crown-4 molecules, and 8979 water molecules. In the absence of 12-crown-4, Aβ40 monomer system contains 8993 water molecules. The system of 12-crown-4 with Aβ42 monomer contains two 12-crown-4 molecules with one Aβ42 monomer and 10658 water molecules. The Aβ42

monomer system, in absence of 12-crown-4, contains 9025 water molecules. Three Na^+ counter ions were added into all systems to achieve overall charge neutrality. Initially, 5000 steps of steepest descent were performed to energy minimize the systems[48], followed by two sequential 100ps equilibration simulations, first in the canonical (NVT) ensemble, then the isobaric-isothermic (NPT) ensemble; NPT ensemble was used for the production simulations. The bond lengths from heavy atoms to hydrogen atoms, of the Aβ40 and Aβ42 monomers and 12-crown-4, were constrained using the LINCS algorithm[49] and the SETTLE algorithm[50] was used for water molecule bond length constraints. Particle mesh Ewald (PME)[51] was used for long-range electrostatics and van der Waals (vdW) interactions with a short-range cut-off of 10Å. In both systems (Aβ40 and Aβ42) Aβ peptide and non-protein components (water, 12-crown-4, and ions) were separately coupled with external pressure and temperature baths. The velocity-rescale algorithm[52] was used for temperature coupling and the Parrinello−Rahman algorithm was used for pressure coupling [53]. Temperature and pressure bath coupling times were set to 0.1 and 0.1 ps respectively. All MD simulations were performed at a pressure of 1 bar and temperature of 300K.

A total of eleven control simulations were performed, one (2 μs), four (200 ns) and six (100 ns), to explore the conformation change in Aβ40 monomer in the absence of 12-crown-4; a total of sixteen simulations were performed in the presence of 12-crown-4 for 12-Aβ40 monomer system, one (2 μs), five (200 ns) and ten (100 ns). For Aβ42 monomer system two simulations were performed, one in the presence of 12-crown-4 and other in the absence of 12-crown-4; each simulation was 2 μS long, in total of 4 μS simulations were performed for the Aβ42 system. In both systems, Aβ40 and Aβ42, one 12-crown-4 molecule was placed near to the N-terminal and the other 12-crown-4 molecule was placed near to the C-terminal of Aβ40 monomer. No prior contacts were formed between Aβ40 and Aβ42 monomer residues and 12-crown-4.

3.3.3 Analysis details

Changes in the conformational topology of the Aβ40 and Aβ 42 peptides was measured via the angle of the α-carbon atoms of HIS14, ASN27, and GLY37 (Figure: 3.1A, B). Aβ peptide has been considered in "U-shaped" if angle value is 60° or less. The number of water molecules has been calculated within 3.5 Å of Lys28 and Val24 residues, using an in-house Tcl script. For H-bond calculations the cut-off distance, between donor and acceptor atoms, was set at 3.5 Å and the angle was considered to be 30°. To understand the dynamics of Lys28 (backbone and sidechain) and the effect of 12-crown-4 binding on its dynamics, we divided the trajectory into 10 ns bins and calculated the average structure for that bin; using the average structure as reference with the "fit none" option of the Gromacs RMS program, RMSD was calculated and averaged for each bin. To investigate conformational entropy of Lys28 (Backbone and sidechain), the mass-weighted covariance matrix was calculated, which was used for quasi-harmonic approximation[54]. Conformational entropy was calculated and averaged for each 10ns bin. An interaction between 12-crown-4 and Aβ peptides

residues were considered when the distance, between the COM of the residues and COM of 12-crown-4, was 10 Å or less. The percentage of contact of Aβ monomers for each residue with 12-crown-4 was calculated by using g_mmpbsa tool[55]. Secondary structure analysis for Aβ40 and Aβ42 monomers were performed using the dictionary secondary structure of protein (DSSP)[56]. The GROMACS[57] sham program was used to construct the free energy contour maps and RMSD (backbone atoms) and Rg (backbone atoms) of Aβ peptides were used as an order parameter to determine free energy (kJ/mol). The initial NMR structure was used for calculating the RMSD (backbone atoms) and Rg (backbone atoms) for in the presence of absence of 12-crown-4, free energy contour maps.

3.4 Results

3.4.1 Conformational transition of Aβ40 and Aβ42 in "U-shaped" structure and loss and gain of water around turn region residue Val24 and Lys28

To investigate the conformational transition for the Aβ40 monomer from the native "I-shaped" structure to the "U-shaped structure" and Aβ42 monomer from the "L-shaped" structure to "U-shaped structure" in the presence and absence of 12-crown-4, we calculated angle of bending for all simulation trajectories (see the method section for more details). It has been reported that the turn formation in Aβ peptide is the first step toward the formation of the misfolded structure and NMR and MD simulations studies have suggested that Val24-Lys28 is the most probable region to form a turn[8, 11]. Another study, however, has suggested that a turn could also form at residue positions Glu22-Asp23[58]. Visual inspection of 11 control trajectories including the 2 μs long of Aβ40 monomer revealed that in six simulations the turn formed between residues Val24-Lys28, in two of the simulations the turn formed at residue position Gly29, and in one simulation the turn was formed at residue position Gul22-Asp23. Visual inspection of Aβ42 monomer 2 μs trajectory revealed that the turn was formed around Val24-Lys28.

To investigate the effect of water molecules on Aβ40 and Aβ42 peptides, on turn formation, we calculated the number of water molecules within 3.5Å of turn region residues. In a total of 11 control simulations for Aβ40 monomer, in 6 simulation trajectories we observed loss of water molecules around residue Val24 and in four simulation trajectories, we observed gain of water molecules around Lys28. In four simulation trajectories we observed loss and gain of water molecules occurring at the same time in Aβ40 monomer system. In case of Aβ42 monomer, we also observed gain and loss of water molecules around Val24-Lys8 residues. The same phenomenon was observed in the long trajectories of Aβ40 and Aβ42 monomers in the presence of 12-crown-4, where turn formation took place.

Figure: 3.2A and 3.2C show the time evolution of the change in angle of Aβ40 and Aβ42 monomer, and Figure: 3.2B and 3.2D show the time evolution of gain and loss of water molecules around Lys28 and Val24 in two of the representative 2 μs long trajectories of Aβ40 and Aβ42 in absence of 12-crown-4. To understand the mechanism of turn formation, we have plotted the change in angle and gain/loss of water for the initial 600ns, until water gain stabilized and the peptide remained stable in "U-shaped" structure. The change in angle of Aβ40 monomer was observed at ~320 ns (Figure: 3.2A) when the peptide changed from native "I-shaped" conformation to "U-shaped" conformation. The peptide was considered in "U-shaped" when angle was 60° or less; in the meantime we observed there was a sudden gain of water molecules around Lys28 (Figure: 3.2B, red line, Table: 3.1) and loss of water molecule around Val24 (Figure: 3.2B, black line, Table:1). On average there was a gain of ~0.907 water molecules around Lys28 and a loss of ~1.275 water molecules around Val24 after "U-shaped" structure formation in the Aβ40 monomer representative simulation.

In Aβ42 monomer, during the transition from "L-shaped" (80°-120°) to "U-shaped" structure (<= 60°), we observed an intermediate state where Aβ42 monomer obtained an "I-shaped" structure(~130° to ~170°). At ~32ns, Aβ42 monomer obtained "I-shaped" structure, which leads to an increase of water molecules around both Lys28 and Val24 (Figure: 3.2D red and black line) and an increase of the angle form ~125° to ~170°. At ~440ns (Figure: 3.2C) the Aβ42 monomer transformed from "I-shaped" structure to "U-shaped" structure; in the meantime, gain of water molecules around Lys28 and loss of water molecules around Val24 took place (Table: 1.1) On average there was a gain of ~1.227 water molecules around Lys28 and a loss of ~1.631 water molecules around Val24, after "U-shaped" structure formation in the Aβ42 monomer simulation. Overall, this data suggest that the gain and loss of water molecules play a crucial role in early stage misfolding of Aβ40 and Aβ42 monomers.

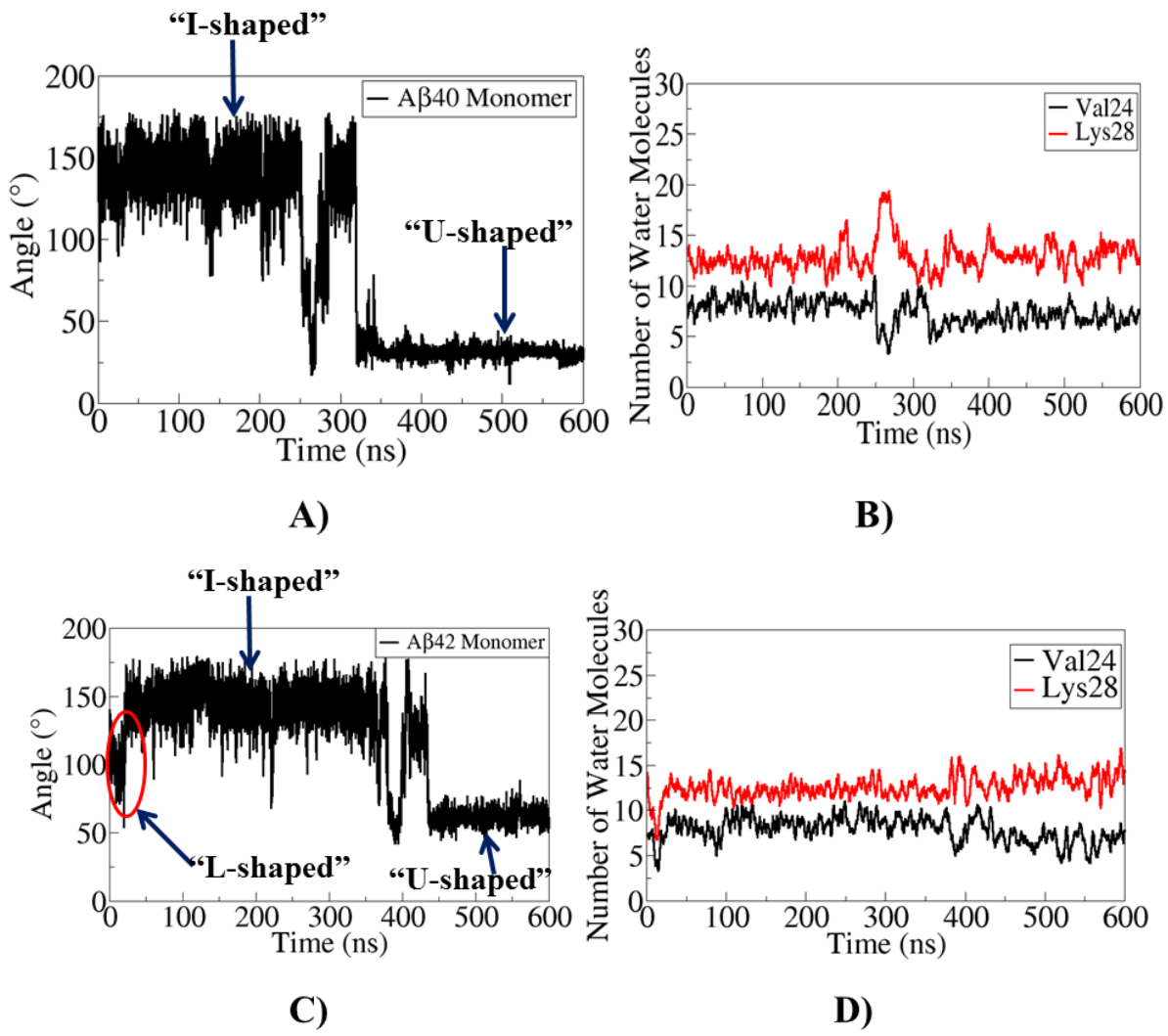

Figure: 3.2 A) Shows the time evoluion of change in angle of Aβ40 monomer. B) Shows the time evolution of number of water molecules around Val24 and Lys28 of Aβ40 monomer. C) Shows the time evolution of change in angle of Aβ42 monomer. D) Shows the time evolution of number of water molecules around Val24 and Lys28 residues of Aβ42 momomer.

Name of the residue	Average number of water molecules in "I-shaped" structure	Average number of water molecules in "U-shaped" structure
Aβ40 and Lys28	12.27	13.18
Aβ40 and Val24	8.25	6.97
Aβ42 and Lys28	12.17	13.40
Aβ42 and Val24	8.29	6.66

Table: 3.1 shows the average number of water molecules around Lys28 and Val24 in Aβ40 and Aβ42 monomers in "I-shaped" and "U-shaped" conformations. In the "I-shaped" conformation, average water molecules were calculated from 50 to 150 ns time period for Aβ40 and Aβ42. In the "U-shaped" structure, average water molecules were calculated for Aβ40 monomer from 400 to 500 ns and for Aβ42 monomer from 450 to 550 ns.

3.4.2 Hydrogen bonds (H-Bonds) formed by Lys28 Backbone in Aβ40 monomer

To further investigate the effect of water gain around the Lys28 backbone, on the formation of the turn, we have calculated the number of intrapeptide H-bonds between amide H-bond donor and carbonyl H-bond acceptor atoms within the Lys28 region of the helix (Figure: 3.3A, black line) in one of the representative trajectories of Aβ40 monomer, in this trajectory turn was formed ~30ns. Before the turn formation, there are two H-bonds, one formed between the amide group of Lys28 and the carbonyl group of Val24 and the other between the carbonyl group of Lys28 and the amide group of Ile32 (Figure: 3.3B). The aforementioned H-bonds are almost completely broken after the turn-formation (Figure: 3.3D) and this indicates the importance of the intrapeptide H-bonds for maintaining Aβ40 peptide stability. H-bonds, between water molecules and the backbone amide and carbonyl groups, replaced the intrapeptide H-bonds during the turn formation (Figure: 3.3A, red line); this leads us to believe that the formation of the water—backbone H-bonds provide a motivation for breaking the intrapeptide H-bonds and, therefore, turn-formation.

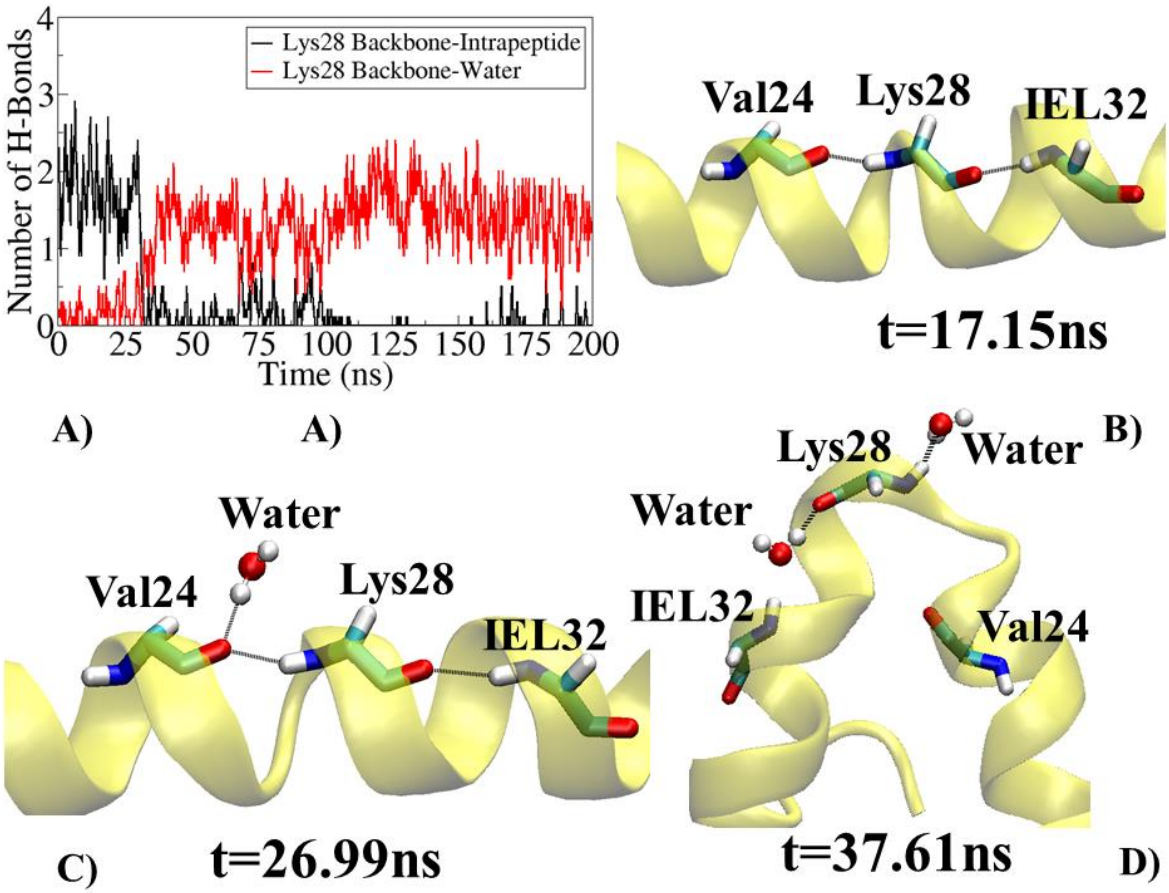

Figure: 3.3 A) Shows the time evolution of number of intrapeptide H-bonds (black line) and number of H-bonds formed with water molecules. B) Shows represented image of H-bonds formed by Lys28 at t=17.15ns. C) Shows represented image of H-bonds formed by Lys28 at t=26.99ns. D) Shows represented image of H-bonds formed by Lys28 at t=37.61ns.

3.4.3 Percentage of contact of 12-crown-4 ether with Aβ40 and Aβ42 monomers

To identify the residues of Aβ40 and Aβ42 monomers, which formed the most contacts with 12-crown-4, we computed the percentage of contacts with each residue in 2 μs long trajectories (Figure: 3.4). 12-crown-4 ether formed major contacts with positively charged residues, Lys16 and Lys28, and N-terminal, Asp1 in Aβ40 monomer (Figure: 3.4A). 12-crown-4 ether also formed contact with central hydrophobic cluster residues (Phe19, Phe20), turn region residues (Ser26 and Gly29). In case of Aβ42 monomer, we observed 12-crown-4 formed major contacts with positively charged Lys16, N-terminal Asp1 and central hydrophobic cluster residue Phe19 (Figure: 3.4B). This analysis revealed that 12-crown-4 ether formed major contact with positively charged residue Lys in case of both peptides, however , we observed in case of Aβ40 it forms contacts with both Lys residues majorly, however; in Aβ42 monomer simulation, 12-crown-4 forms major contact with Lys16 and minor contacts with Lys28. Other than Lys28, which is one of the crucial residues in Aβ misfolding, Lys16 has been reported to play a major role in Aβ toxicity[21]. Various studies have suggested that Lys16 can form a salt-bridge with Glu22, which helps to arrange Aβ into the antiparallel arrangement[59,60]. Karr *et*

.*al.* reveal that Asp1 is a binding site of Cu ions[61] and binding of Cu with Asp1 increases the toxicity of Aβ[62].

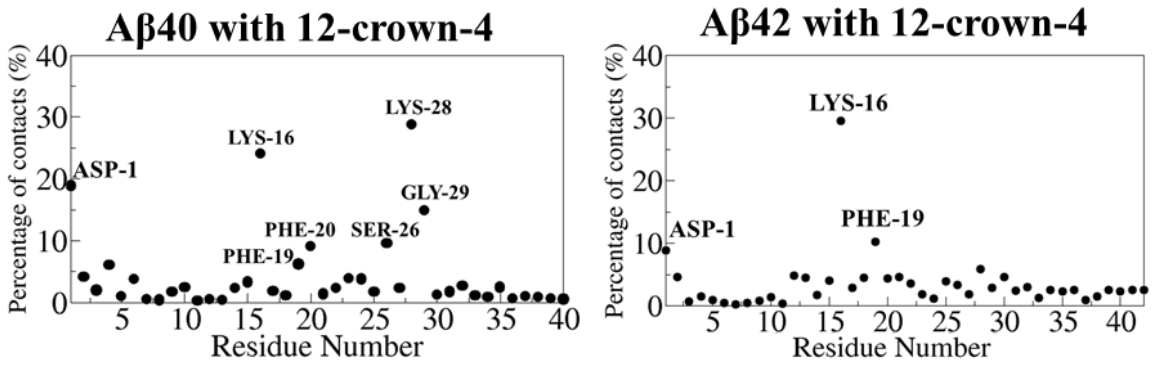

Figure: 3.4 A) Shows the percentage of contacts formed by 12-crown-4 with each residue of Aβ40 monomer in 2 μs simulation trajectory. B) Show the percentage of contacts formed by 12-crown-4 with each residue of Aβ42 monomer in 2 μs simulation trajectory.

3.4.4 Secondary Structure Changes in Aβ40 and Aβ42 monomers in presence and absence of 12-crown-4

Simmons *et. al.*[63] performed structure-activity relationship of Aβ40 and revealed neurotoxicity in the primary neuronal cell; their data showed that Aβ with β-sheet structure was highly toxic and Aβ structure with a random coil is less toxic. To investigate effect of 12-crown-4 binding on secondary structure of Aβ peptides we have performed time evolution of secondary structure analysis of Aβ40 and Aβ42 monomers in the presence and absence of 12-crown-4 (Figure: 3.5)

In the absence of 12-crown-4, at ~600 ns we observed some part of the unstructured region was converted into the β-sheet and the β-bridge in Aβ40 monomer and remained stable until the end of the simulation (Figure: 3.5A). The aforementioned event could be significant since a recent Aβ fibrils structure has revealed that the unstructured region of Aβ forms a β-sheet structure[64]. In the presence of 12-crown-4, no β-sheet formation was observed in the Aβ40 peptide (Figure: 3.5B); however, there is a transition between helix to the coil from ~250ns to ~800ns, but Aβ40 peptide regained its helicity and remained stable until the end of the simulation.

In the case of Aβ42 monomer in absence of 12-crown-4, we observed Helix 2 of the peptide (residue 28-38) was almost completely converted into the turn and coil (Figure: 3.5C); however, in the presence of 12-crown-4, the helix region remained intact until the end of the simulation (Figure: 3.5D). Overall this data suggest that binding of 12-crown-4 could affect the secondary structure change of the Aβ40 and Aβ42 peptides.

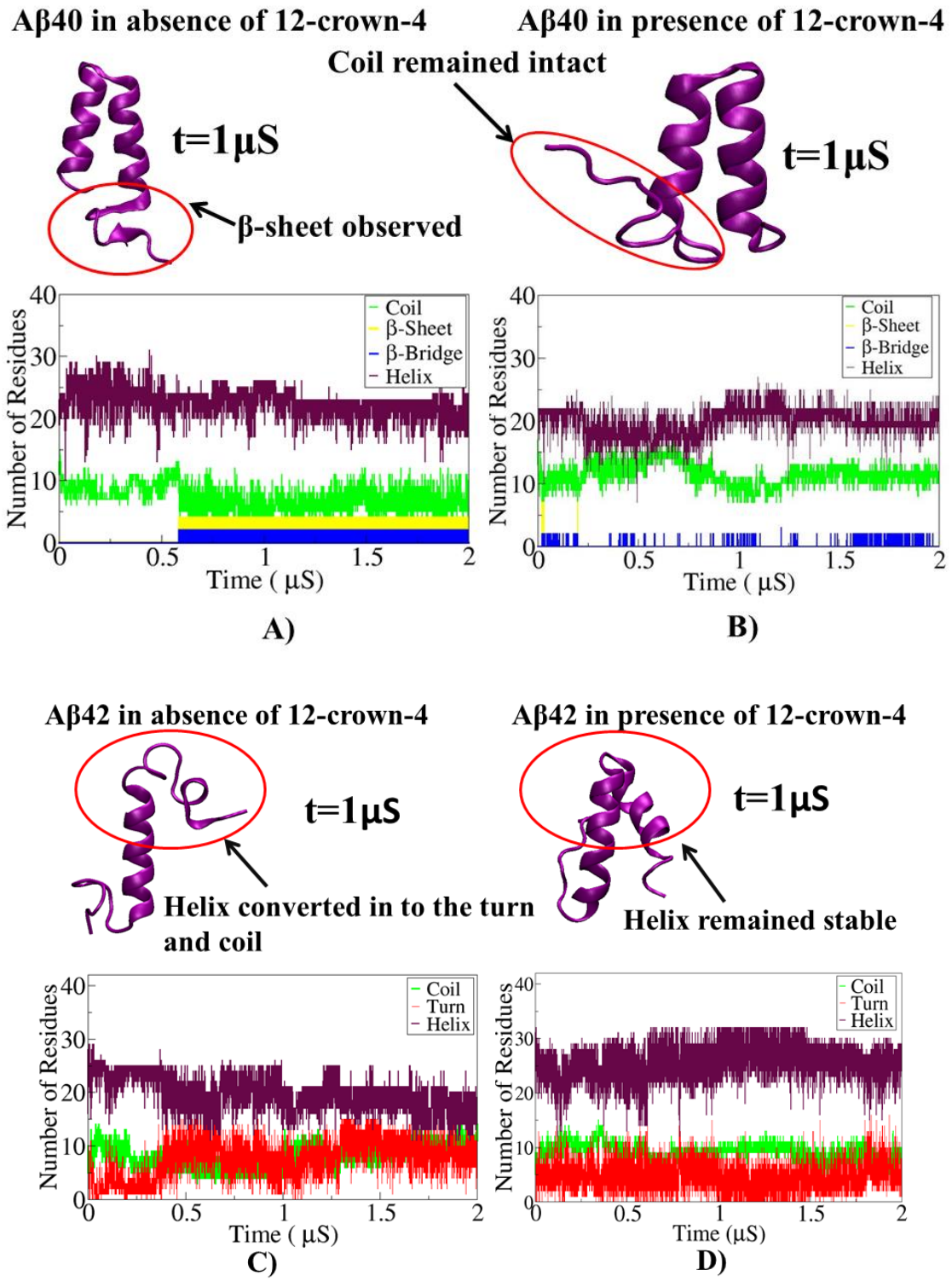

Figure: 3.5 A) Shows time evolution of secondary structure of Aβ40 monomer in the absence of 12-crown-4. B) Shows time evolution of secondary structure of Aβ40 monomer in the presence of 12-crown-4. C) Shows time evolution of secondary structure of Aβ42 monomer in the absence of 12-crown-4. D) Shows time evolution of secondary structure of Aβ42 monomer in the presence of 12-crown-4.

3.4.5 Interaction of 12-crown-4 ether with Asp1, Lys16, and Lys28 of Aβ40 monomer

Figure: 3.6A) shows the time evolution of COM distances between 12-crown-4, with major contact-forming residues. 12-crown-4 interactions with Aβ40 monomer, in the 2 μs long trajectory, can be divided into three steps; in the first step, 12-crown-4 interacted with c-terminal Asp-1 for the period of ~343 ns (350-693 ns) (Figure: 3.6A, black line). In the second step, 12-crown-4 formed an interaction with Lys28 for a total time of ~307 ns (953-1260 ns) (Figure: 3.6A, green line). In the third step, 12-crown-4 formed an interaction with Lys16 for a period of ~ 255 ns (1390-1585 ns) (Figure: 6A, red line).The time evolution of interaction energies, between 12-crown-4 (Figure: 3.6B) and major binding residues, revealed that the interaction energy between Asp1 and 12-crown-4 was slightly less negative (~ -90 kJ/mol, Figure: 3.6B, black line) than the interaction energy of Lys residues with 12-crown-4 was (~ -120 kJ/mol, Figure: 3.6B, red and green line). To investigate the number of water molecules displaced by 12-crown-4, to bind with these residues we calculated the average number of water molecules around these residues before and during the binding of 12-crown-4 (Table: 3.2). It reveals that 12-crown-4, displaced ~3.97, ~3.518 and ~1.84 to interact with Asp1, Lys16 and Lys28 respectively.

Name of the residue (Aβ40 monomer)	**Number of water molecules before 12-crown-4 binding**	**Number of water molecules during 12-crown-4 binding**
Asp-1	14.50	10.53
Lys-16	13.04	9.52
Lys-28	10.76	8.91

Table: 3.2 show the average number of water molecules before and during the binding of 12-crown-4 around Asp1, Lys16, and Lys28. Before binding of 12-crown-4, a number of water molecules averaged from 0 to 100 ns around each residue and during binding for Asp-1(400 to 500 ns), for Lys16 (1400 to 1500 ns) and for Lys28 (1000 to 1100 ns).

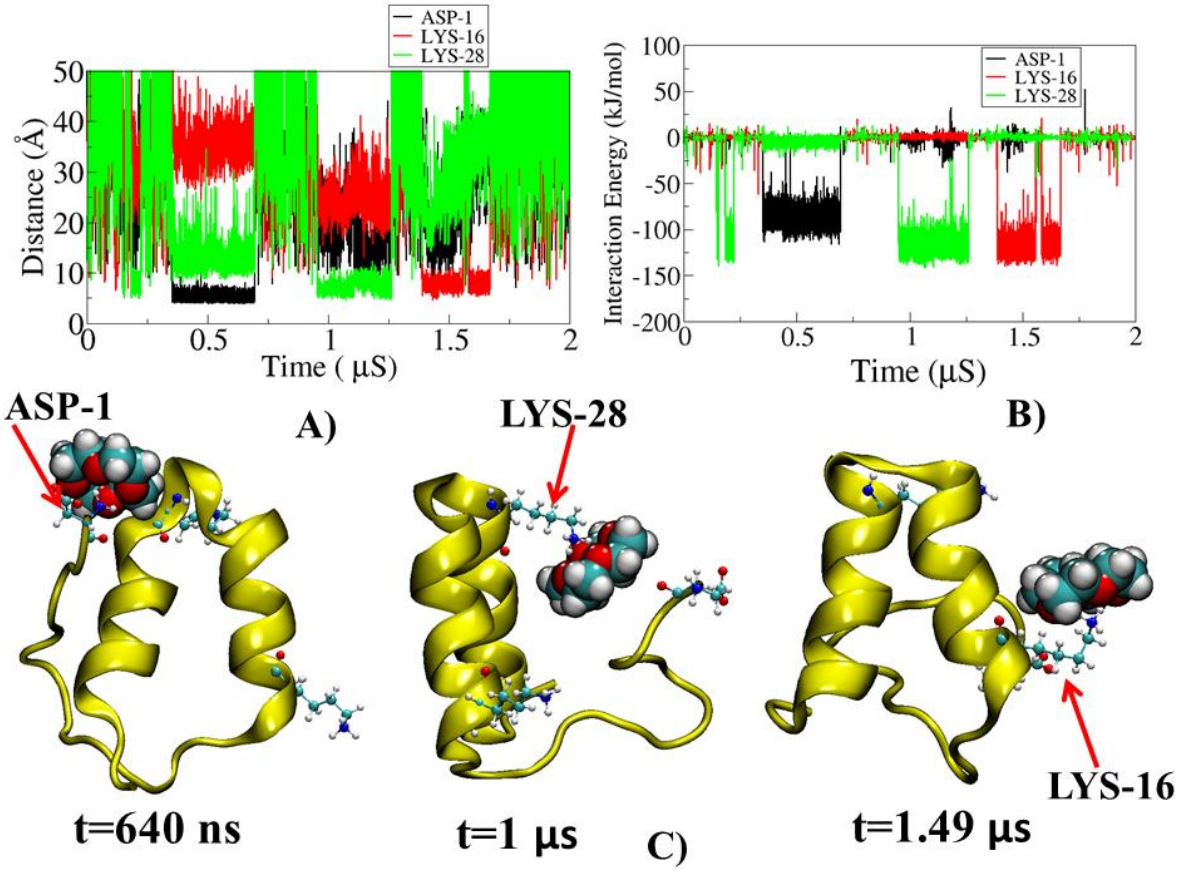

Figure: 3.6 A) Shows time evolution of COM distances between Asp1, Lys16 and Lys28 from COM of 12-crown-4. B) Shows time evolution of interaction energy between 12-crown-4 and Asp1, Lys16 and Lys28. C) Shows three snapshots form 2 μs trajectory of Aβ40 monomer taken at different time points, during 12-crown-4 binding with major contact forming residues.

3.4.6 Interaction of 12-crown-4 ether with Asp1, Lys16, and Phe19 of Aβ42 monomer

Aβ42 monomer simulations with 12-crown-4 revealed that 12-crown-4 formed major contacts with Asp1, Lys16, and Phe19 residues. In 2 μs long simulation of Aβ42 monomer with 12-crown-4, we observed attachment and detachment of 12-crown-4 with these residues at different time points. 12-crown-4 interacted with Asp1 for a total period of ~160 ns in two points of time (166-276 ns, 1230-1280 ns) (Figure: 3.7A, black line). 12-crown-4 interacted for a total of ~506 ns with Lys16 at four different time points (87-142 ns, 285-374 ns, 463-740 ns, 985-1070 ns) (Figure: 3.7A, red line). During its interaction with Lys16, 12-crown-4 also formed interaction with central hydrophobic cluster residue Phe19 (Figure: 3.7A, green line). *In vitro* studies have suggested that a substitution of Lys16 for Ala in Aβ1-28[65] and a substitution of Phe19 or Phe20 for Ala, in Aβ10-23[66] results in the inability for peptides to form Aβ fibril like structures. As for the nature and strength of the interactions of 12-crown-4 and Asp1, Lys16 and Phe19, the 12-crown-4 formed hydrophobic interactions with Phe19 (~8 kJ/mol, Figure: 3.7B, green line) and formed electrostatic interactions with Lys28 and Asp1 (~120 kJ/mol, Figure: 3.7B, red line, ~90 kJ/mol, Figure: 3.7B, black line). To investigate how many water molecules 12-crown-4 has to displace to form interaction with major binding residues, we have calculated average water molecules around these residues before and during 12-crown-4 (Table: 3.3) 12-crown-4 displaced ~4.24, ~4.87 and ~0.0792 water molecules around Asp-1, Lys16 and Phe19 respectively to form the interaction with these residues.

Name of the residue (Aβ42 monomer)	**Number of water molecules before 12-crown-4 binding**	**Number of water molecules during 12-crown-4 binding**
Asp-1	14.62	10.38
Lys-16	11.66	6.79
Phe-19	12.06	11.99

Table: 3.3 show the average number of water molecules before and during the binding of 12-crown-4 around Asp-1, Lys16, and Phe19. For Asp-1 before binding of 12-crown-4, a number of water molecules averaged from 50 to 150 ns and during binding from 170 to 270 ns. For Lys16 and Phe19 before binding of 12-crown, a number of water molecules averaged from 0 to 60 ns and during binding 300 to 360 ns.

In all the simulations we observed that 12-crown-4 binds with Aβ residues for certain periods of time and detaches; however; after detachment we have again observed binding with the same residues, suggesting attachment and detachment of 12-crown-4 with Aβ residues is a spontaneous process. There could be several factors that could contribute to its detachment; for example, 1) Change in the conformation of binding residues. 2) Perturbation of water structure around the binding residue. 3) Competition between water and 12-crown-4 with binding residues.

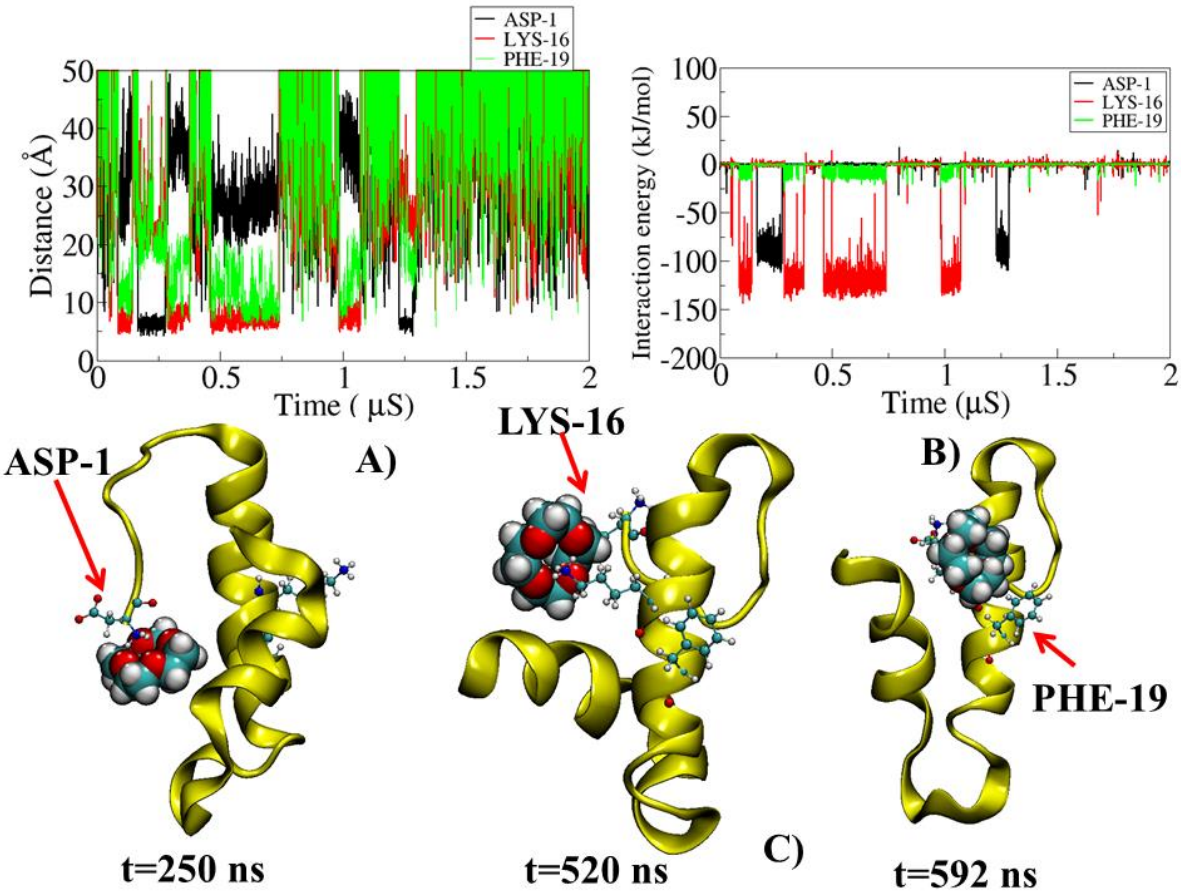

Figure: 3.7 A) Shows time evolution of COM distances between Asp1, Lys16 and Phe19 from COM of 12-crown-4. B) Shows time evolution of interaction energy between 12-crown-4 and Asp1, Lys16 and Phe19. C) Shows three snapshots form 2 µs trajectory of Aβ42 monomer taken at different time points, during 12-crown-4 binding with major contact forming residues.

3.4.7 Free energy landscape of Aβ40 and Aβ42 monomers in absence and presence of 12-crown-4

To investigate the effect of 12-crown-4 on misfolding of Aβ monomers, we have plotted two- -dimensional free energy contour maps as a function of RMSD and RG, in the absence and presence of 12-crown-4, as shown in Figure: 3.8 and Figure: 3.9 with representative structures at each local free energy basin. In the absence of 12-crown-4 (Figure: 3.8A), there was large conformational space explored by the Aβ40 monomer in comparison to the presence of 12-crown-4 (Figure: 3.8B). In the absence of 12-crown-4, we observed two highly populated states of Aβ40 monomer on free energy surface, one native-like structure state and other another one "U-shaped" structure with β-sheet. However, in presence of 12-crown-4 (Figure: 3.8B), there were three most populated energy states. One native-like structure state and two "U-shaped" structures with intact unstructured regions.

In the absence of 12-crown-4 the unstructured region adpoted the β-sheet structure, which made it much less flexible and more compact, compared to the structure in the presence of 12-crown-4. It

should be noted that in the absence of 12-crown-4, the number of states in the transition between the "I-shaped" and "U-shaped" structure are far greater than in the presence of 12-crown-4. A low number of states in the transition region leads to an entropy barrier to transition between the "I-shaped" and "U-shaped" structure, and therefore, a decrease in the opportunity for transition, in the presence of 12-crown-4.

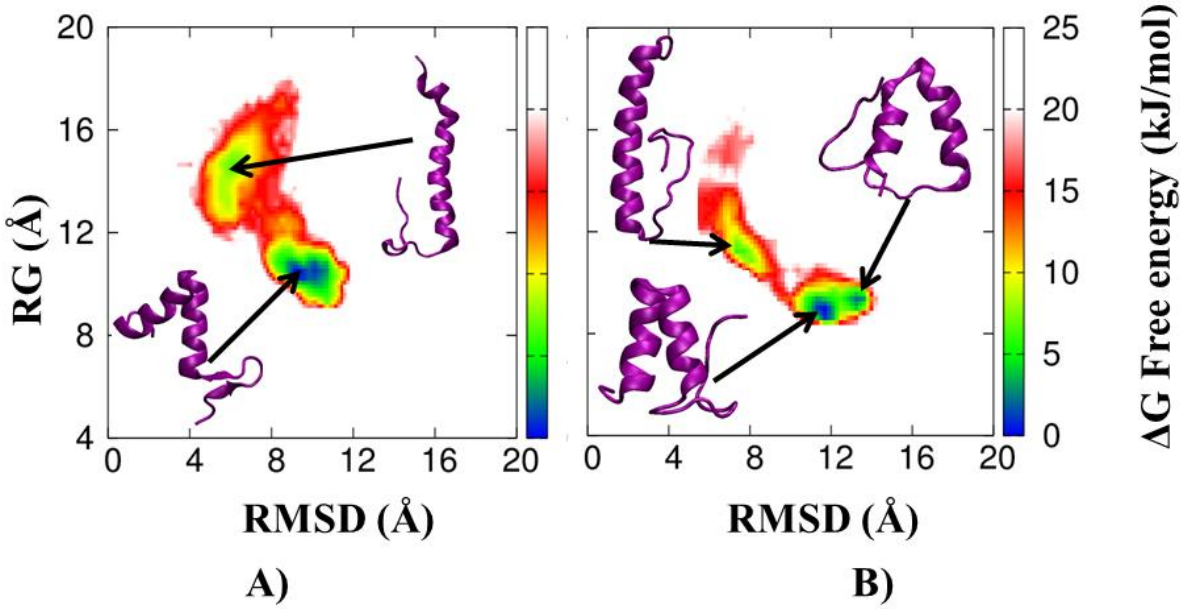

Figure: 3.8 A) free energy landscape of Aβ40 monomer in the absence of 12-crown-4. B) Free energy landscape of Aβ40 monomer in the presence of 12-crown-4.

In Aβ42 monomer, the free energy landscape, in the absence of 12-crown-4 (Figure: 3.9 A), showed a more spread-out profile, with two, low free energy bins; this is due to the conversion of second helical region into coil and turn making the structure unstable. In the presence of 12-crown-4, there is only one low free energy bin populated, the stable state was due to both the helix regions in Aβ42 monomer being intact. Overall this data suggest that the presence of 12-crown-4 affected the free energy landscape of Aβ monomer conformation.

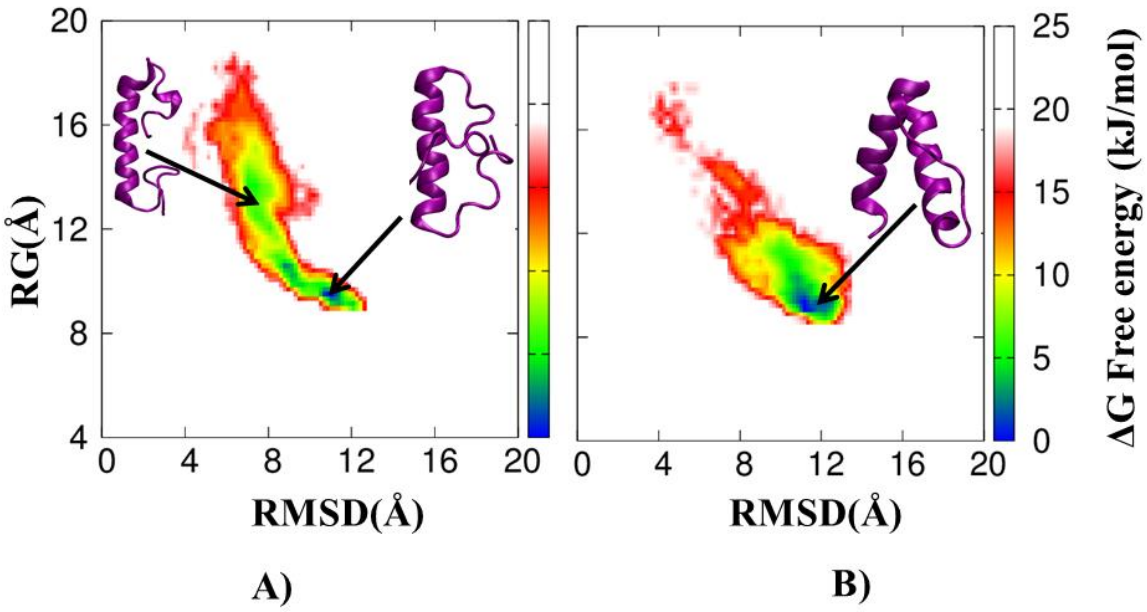

Figure: 3.9 A) free energy landscape of Aβ42 monomer in the absence of 12-crown-4. B) Free energy landscape of Aβ42 monomer in the presence of 12-crown-4.

3.4.8 Lys28 flexibility and conformational entropy in presence and absence of 12-crown-4 of Aβ40 monomer

To provide a better understanding of the interplay between 12-crown-4 and Lys28, we calculated RMSD and conformational entropy (see the method section for more details) for Lys28 in the presence and absence of 12-crown-4, using the quasi-harmonic method. The function/misfolding of the protein is directly linked to its intrinsic flexibility; however, the intrinsic flexibility of a protein can be perturbed by its interaction and binding with other molecules, which could lead to a change in its function. Intuitively, binding between the protein and other molecules is usually considered to restrict the intrinsic flexibility of the binding region in a protein and in its binding partner, which results in a significant loss of conformational entropy[67,68].

The initial RMSD value of Lys28 sidechain (Figure: 3.10A) was ~2.4 Å and increased to ~6.4 Å during the turn formation (30-40 ns), which consequently increased its flexibility. During the turn formation, the number of conformations sampled by the Lys28 sidechain drastically increased (Figure: 3.10A green points). Figure: 3.10B shows the backbone and sidechain conformational entropy of the Lys28 in one of the representative trajectories of the control simulations (in the absence of 12-crown-4). The increase in RMSD correlated with a significant gain in the conformational entropy of the Lys28 backbone and sidechain during the turn formation (30-40ns). The increased conformational entropy of the backbone and sidechain provided a thermodynamic motivation to form the turn in the Aβ40 peptide.

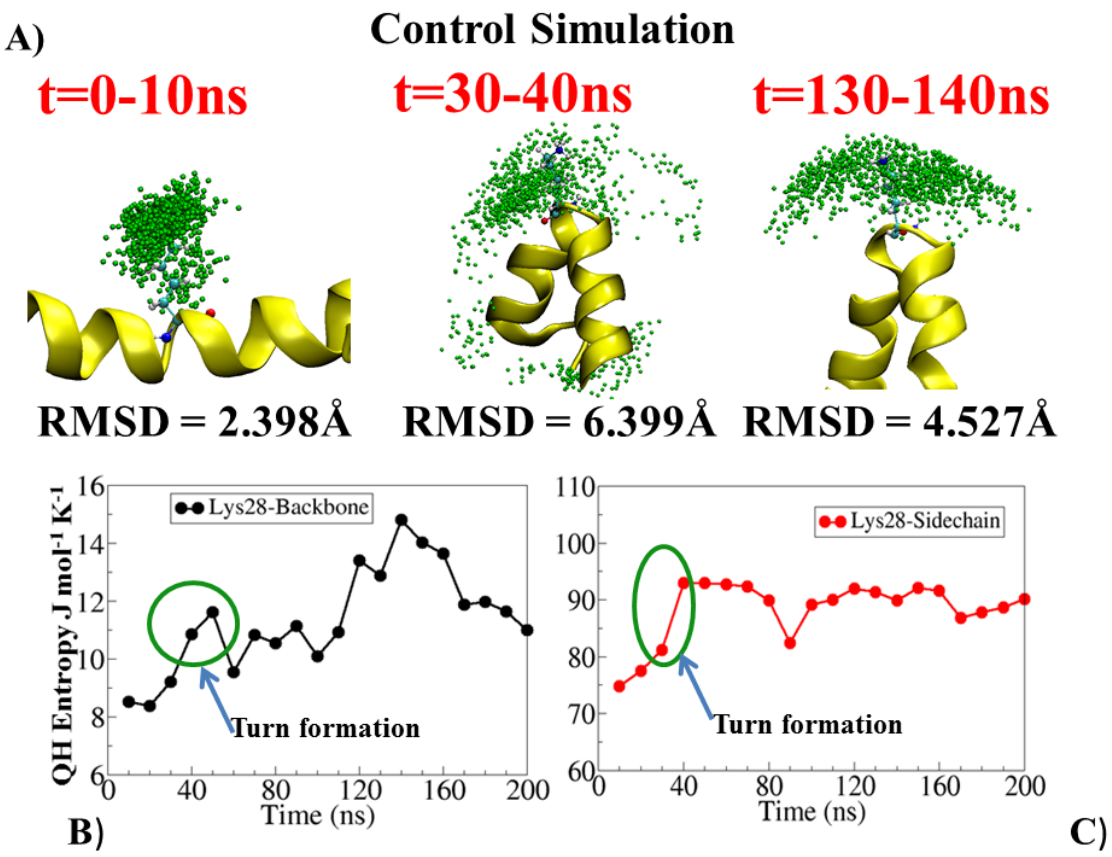

Figure: 3.10A) Shows three representative images of Aβ40 monomer in one of the control simulations at different time point with RMSD values. B) Shows the QH entropy of Lys28 backbone and sidechain averaged for 10ns bin. Green points in the figure represent different number of state visited by the Lys28 side chain.

To investigate how the 12-crown-4 can modify the conformation, we have performed a similar conformational analysis for a representative simulation in the presence of 12-crown-4. Figure: 3.11A shows the RMSD of Lys28 sidechain, in the presence of 12-crown-4, at different time points in the simulation. Initially, from 0-10 ns, before the interaction between Lys28 with 12-crown-4, the RMSD value for Lys28 sidechain was ~3.00Å; during the binding with 12-crown-4, it reduced to ~1.186 Å. Around ~140 ns-160 ns, we again observed a loss of RMSD due to the contacts of unstructured region residues with the Lys28 sidechain. Reduction in RMSD during 12-crown-4 binding resulted in loss of flexibility of Lys28 sidechain; this leads to significant loss of number of states visited by the Lys28 sidechain (Figure: 3.11A green points).

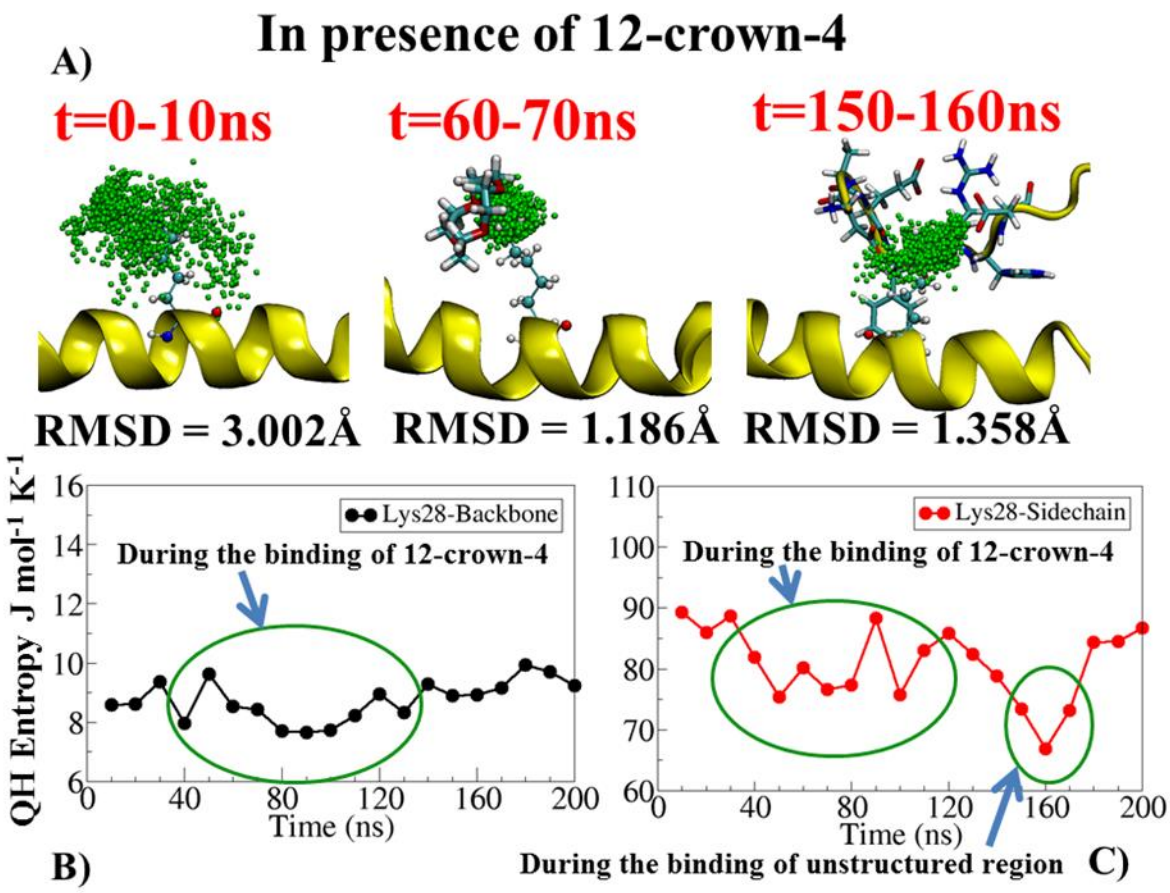

Figure: 3.11A) Shows three representative images of Aβ40 monomer in one of the simulations in the presence of 12-crown-4 at different time point with RMSD values. B) Shows the QH entropy of Lys28 backbone and sidechain averaged for 10ns bin. Green points in the figure represent number of state visited by the Lys28.

Figure: 3.11B and C show the conformational entropy of Lys28 backbone and sidechain. During the binding of 12-crown-4 (~30-110 ns), a significant loss of conformational entropy was observed, as binding of 12-crown-4 restricted the number of conformations obtained by Lys28 backbone and sidechain. At a time point of ~120-160 ns, we also observed binding of the unstructured region with Lys28 sidechain, which resulted in a reduction of its conformational entropy. Despite a loss of entropy upon binding of the 12-crown-4 and Lys28, which should be unfavourable, the attractive interaction between 12-crown-4 and Lys28 more than compensates.

3.5 Discussion

We have performed Aβ40 and Aβ42 monomer simulations in the presence and absence of 12-crown-4. Our simulation data revealed that Aβ40 and Aβ42 peptide misfolding starts with the formation of the turn, in agreement with previous studies[8,9,10]. In our simulations we observed the turn formation, around Val24-Lys28, is initiated by the gain and loss of water molecules around Lys28 and Val24

respectively. Loss of water molecules around Val24 is in agreement with well-established "hydrophobic effect" phenomena[69], which suggest that during the protein folding/misfolding, the nonpolar side chains are removed from contact with water molecules; this leads to the burial of hydrophobic side chains into the core of protein. A previous study[18] suggested that nearby non-polar groups dehydrate backbone hydrogen bonds, which makes it thermodynamically unfavourable to expose the backbone amide and carbonyl groups. Shielding the H-bonds from water molecules helps the protein to maintain secondary structure and warrant them overall stability. In the present study, we observed that the polar/hydrophobic part of the Lys28 sidechain gained a significant number of water molecules, which lead to the water molecules becoming more accessible to the Lys28 backbone. At the same time point in the simulation, there was a significant gain of Lys28 sidechain conformation entropy which leads to a gain in the backbone conformational entropy. Water gain around the Lys28 backbone and entropy gain leads to the lengthening of the intrapeptide H-bonds formed by amide and carbonyl group of Lys28 backbone, and these H-bonds were replaced by water molecules, which destabilizes the Aβ peptide. Loss and gain of water molecules around Val24 and Lys28, conformational entropy gain of Lys28 and breaking of intrapeptide H-bonds are key factors, in turn formation/early stage misfolding of Aβ peptide.

Our simulation data in the presence of 12-crown-4 revealed that it specifically binds to charged residues, Lys16, Lys28, Asp1, and Phe19. 12-crown-4 contains hydrogen and oxygen atoms, this helps 12-crown-4 to form electrostatic interactions with charged Lys, N-terminal Asp, and VdW/hydrophobic interactions with Phe19 residue. These pharmacophore features of 12-crown-4 could be used in designing new highly specific candidate drug molecules or imaging probes. In one previous study, Jiang *et. al.*[70] used pharmacophore features of an Aβ fragment complex with the dye orange G, which specifically binds with Lys16 to search new potential compounds. They identified eight diverse and three compound derivatives that reduced the Aβ cytotoxicity against mammalian cells by up to 90%.

Our data support the hypothesis of Tian *et. al.*[35] that 12-crown-4 can bind with positively charged Lys residues of Aβ peptide and perturb its aggregation and toxicity. 12-crown-4, conjugated with PiB, was shown to cross BBB and inhibit the Aβ aggregation and the present study has highlighted the molecular-level factors with which the inhibition of aggregation may occur. The present study is also in-line with previous studies which suggest that Lys specific candidate drug molecules could perturb the Aβ aggregation and reduce its toxicity[20,21]. Simmons *et. al.*[63] study suggested that the Aβ peptide with β-sheet structure was highly toxic, and Aβ structure with a random coil is less toxic. As we observed in presence of 12-crown-4 secondary structure remained stable in both Aβ0 and Aβ42 monomer, which may affect the toxicity of Aβ monomers.

3.6 Conclusions

In summary, our simulations have shed light on the fundamental understating of turn formation. We observed the gain of water molecules around Lys28 sidechain and increase in its conformational entropy that leads to the break of intra-peptide H-bonds of Lys28 backbone and consequently the turn formation. Our data reveals that 12-crown-4, which has potential as a drug carrier when conjugated with an amyloid targeting agent, is highly specific toward Lys16, Lys28 and Asp1; moreover, we observed contacts formed by 12-crown-4 with central hydrophobic cluster residues, Phe19 and Phe20, and turn region residues Ser26 and Gly29. Secondary structure analysis suggests that 12-crown-4 binding inhibited secondary change in both Aβ40 and Aβ42 monomer. Free energy contour maps revealed that 12-crown-4 can restrict number of conformations explored by Aβ peptides and therefore, affect its misfolding.

The present study deepens our knowledge about the molecular-level factors that contribute to the turn formation in early stage misfolding of the Aβ40 monomer; furthermore, it underpins the importance of Lys residues as potential targets for Aβ inhibition. The present study has, therefore, opened up new avenues in design of potential inhibitors for early stage misfolding of Alzheimer's Aβ monomers.

3.7 Supporting Information

The Supporting Information is available free of charge on the ACS Publications website at DOI: 10.1021/acs.molpharmaceut.7b00966.

Results of gain/loss of water and binding of 12-crown-4 in Aβ40 monomer simulations (PDF)

Movie of Aβ40 monomer in absence and presence of 12- crown-4 (AVI)

Movie of Aβ42 monomer in absence and presence of 12- crown-4 (AVI)

Funding Source: N.A. would like to thank DST-NRF, South Africa for project funding (grant number: 106272). We would like to thank college of Health Sciences at UKZN for funding and infrastructure support.

Notes

The authors declare no competing financial interest.

Acknowledgement: We are indebted to UKZN "hippo" super computer facility, Durban, South Africa, and Centre for High Performance Computing (CHPC) in Cape Town, South Africa for computational resources. We would like to thanks NRF for travel grants.

3.8 References:

1. Uflacker, A.; Doraiswamy, P. M. Alzheimer's Disease: An Overview of Recent Developments and a Look to the Future. *Focus* **2017,** *15*, (1), 13-17.

2. Association, A. s. 2016 Alzheimer's disease facts and figures. *Alzheimer's & Dementia* **2016,** *12*, (4), 459-509.

3. Buxbaum, J. N. Alzheimer's Disease: It's More Than Aβ. *The FASEB Journal* **2017,** *31*, (1), 2-4.

4. Pivi, G. A. K.; de Andrade Vieira, N. M.; da Ponte, J. B.; de Moraes, D. S. C.; Bertolucci, P. H. F. Nutritional management for Alzheimer's disease in all stages: mild, moderate, and severe. *Nutrire* **2017,** *42*, (1), 1.

5. Jakob-Roetne, R.; Jacobsen, H. Alzheimer's disease: from pathology to therapeutic approaches. *Angewandte Chemie International Edition* **2009,** *48*, (17), 3030-3059.

6. Mullard, A. Alzheimer amyloid hypothesis lives on. *Nature Reviews Drug Discovery* **2017,** *16*, (1), 3-5.

7. Bergström, P.; Agholme, L.; Nazir, F. H.; Satir, T. M.; Toombs, J.; Wellington, H.; Strandberg, J.; Bontell, T. O.; Kvartsberg, H.; Holmström, M. Amyloid precursor protein expression and processing are differentially regulated during cortical neuron differentiation. *Scientific reports* **2016,** *6*.

8. Lazo, N. D.; Grant, M. A.; Condron, M. C.; Rigby, A. C.; Teplow, D. B. On the nucleation of amyloid β-protein monomer folding. *Protein Science* **2005,** *14*, (6), 1581-1596.

9. Baumketner, A.; Bernstein, S. L.; Wyttenbach, T.; Lazo, N. D.; Teplow, D. B.; Bowers, M. T.; Shea, J. E. Structure of the 21–30 fragment of amyloid β-protein. *Protein Science* **2006,** *15*, (6), 1239-1247.

10. Cruz, L.; Urbanc, B.; Borreguero, J. M.; Lazo, N. D.; Teplow, D. B.; Stanley, H. E. Solvent and mutation effects on the nucleation of amyloid β-protein folding. *Proceedings of the National Academy of Sciences of the United States of America* **2005,** *102*, (51), 18258-18263.

11. Borreguero, J. M.; Urbanc, B.; Lazo, N. D.; Buldyrev, S. V.; Teplow, D. B.; Stanley, H. E. Folding events in the 21-30 region of amyloid β-protein (Aβ) studied in silico. *Proceedings of the National Academy of Sciences* **2005,** *102*, (17), 6015-6020.

12. Tarus, B.; Straub, J. E.; Thirumalai, D. Dynamics of Asp23− Lys28 Salt-Bridge Formation in Aβ10-35 Monomers. *Journal of the American Chemical Society* **2006,** *128*, (50), 16159-16168.

13. Khatua, P.; Jose, J. C.; Sengupta, N.; Bandyopadhyay, S. Conformational features of the Aβ 42 peptide monomer and its interaction with the surrounding solvent. *Physical Chemistry Chemical Physics* **2016,** *18*, (43), 30144-30159.

14. Melquiond, A.; Dong, X.; Mousseau, N.; Derreumaux, P. Role of the Region 23-28 in Aβ Fibril Formation: Insights from Simulations of the Monomers and Dimers of Alzheimer's Peptides Aβ40 and Aβ42. *Current Alzheimer Research* **2008,** *5*, (3), 244-250.

15. Fleming, P. J.; Rose, G. D. Do all backbone polar groups in proteins form hydrogen bonds? *Protein Science* **2005,** *14*, (7), 1911-1917.

16. Li, J.; Wang, Y.; Chen, J.; Liu, Z.; Bax, A.; Yao, L. Observation of α-helical hydrogen-bond cooperativity in an intact protein. *J. Am. Chem. Soc* **2016,** *138*, (6), 1824-1827.

17. Levy, Y.; Onuchic, J. N. Water and proteins: a love–hate relationship. *Proceedings of the National Academy of Sciences of the United States of America* **2004,** *101*, (10), 3325-3326.

18. Fernández, A.; Scheraga, H. A. Insufficiently dehydrated hydrogen bonds as determinants of protein interactions. *Proceedings of the National Academy of Sciences* **2003,** *100*, (1), 113-118.

19. Hernández-Rodríguez, M.; Correa-Basurto, J.; Benitez-Cardoza, C. G.; Resendiz-Albor, A. A.; Rosales-Hernández, M. C. In silico and in vitro studies to elucidate the role of Cu2+ and galanthamine as the limiting step in the amyloid beta (1–42) fibrillation process. *Protein Science* **2013,** *22*, (10), 1320-1335.

20. Sinha, S.; Lopes, D. H.; Du, Z.; Pang, E. S.; Shanmugam, A.; Lomakin, A.; Talbiersky, P.; Tennstaedt, A.; McDaniel, K.; Bakshi, R. Lysine-specific molecular tweezers are broad-spectrum inhibitors of assembly and toxicity of amyloid proteins. *Journal of the American Chemical Society* **2011,** *133*, (42), 16958-16969.

21. Sinha, S.; Lopes, D. H.; Bitan, G. A key role for lysine residues in amyloid β-protein folding, assembly, and toxicity. *ACS chemical neuroscience* **2012,** *3*, (6), 473-481.

22. Marlow, M. S.; Dogan, J.; Frederick, K. K.; Valentine, K. G.; Wand, A. J. The role of conformational entropy in molecular recognition by calmodulin. *Nature chemical biology* **2010,** *6*, (5), 352-358.

23. Baruah, A.; Rani, P.; Biswas, P. Conformational entropy of intrinsically disordered proteins from amino acid triads. *Scientific reports* **2015,** *5*.

24. Doig, A. J.; Sternberg, M. J. Side-chain conformational entropy in protein folding. *Protein Science* **1995,** *4*, (11), 2247-2251.

25. Frederick, K. K.; Marlow, M. S.; Valentine, K. G.; Wand, A. J. Conformational entropy in molecular recognition by proteins. *Nature* **2007,** *448*, (7151), 325-329.

26. Chia-en, A. C.; Chen, W.; Gilson, M. K. Ligand configurational entropy and protein binding. *Proceedings of the National Academy of Sciences* **2007,** *104*, (5), 1534-1539.

27. Stone, M. J. NMR relaxation studies of the role of conformational entropy in protein stability and ligand binding. *Accounts of chemical research* **2001,** *34*, (5), 379-388.

28. Li, J.; Yim, D.; Jang, W.-D.; Yoon, J. Recent progress in the design and applications of fluorescence probes containing crown ethers. *Chemical Society Reviews* **2017**.

29. Gokel, G. W.; Leevy, W. M.; Weber, M. E. Crown ethers: sensors for ions and molecular scaffolds for materials and biological models. *Chemical reviews* **2004,** *104*, (5), 2723-2750.

30. Marjanović, M.; Kralj, M.; Supek, F.; Frkanec, L.; Piantanida, I.; Šmuc, T.; Tušek-Božić, L. Antitumor potential of crown ethers: structure− activity relationships, cell cycle disturbances, and cell death studies of a series of ionophores. *Journal of medicinal chemistry* **2007,** *50*, (5), 1007-1018.

31. Morrison, P. W.; Porfiryeva, N. N.; Chahal, S.; Salakhov, I. A.; Lacourt, C.; Semina, I. I.; Moustafine, R. I.; Khutoryanskiy, V. V. Crown Ethers: novel permeability enhancers for ocular drug delivery? *Molecular Pharmaceutics* **2017,** *14*, (10), 3528-3538.

32. Oukhatar, F.; Même, S.; Même, W.; Szeremeta, F. d. r.; Logothetis, N. K.; Angelovski, G.; Tóth, E. v. MRI Sensing of Neurotransmitters with a Crown Ether Appended Gd3+ Complex. *ACS chemical neuroscience* **2014,** *6*, (2), 219-225.

33. Gawley, R. E.; Mao, H.; Haque, M. M.; Thorne, J. B.; Pharr, J. S. Visible fluorescence chemosensor for saxitoxin. *The Journal of organic chemistry* **2007,** *72*, (6), 2187.

34. Işık, M.; Guliyev, R.; Kolemen, S.; Altay, Y.; Senturk, B.; Tekinay, T.; Akkaya, E. U. Designing an intracellular fluorescent probe for glutathione: two modulation sites for selective signal transduction. *Organic letters* **2014,** *16*, (12), 3260-3263.

35. Tian, Y.; Zhang, X.; Li, Y.; Shoup, T. M.; Teng, X.; Elmaleh, D. R.; Moore, A.; Ran, C. Crown ethers attenuate aggregation of amyloid beta of Alzheimer's disease. *Chemical Communications* **2014,** *50*, (99), 15792-15795.

36. Lee, C. C.; Maestre-Reyna, M.; Hsu, K. C.; Wang, H. C.; Liu, C. I.; Jeng, W. Y.; Lin, L. L.; Wood, R.; Chou, C. C.; Yang, J. M. Crowning proteins: modulating the protein surface properties using crown ethers. *Angewandte Chemie International Edition* **2014,** *53*, (48), 13054-13058.

37. Agrawal, N.; Skelton, A. A. 12-Crown-4 Ether Disrupts the Patient Brain-Derived Amyloid-β-Fibril Trimer: Insight from All-Atom Molecular Dynamics Simulations. *ACS chemical neuroscience* **2016,** *7*, (10), 1433-1441.

38. Petkova, A. T.; Leapman, R. D.; Guo, Z.; Yau, W.-M.; Mattson, M. P.; Tycko, R. Self-propagating, molecular-level polymorphism in Alzheimer's ß-amyloid fibrils. *Science* **2005,** *307*, (5707), 262-265.

39. Miller, Y.; Ma, B.; Nussinov, R. Polymorphism of Alzheimer's Aβ 17-42 (p3) Oligomers: The Importance of the Turn Location and Its Conformation. *Biophysical journal* **2009,** *97*, (4), 1168-1177.

40. Coles, M.; Bicknell, W.; Watson, A. A.; Fairlie, D. P.; Craik, D. J. Solution Structure of Amyloid β-Peptide (1− 40) in a Water− Micelle Environment. Is the Membrane-Spanning Domain Where We Think It Is?†. *Biochemistry* **1998,** *37*, (31), 11064-11077.

41. Crescenzi, O.; Tomaselli, S.; Guerrini, R.; Salvadori, S.; D'Ursi, A. M.; Temussi, P. A.; Picone, D. Solution structure of the Alzheimer amyloid β-peptide (1–42) in an apolar microenvironment. *The FEBS Journal* **2002,** *269*, (22), 5642-5648.

42. Huang, J.; MacKerell, A. D. CHARMM36 all-atom additive protein force field: Validation based on comparison to NMR data. *Journal of computational chemistry* **2013,** *34*, (25), 2135-2145.

43. Siwy, C. M.; Lockhart, C.; Klimov, D. K. Is the Conformational Ensemble of Alzheimer's Aβ10-40 Peptide Force Field Dependent? *PLOS Computational Biology* **2017,** *13*, (1), e1005314.

44. Wang, Y.; Xiao, J.; Suzek, T. O.; Zhang, J.; Wang, J.; Bryant, S. H. PubChem: a public information system for analyzing bioactivities of small molecules. *Nucleic acids research* **2009,** *37*, (suppl 2), W623-W633.

45. Leong, B. K.; Ts'o, T. O.; Chenoweth, M. B. Testicular atrophy from inhalation of ethylene oxide cyclic tetramer. *Toxicology and applied pharmacology* **1974,** *27*, (2), 342-354.

46. Jana, M.; MacKerell Jr, A. D. CHARMM Drude Polarizable Force Field for Aldopentofuranoses and Methyl-aldopentofuranosides. *The Journal of Physical Chemistry B* **2015,** *119*, (25), 7846-7859.

47. O'Brien, R. J.; Wong, P. C. Amyloid precursor protein processing and Alzheimer's disease. *Annual review of neuroscience* **2011,** *34*, 185-204.

48. Bixon, M.; Lifson, S. Potential functions and conformations in cycloalkanes. *Tetrahedron* **1967,** *23*, (2), 769-784.

49. Hess, B.; Bekker, H.; Berendsen, H. J.; Fraaije, J. G. LINCS: a linear constraint solver for molecular simulations. *Journal of computational chemistry* **1997,** *18*, (12), 1463-1472.

50. Miyamoto, S.; Kollman, P. A. SETTLE: an analytical version of the SHAKE and RATTLE algorithm for rigid water models. *Journal of computational chemistry* **1992,** *13*, (8), 952-962.

51. Darden, T.; York, D.; Pedersen, L. Particle mesh Ewald: An N· log (N) method for Ewald sums in large systems. *The Journal of chemical physics* **1993,** *98*, (12), 10089-10092.

52. Bussi, G.; Donadio, D.; Parrinello, M. Canonical sampling through velocity rescaling. *The Journal of chemical physics* **2007,** *126*, (1), 014101.

53. Parrinello, M.; Rahman, A. Polymorphic transitions in single crystals: A new molecular dynamics method. *Journal of Applied physics* **1981,** *52*, (12), 7182-7190.

54. Levy, R. M.; Karplus, M.; Kushick, J.; Perahia, D. Evaluation of the configurational entropy for proteins: application to molecular dynamics simulations of an a-helix. *Macromolecules* **1984,** *17*, (7), 1370-1374.

55. Kumari, R.; Kumar, R.; Lynn, A. g_mmpbsa□ A GROMACS Tool for High-Throughput MM-PBSA Calculations. *Journal of chemical information and modeling* **2014,** *54*, (7), 1951-1962.

56. Frishman, D.; Argos, P. Seventy-five percent accuracy in protein secondary structure prediction. *Proteins-Structure Function and Genetics* **1997,** *27*, (3), 329-335.

57. Abraham, M. J.; Murtola, T.; Schulz, R.; Páll, S.; Smith, J. C.; Hess, B.; Lindahl, E. GROMACS: High performance molecular simulations through multi-level parallelism from laptops to supercomputers. *SoftwareX* **2015,** *1*, 19-25.

58. Murakami, K.; Masuda, Y.; Shirasawa, T.; Shimizu, T.; Irie, K. The turn formation at positions 22 and 23 in the 42-mer amyloid β peptide: The emerging role in the pathogenesis of Alzheimer's disease. *Geriatrics & gerontology international* **2010,** *10*, (s1), S169-S179.

59. Klimov, D. K.; Thirumalai, D. Dissecting the assembly of Aβ 16–22 amyloid peptides into antiparallel β sheets. *Structure* **2003,** *11*, (3), 295-307.

60. Ma, B.; Nussinov, R. Stabilities and conformations of Alzheimer's β-amyloid peptide oligomers (Aβ16–22, Aβ16–35, and Aβ10–35): sequence effects. *Proceedings of the National Academy of Sciences* **2002,** *99*, (22), 14126-14131.

61. Karr, J. W.; Szalai, V. A. Role of aspartate-1 in Cu (II) binding to the amyloid-β peptide of Alzheimer's disease. *Journal of the American Chemical Society* **2007,** *129*, (13), 3796-3797.

62. Tõugu, V.; Tiiman, A.; Palumaa, P. Interactions of Zn (II) and Cu (II) ions with Alzheimer's amyloid-beta peptide. Metal ion binding, contribution to fibrillization and toxicity. *Metallomics* **2011,** *3*, (3), 250-261.

63. Simmons, L. K.; May, P. C.; Tomaselli, K. J.; Rydel, R. E.; Fuson, K. S.; Brigham, E. F.; Wright, S.; Lieberburg, I.; Becker, G. W.; Brems, D. N. Secondary structure of amyloid beta peptide correlates with neurotoxic activity in vitro. *Molecular Pharmacology* **1994,** *45*, (3), 373-379.

64. Gremer, L.; Schölzel, D.; Schenk, C.; Reinartz, E.; Labahn, J.; Ravelli, R. B.; Tusche, M.; Lopez-Iglesias, C.; Hoyer, W.; Heise, H. Fibril structure of amyloid-β (1–42) by cryo–electron microscopy. *Science* **2017,** *358*, (6359), 116-119.

65. Kirschner, D. A.; Inouye, H.; Duffy, L. K.; Sinclair, A.; Lind, M.; Selkoe, D. J. Synthetic peptide homologous to beta protein from Alzheimer disease forms amyloid-like fibrils in vitro. *Proceedings of the National Academy of Sciences* **1987,** *84*, (19), 6953-6957.

66. Hilbich, C.; Kisters-Woike, B.; Reed, J.; Masters, C. L.; Beyreuther, K. Aggregation and secondary structure of synthetic amyloid βA4 peptides of Alzheimer's disease. *Journal of molecular biology* **1991,** *218*, (1), 149-163.

67. Grünberg, R.; Nilges, M.; Leckner, J. Flexibility and conformational entropy in protein-protein binding. *Structure* **2006,** *14*, (4), 683-693.

68. Teilum, K.; Olsen, J. G.; Kragelund, B. B. Protein stability, flexibility and function. *Biochimica et Biophysica Acta (BBA)-Proteins and Proteomics* **2011,** *1814*, (8), 969-976.

69. Spolar, R. S.; Ha, J.-H.; Record, M. T. Hydrophobic effect in protein folding and other noncovalent processes involving proteins. *Proceedings of the National Academy of Sciences* **1989,** *86*, (21), 8382-8385.

70. Jiang, L.; Liu, C.; Leibly, D.; Landau, M.; Zhao, M.; Hughes, M. P.; Eisenberg, D. S. Structure-based discovery of fiber-binding compounds that reduce the cytotoxicity of amyloid beta. *Elife* **2013,** *2*, e00857.

CHAPTER 4

Published Article

12-crown-4 ether disrupts the Patient Brain-derived Amyloid-βeta Fibril Trimer: Insight from All-atom Molecular Dynamics Simulations

Nikhil Agrawal[1], Adam A. Skelton*[1]

[1]School of Pharmacy and Pharmacology, University of KwaZulu-Natal, Durban, 4001, South Africa

Keywords: Amyloid fibrils, MD simulation, crown ether

Corresponding author: Skelton@ukzn.ac.za (A.A Skelton)

4.1 Abstract

Recent experimental data elucidated that 12-crown-4 ether molecule can disrupt Aβ40 fibrils but the mechanism of disruption remains elusive. We have performed a series of all-atom molecular dynamics simulations to study the molecular mechanism of Aβ40 fibril disruption by 12-crown-4. In the present study we have used the Aβ40 fibril trimer as it is the smallest unit that maintains a stable U-shaped structure, and serves as the nucleus to form larger fibrils. Our study reveals that 12-crown-4 ether can enter into the hydrophobic core region and form competitive, hydrophobic interactions with key hydrophobic residues; these interactions break the inter-sheet hydrophobic interactions and lead to the opening of the U-shaped topology and a loss of β-sheet structure. Furthermore, we observed periods of time when 12-crown-4 was in the hydrophobic core and periods of time when it interacted with Lys28 (chain C), a "tug of war"; the 12-crown-4 binding with Lys28 destabilizes the salt-bridge between Asp23 and Lys28. In addition to the two aforementioned binding modes, the 12-crown-4 binds with Lys16, which is known to form a salt-bridge with Glu22 in antiparallel arranged Aβ fibrils. Our results are in good agreement with experimental results and suggest that molecules that have the ability to interact with both the hydrophobic core region and positively charged residues could serve as potential inhibitors of Aβ fibrils.

4.2 Introduction:

Alzheimer's disease (AD) is the most common form of dementia, accounting for up to 60-80% of all dementia cases[1,2]. AD is caused by misfolding and aggregation of amyloid beta (Aβ) peptide, into amyloid-β-fibrils (Aβ fibrils) and affects the structure and function of neural cells leading to synaptic dysfunction[3,4]. It has been reported that cytotoxicity of Aβ fibrils depends on its morphology and remodeling of Aβ fibrils can significantly reduce its cytotoxicity[5]. Understanding the mechanism of amyloid genesis and disruption allows us to design more effective ways of controlling the disease.

Crown ethers are small, cyclic polyethers that work as cation chelators, and this property of crown ethers has been extensively used in phase-transfer catalysis and in the activation of proteins in organic solvents[6,7,8]. A recent study by Tian *et al*[9] proposed a new strategy to attenuate the aggregation of Aβ through a non-covalent modification at the protein surface. Their experimental results showed that the 12-crown-4 ether caused a reduction in the zeta potential of Aβ40 fibrils, once it was mixed with the 12-crown-4 ether (from -48 mV to -4 mV); this pointed to a reduction in the surface charge upon binding. In addition, anti-aggregation testing results revealed that the presence of 12-crown-4 can reduce the aggregation of Aβ40 peptides in fibrils. Transmission electron microscopy (TEM) images revealed that Aβ40 fibrils, formed in the presence of 12-crown-4, had a different morphology than those in the absence of 12-crown-4 and this could be significant since different morphologies of Aβ fibrils relate to different cytotoxicity[5]. The authors hypothesized that 12-crown-4 interacts with positively charged residues (Lys, Arg, His) and this could attenuate Aβ40 peptide aggregation and affect Aβ fibril conformation.

In another experimental study, Lee *et al.*[10] co-crystallized 18-crown-6 ether with several protein structures and revealed that crown ether specifically interacted with the hydrophobic patches, or with the amine group of Lys; this resulted in dramatic alterations to the protein surface. Das *et al.*[11] revealed by a mutation study that contact between Phe19 and Leu34 are critical for the formation of Aβ40 oligomer; their study showed that altering this interaction drastically reduced the cytotoxicity of Aβ40 oligomers. Chandrakesan *et al.*[12] showed by a Nuclear magnetic resonance spectroscopy (NMR) study that contact between Phe19 and Leu34 plays a crucial role in self-assembly of Aβ fibrils and they suggested that candidate drug molecules, with the ability to disrupt the contact between Phe19 and Leu34, are expected to have a very strong effect on the aggregation of Aβ.

In the present molecular dynamics study, the Aβ40 fibril single trimer unit is used and is shown in Figure: 4.1A; this was taken from the experimental structure formed by three trimeric units (PDB: 2M4J), arranged in three fold symmetry. The particular structure was chosen over other available experimental structures of Aβ40 fibrils because this is the first detailed, experimentally determined structure of any patient brain-derived Aβ aggregate[13]. The Aβ40 fibril structure contains an N-terminal disordered region (residues 1-10), two β-sheets (residues 11-19, and residues 31-38), and a

connecting region. The bend, in the connecting region of two β-sheets in Aβ fibrils, brings the two-sheets in contact through side chain interactions, which leads to a double-sheet structure (U-shaped structure) with a core region (residues 17-36), Figure: 4.1B. The core region can be subdivided into three parts: (1) side chains of Leu17, Phe19, Ala 21, Ile 31, Leu34, and Val36 that form hydrophobic interactions. (2) Side chains of residues Ala 29, Gly30, Ile 32, Gly33, and Met35 face toward the outside and form the hydrophobic face. (3) Side chains of Asp23 and Lys28 form a salt bridge, which plays a crucial role in Aβ fibrils stability[13,14].

Previously, several MD simulation studies have been conducted on the interaction between Aβ fibrils; for example, Lemkul *et al.*[15] has shown that an organic molecule, Morin, can enter into the hydrophobic core and destabilize the salt bridge formed by Asp23-Lsy28. Another study by Tianhan Kai *et al.*[16] has revealed that Tabersonine can interact with β-sheet grooves containing aromatic and hydrophobic residues, which they postulate could affect the elongation process; however, in both of these studies they did not observe the opening of the U-shaped structure of Aβ fibril. To the best of our knowledge no molecular dynamics study of Aβ fibril and an organic molecule has shown the complete opening of the U-shaped topology of Aβ fibril.

In the present study, we aim to find a molecular basis for the Aβ40 fibril remodelling by 12-crown-4. Specifically, the following questions still need to be answered (1) which region does 12-crown-4 bind to? (2) Is there any region on Aβ40 fibril that is particularly favourable or unfavourable for 12-crown-4 binding? (3) What is the impact of 12-crown-4 binding on the conformation of the Aβ40 fibril? To address all these questions we have performed more than 25 all-atom molecular dynamics simulations of Aβ40 fibrils in the presence and absence of 12-crown-4 and investigated the mechanism of Aβ40 disruption by 12-crown-4 ether molecule. 12-crown-4 ether structure has been shown in Figure: 4.1C

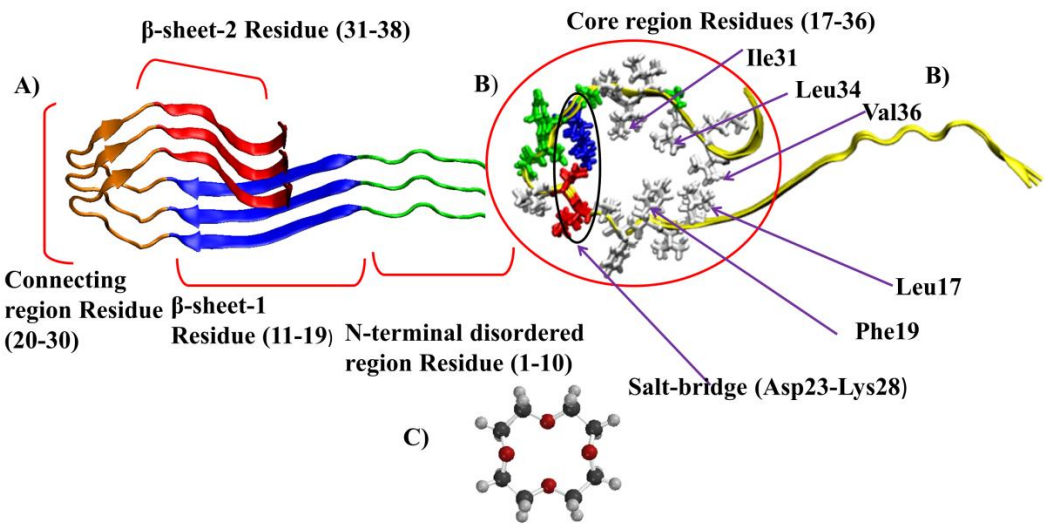

Figure: 4.1 A) Shows the initial structure of Aβ40 fibril containing disordered region (1-10) in green color, β-sheet-1 in blue color (11-19), connecting region in orange color (20-30) and β-sheet-2 in red color (31-38). The Aβ40 fibril trimer is shown in cartoon representation. B) Shows core region residues in liquorice representation colored by residue type: hydrophobic residues (white), negatively charged residues (red), positively charged residues (blue), and polar residues (green). C) Chemical structure of 12-crown-4 molecule.

4.3 Results and Discussion

4.3.1 Insertion of 12-crown-4 in core region and opening of U-shaped structure Aβ40 fibril

Out of a total of 15 independent simulations, 8 simulations showed the spontaneous entering of 12-crown-4 into the core region; in 6 simulations 12-crown-4 interacted with aromatic and hydrophobic residues, was highly stable and an opening event occurred. In all control simulations, the RMSD and "opening" of Aβ40 fibril remained stable and U-shaped topology remained intact (Figure: 4.1S).

Figure: 4.2A shows the time evolution, in one of the representative trajectories, of "entering" of 12-crown-4 in the core region of Aβ40 fibril and U-shaped structure "opening" (see method section for details). Figure: 4.2B shows the change in Aβ40 fibril conformation, monitored by RMSD of residue 11 to 40 backbone atoms. The atomic level representation of the mechanism of entering of 12-crown-4 and the subsequent opening of the U-shaped structure in a step-wise process is shown in Figure: 4.3 (steps A-D).

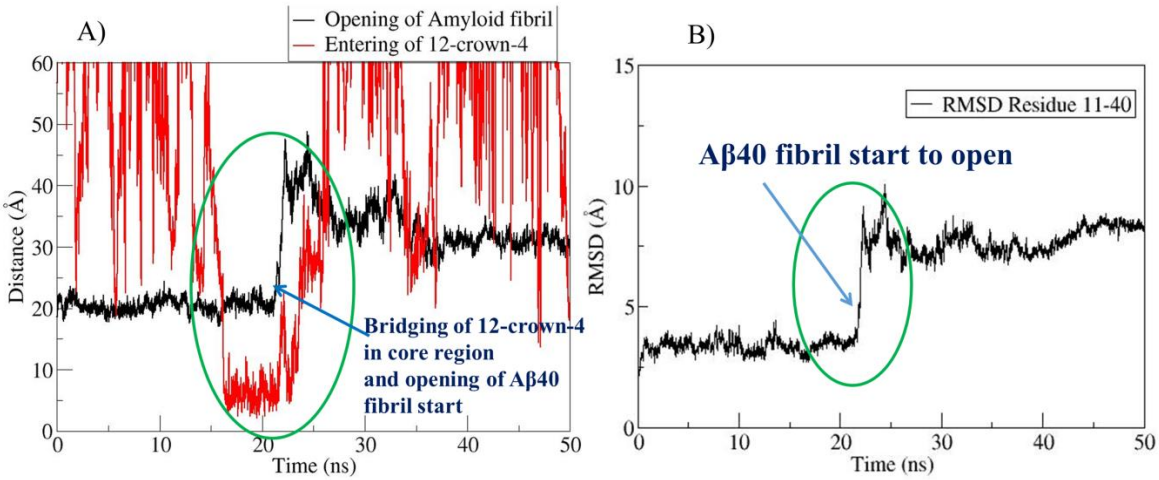

Figure 4.2: A) Shows time evolution of "entering" of 12-crown-4 in core region (red line) and "opening" of U-shaped structure of Aβ40 fibril (black line). B) Shows time evolution of conformational change in Aβ40 fibrils.

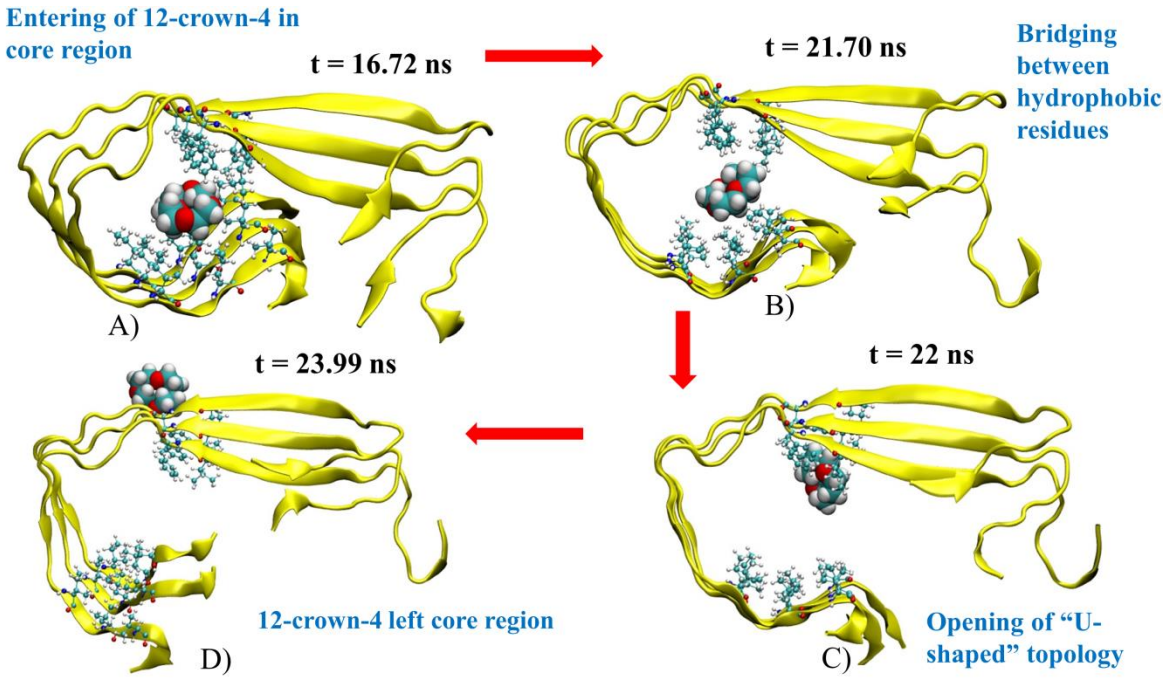

Figure 4.3: Four representative structures taken at different time points in a representative trajectory A) Entering of 12-crown-4 in core region (16.72ns) and making competitive hydrophobic interaction with top and bottom β-sheets residues. B) 12-crown-4 working as a bridge between side chains of top and bottom β-sheets residues (21.70ns). C) Opening of U-shaped topology (22ns). D) 12-crown-4 left the core region.

In step-A, 12-crown-4 enters into the core region at ~16.72 ns, as shown by a decrease in the "entering" value (Figure: 4.2A, red data set); at this time point, competitive interactions were established between 12-crown-4 and, the aromatic and hydrophobic residues of the two opposing β-

sheet residues. In step-B, a bridge is formed between two opposing β-sheet hydrophobic residues (~21.7 ns) (Figure: 4.3B). In step-C, the 12-crown-4/hydrophobic bridge eventually breaks and the two opposing β-sheets do not have the opportunity to reconnect, an opening event occurs (Figure: 4.3C); this results in an increase in the "opening" value (Figure: 4.2A, black data set) and a large increase in RMSD value at 22 ns (Figure: 4.2B). The 12-crown-4 remained bound to the top β-sheet (β-sheet-1) residues for duration of ~2 ns. At ~24 ns there is separation of 12-crown-4 with the core region (Figure: 4.3D).

4.3.2 Deciphering the core region contact sites of 12-crown-4

Now we have observed an event we try to elucidate the mechanism for Aβ40 fibril opening as it is desirable to gain an understanding of the specific interactions and driving forces at play during this process. Figure: 4.4A shows the average distances of all three peptide residues from the COM of 12-crown-4; this illustrates the specific interactions of 12-crown-4, after insertion, in the core region (16 ns to 24 ns). Residues in β-sheet-1 (Leu17 and Phe19) and residues in β-sheet-2, (Ile31, Leu34 and Val36) form a close contact with 12-crown-4 (less than 5 Å). The five aforementioned side chains face each other and form a hydrophobic core (Figure: 4.4B) that plays an important role in maintaining the U-shaped structure of Aβ40 fibril. For further understanding, we calculated the time evolution of the average distance of these residues from the COM of 12-crown-4, during the binding, for all three peptides (Figure: 4.4C). It is revealed that 12-crown-4 first interacts with the bottom β-sheet residues, Leu34, Ile31 and Val36. At the time of bridging and opening (steps B and C), there are increases in the bottom residue—12-crown-4 distances and decreases in the top residue—12-crown-4 distances; these changes occur as 12-crown-4 remains bound to the top residues before completely separating.

Time evolutions of the interaction energy between top (Leu17, Phe19) and bottom residues (Leu34, Val36) (black data set, $\Delta E_{top—bottom}$) and the interaction energy of 12-crown-4 with both top (red data set, $\Delta E_{top—crown}$) and bottom residues (green data set, $\Delta E_{bottom—crown}$), are shown in Figure :4D. Before binding, $\Delta E_{top—bottom}$ is attractive (~ -22 kJ/mol) and at ~14 ns, $\Delta E_{top—bottom}$ becomes less negative when there is a momentary 12-crown-4 interaction. When 12-crown-4 fully enters, at step-A, $\Delta E_{top—bottom}$ is ~ -22 kJ/mol, similar to that of the unbound $\Delta E_{top—bottom}$ value; however, binding of 12-crown-4 causes $\Delta E_{top—bottom}$ to become less negative (~ -13.5 kJ/mol), indicating the role of 12-crown-4 in weakening the interaction between top and bottom residues. When bridging starts, at step-B, $\Delta E_{top—bottom}$ becomes less attractive, becoming zero at step-C; at this point in time, $\Delta E_{bottom—crown}$ abruptly goes to zero as opening starts. $\Delta E_{top—crown}$, however, remains the same at step-C and this value only goes to zero at step-D, as 12-crown-4 completely leaves the core region.

As stated, before entering of 12-crown-4, $\Delta E_{top—bottom}$ is comparable to $\Delta E_{top—crown}$ and $\Delta E_{bottom—crown}$. When taken together $\Delta E_{top—crown}$ and $\Delta E_{bottom—crown}$ (~-24 kJ/mol + ~ -23 kJ/mol = ~-47 kJ/mol) far

exceeds $\Delta E_{top—bottom}$ (~-22 kJ/mol); this provides an energetic basis for the competition between 12-crown-4—hydrophobic residue interaction and top—bottom residues.

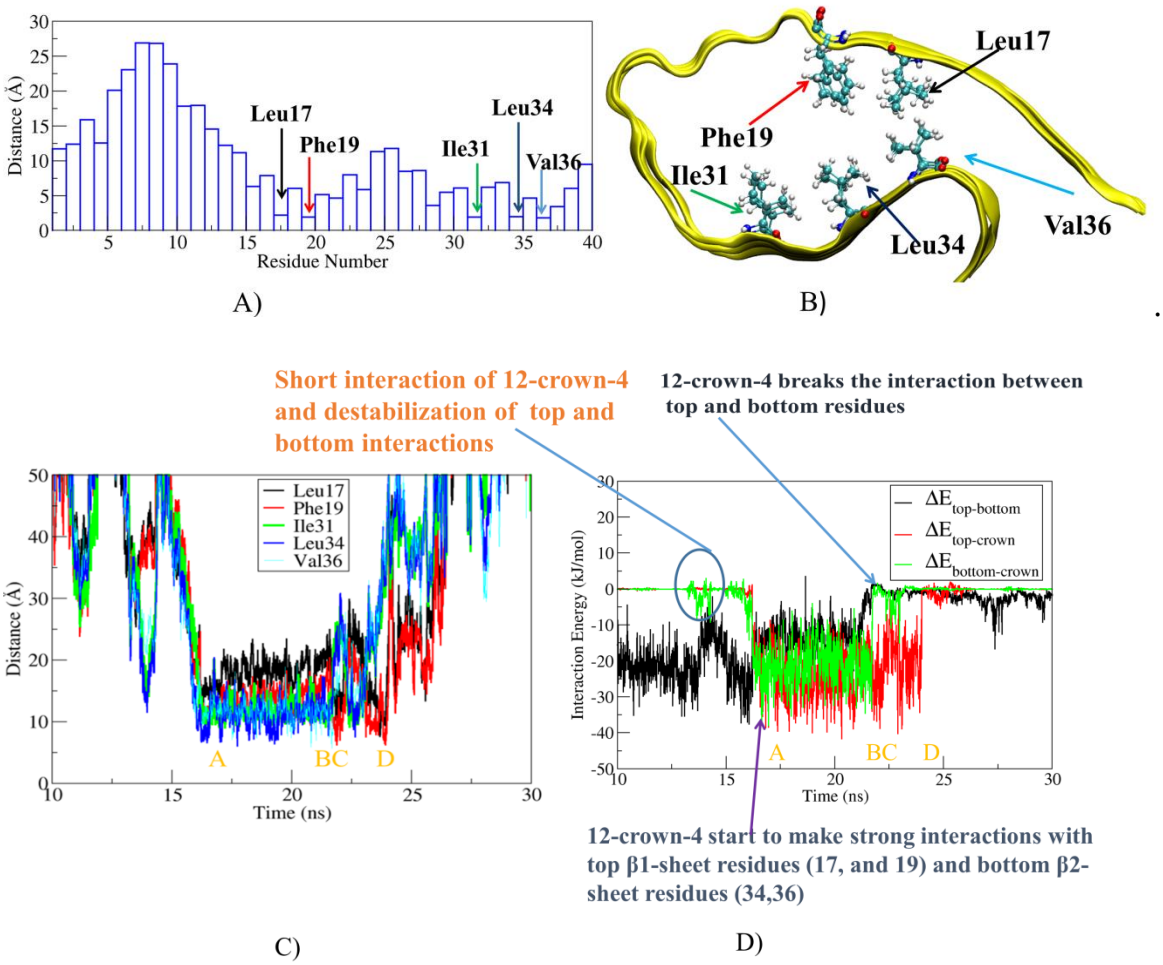

Figure: 4.4: A) The average distance of 12-crown-4 from all three peptide residues during binding (16-24ns). B) The closest distance residues, during binding time, in CPK model and protein has been shown in new cartoon reprsentation. C) Time evolution of distance from closest residues. D) Shows the interaction energy between top and bottom β-sheets residues ($\Delta E_{top—bottom}$), interaction energy between top β-sheet and 12-crown-4 ($\Delta E_{top—crown}$) and bottom β-sheet and 12-crown-4 ($\Delta E_{bottom—crown}$) .

4.3.3 Secondary structure changes

It has previously been shown that the structural stability of the Aβ40 fibril is directly associated with the β-sheet content[17,18]. To investigate the effect of opening of the U-shaped structure on the secondary structure content, we extended one of the simulations for a longer time period; in this simulation opening took place at 10ns. We calculated the time evolution of the secondary structurre

in the bottom β-sheet residues of all three peptide for control (Figure: 4.5 A) and 12-crown-4 (Figure: 4.5 B) simulations.

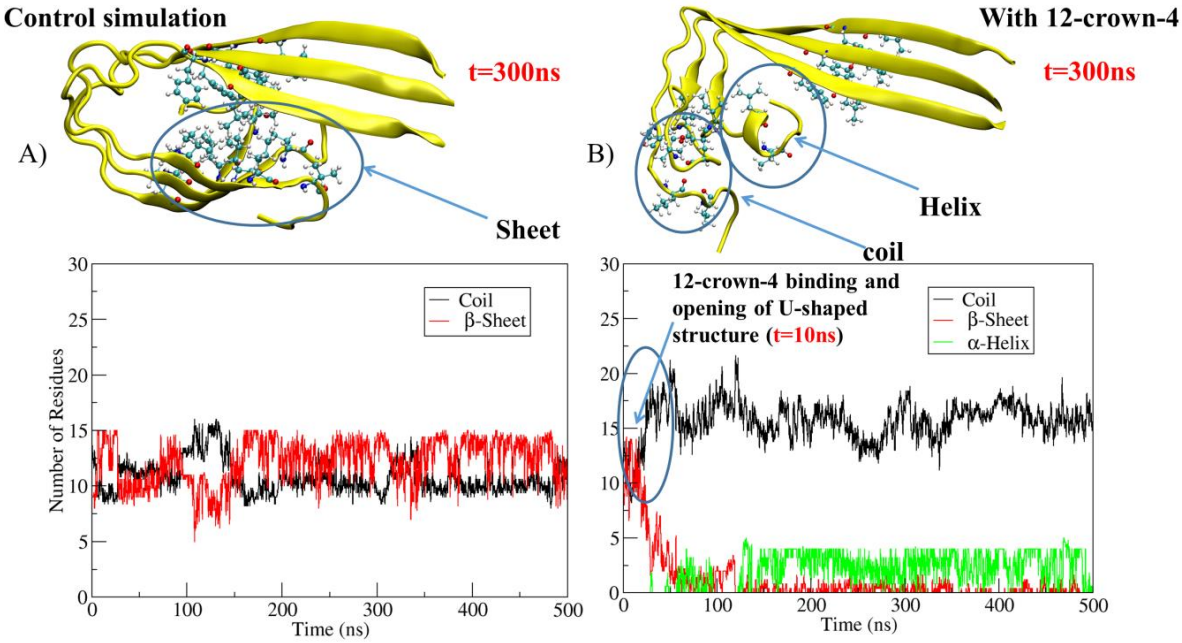

Figure: 4.5 A) Left panel shows representative structure from control simulations at 300ns, and time evoluation of secondary structure change in bottom β-sheets in all three peptides. B) Right panel shows representative structure of Aβ40 fibril with 12-crown-4 simulation at 300ns, and time evoluation of secondary structure change in bottom β-sheets residues of all three peptides.

In the control simulation, the content of β-sheet and coil always remained quiet stable and no α-helix formation was observed; howerver, during the time period between 100-150ns subtle transition were obesrved in β-sheet structute of chain A residues between 32 to 35 in to coil. After that time period they gained there β-sheet content again. In the simulation, in the presence of 12-crown-4; however, we obseved a reduction in β-sheet content and increase in coil content after opening. After ~50ns α-helix content started to form and this stablized after ~150 ns, when ~4 residues maintained the α-helix stucture until the end of the simulation. These results unequivacally show that the 12-crown-4 has not only caused an opening event but when the Aβ40 fibril does open the conformation changes. The result of the conformational changes is that the bottom residues should no longer be able to accommodate the U-shaped structure; therefore, the recombination of top and bottom sheets would require a further comformational change, which should take more time and make this process more unfavorable.

4.3.4 Tug of war of 12-crown-4 between hydrophobic core and Lys28

Since 12-crown-4 contains both oxygen and hydrocarbon groups, it should be able to from both hydrogen bonding/electrostatic interactions with hydrophilic groups and, van der Waals/hydrophobic interactions with hydrophobic residues. This amphiphilic behaviour was observed in two simulations,

where 12-crown-4 entered into the core region yet no opening event took place; however, we obseved periods of time when the 12-crown-4 was in the hydrophobic core and periods of time when it interacted with Lys28 (chain C), a "tug of war" (Figure: 4.6A). First, 12-crown-4 entered into the core region, in a similar fashion to that described above; it entered at ~12 ns and stayed there until ~33ns (Figure : 4.6C, green line). At ~33 ns, 12-crown-4 shifted towards Lys28 of chain C and formed hydrogen bonds (Figure: 4.6B, Figure: 4.6C, black line); this broke the salt-bridge formed by Aps23 and Lys28 (Figure: 4.6 C, red line). At ~70ns the 12-crown-4 broke contract with Lys28, the salt bridge reformed and the 12-crown-4 shifted back to the hydrophobic core region. At ~75ns the 12-crown-4 left the hydrophobic region and in fact the whole Aβ40 fibril.

To understand the enegetic interplay between 12-crown-4 binding with Lys28 and the hyrophobic core, we calculated the time evolution of the interaction energy between 12-crown-4 and Lys28 ($\Delta E_{Lys28—crown}$), the interaction between 12-crown-4 and the hyrophobic core residues ($\Delta E_{hydrophobic—crown}$) and the interaction energy between Asp23 and Lys28 ($\Delta E_{Asp23—Lys28}$); these are shown in Figure: 4.6D, black, green and red lines, respectively. The 12-crown-4 interacts with the hyrophobic core resulting in the $\Delta E_{hydrophobic—crown}$ value of ~-53 kJ/mol and when 12-crown-4 shifts to Lys28, it strongly interacts with a $\Delta E_{Lys28—crown}$ value of ~-230 kJ/mol. At the start of the simulation, when the salt bridge is fully formed, $\Delta E_{Aps23\text{-}Lys28}$ is hugely attractive at ~ -410 kJ/mol (Figure: 4.6D red); 12-crown—Lys28 interaction, however, destablizes the salt-bridge interaction, making $\Delta E_{Asp23\text{-}Lys28}$ less favorable (~ -220 kJ/mol). It should be noted that $\Delta E_{Lys28—crown}$ was much higher than $\Delta E_{hydrophobic—crown}$; there could be three possibile reasons that 12-crown-4 shifted back to the hydrophobic core (1) There are a greater number of residues in the hyrophobic core, so 12-crown-4 has a greater opporunity to interact. (2) There is competition between Asp23 (salt-bridge) and 12-crown-4 for binding to Lys28. (3) There is greater competition of Lys28 with water molecules than that of the hydrophobic residues. In order to bind to Lys28, 12-crown-4 must displace ordered water molecules that are hydrogen bonded to the $-NH_3^+$ group (on average a reduction of 1.50 water molecules in the first solvation shell, see Table: 4.1S). The number of water molecules that are displaced is far fewer for the hyrophobic resdues; for example, on average there is a reduction of 0.04 and 0.19 water molecules, respectively, upon binding to the central chain (chain B) Phe19 and Leu34 residues.

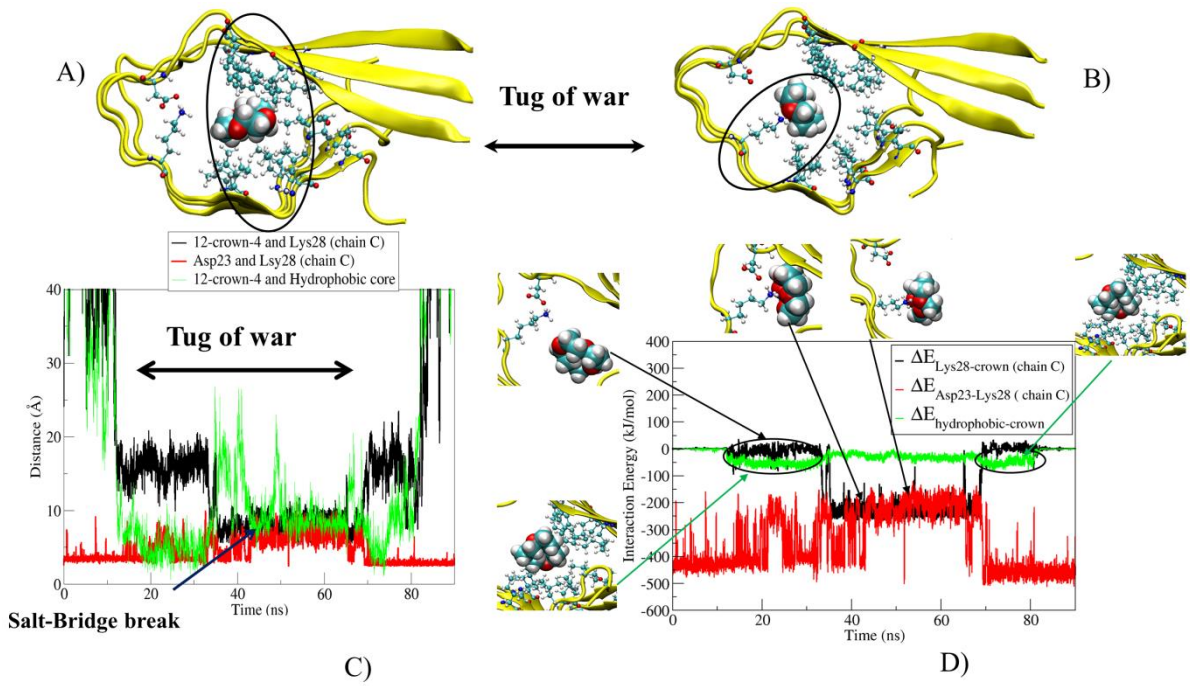

Figure: 4.6 A) Shows the representative structure of 12-crown-4 with hyrophobic core residues during binding. B) Shows the representative structure of 12-crown-4 with Lys28 chain C during binding. C) Shows the distance of 12-crown-4 from hyrophobic core, 12-crown-4 and Lys28 distance and salt-bridge distance between Asp23 and Lys28.

4.3.5 Interaction with Lys16

Various studies have shown that Lys16 and Glu22. with their opposite positive and negative charges, form electrostatic interactions and this favours the Aβ fibrils arrangement in-register antiparallel alignment[19]. An interaction of 12-crown-4, with either Lys16 or Glu22, should therefore, hinder such alignment, decreasing the extent of amyloid fibril formation; 12-crown-4 interaction with Lys16 was, in fact, observed in four simulations.

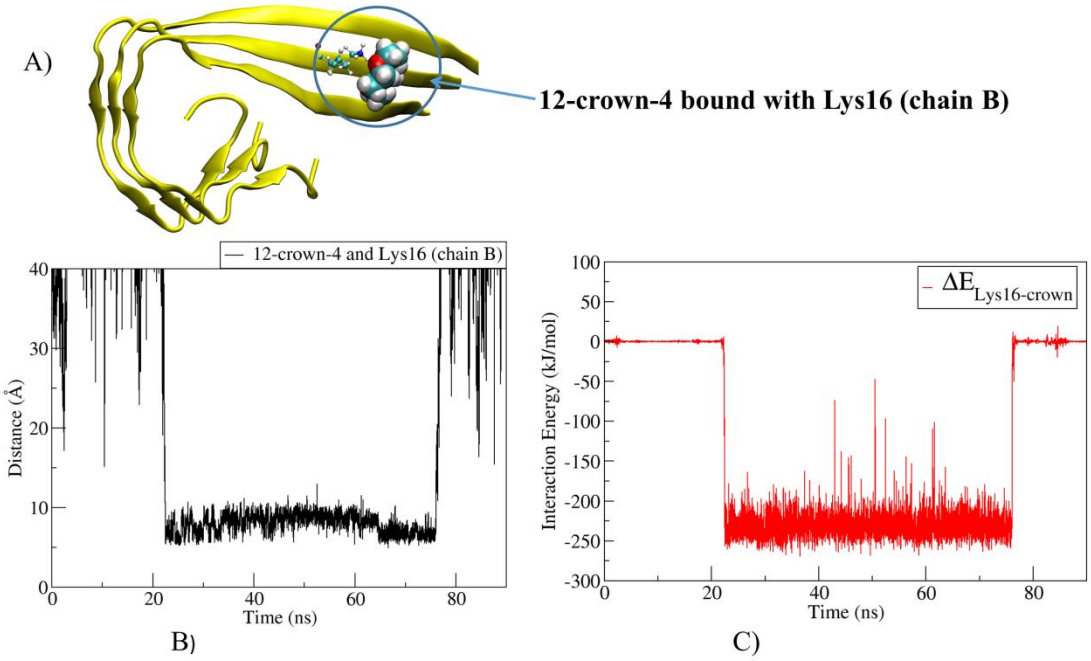

Figure: 4.7 A) Shows the representative structure of 12-crown-4 bound on Aβ40 fibrils. B) Shows the time evolution of distance between 12-crown-4 and Lys16 of chain B. C) Shows the time evolution of interaction energy between 12-crown-4 and Lys16 of chain B.

Figure: 4.7A shows the Lys28—12-crown-4 distance and Figure: 7B shows the interaction energy between Lys 28 and 12-crown-4 ($\Delta E_{Lys16—crown}$). 12-crown-4 binds to Lys16 at ~22 ns and remains bound until ~76 ns (for ~ 45 ns). The $\Delta E_{Lys16—crown}$ value was ~ -230 kJ/mol during the binding, which is similar to that of $\Delta E_{Lys28—crown}$.

To bind to Lys16, 12-crown-4 needs to displace, on average, 2.7 water molecules from the first solvation shell (supplementary table: 4.1S). The number of water molecules that get displaced is greater for Lys16 than for Lys28 because, in the absence of 12-crown-4 interaction, there are more water molecules available to interact with Lys16 (4.62 water molecules) than for Lys28 (3.27), Figure: 4S, 5S; this is because part of the coordination of Lys28 is taken up by the salt-bridge between Asp23 but Lys16 is not engaged in a salt-bridge. The amount of structured water molecules, around –NH_3^+, after coordination with 12-crown-4 is comparable for Lys16 and Lys28 (approximately 1.8 water molecules on average) since the 12-crown-4 causes a break in the Asp23-Lys28 salt-bridge.

4.3.6 Binding free energy and energetic contribution

The binding free energy of 12-crown-4 with Aβ40 fibril (ΔG_{total}) was evaluated by the MM-PBSA method (see the method section for more details), during the time of 12-crown-4 binding with Aβ40 fibril for all three binding modes (Table: 4.1). The contribution to ΔG_{total} from van der Waals and electrostatic interactions is denoted ΔE_{vdw} and ΔE_{elec}. Polar and nonpolar contributions to ΔG_{total} have been denoted by ΔG_{polar} and $\Delta G_{non\text{-}polar}$, respectively. As expected, Mode-3 and Mode-2/*Lys28* have

greater overall binding than Mode-2/*hydrophobic* and Mode-1. Since, in Mode-1 and Mode-2/*hydrophobic*, the binding contains hydrophobic residues, the Van der Waals energy is the most favourable contributor; however, the electrostatic energy is the most favourable contributor in Mode-2/*Lys28* and, Mode-3/*Lys16*. The ΔG_{polar} value, which is always unfavourable for the 12-crown-4-Aβ40 fibril complexes, is less unfavourable in case of the hydrophobic core binding sites compared to Lys binding sites. For the latter case, the total gain in intermolecular electrostatic interaction compensates an increase in polar solvation energy.

Contribution	**Mode-1** ***Hydrophobic*** **Energy (kJ/mol)** **(16-22ns)**	**Mode-2** **Energy (kJ/mol)**		**Mode-3** ***Lys16*** **Energy (kJ/mol)** **(23-50ns)**
		Hydrophobic (12-32ns)	*Lys28* (40-60ns)	
ΔE_{vdw}	-58.28 ± 0.95	-62.83 ± 0.57	-41.69 ± 0.88	-22.11 ± 0.64
ΔE_{elec}	-1.76 ± 0.73	-12.72 ± 1.47	-214.56 ± 2.04	-230.34 ± 1.41
ΔG_{polar}	20.02 ± 0.63	31.41 ± 1.15	160.47 ± 1.24	150.15 ± 0.99
$\Delta G_{non\text{-}polar}$	-9.63 ± 0.12	-10.25 ± 0.07	-9.51 ± 0.10	-6.031 ± 0.05
ΔG_{total}	-49.63 ± 1.18	-54.43 ± 0.99	-105.36 ± 1.27	-108.22 ± 0.76

Table: 4.1 Average binding energy and its components obtained from the MM-PBSA calculations for Aβ40 fibril-12-crown-4 complex, all energies are in kJ/mol.

To gain even more detailed thermodynamic insight into the total binding energy, the binding energies were further decomposed into individual residue contributions and are shown in Figure: 4.8. The decomposition of binding energy per residue constitutes ΔE_{vdw}, ΔE_{elec}, ΔE_{polar} and $\Delta E_{non\text{-}polar}$. It is revealed that, in Mode-1 and Mode-2/*hydrophobic*, the binding energy contribution is distributed amongst several residues of the core region (Phe19, Leu17, Lys28, Lue34, Val36); in the case of Mode-2/*lys28* and Mode-3/*lys16*, however, the only significant binders are Lys28 and Lys16. In Mode-1, Asp23, Val24 and Mode-2 (*hydrophobic* and *Lys28*) the negatively charged Asp23 has unfavourable contributions to the binding energy.

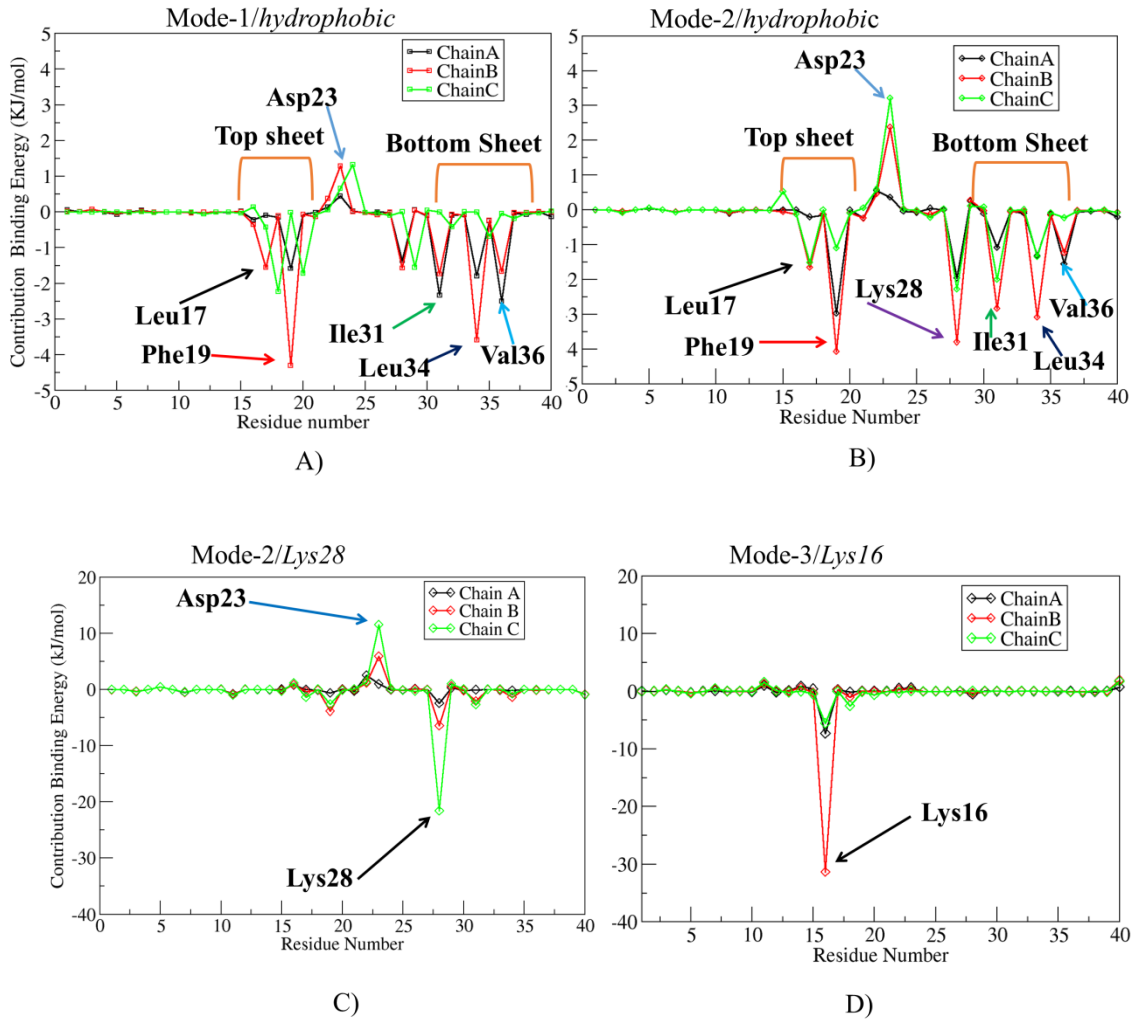

Figure: 4.8 A) Residue contributions to binding energy in Mode-1/ *hydrophobic* (U-shaped structure opening). B) Residue contributions to binding energy in Mode-2/*hydrophobic* (Tug of war). C) Residue contributions to binding energy of Mode-2/*Lys28* (Tug of War). D) Residue contributions to binding energy of Mode-3/*Lys16*.

4.4 Perspective and concluding remarks

Similar binding modes were observed, experimentally and theoretically, for 18-crown-6 with several proteins (but not Aβ fibrils).[10]. The crown ether specially interacts with hydrophobic patches forming Van der Waals interactions with aromatic or aliphatic residues. Moreover, binding between the crown and a single Lys or Lys in the vicinity of hydrophobic residues was observed. Our data also supports the hypothesis by Tian *et. al.*[9] that 12-crown-4 can form hydrogen bonds with positively charged residues, especially with Lys16 and Lys28, and destabilizes the salt-bridges formed by these residues. Various studies have shown that the salt-bridge between Asp23-Lys28 plays a crucial role in structure stability and cytotoxicity[20,21,22]. Other experimentally known, structurally distinct inhibitor molecules, such as Congo red, Naproxen, Ibuprofen, and Curcumin are shown to bind to Lys28 using docking

and MD simulations studies[23,24]. The salt-bridge formed between Lys16-Glu22 plays an important role in stabilizing the structure of Aβ fibrils in antiparallel arrangement. If the 12-crown-4 binds to Lys16, it could destabilize such antiparallel Aβ fibrils.

Many studies have shown that side-chain interlocking of hydrophobic residues in the core region play a crucial role in the U-shaped structure stability[25,26,27]. In particular Chandrakesan *et al.*[12], showed that contact between Phe19 and Leu34 is crucial for Aβ fibrils formation and suggested that Phe19 and Lue34 provides considerable stabilization for aggregation; the authors proposed that disrupting the contact between Phe19 and Leu34 is expected to have a very strong effect on the aggregation of Aβ fibrils. A study by Das *et al.* showed that contact between Phe19 and Leu34 plays an important role in Aβ40 oligomer cytotoxicity[11]. Control simulation data in the present study (Aβ40 fibril trimer in absence of 12-crown-4) revealed that the Aβ40 fibril trimer maintained hydrophobic side-chain contact in the core region in all simulation trajectories; this helped it to retain its U-shaped topology. A MD simulation study by Buchete *et al* [28] suggested that hydrophobic interactions, stabilizing the C-terminal β-sheet, play a crucial role in the elongation of Aβ fibril. A study by Horn *et al.* [29] revealed that the Aβ trimer is the smallest unit that can maintain the U-shaped structure and is a potential seed for fibril elongation. It should, therefore, be considered that a disruption of these hydrophobic interactions and the U-shaped structure, as observed in the present study, could indeed affect elongation. Taken together all these data, we propose that 12-crown-4 binding to hydrophobic core residues (Phe19, Leu34) and positively charged Lys16, Lys28 could significantly reduce the cytotoxicity, structure stability and the elongation process.

Studies on oral toxicity of 12-crown-4 in mice and rats showed that 12-crown-4 had median lethal dose (LD_{50}) values of 3.15 grams/ Kg and 2.8 grams/Kg, respectively[30,31]. A further dermal toxicity study in rabbits revealed that the LD_{50} value was 4.5 grams/Kg[32]. Since different organisms have been used in testing the toxicity, without further studies, it would be difficult to generalize 12-crown-4 toxicity. This study, however, has shown the chemical features that could be required to design an effective Aβ fibril inhibitor; that is, 12-crown-4 contains both hydrophilic oxygen atoms and hydrophobic hydrocarbon groups.

In summary, we have studied the effect of 12-crown-4 on Aβ40 fibril trimer by performing simulations in the presence and absence of 12-crown-4; we observed three possible binding modes of 12-crown-4 on Aβ40 fibril. First, the 12-crown-4 can enter into the hydrophobic core and interact with hydrophobic residues by Van der Waals interactions; when this occurs there is a disruption of the hydrophobic interactions between two β-sheets and this leads to the opening of the U-shaped structure and drastic conversion of β-sheet into random coil and α-helix. The second mode involves a “tug of war”, where the 12-crown-4 enters into the hydrophobic core but instead of causing an opening event, it subsequently moves towards the Asp23-Lys28 salt bridge, causing it to break. Lastly, there is significant binding of 12-crown-4 with Lys16, which is implicated in stabilizing the structure of Aβ fibrils in antiparallel arrangement. The present study deepens our knowledge of how a candidate

molecule can remodel Aβ40 fibril and provides information that can be used in the design of new, potential drugs; therefore, provides new avenues for Aβ40 fibril inhibition.

4.5 Methods

4.5.1 12-crown-4 ether structure and force field

The 12-crown-4 is a cyclic ether molecule and the coordinate for 12-crown-4 ether was taken from PubChem compound library (CID: 9269)[33]. The force field parameters of 12-crown-4 ether molecule were derived from the Charmm Additive and Classical Drude Polarizable Force Fields for Linear and Cyclic Ethers (ACDPFF)[34]. Parameters for 12-crown-4 cyclic ether are provided in Table: 4.2S).

4.5.2 Simulation protocol

All simulations were performed using the GROMACS 4.6.3[35] molecular dynamics program. The Charmm36 force field[36] was used for the Aβ40 fibril trimer, which were solvated using the TIP3P water model[37]. Systems of Aβ40 fibril with 12-crown-4 contain 22518 water molecules and systems of the Aβ40 fibril, in the absence of 12-crown-4, contain 18347 water molecules. Nine Na^+ counter ions were added to neutralize the systems. All systems were energy minimized using 5000 steepest descent steps[38]. The systems were then equilibrated for 100 ps using the cononical (NVT) ensemble, followed by a further 100 ps of equilibration simulation with the isobaric-isothermic (NPT) ensemble. The production run for all systems were performed in the NPT ensemble. The LINCS[39] algorithm was used to constrain the hydrogen bond lengths of the Aβ40 fibril and 12-crown-4 molecule. Water molecule bond lengths were constrained with the SETTLE[40] algorithm, which allowed an integration time step of 2 fs. Long-range electrostatic interactions were calculated using the particle mesh Ewald (PME)[41] method with a real space cut-off of 1.2 nm. The van der Waals (vdW) interactions were calculated using a cut off of 1.2 nm. The Aβ40 fibril was separately coupled to the external temperature and pressure baths and the non-protein components, 12-crown-4, water and ions were together, coupled to the external temperature and pressure baths using velocity-rescale[42], and Parrinello−Rahman[43] methods. All MD simulations were performed at a temperature of 310 K and a pressure of 1 bar. The coupling times of the temperature and pressure were 0.1 ps and 1.0 ps, respectively.

Set I: Control Aβ40 trimer simulations

To explore the inherent conformational changes, and to check the stability of the U-shaped topology in the absence of 12-crown-4, two sets of control simulations were performed, three long (500 ns) and five short simulations (100 ns) using random initial velocities.

Set II. Aβ40 trimer with 12-crown-4

The 12-crown-4 and Aβ40 fibril systems consist of an Aβ40 fibril trimer and six 12-crown-4 molecules randomly placed at a minimum distance of 12 Å from the trimer (Figure: 4.1C). The systems were prepared as described previously and an additional six 12-crown-4 molecules were added before solvating the system. 15 simulations were performed with random initial velocities and the simulation time was different for all trajectories. In our simulations we did not apply any restraints or prior contact between Aβ40 fibril and 12-crown-4 molecule.

4.5.3 Analysis details

Interaction and binding energies between the Aβ40 fibril and the 12-crown-4 was calculated using Molecular Mechanics–Poisson Boltzmann Surface Area (MM-PBSA), implemented in g_mmpbsa package[44]. The structural stability of the trimer was measured by root-mean-square deviation (RMSD) of the backbone atoms, of residues 11-40, with respect to the energy minimized structure. "Opening" of the U-shaped topology was defined by the centre of mass (COM) distance between residue 16- 20 (top β-sheet) and residue 33-40 (bottom β-sheet) of all three peptides (Figure: 4.9A). Entering of 12-crown-4 inside the core region is defined by COM distance between 12-crown-4 and residues 16-36 (Figure: 4.9B). Secondary structure analysis was performed using the dictionary secondary structure of protein (DSSP)[45].

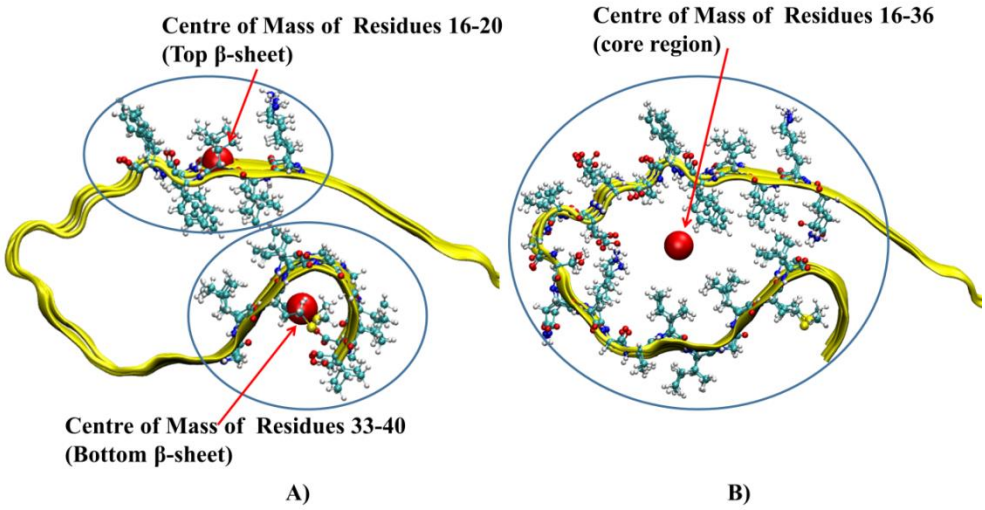

Figure: 4.9 A) Centre of mass (COM) of Residues 16-20 and COM of Residues 33-40. B) COM of Residues 16-36.

4.6 Supporting Information

The Supporting Information is available free of charge on the ACS Publications website at DOI: 10.1021/acschemneuro. 6b00185.

Results for control simulations (500 ns), entering and opening of two other trajectories, displacement of water molecules upon binding, and force field parameters for

12-crown-4 (PDF) Two simulation movies: (1) entering and opening and (2) "Tug of war" (ZIP)

Notes

The authors declare no competing financial interest.

ACKNOWLEDGMENTS

We are indebted to Centre for High Performance Computing (CHPC) in Cape Town, South Africa and UKZN "hippo" super computer facility, Durban, South Africa for computational resources. We would like to thank college of Health Sciences at UKZN for funding and N.A. is in debt to National Research Foundation, South Africa for funding the project (grant number: 101323). N.A. is an "innovation doctoral scholarship" fellow funded by National Research Foundation, South Africa.

4.7 Refernces

[1] Braun, U., Muldoon, S. F., and Bassett, D. S. (2015) On human brain networks in health and disease, *eLS*.

[2] Association, A. s. (2016) 2016 Alzheimer's disease facts and figures, *Alzheimer's & Dementia 12*, 459-509.

[3] Selkoe, D. J., and Hardy, J. (2016) The amyloid hypothesis of Alzheimer's disease at 25 years, *EMBO molecular medicine 8*, 595-608.

[4] Nelson, A. R., Sweeney, M. D., Sagare, A. P., and Zlokovic, B. V. (2016) Neurovascular dysfunction and neurodegeneration in dementia and Alzheimer's disease, *Biochimica et Biophysica Acta (BBA)-Molecular Basis of Disease 1862*, 887-900.

[5] Petkova, A. T., Leapman, R. D., Guo, Z., Yau, W.-M., Mattson, M. P., and Tycko, R. (2005) Self-propagating, molecular-level polymorphism in Alzheimer's ß-amyloid fibrils, *Science 307*, 262-265.

[6] Macdonald, C. L. (2016) Polyether complexes of groups 13 and 14, *Chemical Society Reviews*.

[7] Paul, D., Suzumura, A., Sugimoto, H., Teraoka, J., Shinoda, S., and Tsukube, H. (2003) Chemical activation of cytochrome c proteins via crown ether complexation: cold-active synzymes for enantiomer-selective sulfoxide oxidation in methanol, *Journal of the American Chemical Society 125*, 11478-11479.

[8] Mistarz, U. H., Brown, J. M., Haselmann, K. F., and Rand, K. D. (2016) Probing the Binding Interfaces of Protein Complexes Using Gas-Phase H/D Exchange Mass Spectrometry, *Structure 24*, 310-318.

[9] Tian, Y., Zhang, X., Li, Y., Shoup, T. M., Teng, X., Elmaleh, D. R., Moore, A., and Ran, C. (2014) Crown ethers attenuate aggregation of amyloid beta of Alzheimer's disease, *Chemical Communications 50*, 15792-15795.

[10] Lee, C. C., Maestre-Reyna, M., Hsu, K. C., Wang, H. C., Liu, C. I., Jeng, W. Y., Lin, L. L., Wood, R., Chou, C. C., and Yang, J. M. (2014) Crowning proteins: modulating the protein surface properties using crown ethers, *Angewandte Chemie International Edition 53*, 13054-13058.

[11] Das, A. K., Rawat, A., Bhowmik, D., Pandit, R., Huster, D., and Maiti, S. (2015) An early folding contact between Phe19 and Leu34 is critical for amyloid-β oligomer toxicity, *ACS chemical neuroscience 6*, 1290-1295.

[12] Chandrakesan, M., Bhowmik, D., Sarkar, B., Abhyankar, R., Singh, H., Kallianpur, M., Dandekar, S. P., Madhu, P. K., Maiti, S., and Mithu, V. S. (2015) Steric Crowding of the Turn Region Alters the Tertiary Fold of Amyloid-β18–35 and Makes It Soluble, *Journal of Biological Chemistry 290*, 30099-30107.

[13] Lu, J.-X., Qiang, W., Yau, W.-M., Schwieters, C. D., Meredith, S. C., and Tycko, R. (2013) Molecular structure of β-amyloid fibrils in Alzheimer's disease brain tissue, *Cell 154*, 1257-1268.

[14] Petkova, A. T., Ishii, Y., Balbach, J. J., Antzutkin, O. N., Leapman, R. D., Delaglio, F., and Tycko, R. (2002) A structural model for Alzheimer's β-amyloid fibrils based on experimental constraints from solid state NMR, *Proceedings of the National Academy of Sciences 99*, 16742-16747.

[15] Lemkul, J. A., and Bevan, D. R. (2010) Destabilizing Alzheimer's Aβ42 protofibrils with Morin: mechanistic insights from molecular dynamics simulations, *Biochemistry 49*, 3935-3946.

[16] Kai, T., Zhang, L., Wang, X., Jing, A., Zhao, B., Yu, X., Zheng, J., and Zhou, F. (2015) Tabersonine inhibits amyloid fibril formation and cytotoxicity of Aβ (1–42), *ACS chemical neuroscience 6*, 879-888.

[17] Viet, M. H., Ngo, S. T., Lam, N. S., and Li, M. S. (2011) Inhibition of aggregation of amyloid peptides by beta-sheet breaker peptides and their binding affinity, *The Journal of Physical Chemistry B 115*, 7433-7446.

[18] Zhao, L. N., Chiu, S.-W., Benoit, J. r. m., Chew, L. Y., and Mu, Y. (2012) The effect of curcumin on the stability of Aβ dimers, *The Journal of Physical Chemistry B 116*, 7428-7435.

[19] Klimov, D. K., and Thirumalai, D. (2003) Dissecting the assembly of Aβ 16–22 amyloid peptides into antiparallel β sheets, *Structure 11*, 295-307.

[20] Schledorn, M., Meier, B. H., and Böckmann, A. (2015) Alternative salt bridge formation in Aβ—a hallmark of early-onset Alzheimer's disease?, *Frontiers in Molecular Biosciences 2*.

[21] Tarus, B., Straub, J. E., and Thirumalai, D. (2006) Dynamics of Asp23-Lys28 salt-bridge formation in Aβ10-35 monomers, *Journal of the American Chemical Society 128*, 16159-16168.

[22] Ma, B., and Nussinov, R. (2002) Stabilities and conformations of Alzheimer's β-amyloid peptide oligomers (Aβ16–22, Aβ16–35, and Aβ10–35): sequence effects, *Proceedings of the National Academy of Sciences 99*, 14126-14131.

[23] Ngo, S. T., and Li, M. S. (2012) Curcumin binds to Aβ1–40 peptides and fibrils stronger than ibuprofen and naproxen, *The Journal of Physical Chemistry B 116*, 10165-10175.

[24] Keshet, B., Gray, J. J., and Good, T. A. (2010) Structurally distinct toxicity inhibitors bind at common loci on β-amyloid fibril, *Protein Science 19*, 2291-2304.

[25] Bitan, G., Kirkitadze, M. D., Lomakin, A., Vollers, S. S., Benedek, G. B., and Teplow, D. B. (2003) Amyloid β-protein (Aβ) assembly: Aβ40 and Aβ42 oligomerize through distinct pathways, *Proceedings of the National Academy of Sciences 100*, 330-335.

[26] Kreutzer, A. G., Hamza, I. L., Spencer, R. K., and Nowick, J. S. (2016) X-ray Crystallographic Structures of a Trimer, Dodecamer, and Annular Pore Formed by an Aβ17–36 β-Hairpin, *Journal of the American Chemical Society 138*, 4634-4642.

[27] Ahmed, M., Davis, J., Aucoin, D., Sato, T., Ahuja, S., Aimoto, S., Elliott, J. I., Van Nostrand, W. E., and Smith, S. O. (2010) Structural conversion of neurotoxic amyloid-[beta] 1-42 oligomers to fibrils, *Nature structural & molecular biology 17*, 561-567.

[28] Buchete, N.-V., and Hummer, G. (2007) Structure and dynamics of parallel β-sheets, hydrophobic core, and loops in Alzheimer's Aβ fibrils, *Biophysical journal 92*, 3032-3039.

[29] Horn, A. H., and Sticht, H. (2010) Amyloid-β42 oligomer structures from fibrils: a systematic molecular dynamics study, *The Journal of Physical Chemistry B 114*, 2219-2226.

[30] Hendrixson, R. R., Mack, M. P., Palmer, R. A., Ottolenghi, A., and Ghirardelli, R. G. (1978) Oral toxicity of the cyclic polyethers—12-crown-4, 15-crown-5, and 18-crown-6—in mice, *Toxicology and applied pharmacology 44*, 263-268.

[31] Gad, S., Conroy, W., McKelvey, J., and Turney, K. (1978) Behavioral and Neuropuarmacological Toxicology of the Macrocyclic Ether 18-Ckown-6, *Drug and chemical toxicology 1*, 339-353.

[32] Gad, S., Reilly, C., Siino, K., Gavigan, F., and Witz, G. (1985) Thirteen Cationic I0n0ph0res: Their Acute Toxicity, Neurobehavioral and Membrane Effects, *Drug and chemical toxicology 8*, 451-468.

[33] Wang, Y., Xiao, J., Suzek, T. O., Zhang, J., Wang, J., and Bryant, S. H. (2009) PubChem: a public information system for analyzing bioactivities of small molecules, *Nucleic acids research*, gkp456.

[34] Vorobyov, I., Anisimov, V. M., Greene, S., Venable, R. M., Moser, A., Pastor, R. W., and MacKerell, A. D. (2007) Additive and classical drude polarizable force fields for linear and cyclic ethers, *Journal of chemical theory and computation 3*, 1120-1133.

[35] Van Der Spoel, D., Lindahl, E., Hess, B., Groenhof, G., Mark, A. E., and Berendsen, H. J. (2005) GROMACS: fast, flexible, and free, *Journal of computational chemistry 26*, 1701-1718.

[36] Huang, J., and MacKerell, A. D. (2013) CHARMM36 all-atom additive protein force field: Validation based on comparison to NMR data, *Journal of computational chemistry 34*, 2135-2145.

[37] Jorgensen, W. L., Chandrasekhar, J., Madura, J. D., Impey, R. W., and Klein, M. L. (1983) Comparison of simple potential functions for simulating liquid water, *The Journal of chemical physics 79*, 926-935.

[38] Bixon, M., and Lifson, S. (1967) Potential functions and conformations in cycloalkanes, *Tetrahedron 23*, 769-784.

[39] Hess, B., Bekker, H., Berendsen, H. J., and Fraaije, J. G. (1997) LINCS: a linear constraint solver for molecular simulations, *Journal of computational chemistry 18*, 1463-1472.

[40] Miyamoto, S., and Kollman, P. A. (1992) SETTLE: an analytical version of the SHAKE and RATTLE algorithm for rigid water models, *Journal of computational chemistry 13*, 952-962.

[41] Darden, T., York, D., and Pedersen, L. (1993) Particle mesh Ewald: An N· log (N) method for Ewald sums in large systems, *The Journal of chemical physics 98*, 10089-10092.

[42] Bussi, G., Donadio, D., and Parrinello, M. (2007) Canonical sampling through velocity rescaling, *The Journal of chemical physics 126*, 014101.

[43] Parrinello, M., and Rahman, A. (1981) Polymorphic transitions in single crystals: A new molecular dynamics method, *Journal of Applied physics 52*, 7182-7190.

[44] Kumari, R., Kumar, R., and Lynn, A. (2014) g_mmpbsa A GROMACS Tool for High-Throughput MM-PBSA Calculations, *Journal of chemical information and modeling 54*, 1951-1962.

[45] Frishman, D., and Argos, P. (1997) Seventy-five percent accuracy in protein secondary structure prediction, *Proteins-Structure Function and Genetics 27*, 329-335.

CHAPTER 5

Submitted Article

Binding of Alzheimer's $A\beta_{9-40}$ Fibrils with Cholesterol-rich DPPC Bilayer: Insight from Coarse-Grained Molecular Dynamics Simulations

Nikhil Agrawal* and Adam A Skelton*

College of Health Sciences, Discipline of Pharmaceutical Sciences, University of KwaZulu-Natal, Westville, Durban 4001, South Africa

***corresponding authors:** nikhil.08oct@gmail.com, dradamskelton@gmail.com

5.1 Abstract

Alzheimer's disease is the most common form of dementia characterized by misfolding and aggregation of amyloid-β (Aβ) peptides into β-sheet rich Aβ oligomers/fibrils. Experimental studies have suggested that Aβ oligomers/fibrils interact with the neuronal cell membranes and perturb their structures and dynamics. However, the molecular mechanism of Aβ oligomers/fibrils interaction with the neuronal membranes remained elusive. In present work, we have performed more than 8 μs simulations of $A\beta_{9-40}$ fibrils hexamer with cholesterol-rich DPPC bilayer, which are the most abundant lipids in the neuronal membrane. Our simulation data reveals spontaneous insertion of aqueous $A\beta_{9-40}$ fibrils hexamer into the membrane and the central hydrophobic cluster and C-terminal hydrophobic residues plays a crucial role in the insertion process. Due to the hydrophobic nature of binding residues, VdWs interactions are more dominant than the electrostatic interactions. A decrease in the number of water molecules around $A\beta_{9-40}$ fibrils and loss of conformation entropy in chain B is observed as the distance between $A\beta_{9-40}$ fibrils and membrane decreases. We further observe that the binding of $A\beta_{9-40}$ fibrils causes the localized thinning of the membrane at the point of insertion. The identified binding residues of Aβ fibrils could sever as a potential target region to design new inhibitors, thus open new avenues in structure-based drug design for Aβ oligomer/fibrils membrane interaction inhibitors.

Keywords: Alzheimer's disease, Amyloid βeta, cholesterol, DPPC, MD simulations.

5.2 Introduction

Amyloid fibrils are misfolded β-sheet rich aggregated proteins, which play a key role in over 20 disease conditions that include Alzheimer's disease (AD), Parkinson's disease (PD), type 2 diabetes and different forms of systemic amyloidosis[1-4]. Disease conditions involving amyloid formation are commonly known as protein misfolding diseases, which affect more than 500 million people in the world[2]. According to the Amyloid cascade hypothesis in the AD, the amyloid βeta peptide (Aβ) undergoes conformational changes to form water-insoluble Aβ fibrils in the brain of AD patient[5]. These Aβ fibrils then form extracellular neuronal plaques, which have been suggested as the major pathological hallmark of AD[6].

Toxicity of Alzheimer's Aβ is still not completely understood; however, several mechanisms have been proposed to explain it; these are 1) Aβ monomer itself is neurotoxic, or Aβ monomer at higher concertation are neurotoxic[7-8] 2) Aβ aggregate/oligomers interact with membranes and increase membrane permeability[9]. 3) Aβ oligomers form ion channels in the membrane that disrupt the cellular ionic homeostasis of influx[10]. 4) Membrane lipids can convert inert Aβ fibrils into neurotoxic protofibrils[11]. Most of these studies have highlighted that Aβ binding with membrane lipids leads to neurotoxicity.

Various studies have been performed using different experimental techniques to reveal the interaction of Aβ fibrils with lipids. A recent study by Han *et al.*[12], using the Electron tomography technique revealed that Aβ fibrils interaction with lipids of different sizes and their work further revealed that intracellular fibrils deform the structure of intracellular lipid vesicles and puncture through the vesicular membrane into the cytoplasm. Kiskis *et al.*[13], using simultaneous coherent anti-Stokes Raman scattering (CARS) and 2-photon fluorescence microscopy of Thioflavin-S techniques showed that lipids co-localize with fibrillar β-amyloid (Aβ) plaques. In another study, Burns *et al.*[14] experimental study revealed co-localization of cholesterol in Aβ plaques. Ji *et al.*[15] revealed the role of cholesterol concentration on the $A\beta_{1-40}$ insertion in the membrane and secondary structure. They prepared dipalmitoylphosphatidylcholine (DPPC) monolayer with 20, 25, 33, 56, and 74 mol% cholesterol, respectively; their data suggested that $A\beta_{1-40}$ can only able to insert into the membrane when the cholesterol content was greater than 30%. Their results further suggested that at the low concentration of cholesterol (30% or less) Aβ prefers to stay on membrane surface in the β-sheet conformation.

Previously, several MD simulations studies have been performed on the interaction between membranes and Aβ oligomers/fibrils; for example, Yu *et al.*[16] performed MD simulations of $A\beta_{17-42}$ fibrils with mixed anionic POPC–POPG bilayer. Their data revealed that anionic lipids help the

absorption of $A\beta_{17-42}$ pentamer in the membrane and Ca^{+} mediate negatively charged residues Glu22 and Aps23 interactions with phosphate head groups. Tofoleanu[17] *et al*. conducted Aβ fibrils MD simulations with POPE lipid bilayer, and their data revealed that charged residues Glu22, Aps23 and Lys28 form electrostatic interactions with head group atoms. In another study, Tofoleanu[18] performed MD simulations of Aβ fibrils with POPC and POPE bilayers and revealed that Aβ fibrils formed short-lived contacts with POPC headgroups and strong contacts with POPE headgroups and suggested the interaction of Aβ fibrils oligomers with membranes would be more notorious in case of the biological condition in the presence of cholesterol. In a recent work Dong *et al.*[19] performed MD simulations of $A\beta_{9-40}$ fibrils trimers with POPG bilayer and revealed that N-terminal β-sheet forms contact with POPG bilayer. In all the aforementioned studies, Aβ fibrils were placed near to the membrane, and to best of our knowledge, no previous MD simulation study has been performed to investigate Aβ fibrils in contact with a lipid bilayer consisting of cholesterol lipids, which is one of the most important contents of the neuronal cell membranes[20].

In the present study, we aim to capture spontaneous insertion of $A\beta_{9-40}$ fibrils hexamer in the DPPC and Cholesterol mixed bilayer. To fulfill this aim, we have performed 4 Coarse-grained MD simulations, for more than 8 μs. The MD study will allow us to answer the following questions: 1) Does Aβ fibrils oligomer spontaneously insert inside the bilayer? 2) Which region of Aβ fibrils binds with the membrane? 3) What kinds of interactions dominate Aβ fibrils interactions with membrane VdW or electrostatics? 4) What is the role of water molecules in Aβ fibrils interaction with membrane? 5) Does the binding of Aβ fibrils affect the thickness of the bilayer?

5.3 Methods

5.3.1 Structure and force field of $A\beta_{9-40}$ hexamer fibrils initial structure

In the present study, coarse-grained molecular dynamics simulations were performed where the NMR-derived $A\beta_{9-40}$ fibrils hexamer (PDB id: 2LMN) single layer was taken from two-fold symmetry structure. $A\beta_{9-40}$ fibrils structure contains two β-sheets (residue 13-19 and residue 32-40)[21]. The atomistic structure (Figure: 5.1A) was converted into the CG model (Figure: 5.1B) using the CHARMM-GUI Martini maker[22, 23]. Martini2.2 force field[24] parameters were used for the $A\beta_{9-40}$ hexamer.

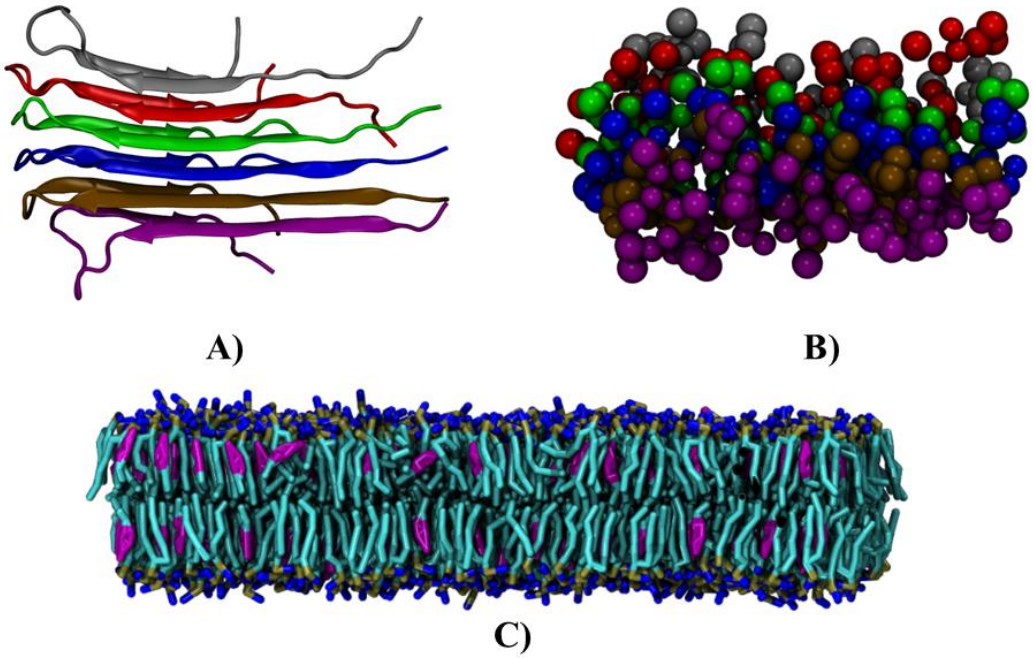

Figure: 5.1 A) Shows NMR structure of $A\beta_{9-40}$ fibrils (PDB id: 2LMN). B) Shows the CG model of $A\beta_{9-40}$ fibrils. C) Shows cholesterol mixed DPPC bilayer.

5.3.2 Structure and force field parameters for the DPPC-Cholesterol membrane

It has been reported that in neuronal cells, membrane lipids are not randomly distributed, instead form lipid domains, where sphingolipids and cholesterol are segregated in DPPC rich membrane areas[25]. In the present study, we have used ~70.37% DPPC and ~29.63% cholesterol as used in the experimental study by Ji *et al.*[15]. The initial structure of DPPC-cholesterol was downloaded from CG martini website[26] and to make the larger patch of the membrane it was replicated in x and y-direction. The larger patch of bilayer contains 1368 DPPC molecules and 576 cholesterol molecules (Figure: 5.1C); the structure was equilibrated for 15 ns before being used for MD simulations with $A\beta_{9-40}$ fibrils. Martini 2.0 force field parameters were used for the membrane and water.

5.3.3 Simulation protocol

The system contains one $A\beta_{9-40}$ hexamer, DPPC-cholesterol bilayer, and 107194 water molecules. To neutralize the system 6 Na^+ ions were added. Initially, 5000 steps of steepest descent[27] were performed to energy minimize the systems, followed by 30 ns equilibration using canonical ensemble (NVT) followed by 100ns equilibration using the isobaric-isothermal ensemble (NPT). The production run was performed using the NPT ensemble. The Berendsen algorithm[28] was used for pressure coupling and velocity-rescale algorithm[29] was used for temperature coupling. Pressure coupling and temperature bath times were set 5.0 and 1.0 ps, respectively. All simulations were performed at a temperature of 303.15K and 1 atm pressure. The Particle mesh Ewald (PME) algorithm[30] was used for long-range electrostatic interactions and van der Waals (vdW) interactions

were calculated using the switch function from 9 to 12 Å; 20 fs time step was used for integration of Newton's equations of motion.

A total of 4 simulations were performed using initial random velocity generated by the GROMACS[31]. Each trajectory simulation time was more than 2 μs.

5.3.4 Analysis details

The centre of mass (COM) distances in Z-dimension was calculated between each chain of the $A\beta_{9-40}$ fibrils and PO4 groups of upper-leaflet of the membrane using an in-house Tcl script. The interaction energy between $A\beta_{9-40}$ fibrils each chain with the membrane was calculated using GROMACS MDRUN program using "rerun" option. An interaction between $A\beta_{9-40}$ fibrils residues was considered when the distance between COM of residues and COM of membrane lipids (DPPC/cholesterol) was 10 Å or less. The percentage of contacts of the $A\beta_{9-40}$ fibrils and chain B was calculated by counting the number of times an interaction occurred. The number of water molecules has been calculated within 5Å and number of DPPC and cholesterol within 10Å using in-house Tcl script. The bilayer thickness was calculated using g_thickness[32] tool for different time point's average over 100ns. The thickness was calculated using the distance between two PO4 head groups of upper and lower leaflets of the membrane. To investigate the conformational entropy of chain B of $A\beta_{9-40}$ fibrils the mass-weighted covariance matrix was calculated, which was used for the quasi-harmonic approximation[33].

5.4 Results

5.4.1 Insertion of $A\beta_{9-40}$ fibrils chains inside membrane

Out of a total 4 independent trajectories, we observed insertion of $A\beta_{9-40}$ fibrils chains in two trajectories. In the other two trajectories, we observed transient contacts between $A\beta_{9-40}$ fibrils and membrane. Figure: 5.2A shows the time evolution of the centre of mass distance between each chain with upper leaflet PO4 beads. Figure: 5.2B shows the time evolution of interaction energy between membranes (DPPC/CHO). The stepwise process of the spontaneous insertion of $A\beta_{9-40}$ fibrils has been shown in Figure: 5.3. Insertion of $A\beta_{9-40}$ fibrils in mixed lipids bilayer took places in sequential steps: in step A ~400 ns the protein came near to the membrane, as shown by a decrease in the distances of each chain from the PO4 beads; however, $A\beta_{9-40}$ fibrils does not form any contact with the membrane at this time. In step B at ~500ns, $A\beta_{9-40}$ fibrils reoriented and Chain B and Chain C form contacts with the membrane, as shown by a further decrease in distances of Chain B and Chain C from the PO4 beads (Figure: 5.2A red and green lines), during this time, the interaction energy between chain B and the membrane was ~-700 kJ/mol and chain C and the membrane was ~-473 kJ/mol. In step-c ~1.55 μs we observed insertion of Chain B inside the bilayer, and we observed binding of

$A\beta_{9\text{-}40}$ until the end of simulation. To understand what kind of interactions drive the binding of Aβ fibrils with the membrane, we further calculated non-bonded interaction energy components between Chain B, Chain C and the membrane. Energy decomposition revealed that VdW interaction is more attractive and, therefore, drives the binding between membrane and $A\beta_{9\text{-}40}$ fibrils hexamer (Figure: 5.2D).

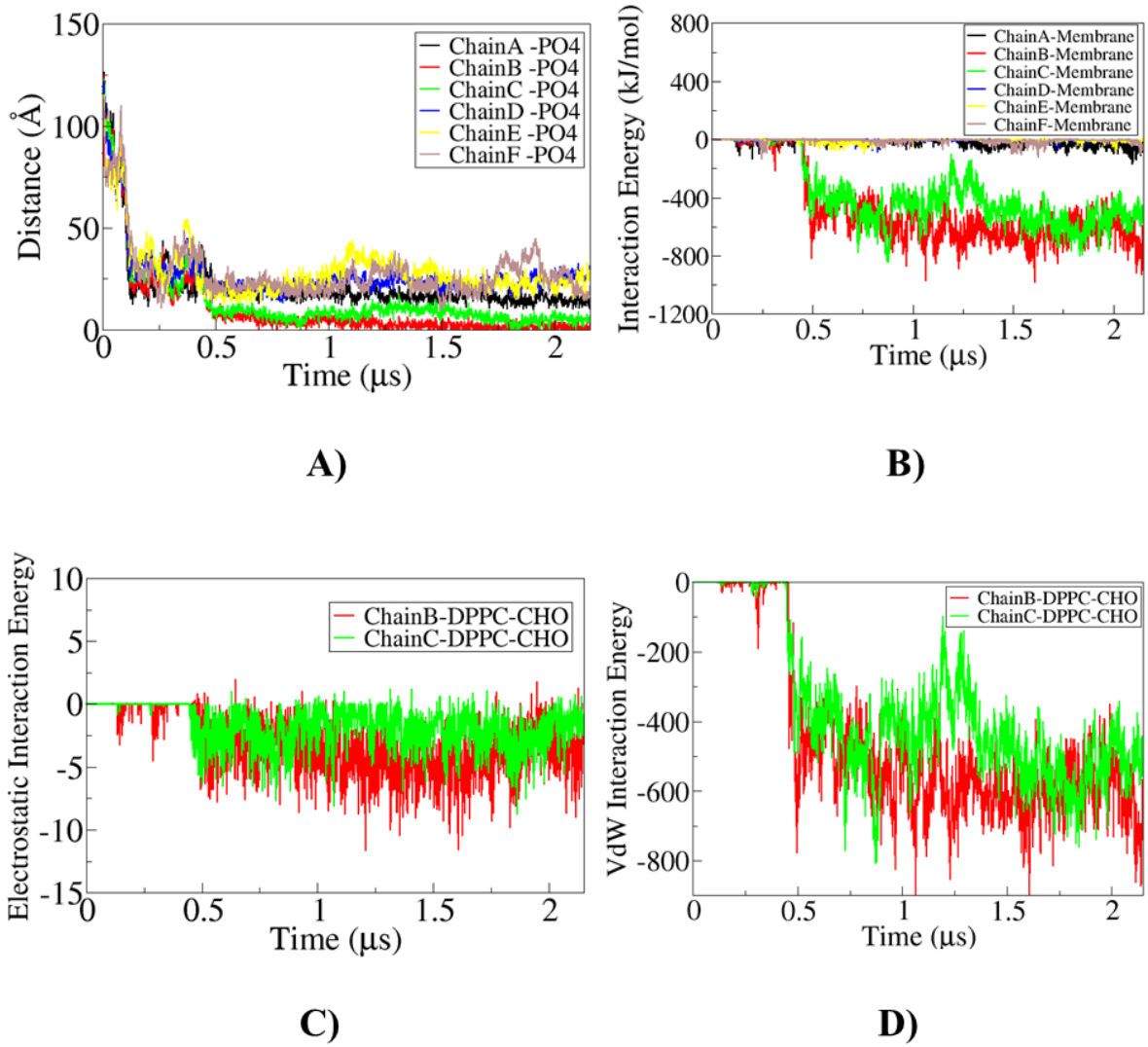

Figure: 5.2 A) Shows time evolution of centre of mass (COM) distance between each chains of $A\beta fibril_{9\text{-}40}$ from COM of PO4 bead of upper leaflet. B) Shows the time evolution of interaction energy between $A\beta fibril_{9\text{-}40}$ each chain from the membrane. C) Shows the electrostatic interaction between chain B and C with membrane. D) Shows VdW interaction energy between chain B-membrane and chain C- membrane.

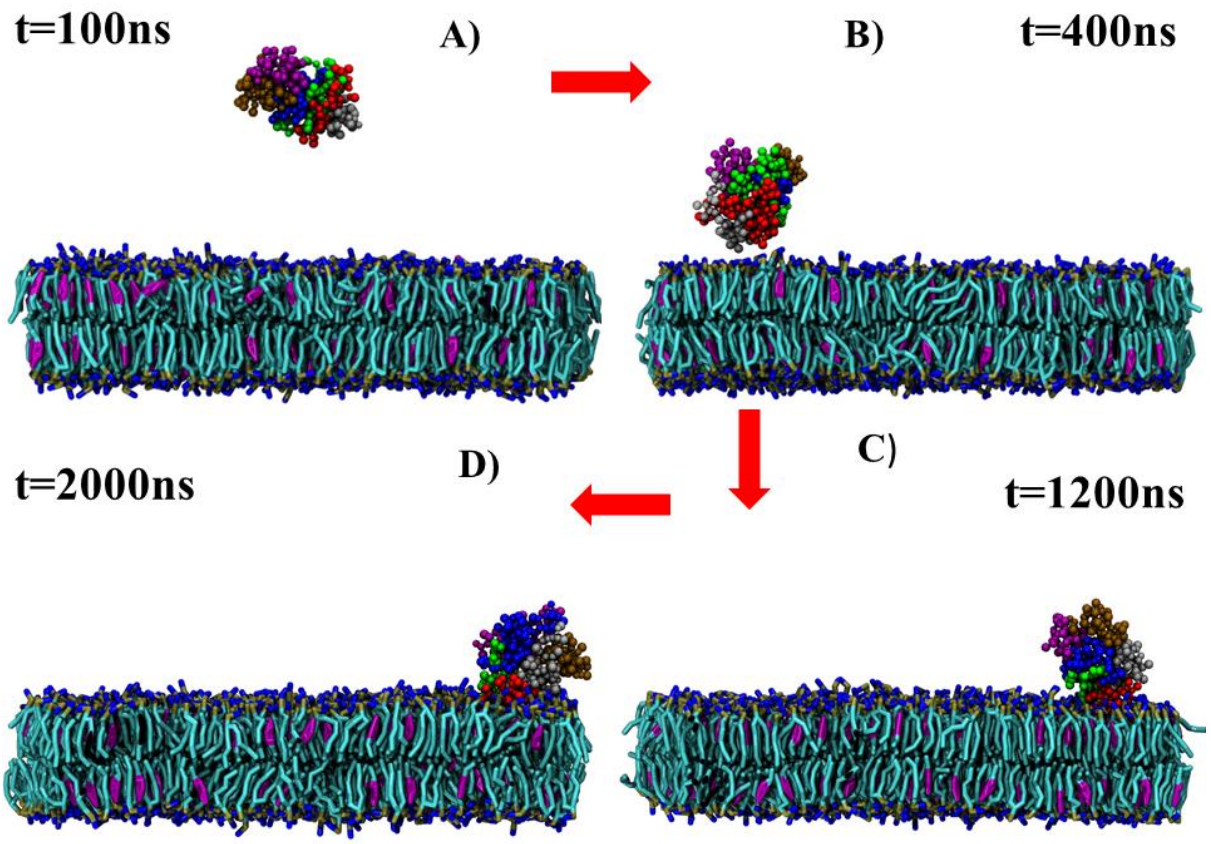

Figure: 5.3 Shows structures of $A\beta_{9-40}$ fibrils at four different time points taken from the representative trajectory. A) Shows representative image at 100 ns. B) Shows representative image at 400 ns. C) Shows representative image at 1200 ns (1.2 µs). D) Shows representative image at 2000 ns (2µs). Each chain of protein has been shown in different colour, Chain A silver, Chain B red, Chain C green, Chain D blue, Chain E ochre and Chain F in purple. Protein beads are represented in VdW and membrane in Licorice. DPPC lipid molecules have been shown in cyan colour and cholesterol lipid molecules have been shown in maroon.

5.4.2 Percentage of contacts

To identify chain B residues that more strongly bind with the upper leaflet and, therefore, assist Aβ fibrils insertion into the membrane, we have calculated the percentage of contacts of each residue of Chain B with PO4 beads of DPPC and ROH beads of cholesterol. Figure: 5.4B shows the percentage of contacts formed by Chain B residues with PO4 beads. We observed central hydrophobic cluster (CHC) residues Lys16, Leu17, Val18, Phe19 and Phe20 (Aβ16-20), turn region residues Gly29 and Ala30 and second β-sheet residues (32-40) form major contacts with the membrane. This could be significant since the binding of Aβ fibrils with the membrane was governed by VdW's rather than electrostatic interactions. The CHC region and turn region residues have been previously reported to form interactions with the membrane[19, 34]. Ji[15] *et al.* experimental study revealed that Aβ peptide entered inside the cholesterol-containing vesicles by its C-terminal domain.

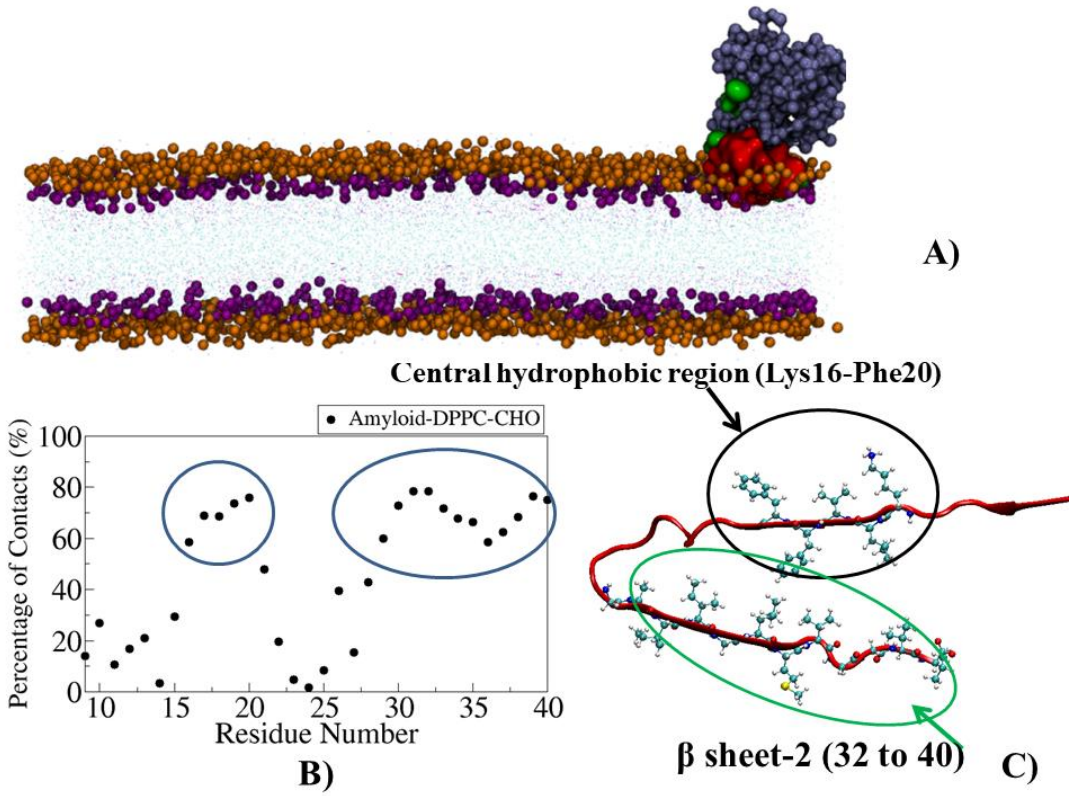

Figure: 5.4 A) Shows $A\beta_{9-40}$ fibrils binding with the membrane. Protein has been shown in ice blue colour with surf representation and chain B and Chain C have been shown in red and green colours, respectively. PO4 and ROH beads have been shown in VdW representation in orange and maroon colour. B) Shows percentage of contacts of graph of Chain B with DPPC and Cholesterol lipids and CHC region and C-terminal residues have been shown in circles. D) Shows the major binding residues of Chain B on atomistic model.

5.4.3 Time evolution of number of water, lipid molecules around $A\beta_{9-40}$ fibrils and change in the conformational entropy

To investigate how many water molecules $A\beta_{9-40}$ fibrils have to displace to interact with the membrane, we calculated the time evolution of the number of water molecules within 5Å of $A\beta_{9-40}$ fibril (Figure: 5.5A). We observed that, as the distance of $A\beta_{9-40}$ fibrils decreases from the membrane, the number of water molecules also decreases. In the beginning (0 to 450 ns), before Aβ fibrils form interactions with the membrane there were ~164 ± 11.3 water molecules around $A\beta_{9-40}$ fibrils, which decreased to ~142.5 ± 9.5, during the period from 500 ns to 1.3 μs, when $A\beta_{9-40}$ fibrils established interactions with the membrane. A further displacement of water molecules was observed ~1.3 μs, when $A\beta_{9-40}$ fibrils inserted deeply inside the membrane. On average there were ~131 ± 8.8 water molecules around $A\beta_{9-40}$ fibrils during the period from 1.3 μs to 2.15 μs. Overall, aqueous phase $A\beta_{9-40}$ fibrils have to displace ~33 water molecules to insert into the cholesterol-rich DPPC membrane.

To investigate the number of lipids molecules around $A\beta_{9-40}$ fibrils, we calculated the time evolution of DPPC and cholesterol lipid molecules within 10 Å of $A\beta_{9-40}$ fibrils (Figure: 5.5B). During 0 to 450 ns, before Aβ fibrils formed interactions with the membrane, we observed on average 0 DPPC lipid molecules and 0 cholesterol lipid molecules. The number of lipid molecules around $A\beta_{9-40}$ fibrils increased in two phases in the first phase during the period from 500 ns to 1.3 µs, when $A\beta_{9-40}$ fibrils established the interactions with the membrane, there were on average ~16.6 ± 3.8 DPPC molecules and ~5.01 ± 2.03 cholesterol molecules around $A\beta_{9-40}$ fibrils. In the second phase, when $A\beta_{9-40}$ fibrils inserted deeply inside the membrane; during 1.3 µs to 2.15 µs, there were on average ~16.9 ± 3.5 DPPC lipid molecules and ~6.45 ± 1.6 cholesterol lipid molecules around $A\beta_{9-40}$ fibrils. A significant gain of ~1.44 cholesterol molecules during the second phase indicates that cholesterol lipids play a crucial role in the insertion of $A\beta_{9-40}$ fibrils in the membrane.

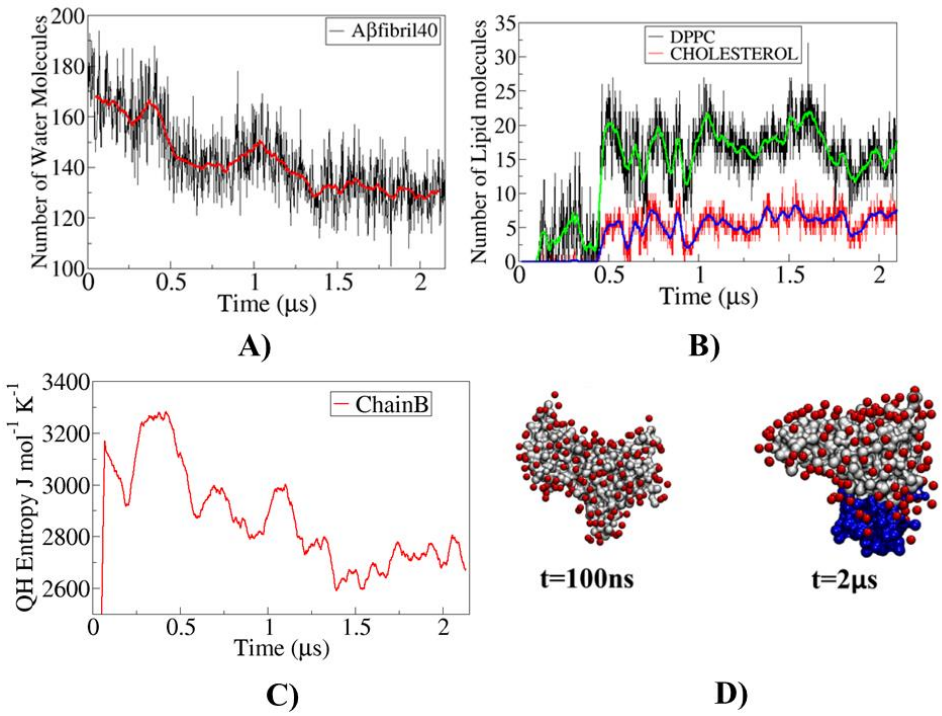

Figure: 5.5 A) Shows the time evolution of number of water molecules around the $A\beta_{9-40}$ fibrils. B) Shows the time evolution of number of DPPC and cholesterol lipid molecules around the $A\beta_{9-40}$ fibrils. C) Show the change in conformation entropy of chain B and C with respect to the time. D) Shows the water molecules on surface of $A\beta_{9-40}$ fibrils at two different time point. Protein has been shown in white in surf representation and residues with 10Å of the membrane have been shown in blue color. Water has been shown in VdW representation in red color.

The time evolution of change in the conformational entropy of the membrane binding chain B (Figure: 5.5C) revealed that conformation entropy of chain B decreased as the number of water molecules decreased or the number of lipids molecules increased around $A\beta_{9-40}$ fibrils. Change in conformation entropy of chain B can be divided into three stages, the first stage was from 0 to 450 ns,

before the $A\beta_{9-40}$ fibrils formed interactions with the membrane. The second stage (500 ns to 1.3 μs) was when $A\beta_{9-40}$ fibrils established interactions with the membrane, and the third stage, when it deeply inserted inside the membrane (1.3 μs to 2.15 μs). In the first phase on average conformation entropy of chain B was ~2925.87 ± 634.54, in the second phase ~2892.45 ± 88.31 and in the third phase ~2700.94 ± 54.79 J mol^{-1} K^{-1}, respectively. This result revealed that chain B has high conformational entropy in aqueous environment compare to the membrane environment. It could be significant since water molecules are mobile than lipid molecules. Also, the loss of entropy must be offset by the interaction between chain B and the membrane (Figure: 5.2D).

5.4.4 Perturbation of thickness of bilayer

To investigate the effect of binding of $A\beta_{9-40}$ fibril on the membrane, we have calculated the thickness of the membrane before (300 ns to 400 ns) and after binding (1.7 μs to 1.8 μs) of the $A\beta_{9-40}$ fibrils. On average, the thickness of the bilayer before $A\beta_{9-40}$ fibrils insertion throughout the box was uniform (Figure: 5.6A). However, after the insertion of $A\beta_{9-40}$ fibrils, localized thinning in the region of insertion was observed. (Figure: 5.6B). These results revealed that $A\beta_{9-40}$ fibrils binding affected the local lipid distribution in the membrane, which leads to thinning in one region and increased thickness in the rest of the membrane. Previous experimental studies have revealed that peptide/protein binding on the surface membrane cause membrane thinning, which is directly dependent on the concentration of the peptide[35, 36]. Insertion of the peptides inside the membrane could lead to the formation of pores in the membrane[35, 37]. Our results revealed that binding of a single molecule of Aβ fibril (6 peptides) lead to the localized thinning in the membrane; however, *in-vivo*, the number of Aβ peptides, which interact with the membrane, could be greater causing significantly thinning of the membrane, which could lead to further pore formation in the membrane.

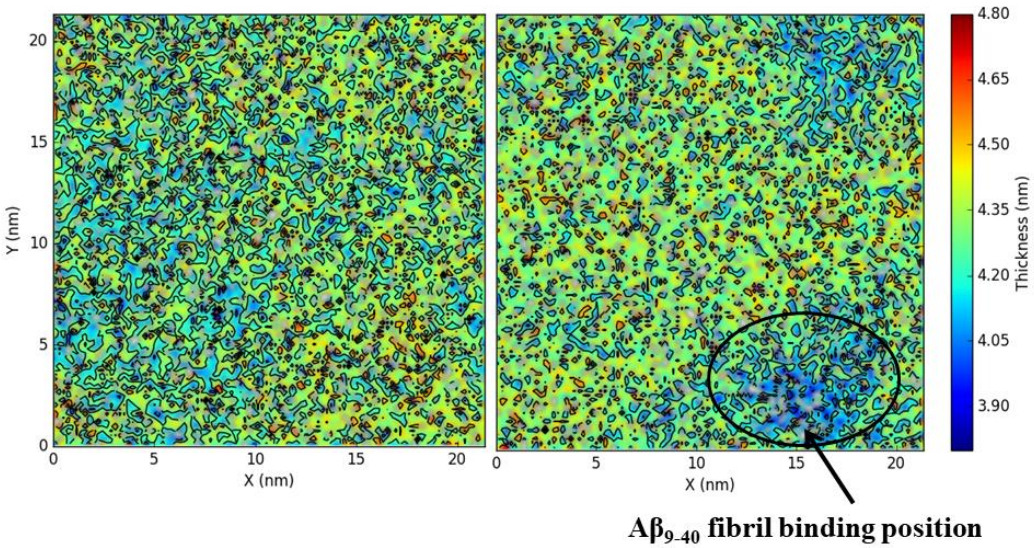

Figure: 5.6A) Shows the thickness of the membrane during 300-400 ns b) Shows the thickness of the membrane during 1.7 μs to 1.8 μs.

5.5 Discussion

Aβ protein interaction with the membranes plays a key role in the toxicity of Alzheimer's and cholesterol lipids have been reported to play an important role in Aβ protein interaction with the membrane[38, 39]. Computer simulations have helped to reveal the molecular details of Aβ proteins interaction with candidate drug molecules and biological membranes[40-42]. In the present study, we have performed $A\beta_{9-40}$ simulations with cholesterol-rich DPPC bilayer. In all previous studies, simulations of Aβ proteins begin from a membrane-bound conformation, and therefore, details key transition events such as membrane binding remains elusive. In the present work, we have revealed the spontaneous insertion of aqueous phase $A\beta_{9-40}$ fibrils into the cholesterol-rich DPPC membrane using more than 8 μs long simulations at physiological temperature.

Our simulation data reveals that CHC region and second β-sheet residues of $A\beta_{9-40}$ fibrils forms major contacts with the membrane. CHC region residues have been previously reported to make interaction with membrane[34] and also been reported to play a key role in aggregation of Aβ peptides[43]. The present simulations data revealed that $A\beta_{9-40}$ fibrils interaction with the membrane is majorly governed by the hydrophobic residues and to form the interaction with the membrane $A\beta_{9-40}$ fibrils rearranged itself so that hydrophobic residues face to the membrane. We also observed a loss of water molecules and increase in the number of lipid molecules around chain B, which leads to a significant loss of conformation entropy of chain B and may play a crucial role in the binding of $A\beta_{9-40}$ fibrils to the membrane. Our data is also in agreement with the previous studies[44, 45], which suggested that cholesterol promotes Aβ interaction with the membrane; we observed that after insertion into the membrane, the interaction between Aβ fibrils and cholesterol molecules increases. At the position where $A\beta_{9-40}$ fibrils inserted, the thickness was locally decreased; in this way, Aβ fibril/aggregate could lead to the formation of a pore, which would disrupt the membrane and result in neuronal cytotoxicity.

5.6 Conclusions

In summary, our simulations have shed light on the fundamental understating Aβ fibrils interaction with the membrane. Our simulation data revealed spontaneous insertion of aqueous $A\beta_{9-40}$ fibrils in cholesterols-rich DPPC bilayer. To the best of our knowledge, this is the first report to show spontaneous insertion of Aβ fibrils using the most abundant lipid molecules in the neuronal cell membrane. Our simulation revealed the key binding residues, which stabilized the interaction of Aβ fibril. Our simulation data further revealed loss in the conformational entropy of membrane binding chain of $A\beta_{9-40}$ fibrils as the number of water molecules decreased around $A\beta_{9-40}$ fibrils. The identified $A\beta_{9-40}$ fibrils residues of CHC region and second β-sheet could be used as a target site to design new candidate drug molecules, which could inhibit its association with the membrane, and further stop the

pore formation in the membrane Thus, open new avenues in drug design of Aβ peptides membrane interaction inhibitors.

Acknowledgments

We are indebted to Centre for High Performance Computing (CHPC) in Cape Town, South Africa and UKZN hippo super computer facility, Durban, South Africa for computational resources. We would like to thank college of Health Sciences at UKZN for funding and Nikhil Agrawal is in debt to National Research Foundation, South Africa.

Supplementary Information Available

Supplementary information contains simulation video of $A\beta_{9\text{-}40}$ fibrils insertion into the cholesterol-rich DPPC bilayer.

5.7 References:

1. Chiti, F.; Dobson, C. M. Protein Misfolding, Amyloid Formation, and Human Disease: A Summary of Progress Over the Last Decade. *Annual Review of Biochemistry* **2017**, (0).

2. Dobson, C. M. The Amyloid Phenomenon and Its Links with Human Disease. *Cold Spring Harbor perspectives in biology* **2017,** *9*, (6), a023648.

3. Hazenberg, B. P. Amyloidosis. *Rheumatic Disease Clinics* **2013,** *39*, (2), 323-345.

4. Hirschfield, G. M. In *Amyloidosis: a clinico-pathophysiological synopsis*, Seminars in cell & developmental biology, 2004; Elsevier: pp 39-44.

5. Mullard, A. Alzheimer amyloid hypothesis lives on. *Nature Reviews Drug Discovery* **2017,** *16*, (1), 3-5.

6. Harrison, R.; Sharpe, P.; Singh, Y.; Fairlie, D., Amyloid peptides and proteins in review. In *Reviews of physiology, biochemistry and pharmacology*, Springer: 2007; pp 1-77.

7. Stroud, J. C.; Liu, C.; Teng, P. K.; Eisenberg, D. Toxic fibrillar oligomers of amyloid-β have cross-β structure. *Proceedings of the National Academy of Sciences* **2012,** *109*, (20), 7717-7722.

8. Vestergaard, M. d.; Hamada, T.; Takagi, M. Using model membranes for the study of amyloid beta: lipid interactions and neurotoxicity. *Biotechnology and Bioengineering* **2008,** *99*, (4), 753-763.

9. Kayed, R.; Lasagna-Reeves, C. A. Molecular mechanisms of amyloid oligomers toxicity. *Journal of Alzheimer's Disease* **2013,** *33*, (s1), S67-S78.

10. Quist, A.; Doudevski, I.; Lin, H.; Azimova, R.; Ng, D.; Frangione, B.; Kagan, B.; Ghiso, J.; Lal, R. Amyloid ion channels: a common structural link for protein-misfolding disease. *Proceedings of the National Academy of Sciences of the United States of America* **2005,** *102*, (30), 10427-10432.

11. Martins, I. C.; Kuperstein, I.; Wilkinson, H.; Maes, E.; Vanbrabant, M.; Jonckheere, W.; Van Gelder, P.; Hartmann, D.; D'Hooge, R.; De Strooper, B. Lipids revert inert Aβ amyloid fibrils to neurotoxic protofibrils that affect learning in mice. *The EMBO journal* **2008,** *27*, (1), 224-233.

12. Han, S.; Kollmer, M.; Markx, D.; Claus, S.; Walther, P.; Fändrich, M. Amyloid plaque structure and cell surface interactions of β-amyloid fibrils revealed by electron tomography. *Scientific Reports* **2017,** *7*, 43577.

13. Kiskis, J.; Fink, H.; Nyberg, L.; Thyr, J.; Li, J.-Y.; Enejder, A. Plaque-associated lipids in Alzheimer's diseased brain tissue visualized by nonlinear microscopy. *Scientific reports* **2015,** *5*, 13489.

14. Burns, M. P.; Noble, W. J.; Olm, V.; Gaynor, K.; Casey, E.; LaFrancois, J.; Wang, L.; Duff, K. Co-localization of cholesterol, apolipoprotein E and fibrillar Aβ in amyloid plaques. *Molecular Brain Research* **2003,** *110*, (1), 119-125.

15. Ji, S.-R.; Wu, Y.; Sui, S.-f. Cholesterol is an important factor affecting the membrane insertion of β-amyloid peptide (Aβ1–40), which may potentially inhibit the fibril formation. *Journal of Biological Chemistry* **2002,** *277*, (8), 6273-6279.

16. Yu, X.; Wang, Q.; Pan, Q.; Zhou, F.; Zheng, J. Molecular interactions of Alzheimer amyloid-β oligomers with neutral and negatively charged lipid bilayers. *Physical Chemistry Chemical Physics* **2013,** *15*, (23), 8878-8889.

17. Tofoleanu, F.; Buchete, N.-V. Molecular interactions of Alzheimer's Aβ protofilaments with lipid membranes. *Journal of molecular biology* **2012,** *421*, (4), 572-586.

18. Tofoleanu, F.; Brooks, B. R.; Buchete, N.-V. Modulation of Alzheimer's Aβ protofilament-membrane interactions by lipid headgroups. *ACS chemical neuroscience* **2015,** *6*, (3), 446-455.

19. Dong, X.; Sun, Y.; Wei, G.; Nussinov, R.; Ma, B. Binding of protofibrillar Aβ trimers to lipid bilayer surface enhances Aβ structural stability and causes membrane thinning. *Physical Chemistry Chemical Physics* **2017,** *19*, (40), 27556-27569.

20. Calderon, R.; Attema, B.; DeVries, G. Lipid composition of neuronal cell bodies and neurites from cultured dorsal root ganglia. *Journal of neurochemistry* **1995,** *64*, (1), 424-429.

21. Paravastu, A. K.; Leapman, R. D.; Yau, W.-M.; Tycko, R. Molecular structural basis for polymorphism in Alzheimer's β-amyloid fibrils. *Proceedings of the National Academy of Sciences* **2008,** *105*, (47), 18349-18354.

22. Jo, S.; Kim, T.; Iyer, V. G.; Im, W. CHARMM-GUI: a web-based graphical user interface for CHARMM. *Journal of computational chemistry* **2008,** *29*, (11), 1859-1865.

23. Qi, Y.; Ingólfsson, H. I.; Cheng, X.; Lee, J.; Marrink, S. J.; Im, W. CHARMM-GUI martini maker for coarse-grained simulations with the martini force field. *Journal of chemical theory and computation* **2015,** *11*, (9), 4486-4494.

24. Marrink, S. J.; Risselada, H. J.; Yefimov, S.; Tieleman, D. P.; De Vries, A. H. The MARTINI force field: coarse grained model for biomolecular simulations. *The journal of physical chemistry B* **2007,** *111*, (27), 7812-7824.

25. Ottico, E.; Prinetti, A.; Prioni, S.; Giannotta, C.; Basso, L.; Chigorno, V.; Sonnino, S. Dynamics of membrane lipid domains in neuronal cells differentiated in culture. *Journal of lipid research* **2003,** *44*, (11), 2142-2151.

26. "Lipid Membranes." Cgmartini.nl. N.p., 2017. Web. 21 Dec. 2017. http://www.cgmartini.nl/index.php/example-applications2/lipid-membranes

27. Bixon, M.; Lifson, S. Potential functions and conformations in cycloalkanes. *Tetrahedron* **1967,** *23*, (2), 769-784.

28. Berendsen, H.; Postma, J.; van Gunsteren, W.; Dinola, A.; Haak, J. 571 1984. Molecular-dynamics with coupling to an external bath. *J. Chem. Phys 81*, 3684-572.

29. Bussi, G.; Donadio, D.; Parrinello, M. Canonical sampling through velocity rescaling. *The Journal of chemical physics* **2007,** *126*, (1), 014101.

30. Darden, T.; York, D.; Pedersen, L. Particle mesh Ewald: An N· log (N) method for Ewald sums in large systems. *The Journal of chemical physics* **1993,** *98*, (12), 10089-10092.

31. Abraham, M. J.; Murtola, T.; Schulz, R.; Páll, S.; Smith, J. C.; Hess, B.; Lindahl, E. GROMACS: High performance molecular simulations through multi-level parallelism from laptops to supercomputers. *SoftwareX* **2015,** *1*, 19-25.
32. Castillo, N.; Monticelli, L.; Barnoud, J.; Tieleman, D. P. Free energy of WALP23 dimer association in DMPC, DPPC, and DOPC bilayers. *Chemistry and physics of lipids* **2013,** *169*, 95-105.
33. Levy, R. M.; Karplus, M.; Kushick, J.; Perahia, D. Evaluation of the configurational entropy for proteins: application to molecular dynamics simulations of an α-helix. *Macromolecules* **1984,** *17*, (7), 1370-1374.
34. Usachev, K. S.; Efimov, S. V.; Yulmetov, A. R.; Filippov, A. V.; Antzutkin, O. N.; Afonin, S.; Klochkov, V. V. Spatial structure of heptapeptide Aβ16–22 (beta-amyloid Aβ1–40 active fragment) in solution and in complex with a biological membrane model. *Magnetic Resonance in Chemistry* **2012,** *50*, (12), 784-792.
35. Chen, F.-Y.; Lee, M.-T.; Huang, H. W. Evidence for membrane thinning effect as the mechanism for peptide-induced pore formation. *Biophysical journal* **2003,** *84*, (6), 3751-3758.
36. Bechinger, B.; Kim, Y.; Chirlian, L.; Gesell, J.; Neumann, J.-M.; Montal, M.; Tomich, J.; Zasloff, M.; Opella, S. Orientations of amphipathic helical peptides in membrane bilayers determined by solid-state NMR spectroscopy. *Journal of biomolecular NMR* **1991,** *1*, (2), 167-173.
37. Yang, L.; Harroun, T. A.; Weiss, T. M.; Ding, L.; Huang, H. W. Barrel-stave model or toroidal model? A case study on melittin pores. *Biophysical journal* **2001,** *81*, (3), 1475-1485.
38. Smith, R. A.; Nabok, A.; Blakeman, B. J.; Xue, W.-F.; Abell, B.; Smith, D. P. Analysis of toxic amyloid fibril interactions at natively derived membranes by ellipsometry. *PloS one* **2015,** *10*, (7), e0132309.
39. Williams, T. L.; Serpell, L. C. Membrane and surface interactions of Alzheimer's Aβ peptide–insights into the mechanism of cytotoxicity. *The FEBS journal* **2011,** *278*, (20), 3905-3917.
40. Agrawal, N.; Skelton, A. A. 12-Crown-4 Ether Disrupts the Patient Brain-Derived Amyloid-β-Fibril Trimer: Insight from All-Atom Molecular Dynamics Simulations. *ACS chemical neuroscience* **2016,** *7*, (10), 1433-1441.
41. Agrawal, N.; Skelton, A. A. Binding of 12-crown-4 with Alzheimer's Aβ40 and Aβ42 monomers and its effect on their conformation: insight from molecular dynamics simulations. *Molecular pharmaceutics* **2017**.
42. Brown, A. M.; Bevan, D. R. Molecular Dynamics Simulations of Amyloid β-Peptide (1-42): Tetramer Formation and Membrane Interactions. *Biophysical journal* **2016,** *111*, (5), 937-949.
43. Liu, R.; McAllister, C.; Lyubchenko, Y.; Sierks, M. R. Residues 17–20 and 30–35 of beta-amyloid play critical roles in aggregation. *Journal of neuroscience research* **2004,** *75*, (2), 162-171.
44. Di Scala, C.; Yahi, N.; Boutemeur, S.; Flores, A.; Rodriguez, L.; Chahinian, H.; Fantini, J. Common molecular mechanism of amyloid pore formation by Alzheimer's β-amyloid peptide and α-synuclein. *Scientific reports* **2016,** *6*, 28781.

45. Dies, H.; Toppozini, L.; Rheinstädter, M. C. The interaction between amyloid-β peptides and anionic lipid membranes containing cholesterol and melatonin. *PLoS One* **2014,** *9*, (6), e99124.

CHAPTER 6

CONCLUSIONS AND FUTURE PERSPECTIVE

Toxicity of Aβ peptides is still not completely understood; however, various mechanisms have been proposed to explain it; these are 1) Aβ monomers are toxic, 2) Aβ fibrils are toxic 3) Aβ fibrils interaction with membrane lipids leads to toxicity. Experimental studies have demonstrated that perturbing the Aβ monomers misfolding, disrupting the Aβ fibrils structure, and inhibiting the Aβ fibrils interactions with the membrane could reduce toxicity caused by them.

The body of work assembled here sought to explore binding of 12-crown-4, with Aβ1-40, Aβ1-42 monomers and Aβ1-40 fibril and binding of $A\beta_{9-40}$ hexamer fibrils with cholesterol-rich DPPC bilayer. This overall aim of the present thesis was to identify the key pharmacophore features required in candidate drug molecule to bind with Aβ monomer, Aβ fibrils, and the key pharmacophore features of Aβ fibrils that requited it to bind with the most abundant lipids of neuronal cell membrane. Identification of these pharmacophore features will help to design the new candidate drug molecule, which could reduce toxicity caused by Aβ monomers and fibrils. To achieve our aims we have conducted all-atom MD simulations of Aβ1-40 and Aβ1-42 monomers and Aβ1-40 fibrils in the presence and absence of 12-crown-4 and CG MD simulations of $A\beta_{9-40}$ fibrils hexamer with

Simulations of Aβ1-40 and Aβ1-42 monomers with 12-crown-4 shows that the molecule is highly specific toward positively charged Lys residues and the region around Val24-Lys28 is most prevalent for turn formation. Simulations results of Aβ1-40 fibril trimer with 12-crown-4 simulations reveals that it spontaneously, inserted into the hydrophobic core and opened the “U-shaped” topology of Aβ fibrils trimer and also disrupted Lys28-Asp23 salt bridge. Aβ fibrils hexamer with cholesterol-rich DPPC bilayer simulations reveals that $A\beta_{9-40}$ fibrils hexamer spontaneously inserted to the mixed bilayer and hydrophobic residues played a key role in its binding, especially central hydrophobic cluster region (Lys16-Phe20) and C-terminal residues (Ile32-Val40). Insertion of $A\beta_{9-40}$ fibrils hexamer leads to localized thinning of the membrane.

Results of Aβ monomers and Aβ fibrils trimer with 12-crown-4 ether reveals key pharmacophore features required in molecules to specifically bind with Aβ peptides. Data of Aβ fibrils hexamer identifies key pharmacophore features of Aβ protein to bind with the mixed lipid bilayer. The identified pharmacophore features will not only help in designing new candidate drug molecules, which are specific to Aβ peptides but could also be used to design new imaging probe molecules for labeling Aβ peptides.

APPENDIX

APPENDIX: A

Agrawal, N., and Skelton, A. A. (2017) Binding of 12-crown-4 with Alzheimer's Aβ40 and Aβ42 monomers and its effect on their conformation: insight from molecular dynamics simulations, *Molecular pharmaceutics* 15, 289-299.

APPENDIX: B

Agrawal, N., and Skelton, A. A. (2016) 12-Crown-4 Ether Disrupts the Patient Brain-Derived Amyloid-β-Fibril Trimer: Insight from All-Atom Molecular Dynamics Simulations, *ACS chemical neuroscience 7*, 1433-1441.

molecular pharmaceutics

Article

Cite This: Mol. Pharmaceutics 2018, 15, 289−299

Binding of 12-Crown-4 with Alzheimer's Aβ40 and Aβ42 Monomers and Its Effect on Their Conformation: Insight from Molecular Dynamics Simulations

Nikhil Agrawal*,† and Adam A. Skelton*,†

†College of Health Sciences, Discipline of Pharmaceutical Sciences, University of KwaZulu-Natal, Westville, Durban 4041, South Africa

Supporting Information

ABSTRACT: Alzheimer's disease is the most common form of dementia and is considered to be caused by the conformational change of Aβ monomers, from their native monomeric states, to form Aβ oligomers/aggregates in the brain. Turn formation in Aβ monomer has been suggested to be the nucleation step for Aβ misfolding. In the present work, we have performed a series of all-atom molecular dynamics simulations, a total time of 11.4 μs, to elucidate factor that contributes for early stage misfolding of Aβ40 and Aβ42 monomers and reveals the binding modes of 12-crown-4 on Aβ40 and Aβ42 monomer and effect of its binding on structural stability. Our simulation data revealed that the region around Val24-Lys28 is most prevalent for turn formation and a gain of water molecules around Lys28 side chains occurs at the same time as a significant gain in conformational entropy of the side chain. The initiation steps lead a greater number of water molecules available and enhancement of the conformational entropy of the backbone atoms; this leads to greater probability of breaking Lys28 backbone intrapeptide H-bonds, and consequently turns formation. Simulations of Aβ40 and Aβ42 monomers with 12-crown-4 showed that the molecule is highly specific toward positively charged Lys16, Lys28 residues, and N-terminal Asp1. Lys16 and Asp1 have been previously reported to make Aβ peptide toxic. Our secondary structure analysis revealed that in the absence of 12-crown-4 there was a β-sheet formed in the Aβ40 peptide. In case of Aβ42 monomer, in the absence of 12-crown-4, we observed that the second helix region converted into a coil and turn; however, in the presence of 12-crown-4 it remained stable. Observed pharmacophore features of, 12-crown-4 will not only help in designing new candidate drug molecules, which are specific to Aβ peptides but could also be used to design new imaging probe molecules, which could be used for labeling Aβ peptide

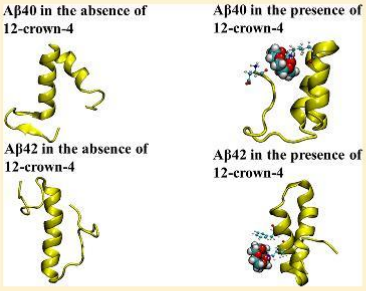

KEYWORDS: *Alzheimer, amyloid βeta, crown ethers, MD simulations*

INTRODUCTION

Alzheimer's disease (AD) is the most prevalent form of neurodegenerative disease, affecting around 40 million people worldwide.[1,2] Since its first description by a psychiatrist and neuropathologist Alois Alzheimer, in 1907, there is still no known cure for this illness, majorly due to lack of complete understanding of the disease etiology.[3−5] The most widely accepted amyloid cascade hypothesis suggests that amyloid-β (Aβ) peptide misfolding and aggregation is the principal culprit for AD.[6] The Aβ peptide is produced from the amyloid precursor protein (APP) by the proteolytic activities of β and γ-secretase. Since γ-secretase is unable to cleave Aβ peptide precisely, this results in a variable length of Aβ peptides; the most common isoforms being Aβ40 and Aβ42.[7]

NMR and MD simulations studies have suggested that Aβ monomer misfolding is nucleated by the formation of a turn around Val24-Lys28 and these studies have further highlighted various important factors that contribute to the turn formation and stabilization of misfolded Aβ monomer; these factors are (1) the intrinsic, conformational properties of the Val-Gly-Ser-Asn and Gly-Ser-Asn-Lys sequences to form the turn.[8] (2) The long-range electrostatic interactions between Lys28 and Glu22 or Asp23.[9,10] (3) Hydrophobic interactions between Val24 and Lys28 side chains.[8,9,11,12] (4) Hydrogen bond formation between the negatively charged Asp23 side chain with the backbone atoms of the turn region residues, Gly25, Ser26, Asn27, and Lys28.[9]

Various MD simulation studies of Aβ peptide, in an explicit water environment, have suggested the importance of the displacement of water molecules around the hydrophobic and hydrophilic region in Aβ misfolding and aggregation. Khatua et al.[13] revealed that water molecules around the hydrophobic region are relatively weakly bound and expected to be easily

Received: November 10, 2017
Revised: November 27, 2017
Accepted: December 4, 2017
Published: December 4, 2017

DOI: 10.1021/acs.molpharmaceut.7b00966
Mol. Pharmaceutics 2018, 15, 289−299

displaced during the hydrophobic collapse. In another study, Melquiond et.al.[14] revealed that water molecule expulsion took place in the hydrophilic region between residue 22 and residue 28 to form the aggregates/fibrils. Tarus et al.[12] revealed that an early event in the oligomerization process is the expulsion of water molecules that facilitate the turn formation around residues 24−27. It has been suggested that intrapeptide H-bonds play a key role in stabilizing the folded forms of proteins and H-bond cooperativity plays an important role in stabilization of a α-helix.[15,16] It is widely appreciated that water molecules, around proteins, form H-bond networks and play a crucial role in dynamics and stabilization of protein structure.[17] The presence of water molecules around the backbone causes lengthening of intrapeptide H-bonds within the backbone, thus loosening the structure.[18]

To investigate the inhibition of the Aβ peptide misfolding and aggregation by a candidate drug molecule, several studies have been performed. Hernández-Rodríguez et al.[19] performed an *in-silico* and *in vitro* study of galanthamine with Aβ42 their results revealed that galanthamine binds with Lys28, which helped the Aβ42 monomer to remain in an unfolded conformation. Sinha et al.,[20] by a mass spectrometry and solution-state NMR study, revealed that a "molecular tweezer", CLR01, specifically binds with Lys16 and Lys28 at the monomer stage which resulted in the formation of nontoxic structures of Aβ. Sinha et al.[21] revealed, by a mutational study, that substitution of Lys16 for Ala significantly reduced Aβ toxicity. All these studies have highlighted the importance of Lys16 and Lys28 in the conversion of Aβ monomers to Aβ aggregates/fibrils and their toxicity.

The conformational entropy of proteins is a proxy measure of its conformational dynamics, which is directly related to a number of conformation obtained by it.[22,23] It has been suggested that loss of backbone and side chain conformational entropy plays an important role in protein stability.[23,24] Conformational entropy significantly contributes to binding affinity and specific association between a protein and its ligand[25] and it has been revealed that binding of a ligand with a protein leads to the loss of conformation entropy of both ligand and protein binding residue.[26,27] A candidate molecule that can bind strongly to key residues should be able to counteract conformational entropy losses upon binding, and, therefore, could play an important role in the stability of the protein.

Crown ethers are small cyclic polyethers, first discovered by Nobel Prize winner Charles Pedersen more than 50 years ago. Due to their strong binding affinities to various metal ions and primary amines, members of the crown ether family have been widely applied in biological chemistry and probe chemistry.[28−31] Oukhatar et al.[32] used crown ethers to design molecular magnetic resonance imaging (MRI) sensing probe for neurotransmitters. Gawley et al.[33] used crown ethers to design visible fluorescence chemosensors for Saxitoxin (a potent neurotoxin). In another study, Işık et.al.[34] used crown ethers to design an intracellular fluorescent probe for Glutathione (GSH), that worked satisfactorily inside the human breast adenocarcinoma cells, and highlighted GSH distribution in the cytosol. All these aforementioned studies revealed that crown ethers can be used for imaging probes.

A recent study by Tian et al.[35] showed the testing of 12-crown-4 and 12-crown-4 conjugated with Pittsburgh compound B (PiB) a positron emission tomography (PET) tracer and targeting agent widely used for Aβ imaging. It was shown that 12-crown-4 ether and 12-crown-4 conjugated Pittsburgh compound B (PiB-C) inhibits the Aβ40 aggregation. It was revealed that the aggregation of Aβ40 was significantly reduced by 12-crown-4 and PiB-C. Furthermore, a dot blot experiment showed that in the presence of 12-crown-4 and PiB-C, a significantly lower number of fibrillar/prefibrillar structures were formed than in its absence or with PiB (PiB without conjugation). To investigate whether 12-crown-4 can reduce the Aβ42 toxicity, the authors treated SH-SY5Y neuronal cells with Aβ42 in the absence and presence of 12-crown-4, PiB and PiB-C; their data revealed that 12-crown-4 and PiBC could significantly reduce the toxicity of Aβ42. Two-photon microscopic imaging data revealed that PiB-C could readily penetrate the blood−brain barrier (BBB) and efficiently label Aβ. Overall the data of the aforementioned study suggested that 12-crown-4 and PiB-C could efficiently inhibit the aggregation of Aβ monomers into protofibrils/fibrils. The authors hypothesized that hydrogen bonds between crown ethers and positively charged amino acids of Aβ, such as Arg5, Lys16, Lys28, His13, and His14, inhibited/modified its aggregation. An experimental and computational study by Lee et al.[36] revealed that crown ethers can modify protein surface behavior dramatically by forming intra- or intermolecular interactions and they proposed that crown ethers can be used to modulate protein oligomerization/aggregation. In our previous study, we performed MD simulation of 12-crown-4 with Aβ40 fibrils trimer[37] and revealed three binding modes of 12-crown-4 on Aβ40 fibrils trimer. In the first binding mode, 12-crown-4 ether entered into the hydrophobic core and opened the "U-shaped" topology of Aβ40 fibril trimer, which is important for its cytotoxicity.[38] In the second binding mode, 12-crown-4 interacted with Lys28 breaking the salt-bridge formed between Asp23-Lys28, which plays an important role in aggregate/fibril stability.[39] Lastly, 12-crown-4 specifically interacted with Lys16, which is important for toxicity.[20]

In the present study, we aim to find a molecular basis for the early steps misfolding of Aβ peptides and effect of 12-crown-4 ether on Aβ40 and Aβ42 monomers misfolding, To fulfill this aim we have performed 29 all-atom molecular dynamics (MD) simulations, with a total simulation time of 11.4 μs, in the presence and absence of 12-crown-4; these methods allow us to study the Aβ40 and Aβ42 monomers conformation dynamics and monitor the interaction between the 12-crown-4 and the Aβ40 and Aβ42 monomers. The MD study will allow us to answer the following questions: (1) How does turn-formation take place in Aβ monomers? (2) What is the role of water solvation around turn-region residues in turn-formation? (3) Which region does 12-crown-4 bind to? (4) What is the impact of 12-crown-4 binding on Aβ40 and Aβ42 monomers? (5) How does 12-crown-4 binding with Aβ40 residues affect its conformational entropy and what are the implications of such entropy changes?

■ METHODS

Structure and Force Field for Aβ40 Monomer. In the present molecular dynamics study, NMR derived Aβ40 monomer (PDB id: 1BA4) and Aβ42 monomer (PDB id:1IYT) structures have been used (Figure: 1A, B). The Aβ40 monomer structure contains 1−14 unstructured region; the rest of the peptide adopts α-helical conformation.[40] The Aβ42 monomer structure contains two helical regions first one from residues 8−25 and the second one from 28−38, both regions connected by a regular a β-turn.[41] In this study we have used Charmm36 force field[42] for Aβ40 and Aβ42 monomer; a

DOI: 10.1021/acs.molpharmaceut.7b00966
Mol. Pharmaceutics 2018, 15, 289−299

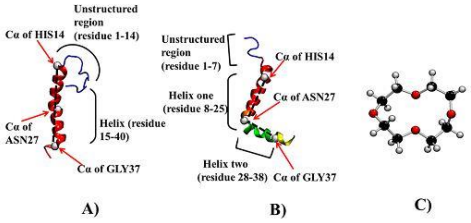

Figure 1. (A) The initial structure of Aβ40 monomer in cartoon representation. The unstructured region (residue 1 to 14) is shown in blue color, helix region (residue 15 to 40) is shown in red color. (B) The structure of Aβ42 monomer in cartoon representation. The unstructured region (residue 1 to 7) is shown in blue color; helix one region (residue 8 to 25) is shown in red color and helix two regions (residue 28 to 38) has been shown in green color. Cα atoms of His14, Asn27, and Gly37 used in angle calculation have been represented in VdW representation for both peptides in white color. (C) The structure of 12-crown-4 in CPK representation.

recent study Siwy *et.al.*[43] performed a comparative MD simulation study of $A\beta_{10-40}$ using four different protein force fields and two water models (standard TIP3P and modified TIP3P). Their data revealed that J-coupling and residual dipolar coupling constants of the Charmm36 force field, with standard TIP3P water model, was in the close agreement with experimental values. Thus, Charmm36 produces an accurate representation of the $A\beta_{10-40}$ conformational ensemble.

Structure and Force Field Parameters for 12-Crown-4 Ether. The structure of 12-crown-4 ether was taken from PubChem compound library (CID: 9269)[44] and is shown in Figure: 1C. The 12-crown-4 is a cyclic tetramer of ethylene oxide; its chemical formula is $C_8H_{16}O_4$.[45] 12-Crown-4 ether force field parameters were derived from the Charmm Additive and Classical Drude Polarizable Force Fields for Linear and Cyclic Ethers (ACDPFF).[46] ACDPFF is force field for linear and cyclic ether molecules and the same force field parameters for 12-crown-4 ether were used in our previous MD simulation work.[37] Aβ40/42 peptides are generated through a serial cleavage of amyloid precursor protein (APP) by β- and γ-secretase enzymes.[7,47] After cleavage, Aβ40/42 peptides are independent peptides, not associated with APP and contain their own N and C-terminals. In the present work, in the case of Aβ40, we have treated ASP-1 as an N-terminal residue and VAL-40 as a C-terminal. In the case of Aβ42, we have treated ASP-1 as an N-terminal residue and ALA-42 as a C-terminal residue.

Simulation Protocol. The system, in the presence of the 12-crown-4, contains one Aβ40 monomer, two 12-crown-4 molecules, and 8979 water molecules. In the absence of 12-crown-4, Aβ40 monomer system contains 8993 water molecules. The system of 12-crown-4 with Aβ42 monomer contains two 12-crown-4 molecules with one Aβ42 monomer and 10658 water molecules. The Aβ42 monomer system, in absence of 12-crown-4, contains 9025 water molecules. Three Na^+ counterions were added into all systems to achieve overall charge neutrality. Initially, 5000 steps of steepest descent were performed to energy minimize the systems,[48] followed by two sequential 100 ps equilibration simulations, first in the canonical (NVT) ensemble, then the isobaric−isothermic (NPT) ensemble; NPT ensemble was used for the production simulations. The bond lengths from heavy atoms to hydrogen atoms, of the Aβ40 and Aβ42 monomers and 12-crown-4, were constrained using the LINCS algorithm[49] and the SETTLE algorithm[50] was used for water molecule bond length constraints. Particle mesh Ewald (PME)[51] was used for long-range electrostatics and van der Waals (vdW) interactions with a short-range cutoff of 10 Å. In both systems (Aβ40 and Aβ42) Aβ peptide and nonprotein components (water, 12-crown-4, and ions) were separately coupled with external pressure and temperature baths. The velocity-rescale algorithm[52] was used for temperature coupling and the Parrinello−Rahman algorithm was used for pressure coupling.[53] Temperature and pressure bath coupling times were set to 0.1 and 0.1 ps, respectively. All MD simulations were performed at a pressure of 1 bar and temperature of 300 K.

A total of 11 control simulations were performed, one (2 μs), four (200 ns), and six (100 ns), to explore the conformation change in Aβ40 monomer in the absence of 12-crown-4; a total of 16 simulations were performed in the presence of 12-crown-4 for 12-Aβ40 monomer system, one (2 μs), five (200 ns), and ten (100 ns). For Aβ42 monomer system two simulations were performed, one in the presence of 12-crown-4 and other in the absence of 12-crown-4; each simulation was 2 μs long, in total of 4 μs simulations were performed for the Aβ42 system. In both systems, Aβ40 and Aβ42, one 12-crown-4 molecule was placed near to the N-terminal and the other 12-crown-4 molecule was placed near to the C-terminal of Aβ40 monomer. No prior contacts were formed between Aβ40 and Aβ42 monomer residues and 12-crown-4.

Analysis Details. Changes in the conformational topology of the Aβ40 and Aβ42 peptides was measured via the angle of the α-carbon atoms of HIS14, ASN27, and GLY37 (Figure: 1A, B). Aβ peptide has been considered in "U-shaped" if angle value is 60° or less. The number of water molecules has been calculated within 3.5 Å of Lys28 and Val24 residues, using an in-house Tcl script. For H-bond calculations the cutoff distance, between donor and acceptor atoms, was set at 3.5 Å and the angle was considered to be 30°. To understand the dynamics of Lys28 (backbone and side chain) and the effect of 12-crown-4 binding on its dynamics, we divided the trajectory into 10 ns bins and calculated the average structure for that bin; using the average structure as reference with the "fit none" option of the Gromacs RMS program, RMSD was calculated and averaged for each bin. To investigate conformational entropy of Lys28 (Backbone and side chain), the mass-weighted covariance matrix was calculated, which was used for quasi-harmonic approximation.[54] Conformational entropy was calculated and averaged for each 10 ns bin. An interaction between 12-crown-4 and Aβ peptides residues were considered when the distance, between the COM of the residues and COM of 12-crown-4, was 10 Å or less. The percentage of contact of Aβ monomers for each residue with 12-crown-4 was calculated by counting the number of times an interaction occurred. Interaction energy between Aβ peptides residues and 12-crown-4 was calculated by using g_mmpbsa tool.[55] Secondary structure analysis for Aβ40 and Aβ42 monomers were performed using the dictionary secondary structure of protein (DSSP).[56] The GROMACS[57] sham program was used to construct the free energy contour maps and RMSD (backbone atoms) and Rg (backbone atoms) of Aβ peptides were used as an order parameter to determine free energy (kJ/mol). The initial NMR structure was used for calculating the RMSD (backbone atoms) and Rg (backbone atoms) for in the presence of absence of 12-crown-4, free energy contour maps.

DOI: 10.1021/acs.molpharmaceut.7b00966
Mol. Pharmaceutics 2018, 15, 289−299

RESULTS

Conformational Transition of Aβ40 and Aβ42 in "U-Shaped" Structure and Loss and Gain of Water Around Turn Region Residue Val24 and Lys28. To investigate the conformational transition for the Aβ40 monomer from the native "I-shaped" structure to the "U-shaped structure" and Aβ42 monomer from the "L-shaped" structure to "U-shaped structure" in the presence and absence of 12-crown-4, we calculated angle of bending for all simulation trajectories (see the Method Section for more details). It has been reported that the turn formation in Aβ peptide is the first step toward the formation of the misfolded structure and NMR and MD simulations studies have suggested that Val24-Lys28 is the most probable region to form a turn.[8,11] Another study, however, has suggested that a turn could also form at residue positions Glu22-Asp23.[58] Visual inspection of 11 control trajectories including the 2 μs long of Aβ40 monomer revealed that in six simulations the turn formed between residues Val24-Lys28, in two of the simulations the turn formed at residue position Gly29, and in one simulation the turn was formed at residue position Gul22-Asp23. Visual inspection of Aβ42 monomer 2 μs trajectory revealed that the turn was formed around Val24-Lys28.

To investigate the effect of water molecules on Aβ40 and Aβ42 peptides, on turn formation, we calculated the number of water molecules within 3.5 Å of turn region residues. In a total of 11 control simulations for Aβ40 monomer, in 6 simulation trajectories we observed loss of water molecules around residue Val24 and in four simulation trajectories, we observed gain of water molecules around Lys28. In four simulation trajectories we observed loss and gain of water molecules occurring at the same time in Aβ40 monomer system. In case of Aβ42 monomer, we also observed gain and loss of water molecules around Val24-Lys8 residues. The same phenomenon was observed in the long trajectories of Aβ40 and Aβ42 monomers in the presence of 12-crown-4, where turn formation took place.

Figure 2A and C show the time evolution of the change in angle of Aβ40 and Aβ42 monomer, and Figure 2B and D show the time evolution of gain and loss of water molecules around Lys28 and Val24 in two of the representative 2 μs long trajectories of Aβ40 and Aβ42 in absence of 12-crown-4. To understand the mechanism of turn formation, we have plotted the change in angle and gain/loss of water for the initial 600 ns, until water gain stabilized and the peptide remained stable in "U-shaped" structure. The change in angle of Aβ40 monomer was observed at ∼320 ns (Figure: 2A) when the peptide changed from native "I-shaped" conformation to "U-shaped" conformation. The peptide was considered in "U-shaped" when angle was 60° or less; in the meantime we observed there was a sudden gain of water molecules around Lys28 (Figure 2B, red line, Table 1) and loss of water molecule around Val24 (Figure 2B, black line, Table 1). On average there was a gain of ∼0.91 water molecules around Lys28 and a loss of ∼1.28 water molecules around Val24 after "U-shaped" structure formation in the Aβ40 monomer representative simulation.

In Aβ42 monomer, during the transition from "L-shaped" (80°−120°) to "U-shaped" structure (≤60°), we observed an intermediate state where Aβ42 monomer obtained an "I-shaped" structure(∼130° to ∼170°). At ∼ 32 ns, Aβ42 monomer obtained "I-shaped" structure, which leads to an increase of water molecules around both Lys28 and Val24

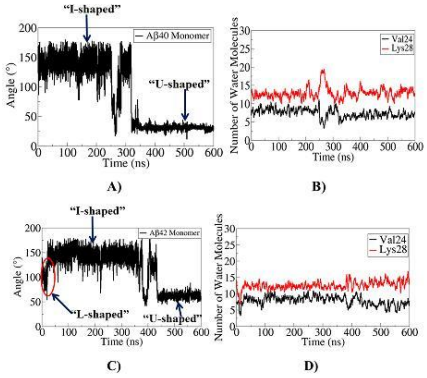

Figure 2. (A) The time evoluion of change in angle of Aβ40 monomer. (B) The time evolution of number of water molecules around Val24 and Lys28 of Aβ40 monomer. (C) The time evolution of change in angle of Aβ42 monomer. (D) The time evolution of number of water molecules around Val24 and Lys28 residues of Aβ42 momomer.

Table 1. Average Number of Water Molecules Around Lys28 and Val24 in Aβ40 and Aβ42 Monomers in "I-Shaped" and "U-Shaped" Conformations[a]

name of the residue	average number of water molecules in "I-shaped" structure	average number of water molecules in "U-shaped" structure
Aβ40 and Lys28	12.27	13.18
Aβ40 and Val24	8.25	6.97
Aβ42 and Lys28	12.17	13.40
Aβ42 and Val24	8.29	6.66

[a]In the "I-shaped" conformation, average water molecules were calculated from 50 to 150 ns time period for Aβ40 and Aβ42. In the "U-shaped" structure, average water molecules were calculated for Aβ40 monomer from 400 to 500 ns and for Aβ42 monomer from 450 to 550 ns.

(Figure 2D red and black line) and an increase of the angle form ∼125° to ∼170°. At ∼ 440 ns (Figure 2C) the Aβ42 monomer transformed from "I-shaped" structure to "U-shaped" structure; in the meantime, gain of water molecules around Lys28 and loss of water molecules around Val24 took place (Table 1) On average there was a gain of ∼1.227 water molecules around Lys28 and a loss of ∼1.631 water molecules around Val24, after "U-shaped" structure formation in the Aβ42 monomer simulation. Overall, this data suggest that the gain and loss of water molecules play a crucial role in early stage misfolding of Aβ40 and Aβ42 monomers.

Hydrogen bonds (H-Bonds) Formed by Lys28 Backbone in Aβ40 Monomer. To further investigate the effect of water gain around the Lys28 backbone, on the formation of the turn, we have calculated the number of intrapeptide H-bonds between amide H-bond donor and carbonyl H-bond acceptor atoms within the Lys28 region of the helix (Figure 3A, black line) in one of the representative trajectories of Aβ40 monomer, in this trajectory turn was formed ∼30 ns. Before

DOI: 10.1021/acs.molpharmaceut.7b00966
Mol. Pharmaceutics 2018, 15, 289−299

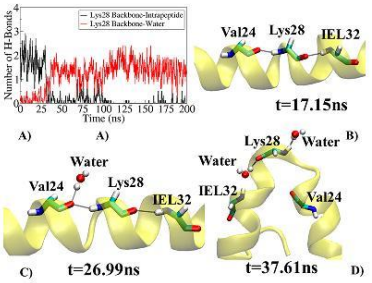

Figure 3. (A) The time evolution of number of intrapeptide H-bonds (black line) and number of H-bonds formed with water molecules. (B) Represented image of H-bonds formed by Lys28 at t = 17.15 ns. (C) Represented image of H-bonds formed by Lys28 at t = 26.99 ns. (D) Represented image of H-bonds formed by Lys28 at t = 37.61 ns.

the turn formation, there are two H-bonds, one formed between the amide group of Lys28 and the carbonyl group of Val24 and the other between the carbonyl group of Lys28 and the amide group of Ile32 (Figure 3B). The aforementioned H-bonds are almost completely broken after the turn-formation (Figure: 3D) and this indicates the importance of the intrapeptide H-bonds for maintaining Aβ40 peptide stability. H-bonds, between water molecules and the backbone amide and carbonyl groups, replaced the intrapeptide H-bonds during the turn formation (Figure 3A, red line); this leads us to believe that the formation of the water—backbone H-bonds provide a motivation for breaking the intrapeptide H-bonds and, therefore, turn-formation.

Percentage of Contact of 12-Crown-4 Ether with Aβ40 and Aβ42 Monomers. To identify the residues of Aβ40 and Aβ42 monomers, which formed the most contacts with 12-crown-4, we computed the percentage of contacts with each residue in 2 μs long trajectories (Figure 4). 12-Crown-4 ether

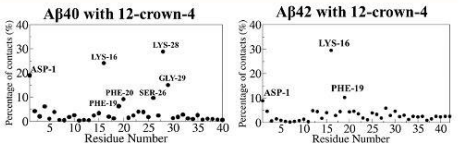

Figure 4. (A) The percentage of contacts formed by 12-crown-4 with each residue of Aβ40 monomer in 2 μs simulation trajectory. (B) The percentage of contacts formed by 12-crown-4 with each residue of Aβ42 monomer in 2 μs simulation trajectory.

formed major contacts with positively charged residues, Lys16 and Lys28, and N-terminal, Asp1 in Aβ40 monomer (Figure 4A). 12-Crown-4 ether also formed contact with central hydrophobic cluster residues (Phe19, Phe20), turn region residues (Ser26 and Gly29). In case of Aβ42 monomer, we observed 12-crown-4 formed major contacts with positively charged Lys16, N-terminal Asp1, and central hydrophobic cluster residue Phe19 (Figure 4B). This analysis revealed that 12-crown-4 ether formed major contact with positively charged residue Lys in case of both peptides, we observed in case of Aβ40 it forms contacts with both Lys residues majorly, however; in Aβ42 monomer simulation, 12-crown-4 forms major contact with Lys16 and minor contacts with Lys28. Other than Lys28, which is one of the crucial residues in Aβ misfolding, Lys16 has been reported to play a major role in Aβ toxicity.[21] Various studies have suggested that Lys16 can form a salt-bridge with Glu22, which helps to arrange Aβ into the antiparallel arrangement.[59,60] Karr et.al. reveal that Asp1 is a binding site of Cu ions[61] and binding of Cu with Asp1 increases the toxicity of Aβ.[62]

Secondary Structure Changes in Aβ40 and Aβ42 Monomers in Presence and Absence of 12-Crown-4. Simmons et al.[63] performed structure−activity relationship of Aβ40 and revealed neurotoxicity in the primary neuronal cell; their data showed that Aβ with β-sheet structure was highly toxic and Aβ structure with a random coil is less toxic. To investigate effect of 12-crown-4 binding on secondary structure of Aβ peptides we have performed time evolution of secondary structure analysis of Aβ40 and Aβ42 monomers in the presence and absence of 12-crown-4 (Figure 5).

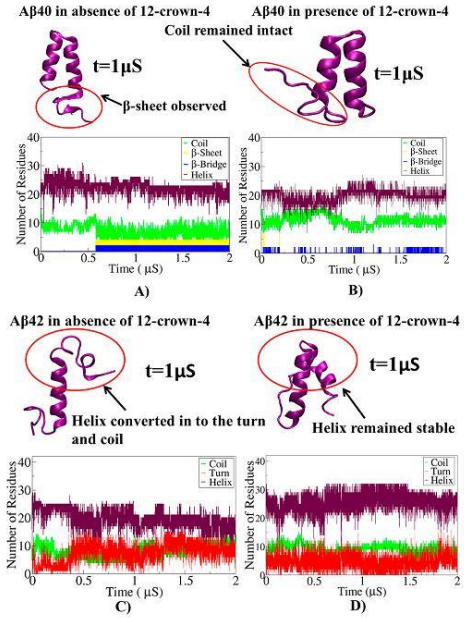

Figure 5. (A) Time evolution of secondary structure of Aβ40 monomer in the absence of 12-crown-4. (B) Time evolution of secondary structure of Aβ40 monomer in the presence of 12-crown-4. (C) Time evolution of secondary structure of Aβ42 monomer in the absence of 12-crown-4. (D) Time evolution of secondary structure of Aβ42 monomer in the presence of 12-crown-4.

In the absence of 12-crown-4, at ∼600 ns we observed some part of the unstructured region was converted into the β-sheet and the β-bridge in Aβ40 monomer and remained stable until the end of the simulation (Figure 5A). The aforementioned event could be significant since a recent Aβ fibrils structure has revealed that the unstructured region of Aβ forms a β-sheet structure.[64] In the presence of 12-crown-4, no β-sheet

DOI: 10.1021/acs.molpharmaceut.7b00966
Mol. Pharmaceutics 2018, 15, 289−299

formation was observed in the Aβ40 peptide (Figure 5B); however, there is a transition between helix to the coil from ∼250 ns to ∼800 ns, but Aβ40 peptide regained its helicity and remained stable until the end of the simulation.

In the case of Aβ42 monomer in absence of 12-crown-4, we observed helix 2 of the peptide (residue 28−38) was almost completely converted into the turn and coil (Figure 5C); however, in the presence of 12-crown-4, the helix region remained intact until the end of the simulation (Figure 5D). Overall this data suggest that binding of 12-crown-4 could affect the secondary structure change of the Aβ40 and Aβ42 peptides.

Interaction of 12-Crown-4 Ether with Asp1, Lys16, and Lys28 of Aβ40 Monomer. Figure 6A shows the time evolution of COM distances between 12-crown-4, with major contact-forming residues. 12-crown-4 interactions with Aβ40 monomer, in the 2 μs long trajectory, can be divided into three steps; in the first step, 12-crown-4 interacted with c-terminal Asp-1 for the period of ∼343 ns (350−693 ns) (Figure 6A, black line). In the second step, 12-crown-4 formed an interaction with Lys28 for a total time of ∼307 ns (953−1260 ns) (Figure 6A, green line). In the third step, 12-crown-4 formed an interaction with Lys16 for a period of ∼255 ns (1390−1585 ns) (Figure 6A, red line).The time evolution of interaction energies, between 12-crown-4 (Figure 6B) and major binding residues, revealed that the interaction energy between Asp1 and 12-crown-4 was slightly less negative (∼ −90 kJ/mol, Figure 6B, black line) than the interaction energy of Lys residues with 12-crown-4 was (∼ −120 kJ/mol, Figure 6B, red and green line). To investigate the number of water molecules displaced by 12-crown-4, to bind with these residues we calculated the average number of water molecules around these residues before and during the binding of 12-crown-4 (Table 2). It reveals that 12-crown-4, displaced ∼3.97, ∼3.52, and ∼1.84 to interact with Asp1, Lys16, and Lys28, respectively.

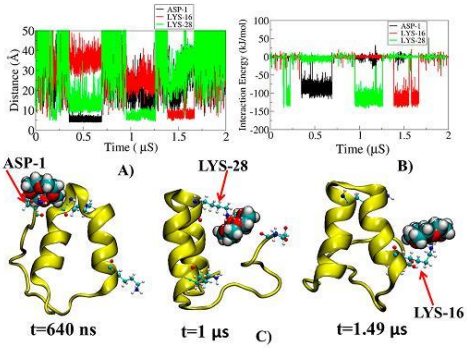

Figure 6. (A) Time evolution of COM distances between Asp1, Lys16, and Lys28 from COM of 12-crown-4. (B) Time evolution of interaction energy between 12-crown-4 and Asp1, Lys16, and Lys28. (C) Three snapshots form 2 μs trajectory of Aβ40 monomer taken at different time points during 12-crown-4 binding with major contact forming residues.

Interaction of 12-Crown-4 Ether with Asp1, Lys16, and Phe19 of Aβ42 Monomer. Aβ42 monomer simulations with 12-crown-4 revealed that 12-crown-4 formed major contacts with Asp1, Lys16, and Phe19 residues. In 2 μs long simulation of Aβ42 monomer with 12-crown-4, we observed attachment and detachment of 12-crown-4 with these residues at different time points. 12-Crown-4 interacted with Asp1 for a total period of ∼160 ns in two points of time (166−276 ns, 1230−1280 ns) (Figure 7A, black line). 12-Crown-4 interacted for a total of ∼506 ns with Lys16 at four different time points (87−142 ns, 285−374 ns, 463−740 ns, 985−1070 ns) (Figure 7A, red line). During its interaction with Lys16, 12-crown-4 also formed interaction with central hydrophobic cluster residue Phe19 (Figure 7A, green line). *In vitro* studies have suggested that a substitution of Lys16 for Ala in Aβ1−28[65] and a substitution of Phe19 or Phe20 for Ala, in Aβ10−23[66] results in the inability for peptides to form Aβ fibril like structures. As for the nature and strength of the interactions of 12-crown-4 and Asp1, Lys16 and Phe19, the 12-crown-4 formed hydrophobic interactions with Phe19 (∼8 kJ/mol, Figure 7B, green line) and formed electrostatic interactions with Lys28 and Asp1 (∼120 kJ/mol, Figure 7B, red line, ∼ 90 kJ/mol, Figure 7B, black line). To investigate how many water molecules 12-crown-4 has to displace to form interaction with major binding residues, we have calculated average water molecules around these residues before and during 12-crown-4 (Table 3). 12-

Table 2. Average Number of Water Molecules before and during the Binding of 12-Crown-4 Around Asp1, Lys16, and Lys28[a]

name of the residue (Aβ40 monomer)	number of water molecules before 12-crown-4 binding	number of water molecules during 12-crown-4 binding
Asp-1	14.50	10.53
Lys-16	13.04	9.52
Lys-28	10.76	8.91

[a]Before binding of 12-crown-4, a number of water molecules averaged from 0 to 100 ns around each residue and during binding for Asp-1(400 to 500 ns), for Lys16 (1400 to 1500 ns) and for Lys28 (1000 to 1100 ns).

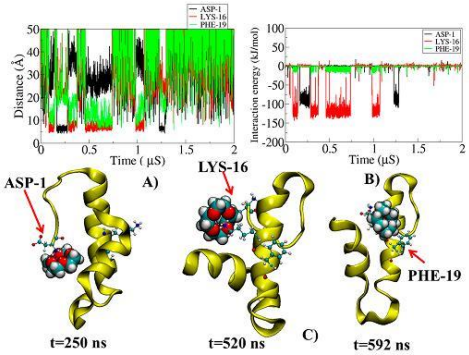

Figure 7. (A) Time evolution of COM distances between Asp1, Lys16, and Phe19 from COM of 12-crown-4. (B) Time evolution of interaction energy between 12-crown-4 and Asp1, Lys16, and Phe19. (C) Three snapshots form 2 μs trajectory of Aβ42 monomer taken at different time points during 12-crown-4 binding with major contact forming residues.

DOI: 10.1021/acs.molpharmaceut.7b00966
Mol. Pharmaceutics 2018, 15, 289−299

Crown-4 displaced ~4.24, ~4.87, and ~0.07 water molecules around Asp-1, Lys16, and Phe19, respectively, to form the interaction with these residues.

Table 3. Average Number of Water Molecules before and during the Binding of 12-Crown-4 Around Asp-1, Lys16, and Phe19[a]

name of the residue (Aβ42 monomer)	number of water molecules before 12-crown-4 binding	number of water molecules during 12-crown-4 binding
Asp-1	14.62	10.38
Lys-16	11.66	6.79
Phe-19	12.06	11.99

[a]For Asp-1 before binding of 12-crown-4, a number of water molecules averaged from 50 to 150 ns and during binding from 170 to 270 ns. For Lys16 and Phe19 before binding of 12-crown, a number of water molecules averaged from 0 to 60 ns and during binding 300 to 360 ns.

In all the simulations we observed that 12-crown-4 binds with Aβ residues for certain periods of time and detaches; however; after detachment we have again observed binding with the same residues, suggesting attachment and detachment of 12-crown-4 with Aβ residues is a spontaneous process. There could be several factors that could contribute to its detachment; for example, (1) change in the conformation of binding residues. (2) Perturbation of water structure around the binding residue. (3) Competition between water and 12-crown-4 with binding residues.

Free Energy Landscape of Aβ40 and Aβ42 Monomers in Absence and Presence of 12-Crown-4. To investigate the effect of 12-crown-4 on misfolding of Aβ monomers, we have plotted two-dimensional free energy contour maps as a function of RMSD and RG, in the absence and presence of 12-crown-4, as shown in Figures 8 and 9 with representative

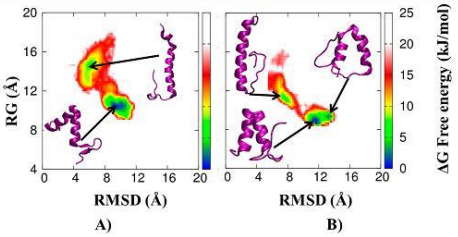

Figure 8. (A) Free energy landscape of Aβ40 monomer in the absence of 12-crown-4. (B) Free energy landscape of Aβ40 monomer in the presence of 12-crown-4.

structures at each local free energy basin. In the absence of 12-crown-4 (Figure 8A), there was large conformational space explored by the Aβ40 monomer in comparison to the presence of 12-crown-4 (Figure 8B). In the absence of 12-crown-4, we observed two highly populated states of Aβ40 monomer on free energy surface, one native-like structure state and other another one "U-shaped" structure with β-sheet. However, in the presence of 12-crown-4 (Figure 8B), there were three most populated energy states. One native-like structure state and two "U-shaped" structures with intact unstructured regions.

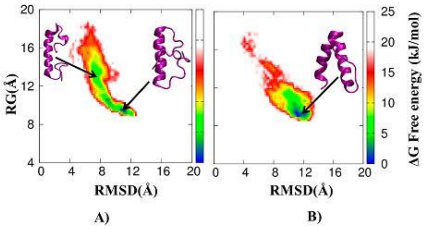

Figure 9. (A) Free energy landscape of Aβ42 monomer in the absence of 12-crown-4. (B) Free energy landscape of Aβ42 monomer in the presence of 12-crown-4.

In the absence of 12-crown-4 the unstructured region adpoted the β-sheet structure, which made it much less flexible and more compact, compared to the structure in the presence of 12-crown-4. It should be noted that in the absence of 12-crown-4, the number of states in the transition between the "I-shaped" and "U-shaped" structure are far greater than in the presence of 12-crown-4. A low number of states in the transition region leads to an entropy barrier to transition between the "I-shaped" and "U-shaped" structure, and therefore, a decrease in the opportunity for transition, in the presence of 12-crown-4.

In Aβ42 monomer, the free energy landscape, in the absence of 12-crown-4 (Figure 9A), showed a more spread-out profile, with two, low free energy bins; this is due to the conversion of second helical region into coil and turn making the structure unstable.

In the presence of 12-crown-4, there is only one low free energy bin populated, the stable state was due to both the helix regions in Aβ42 monomer being intact. Overall this data suggest that the presence of 12-crown-4 affected the free energy landscape of Aβ monomer conformation.

Lys28 Flexibility and Conformational Entropy in Presence and Absence of 12-Crown-4 of Aβ40 Monomer. To provide a better understanding of the interplay between 12-crown-4 and Lys28, we calculated RMSD and conformational entropy (see the method section for more details) for Lys28 in the presence and absence of 12-crown-4, using the quasi-harmonic method. The function/misfolding of the protein is directly linked to its intrinsic flexibility; however, the intrinsic flexibility of a protein can be perturbed by its interaction and binding with other molecules, which could lead to a change in its function. Intuitively, binding between the protein and other molecules is usually considered to restrict the intrinsic flexibility of the binding region in a protein and in its binding partner, which results in a significant loss of conformational entropy.[67,68]

The initial RMSD value of Lys28 side chain (Figure 10A) was ~2.4 Å and increased to ~6.4 Å during the turn formation (30−40 ns), which consequently increased its flexibility. During the turn formation, the number of conformations sampled by the Lys28 side chain drastically increased (Figure 10A green points). Figure 10B shows the backbone and side chain conformational entropy of the Lys28 in one of the representative trajectories of the control simulations (in the absence of 12-crown-4). The increase in RMSD correlated with a significant gain in the conformational entropy of the Lys28 backbone and side chain during the turn formation (30−40 ns). The increased conformational entropy of the backbone and

DOI: 10.1021/acs.molpharmaceut.7b00966
Mol. Pharmaceutics 2018, 15, 289−299

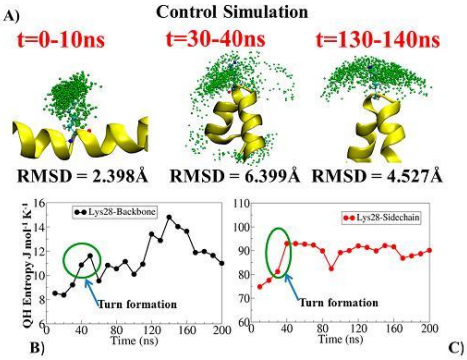

Figure 10. (A) Three representative images of Aβ40 monomer in one of the control simulations at different time point with RMSD values. (B) QH entropy of Lys28 backbone and side chain averaged for 10 ns bin. Green points in the figure represent different number of state visited by the Lys28 side chain.

side chain provided a thermodynamic motivation to form the turn in the Aβ40 peptide.

To investigate how the 12-crown-4 can modify the conformation, we have performed a similar conformational analysis for a representative simulation in the presence of 12-crown-4. Figure 11A shows the RMSD of Lys28 side chain, in

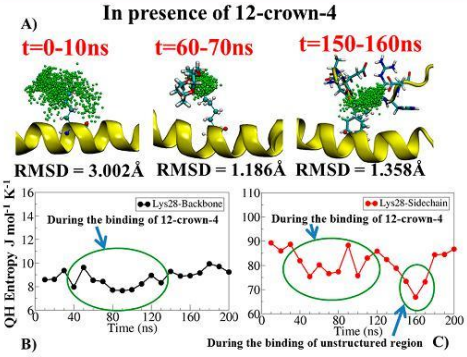

Figure 11. (A) Three representative images of Aβ40 monomer in one of the simulations in the presence of 12-crown-4 at different time point with RMSD values. (B) QH entropy of Lys28 backbone and side chain averaged for 10 ns bin. Green points in the figure represent number of state visited by the Lys28.

the presence of 12-crown-4, at different time points in the simulation. Initially, from 0 to 10 ns, before the interaction between Lys28 with 12-crown-4, the RMSD value for Lys28 side chain was ~3.00 Å; during the binding with 12-crown-4, it reduced to ~1.186 Å. Around ~140−160 ns, we again observed a loss of RMSD due to the contacts of unstructured region residues with the Lys28 side chain. Reduction in RMSD during 12-crown-4 binding resulted in loss of flexibility of Lys28 side chain; this leads to significant loss of number of states visited by the Lys28 side chain (Figure 11A green points).

Figure 11B and C shows the conformational entropy of Lys28 backbone and side chain. During the binding of 12-crown-4 (~30−110 ns), a significant loss of conformational entropy was observed, as binding of 12-crown-4 restricted the number of conformations obtained by Lys28 backbone and side chain. At a time point of ~120−160 ns, we also observed binding of the unstructured region with Lys28 side chain, which resulted in a reduction of its conformational entropy. Despite a loss of entropy upon binding of the 12-crown-4 and Lys28, which should be unfavorable, the attractive interaction between 12-crown-4 and Lys28 more than compensates.

■ DISCUSSION

We have performed Aβ40 and Aβ42 monomer simulations in the presence and absence of 12-crown-4. Our simulation data revealed that Aβ40 and Aβ42 peptide misfolding starts with the formation of the turn, in agreement with previous studies.[8−10] In our simulations we observed the turn formation, around Val24-Lys28, is initiated by the gain and loss of water molecules around Lys28 and Val24, respectively. Loss of water molecules around Val24 is in agreement with well-established "hydrophobic effect" phenomena,[69] which suggest that during the protein folding/misfolding, the nonpolar side chains are removed from contact with water molecules; this leads to the burial of hydrophobic side chains into the core of protein. A previous study[18] suggested that nearby nonpolar groups dehydrate backbone hydrogen bonds, which makes it thermodynamically unfavorable to expose the backbone amide and carbonyl groups. Shielding the H-bonds from water molecules helps the protein to maintain secondary structure and warrant them overall stability. In the present study, we observed that the polar/hydrophobic part of the Lys28 side chain gained a significant number of water molecules, which lead to the water molecules becoming more accessible to the Lys28 backbone. At the same time point in the simulation, there was a significant gain of Lys28 side chain conformation entropy which leads to a gain in the backbone conformational entropy. Water gain around the Lys28 backbone and entropy gain leads to the lengthening of the intrapeptide H-bonds formed by amide and carbonyl group of Lys28 backbone, and these H-bonds were replaced by water molecules, which destabilizes the Aβ peptide. Loss and gain of water molecules around Val24 and Lys28, conformational entropy gain of Lys28, and breaking of intrapeptide H-bonds are key factors, in turn formation/early stage misfolding of Aβ peptide.

Our simulation data in the presence of 12-crown-4 revealed that it specifically binds to charged residues, Lys16, Lys28, Asp1, and Phe19. 12-Crown-4 contains hydrogen and oxygen atoms, this helps 12-crown-4 to form electrostatic interactions with charged Lys, N-terminal Asp, and VdW/hydrophobic interactions with Phe19 residue. These pharmacophore features of 12-crown-4 could be used in designing new highly specific candidate drug molecules or imaging probes. In one previous study, Jiang et al.[70] used pharmacophore features of an Aβ fragment complex with the dye orange G, which specifically binds with Lys16 to search new potential compounds. They identified eight diverse and three compound derivatives that reduced the Aβ cytotoxicity against mammalian cells by up to 90%.

Our data support the hypothesis of Tian et al.[35] that 12-crown-4 can bind with positively charged Lys residues of Aβ peptide and perturb its aggregation and toxicity. 12-Crown-4,

DOI: 10.1021/acs.molpharmaceut.7b00966
Mol. Pharmaceutics 2018, 15, 289−299

conjugated with PiB, was shown to cross BBB and inhibit the Aβ aggregation and the present study has highlighted the molecular-level factors with which the inhibition of aggregation may occur. The present study is also in-line with previous studies which suggest that Lys specific candidate drug molecules could perturb the Aβ aggregation and reduce its toxicity.[20,21] Simmons et al.[63] study suggested that the Aβ peptide with β-sheet structure was highly toxic, and Aβ structure with a random coil is less toxic. As we observed in the presence of 12-crown-4 secondary structure remained stable in both Aβ0 and Aβ42 monomer, which may affect the toxicity of Aβ monomers.

■ CONCLUSION

In summary, our simulations have shed light on the fundamental understating of turn formation. We observed the gain of water molecules around Lys28 side chain and increase in its conformational entropy that leads to the break of intrapeptide H-bonds of Lys28 backbone and consequently the turn formation. Our data reveals that 12-crown-4, which has potential as a drug carrier when conjugated with an amyloid targeting agent, is highly specific toward Lys16, Lys28, and Asp1; moreover, we observed contacts formed by 12-crown-4 with central hydrophobic cluster residues, Phe19 and Phe20, and turn region residues Ser26 and Gly29. Secondary structure analysis suggests that 12-crown-4 binding inhibited secondary change in both Aβ40 and Aβ42 monomer. Free energy contour maps revealed that 12-crown-4 can restrict number of conformations explored by Aβ peptides and therefore, affect its misfolding.

The present study deepens our knowledge about the molecular-level factors that contribute to the turn formation in early stage misfolding of the Aβ40 monomer; furthermore, it underpins the importance of Lys residues as potential targets for Aβ inhibition. The present study has, therefore, opened up new avenues in design of potential inhibitors for early stage misfolding of Alzheimer's Aβ monomers.

■ ASSOCIATED CONTENT

Supporting Information

The Supporting Information is available free of charge on the ACS Publications website at DOI: 10.1021/acs.molpharmaceut.7b00966.

Results of gain/loss of water and binding of 12-crown-4 in Aβ40 monomer simulations (PDF)

Movie of Aβ40 monomer in absence and presence of 12-crown-4 (AVI)

Movie of Aβ42 monomer in absence and presence of 12-crown-4 (AVI)

■ AUTHOR INFORMATION

Corresponding Authors

*E-mail: nikhil.08oct@gmail.com.

*E-mail: skelton@ukzn.ac.za.

ORCID

Nikhil Agrawal: 0000-0002-5365-6332

Adam A. Skelton: 0000-0003-0155-8287

Funding

N.A. would like to thank DST-NRF, South Africa, for project funding (grant number: 106272). We would like to thank college of Health Sciences at UKZN for funding and infrastructure support.

Notes

The authors declare no competing financial interest.

■ ACKNOWLEDGMENTS

We are indebted to UKZN "hippo" super computer facility, Durban, South Africa, and Centre for High Performance Computing (CHPC) in Cape Town, South Africa, for computational resources. We would like to thanks NRF for travel grants.

■ REFERENCES

(1) Uflacker, A.; Doraiswamy, P. M. Alzheimer's Disease: An Overview of Recent Developments and a Look to the Future. *Focus* **2017**, *15*, 13−17.

(2) Association, A. 2016 Alzheimer's disease facts and figures. *Alzheimer's Dementia* **2016**, *12*, 459−509.

(3) Buxbaum, J. N. Alzheimer's Disease: It's More Than Aβ. *FASEB J.* **2017**, *31*, 2−4.

(4) Pivi, G. A. K.; de Andrade Vieira, N. M.; da Ponte, J. B.; de Moraes, D. S. C.; Bertolucci, P. H. F. Nutritional management for Alzheimer's disease in all stages: mild, moderate, and severe. *Nutrire* **2017**, *42*, 1.

(5) Jakob-Roetne, R.; Jacobsen, H. Alzheimer's disease: from pathology to therapeutic approaches. *Angew. Chem., Int. Ed.* **2009**, *48*, 3030−3059.

(6) Mullard, A. Alzheimer amyloid hypothesis lives on. *Nat. Rev. Drug Discovery* **2016**, *16*, 3−5.

(7) Bergström, P.; Agholme, L.; Nazir, F. H.; Satir, T. M.; Toombs, J.; Wellington, H.; Strandberg, J.; Bontell, T. O.; Kvartsberg, H.; Holmström, M.; et al. Amyloid precursor protein expression and processing are differentially regulated during cortical neuron differentiation. *Sci. Rep.* **2016**, *6*, 6.

(8) Lazo, N. D.; Grant, M. A.; Condron, M. C.; Rigby, A. C.; Teplow, D. B. On the nucleation of amyloid β-protein monomer folding. *Protein Sci.* **2005**, *14*, 1581−1596.

(9) Baumketner, A.; Bernstein, S. L.; Wyttenbach, T.; Lazo, N. D.; Teplow, D. B.; Bowers, M. T.; Shea, J. E. Structure of the 21−30 fragment of amyloid β-protein. *Protein Sci.* **2006**, *15*, 1239−1247.

(10) Cruz, L.; Urbanc, B.; Borreguero, J. M.; Lazo, N. D.; Teplow, D. B.; Stanley, H. E. Solvent and mutation effects on the nucleation of amyloid β-protein folding. *Proc. Natl. Acad. Sci. U. S. A.* **2005**, *102*, 18258−18263.

(11) Borreguero, J. M.; Urbanc, B.; Lazo, N. D.; Buldyrev, S. V.; Teplow, D. B.; Stanley, H. E. Folding events in the 21−30 region of amyloid β-protein (Aβ) studied in silico. *Proc. Natl. Acad. Sci. U. S. A.* **2005**, *102*, 6015−6020.

(12) Tarus, B.; Straub, J. E.; Thirumalai, D. Dynamics of Asp23−Lys28 Salt-Bridge Formation in Aβ10−35 Monomers. *J. Am. Chem. Soc.* **2006**, *128*, 16159−16168.

(13) Khatua, P.; Jose, J. C.; Sengupta, N.; Bandyopadhyay, S. Conformational features of the Aβ 42 peptide monomer and its interaction with the surrounding solvent. *Phys. Chem. Chem. Phys.* **2016**, *18*, 30144−30159.

(14) Melquiond, A.; Dong, X.; Mousseau, N.; Derreumaux, P. Role of the Region 23−28 in Aβ Fibril Formation: Insights from Simulations of the Monomers and Dimers of Alzheimer's Peptides Aβ40 and Aβ42. *Curr. Alzheimer Res.* **2008**, *5*, 244−250.

(15) Fleming, P. J.; Rose, G. D. Do all backbone polar groups in proteins form hydrogen bonds? *Protein Sci.* **2005**, *14*, 1911−1917.

(16) Li, J.; Wang, Y.; Chen, J.; Liu, Z.; Bax, A.; Yao, L. Observation of α-helical hydrogen-bond cooperativity in an intact protein. *J. Am. Chem. Soc.* **2016**, *138*, 1824−1827.

(17) Levy, Y.; Onuchic, J. N. Water and proteins: a love−hate relationship. *Proc. Natl. Acad. Sci. U. S. A.* **2004**, *101*, 3325−3326.

(18) Fernández, A.; Scheraga, H. A. Insufficiently dehydrated hydrogen bonds as determinants of protein interactions. *Proc. Natl. Acad. Sci. U. S. A.* **2003**, *100*, 113−118.
(19) Hernández-Rodríguez, M.; Correa-Basurto, J.; Benitez-Cardoza, C. G.; Resendiz-Albor, A. A.; Rosales-Hernández, M. C. In silico and in vitro studies to elucidate the role of Cu2+ and galanthamine as the limiting step in the amyloid beta (1−42) fibrillation process. *Protein Sci.* **2013**, *22*, 1320−1335.
(20) Sinha, S.; Lopes, D. H.; Du, Z.; Pang, E. S.; Shanmugam, A.; Lomakin, A.; Talbiersky, P.; Tennstaedt, A.; McDaniel, K.; Bakshi, R.; et al. Lysine-specific molecular tweezers are broad-spectrum inhibitors of assembly and toxicity of amyloid proteins. *J. Am. Chem. Soc.* **2011**, *133*, 16958−16969.
(21) Sinha, S.; Lopes, D. H.; Bitan, G. A key role for lysine residues in amyloid β-protein folding, assembly, and toxicity. *ACS Chem. Neurosci.* **2012**, *3*, 473−481.
(22) Marlow, M. S.; Dogan, J.; Frederick, K. K.; Valentine, K. G.; Wand, A. J. The role of conformational entropy in molecular recognition by calmodulin. *Nat. Chem. Biol.* **2010**, *6*, 352−358.
(23) Baruah, A.; Rani, P.; Biswas, P. Conformational entropy of intrinsically disordered proteins from amino acid triads. *Sci. Rep.* **2015**, *5*, 5.
(24) Doig, A. J.; Sternberg, M. J. Side-chain conformational entropy in protein folding. *Protein Sci.* **1995**, *4*, 2247−2251.
(25) Frederick, K. K.; Marlow, M. S.; Valentine, K. G.; Wand, A. J. Conformational entropy in molecular recognition by proteins. *Nature* **2007**, *448*, 325−329.
(26) Chang, A. C.; Chen, W.; Gilson, M. K. Ligand configurational entropy and protein binding. *Proc. Natl. Acad. Sci. U. S. A.* **2007**, *104*, 1534−1539.
(27) Stone, M. J. NMR relaxation studies of the role of conformational entropy in protein stability and ligand binding. *Acc. Chem. Res.* **2001**, *34*, 379−388.
(28) Li, J.; Yim, D.; Jang, W.-D.; Yoon, J. Recent progress in the design and applications of fluorescence probes containing crown ethers. *Chem. Soc. Rev.* **2017**.46243710.1039/C6CS00619A
(29) Gokel, G. W.; Leevy, W. M.; Weber, M. E. Crown ethers: sensors for ions and molecular scaffolds for materials and biological models. *Chem. Rev.* **2004**, *104*, 2723−2750.
(30) Marjanović, M.; Kralj, M.; Supek, F.; Frkanec, L.; Piantanida, I.; Šmuc, T.; Tušek-Božić, L. Antitumor potential of crown ethers: structure− activity relationships, cell cycle disturbances, and cell death studies of a series of ionophores. *J. Med. Chem.* **2007**, *50*, 1007−1018.
(31) Morrison, P. W.; Porfiryeva, N. N.; Chahal, S.; Salakhov, I. A.; Lacourt, C.; Semina, I. I.; Moustafine, R. I.; Khutoryanskiy, V. V. Crown Ethers: novel permeability enhancers for ocular drug delivery? *Mol. Pharmaceutics* **2017**, *14*, 3528−3538.
(32) Oukhatar, F.; Même, S.; Même, W.; Szeremeta, F. d. r.; Logothetis, N. K.; Angelovski, G.; Tóth, E. v. MRI Sensing of Neurotransmitters with a Crown Ether Appended Gd3+ Complex. *ACS Chem. Neurosci.* **2015**, *6*, 219−225.
(33) Gawley, R. E.; Mao, H.; Haque, M. M.; Thorne, J. B.; Pharr, J. S. Visible fluorescence chemosensor for saxitoxin. *J. Org. Chem.* **2007**, *72*, 2187.
(34) Işık, M.; Guliyev, R.; Kolemen, S.; Altay, Y.; Senturk, B.; Tekinay, T.; Akkaya, E. U. Designing an intracellular fluorescent probe for glutathione: two modulation sites for selective signal transduction. *Org. Lett.* **2014**, *16*, 3260−3263.
(35) Tian, Y.; Zhang, X.; Li, Y.; Shoup, T. M.; Teng, X.; Elmaleh, D. R.; Moore, A.; Ran, C. Crown ethers attenuate aggregation of amyloid beta of Alzheimer's disease. *Chem. Commun.* **2014**, *50*, 15792−15795.
(36) Lee, C. C.; Maestre-Reyna, M.; Hsu, K. C.; Wang, H. C.; Liu, C. I.; Jeng, W. Y.; Lin, L. L.; Wood, R.; Chou, C. C.; Yang, J. M.; Wang, A. H.-J. Crowning proteins: modulating the protein surface properties using crown ethers. *Angew. Chem., Int. Ed.* **2014**, *53*, 13054−13058.
(37) Agrawal, N.; Skelton, A. A. 12-Crown-4 Ether Disrupts the Patient Brain-Derived Amyloid-β-Fibril Trimer: Insight from All-Atom Molecular Dynamics Simulations. *ACS Chem. Neurosci.* **2016**, *7*, 1433−1441.
(38) Petkova, A. T.; Leapman, R. D.; Guo, Z.; Yau, W.-M.; Mattson, M. P.; Tycko, R. Self-propagating, molecular-level polymorphism in Alzheimer's ß-amyloid fibrils. *Science* **2005**, *307*, 262−265.
(39) Miller, Y.; Ma, B.; Nussinov, R. Polymorphism of Alzheimer's Aβ 17−42 (p3) Oligomers: The Importance of the Turn Location and Its Conformation. *Biophys. J.* **2009**, *97*, 1168−1177.
(40) Coles, M.; Bicknell, W.; Watson, A. A.; Fairlie, D. P.; Craik, D. J. Solution Structure of Amyloid β-Peptide (1− 40) in a Water− Micelle Environment. Is the Membrane-Spanning Domain Where We Think It Is?†. *Biochemistry* **1998**, *37*, 11064−11077.
(41) Crescenzi, O.; Tomaselli, S.; Guerrini, R.; Salvadori, S.; D'Ursi, A. M.; Temussi, P. A.; Picone, D. Solution structure of the Alzheimer amyloid β-peptide (1−42) in an apolar microenvironment. *Eur. J. Biochem.* **2002**, *269*, 5642−5648.
(42) Huang, J.; MacKerell, A. D. CHARMM36 all-atom additive protein force field: Validation based on comparison to NMR data. *J. Comput. Chem.* **2013**, *34*, 2135−2145.
(43) Siwy, C. M.; Lockhart, C.; Klimov, D. K. Is the Conformational Ensemble of Alzheimer's Aβ10−40 Peptide Force Field Dependent? *PLoS Comput. Biol.* **2017**, *13*, e1005314.
(44) Wang, Y.; Xiao, J.; Suzek, T. O.; Zhang, J.; Wang, J.; Bryant, S. H. PubChem: a public information system for analyzing bioactivities of small molecules. *Nucleic Acids Res.* **2009**, *37*, W623−W633.
(45) Leong, B. K.; Ts'o, T. O.; Chenoweth, M. B. Testicular atrophy from inhalation of ethylene oxide cyclic tetramer. *Toxicol. Appl. Pharmacol.* **1974**, *27*, 342−354.
(46) Jana, M.; MacKerell, A. D., Jr CHARMM Drude Polarizable Force Field for Aldopentofuranoses and Methyl-aldopentofuranosides. *J. Phys. Chem. B* **2015**, *119*, 7846−7859.
(47) O'Brien, R. J.; Wong, P. C. Amyloid precursor protein processing and Alzheimer's disease. *Annu. Rev. Neurosci.* **2011**, *34*, 185−204.
(48) Bixon, M.; Lifson, S. Potential functions and conformations in cycloalkanes. *Tetrahedron* **1967**, *23*, 769−784.
(49) Hess, B.; Bekker, H.; Berendsen, H. J.; Fraaije, J. G. LINCS: a linear constraint solver for molecular simulations. *J. Comput. Chem.* **1997**, *18*, 1463−1472.
(50) Miyamoto, S.; Kollman, P. A. SETTLE: an analytical version of the SHAKE and RATTLE algorithm for rigid water models. *J. Comput. Chem.* **1992**, *13*, 952−962.
(51) Darden, T.; York, D.; Pedersen, L. Particle mesh Ewald: An N·log (N) method for Ewald sums in large systems. *J. Chem. Phys.* **1993**, *98*, 10089−10092.
(52) Bussi, G.; Donadio, D.; Parrinello, M. Canonical sampling through velocity rescaling. *J. Chem. Phys.* **2007**, *126*, 014101.
(53) Parrinello, M.; Rahman, A. Polymorphic transitions in single crystals: A new molecular dynamics method. *J. Appl. Phys.* **1981**, *52*, 7182−7190.
(54) Levy, R. M.; Karplus, M.; Kushick, J.; Perahia, D. Evaluation of the configurational entropy for proteins: application to molecular dynamics simulations of an a-helix. *Macromolecules* **1984**, *17*, 1370−1374.
(55) Kumari, R.; Kumar, R.; Lynn, A. g_mmpbsa— A GROMACS Tool for High-Throughput MM-PBSA Calculations. *J. Chem. Inf. Model.* **2014**, *54*, 1951−1962.
(56) Frishman, D.; Argos, P. Seventy-five percent accuracy in protein secondary structure prediction. *Proteins: Struct., Funct., Genet.* **1997**, *27*, 329−335.
(57) Abraham, M. J.; Murtola, T.; Schulz, R.; Páll, S.; Smith, J. C.; Hess, B.; Lindahl, E. GROMACS: High performance molecular simulations through multi-level parallelism from laptops to supercomputers. *SoftwareX* **2015**, *1*, 19−25.
(58) Murakami, K.; Masuda, Y.; Shirasawa, T.; Shimizu, T.; Irie, K. The turn formation at positions 22 and 23 in the 42-mer amyloid β peptide: The emerging role in the pathogenesis of Alzheimer's disease. *Geriatrics & gerontology international* **2010**, *10*, S169−S179.
(59) Klimov, D. K.; Thirumalai, D. Dissecting the assembly of Aβ 16−22 amyloid peptides into antiparallel β sheets. *Structure* **2003**, *11*, 295−307.

DOI: 10.1021/acs.molpharmaceut.7b00966
Mol. Pharmaceutics 2018, 15, 289−299

(60) Ma, B.; Nussinov, R. Stabilities and conformations of Alzheimer's β-amyloid peptide oligomers (Aβ16−22, Aβ16−35, and Aβ10−35): sequence effects. *Proc. Natl. Acad. Sci. U. S. A.* **2002**, *99*, 14126−14131.
(61) Karr, J. W.; Szalai, V. A. Role of aspartate-1 in Cu (II) binding to the amyloid-β peptide of Alzheimer's disease. *J. Am. Chem. Soc.* **2007**, *129*, 3796−3797.
(62) Tõugu, V.; Tiiman, A.; Palumaa, P. Interactions of Zn (II) and Cu (II) ions with Alzheimer's amyloid-beta peptide. Metal ion binding, contribution to fibrillization and toxicity. *Metallomics* **2011**, *3*, 250−261.
(63) Simmons, L. K.; May, P. C.; Tomaselli, K. J.; Rydel, R. E.; Fuson, K. S.; Brigham, E. F.; Wright, S.; Lieberburg, I.; Becker, G. W.; Brems, D. N. Secondary structure of amyloid beta peptide correlates with neurotoxic activity in vitro. *Mol. Pharmacol.* **1994**, *45*, 373−379.
(64) Gremer, L.; Schölzel, D.; Schenk, C.; Reinartz, E.; Labahn, J.; Ravelli, R. B.; Tusche, M.; Lopez-Iglesias, C.; Hoyer, W.; Heise, H.; et al. Fibril structure of amyloid-β (1−42) by cryo−electron microscopy. *Science* **2017**, *358*, 116−119.
(65) Kirschner, D. A.; Inouye, H.; Duffy, L. K.; Sinclair, A.; Lind, M.; Selkoe, D. J. Synthetic peptide homologous to beta protein from Alzheimer disease forms amyloid-like fibrils in vitro. *Proc. Natl. Acad. Sci. U. S. A.* **1987**, *84*, 6953−6957.
(66) Hilbich, C.; Kisters-Woike, B.; Reed, J.; Masters, C. L.; Beyreuther, K. Aggregation and secondary structure of synthetic amyloid βA4 peptides of Alzheimer's disease. *J. Mol. Biol.* **1991**, *218*, 149−163.
(67) Grünberg, R.; Nilges, M.; Leckner, J. Flexibility and conformational entropy in protein-protein binding. *Structure* **2006**, *14*, 683−693.
(68) Teilum, K.; Olsen, J. G.; Kragelund, B. B. Protein stability, flexibility and function. *Biochim. Biophys. Acta, Proteins Proteomics* **2011**, *1814*, 969−976.
(69) Spolar, R. S.; Ha, J.-H.; Record, M. T. Hydrophobic effect in protein folding and other noncovalent processes involving proteins. *Proc. Natl. Acad. Sci. U. S. A.* **1989**, *86*, 8382−8385.
(70) Jiang, L.; Liu, C.; Leibly, D.; Landau, M.; Zhao, M.; Hughes, M. P.; Eisenberg, D. S. Structure-based discovery of fiber-binding compounds that reduce the cytotoxicity of amyloid beta. *eLife* **2013**, 2, e00857 DOI: 10.7554/eLife.00857.

DOI: 10.1021/acs.molpharmaceut.7b00966
Mol. Pharmaceutics 2018, 15, 289−299

ACS Chemical Neuroscience

Research Article

pubs.acs.org/chemneuro

12-Crown-4 Ether Disrupts the Patient Brain-Derived Amyloid-β-Fibril Trimer: Insight from All-Atom Molecular Dynamics Simulations

Nikhil Agrawal and Adam A. Skelton*

School of Pharmacy and Pharmacology, University of KwaZulu-Natal, Durban 4001, South Africa

Supporting Information

ABSTRACT: Recent experimental data elucidated that 12-crown-4 ether molecule can disrupt Aβ40 fibrils but the mechanism of disruption remains elusive. We have performed a series of all-atom molecular dynamics simulations to study the molecular mechanism of Aβ40 fibril disruption by 12-crown-4. In the present study we have used the Aβ40 fibril trimer as it is the smallest unit that maintains a stable U-shaped structure, and serves as the nucleus to form larger fibrils. Our study reveals that 12-crown-4 ether can enter into the hydrophobic core region and form competitive, hydrophobic interactions with key hydrophobic residues; these interactions break the intersheet hydrophobic interactions and lead to the opening of the U-shaped topology and a loss of β-sheet structure. Furthermore, we observed periods of time when 12-crown-4 was in the hydrophobic core and periods of time when it interacted with Lys28 (chain C), a "tug of war"; the 12-crown-4 binding with Lys28 destabilizes the salt-bridge between Asp23 and Lys28. In addition to the two aforementioned binding modes, the 12-crown-4 binds with Lys16, which is known to form a salt-bridge with Glu22 in antiparallel arranged Aβ fibrils. Our results are in good agreement with experimental results and suggest that molecules that have the ability to interact with both the hydrophobic core region and positively charged residues could serve as potential inhibitors of Aβ fibrils.

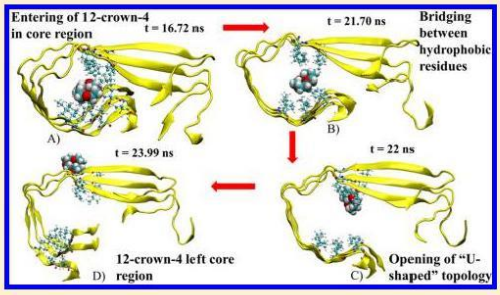

KEYWORDS: *Amyloid fibrils, MD simulation, Crown ether*

Alzheimer's disease (AD) is the most common form of dementia, accounting for up to 60−80% of all dementia cases.[1,2] AD is caused by misfolding and aggregation of amyloid beta (Aβ) peptide, into amyloid-β-fibrils (Aβ fibrils) and affects the structure and function of neural cells leading to synaptic dysfunction.[3,4] It has been reported that cytotoxicity of Aβ fibrils depends on its morphology and remodeling of Aβ fibrils can significantly reduce its cytotoxicity.[5] Understanding the mechanism of amyloid genesis and disruption allows us to design more effective ways of controlling the disease.

Crown ethers are small, cyclic polyethers that work as cation chelators, and this property of crown ethers has been extensively used in phase-transfer catalysis and in the activation of proteins in organic solvents.[6−8] A recent study by Tian et al.[9] proposed a new strategy to attenuate the aggregation of Aβ through a noncovalent modification at the protein surface. Their experimental results showed that the 12-crown-4 ether caused a reduction in the zeta potential of Aβ40 fibrils, once it was mixed with the 12-crown-4 ether (from −48 mV to −4 mV); this pointed to a reduction in the surface charge upon binding. In addition, antiaggregation testing results revealed that the presence of 12-crown-4 can reduce the aggregation of Aβ40 peptides in fibrils. Transmission electron microscopy (TEM) images revealed that Aβ40 fibrils, formed in the presence of 12-crown-4, had a different morphology than those in the absence of 12-crown-4 and this could be significant since different morphologies of Aβ fibrils relate to different cytotoxicity.[5] The authors hypothesized that 12-crown-4 interacts with positively charged residues (Lys, Arg, His) and this could attenuate Aβ40 peptide aggregation and affect Aβ fibril conformation.

In another experimental study, Lee et al.[10] cocrystallized 18-crown-6 ether with several protein structures and revealed that crown ether specifically interacted with the hydrophobic patches, or with the amine group of Lys; this resulted in dramatic alterations to the protein surface. Das et al.[11] revealed by a mutation study that contact between Phe19 and Leu34 are critical for the formation of Aβ40 oligomer; their study showed that altering this interaction drastically reduced the cytotoxicity of Aβ40 oligomers. Chandrakesan et al.[12] showed by a nuclear magnetic resonance spectroscopy (NMR) study that contact between Phe19 and Leu34 plays a crucial role in self-assembly of Aβ fibrils and they suggested that candidate drug molecules, with the ability to disrupt the contact between Phe19 and Leu34, are expected to have a very strong effect on the aggregation of Aβ.

Received: June 24, 2016
Accepted: July 25, 2016
Published: July 25, 2016

DOI: 10.1021/acschemneuro.6b00185
ACS Chem. Neurosci. 2016, 7, 1433−1441

In the present molecular dynamics study, the Aβ40 fibril single trimer unit is used and is shown in Figure 1A; this was taken from the experimental structure formed by three trimeric units (PDB: 2M4J), arranged in 3-fold symmetry. The particular structure was chosen over other available experimental structures of Aβ40 fibrils because this is the first detailed, experimentally determined structure of any patient brain-derived Aβ aggregate.[13] The Aβ40 fibril structure contains an N-terminal disordered region (residues 1−10), two β-sheets (residues 11−19 and residues 31−38), and a connecting region. The bend, in the connecting region of two β-sheets in Aβ fibrils, brings the two-sheets in contact through side chain interactions, which leads to a double-sheet structure (U-shaped structure) with a core region (residues 17−36), Figure 1B. The core region can be subdivided into three parts: (1) side chains of Leu17, Phe19, Ala 21, Ile 31, Leu34, and Val36 that form hydrophobic interactions. (2) Side chains of residues Ala 29, Gly30, Ile 32, Gly33, and Met35 face toward the outside and form the hydrophobic face. (3) Side chains of Asp23 and Lys28 form a salt bridge, which plays a crucial role in Aβ fibrils stability.[13,14]

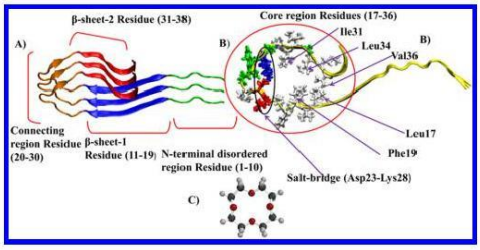

Figure 1. (A) Shows the initial structure of Aβ40 fibril containing disordered region (1−10) in green color, β-sheet-1 in blue color (11−19), connecting region in orange color (20−30), and β-sheet-2 in red color (31−38). The Aβ40 fibril trimer is shown in cartoon representation. (B) Shows core region residues in liquorice representation colored by residue type: hydrophobic residues (white), negatively charged residues (red), positively charged residues (blue), and polar residues (green). (C) Chemical structure of 12-crown-4 molecule.

Previously, several MD simulation studies have been conducted on the interaction between Aβ fibrils; for example, Lemkul et al.[15] has shown that an organic molecule, Morin, can enter into the hydrophobic core and destabilize the salt bridge formed by Asp23−Lsy28. Another study by Tianhan Kai et al.[16] has revealed that Tabersonine can interact with β-sheet grooves containing aromatic and hydrophobic residues, which they postulate could affect the elongation process; however, in both of these studies they did not observe the opening of the U-shaped structure of Aβ fibril. To the best of our knowledge no molecular dynamics study of Aβ fibril and an organic molecule has shown the complete opening of the U-shaped topology of Aβ fibril.

In the present study, we aim to find a molecular basis for the Aβ40 fibril remodelling by 12-crown-4. Specifically, the following questions still need to be answered, (1) which region does 12-crown-4 bind to? (2) Is there any region on Aβ40 fibril that is particularly favorable or unfavorable for 12-crown-4 binding? (3) What is the impact of 12-crown-4 binding on the conformation of the Aβ40 fibril? To address all these questions we have performed more than 25 all-atom molecular dynamics simulations of Aβ40 fibrils in the presence and absence of 12-crown-4 and investigated the mechanism of Aβ40 disruption by 12-crown-4 ether molecule. The 12-crown-4 ether structure is been shown in Figure 1C

■ RESULTS AND DISCUSSION

Insertion of 12-Crown-4 in Core Region and Opening of U-Shaped Structure Aβ40 Fibril. Out of a total of 15 independent simulations, 8 simulations showed the spontaneous entering of 12-crown-4 into the core region; in 6 simulations 12-crown-4 interacted with aromatic and hydrophobic residues, was highly stable, and an opening event occurred. In all control simulations, the RMSD and "opening" of Aβ40 fibril remained stable and U-shaped topology remained intact (Figure: 1S).

Figure 2A shows the time evolution, in one of the representative trajectories, of "entering" of 12-crown-4 in the core region of Aβ40 fibril and U-shaped structure "opening" (see Methods Section for details). Figure 2B shows the change in Aβ40 fibril conformation, monitored by RMSD of residue 11 to 40 backbone atoms. The atomic level representation of the mechanism of entering of 12-crown-4 and the subsequent opening of the U-shaped structure in a stepwise process is shown in Figure 3 (steps A−D).

In step-A, 12-crown-4 enters into the core region at ∼16.72 ns, as shown by a decrease in the "entering" value (Figure 2A, red data set); at this time point, competitive interactions were established between 12-crown-4 and the aromatic and hydro-

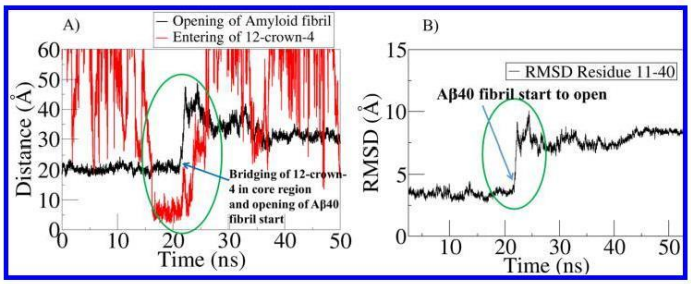

Figure 2. (A) Shows time evolution of "entering" of 12-crown-4 in core region (red line) and "opening" of U-shaped structure of Aβ40 fibril (black line). (B) Shows time evolution of conformational change in Aβ40 fibrils.

DOI: 10.1021/acschemneuro.6b00185
ACS Chem. Neurosci. 2016, 7, 1433−1441

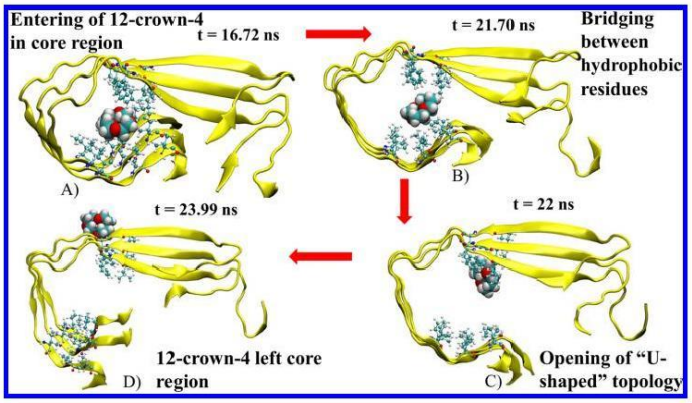

Figure 3. Four representative structures taken at different time points in a representative trajectory. (A) Entering of 12-crown-4 in core region (16.72 ns) and making competitive hydrophobic interaction with top and bottom β-sheets residues. (B) 12-Crown-4 working as a bridge between side chains of top and bottom β-sheets residues (21.70 ns). (C) Opening of U-shaped topology (22 ns). (D) 12-Crown-4 left the core region.

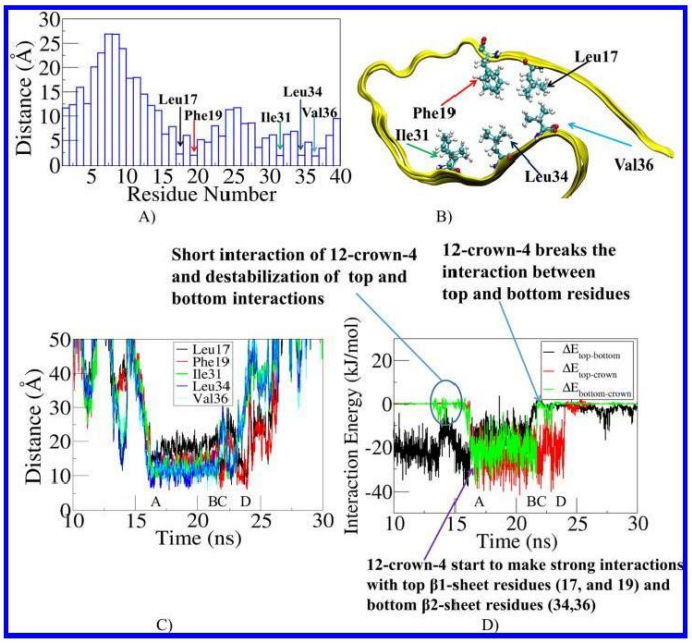

Figure 4. (A) The average distance of 12-crown-4 from all three peptide residues during binding (16−24 ns). (B) The closest distance residues, during binding time, in CPK model and protein has been shown in new cartoon representation. C) Time evolution of distance from closest residues. (D) Shows the interaction energy between top and bottom β-sheets residues ($\Delta E_{top-bottom}$), interaction energy between top β-sheet and 12-crown-4 ($\Delta E_{top-crown}$) and bottom β-sheet and 12-crown-4 ($\Delta E_{bottom-crown}$) .

phobic residues of the two opposing β-sheet residues. In step-B, a bridge is formed between two opposing β-sheet hydrophobic residues (~21.7 ns) (Figure 3B). In step-C, the 12-crown-4/*hydrophobic* bridge eventually breaks and the two opposing β-sheets do not have the opportunity to reconnect, an opening event occurs (Figure 3C); this results in an increase in the "opening" value (Figure 2A, black data set) and a large increase in RMSD value at 22 ns (Figure 2B). The 12-crown-4 remained bound to the top β-sheet (β-sheet-1) residues for duration of

DOI: 10.1021/acschemneuro.6b00185
ACS Chem. Neurosci. 2016, 7, 1433−1441

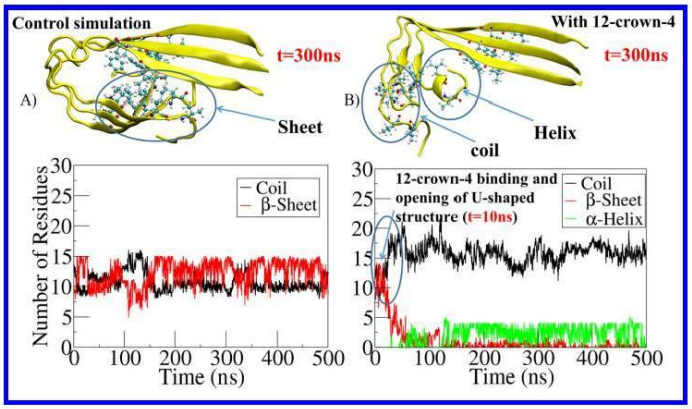

Figure 5. (A) Left panel shows representative structure from control simulations at 300 ns, and time evoluation of secondary structure change in bottom β-sheets in all three peptides. (B) Right panel shows representative structure of Aβ40 fibril with 12-crown-4 simulation at 300 ns, and time evoluation of secondary structure change in bottom β-sheests residues of all three peptides.

~2 ns. At ~ 24 ns there is separation of 12-crown-4 with the core region (Figure 3D).

Deciphering the Core Region Contact Sites of 12-Crown-4. Now that we have observed the opening event we aim to gain an understanding of the specific interactions and driving forces at play during this process. Figure 4A shows the average distances of all three peptide residues from the COM of 12-crown-4; this illustrates the specific interactions of 12-crown-4, after insertion, in the core region (16 to 24 ns). Residues in β-sheet-1 (Leu17 and Phe19) and residues in β-sheet-2, (Ile31, Leu34, and Val36) form a close contact with 12-crown-4 (less than 5 Å). The five aforementioned side chains face each other and form a hydrophobic core (Figure 4B) that plays an important role in maintaining the U-shaped structure of Aβ40 fibril. For further understanding, we calculated the time evolution of the average distance of these residues from the COM of 12-crown-4, during the binding, for all three peptides (Figure 4C). It is revealed that 12-crown-4 first interacts with the bottom β-sheet residues, Leu34, Ile31, and Val36. At the time of bridging and opening (steps B and C), there are increases in the bottom residue−12-crown-4 distances and decreases in the top residue−12-crown-4 distances; these changes occur as 12-crown-4 remains bound to the top residues before completely separating.

Time evolutions of the interaction energy between top (Leu17, Phe19) and bottom residues (Leu34, Val36) (black data set, $\Delta E_{\text{top-bottom}}$) and the interaction energy of 12-crown-4 with both top (red data set, $\Delta E_{\text{top-crown}}$) and bottom residues (green data set, $\Delta E_{\text{bottom-crown}}$), are shown in Figure4D. Before binding, $\Delta E_{\text{top-bottom}}$ is attractive (~ −22 kJ/mol) and at ~14 ns, $\Delta E_{\text{top-bottom}}$ becomes less negative when there is a momentary 12-crown-4 interaction. When 12-crown-4 fully enters, at step-A, $\Delta E_{\text{top-bottom}}$ is ~ −22 kJ/mol, similar to that of the unbound $\Delta E_{\text{top-bottom}}$ value; however, binding of 12-crown-4 causes $\Delta E_{\text{top-bottom}}$ to become less negative (~ −13.5 kJ/mol), indicating the role of 12-crown-4 in weakening the interaction between top and bottom residues. When bridging starts, at step-B, $\Delta E_{\text{top-bottom}}$ becomes less attractive, becoming zero at step-C; at this point in time, $\Delta E_{\text{bottom-crown}}$ abruptly goes to zero as opening starts. $\Delta E_{\text{top-crown}}$, however, remains the same at step-C and this value only goes to zero at step-D, as 12-crown-4 completely leaves the core region.

As stated, before entering of 12-crown-4, $\Delta E_{\text{top-bottom}}$ is comparable to $\Delta E_{\text{top-crown}}$ and $\Delta E_{\text{bottom-crown}}$. When taken together $\Delta E_{\text{top-crown}}$ and $\Delta E_{\text{bottom-crown}}$ (~-24 kJ/mol + ~ −23 kJ/mol = ~ −47 kJ/mol) far exceeds $\Delta E_{\text{top-bottom}}$ (~-22 kJ/mol); this provides an energetic basis for the competition between 12-crown-4−hydrophobic residue interaction and top−bottom residues.

Secondary Structure Changes. It has previously been shown that the structural stability of the Aβ40 fibril is directly associated with the β-sheet content.[17,18] To investigate the effect of opening of the U-shaped structure on the secondary structure content, we extended one of the simulations for a longer time period; in this simulation, opening took place at 10 ns. We calculated the time evolution of the secondary structurre in the bottom β-sheet residues of all three peptide for control (Figure 5A) and 12-crown-4 (Figure 5B) simulations.

In the control simulation, the content of β-sheet and coil always remained reasonably stable and no α-helix formation was observed; however, during the time period between 100 and 150 ns, transitions from β-sheet to coil were observed for chain A, residues 32 to 35. After that time period the β-sheet content of residues 32 to 35 was regained. In the simulation, in the presence of 12-crown-4, however, we obseved a reduction in β-sheet content and increase in coil content after opening. After ~50 ns, α-helix content started to form and this stabilized after ~150 ns, when ~4 residues maintained the α-helix stucture until the end of the simulation. These results unequivacally show that the 12-crown-4 has not only caused an opening event but when the Aβ40 fibril does open the conformation changes. The result of the conformational changes is that the bottom residues should no longer be able to accommodate the U-shaped structure; therefore, the recombination of top and bottom sheets would require a further comformational change, which should take more time and make this process more unfavorable.

Tug of War of 12-Crown-4 between Hydrophobic Core and Lys28. Since 12-crown-4 contains both oxygen and hydrocarbon groups, it should be able to form both hydrogen

DOI: 10.1021/acschemneuro.6b00185
ACS Chem. Neurosci. 2016, 7, 1433−1441

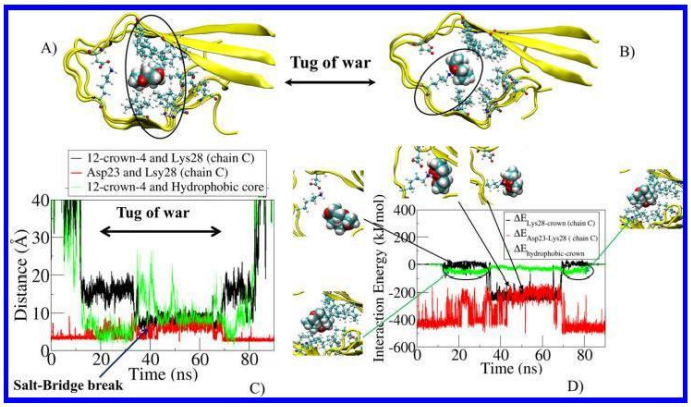

Figure 6. (A) Shows the representative structure of 12-crown-4 with hyrophobic core residues during binding. (B) Shows the representative structure of 12-crown-4 with Lys28 chain C during binding. (C) Shows the distance of 12-crown-4 from hyrophobic core, 12-crown-4 and Lys28 distance, and salt-bridge distance between Asp23 and Lys28.

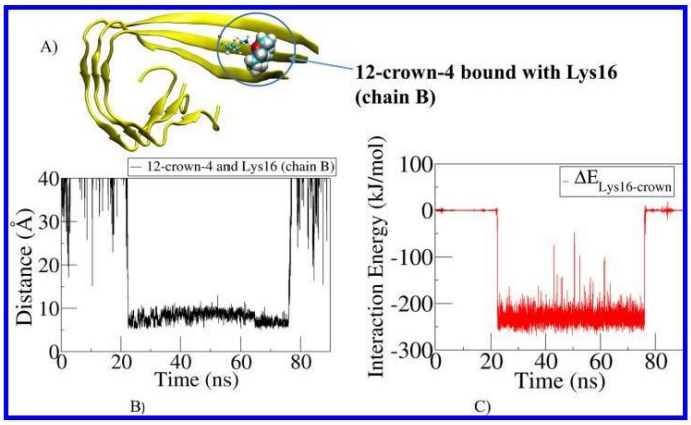

Figure 7. (A) Shows the representative structure of 12-crown-4 bound on Aβ40 fibrils. (B) Shows the time evolution of distance between 12-crown-4 and Lys16 of chain B. (C) Shows the time evolution of interaction energy between 12-crown-4 and Lys16 of chain B.

bonding/electrostatic interactions with hydrophilic groups and van der Waals/hydrophobic interactions with hydrophobic residues. This amphiphilic behavior was observed in two simulations, where 12-crown-4 entered into the core region yet no opening event took place; however, we obseved periods of time when the 12-crown-4 was in the hydrophobic core and periods of time when it interacted with Lys28 (chain C), a "tug of war" (Figure 6A). First, 12-crown-4 entered into the core region, in a similar fashion to that described above; it entered at ~12 ns and stayed there until ~33 ns (Figure6C, green line). At ~ 33 ns, 12-crown-4 shifted toward Lys28 of chain C and formed hydrogen bonds (Figure 6B,C, black line); this broke the salt-bridge formed by Aps23 and Lys28 (Figure 6C, red line). At ~ 70 ns the 12-crown-4 broke contact with Lys28, the salt bridge reformed and the 12-crown-4 shifted back to the hydrophobic core region. At ~ 75 ns the 12-crown-4 left the hydrophobic region and in fact the whole Aβ40 fibril.

To understand the enegetic interplay between 12-crown-4 binding with Lys28 and the hyrophobic core, we calculated the time evolution of the interaction energy between 12-crown-4 and Lys28 ($\Delta E_{\mathrm{Lys28-crown}}$), the interaction between 12-crown-4 and the hyrophobic core residues ($\Delta E_{\mathrm{hydrophobic-crown}}$), and the interaction energy between Asp23 and Lys28 ($\Delta E_{\mathrm{Asp23-Lys28}}$); these are shown in Figure 6D, black, green, and red lines, respectively. The 12-crown-4 interacts with the hyrophobic core resulting in the $\Delta E_{\mathrm{hydrophobic-crown}}$ value of ~−53 kJ/mol and when 12-crown-4 shifts to Lys28, it strongly interacts with a $\Delta E_{\mathrm{Lys28-crown}}$ value of ~ −230 kJ/mol. At the start of the simulation, when the salt bridge is fully formed, $\Delta E_{\mathrm{Aps23-Lys28}}$ is hugely attractive at ~−410 kJ/mol (Figure 6D, red); 12-crown−Lys28 interaction, however, destabilizes the salt-bridge interaction, making $\Delta E_{\mathrm{Asp23-Lys28}}$ less favorable (~−220 kJ/mol). It should be noted that $\Delta E_{\mathrm{Lys28-crown}}$ was much higher than $\Delta E_{\mathrm{hydrophobic-crown}}$; there could be three possibile reasons

DOI: 10.1021/acschemneuro.6b00185
ACS Chem. Neurosci. 2016, 7, 1433−1441

Table 1. Average Binding Energy and its Components Obtained from the MM-PBSA Calculations for Aβ40 Fibril-12-Crown-4 Complex[a]

		mode-2 energy (kJ/mol)		
contribution	mode-1 *hydrophobic* energy (kJ/mol) (16−22 ns)	*hydrophobic* (12−32 ns)	*Lys28* (40−60 ns)	mode-3 *Lys16* energy (kJ/mol) (23−50 ns)
ΔE_{vdw}	−58.28 ± 0.95	−62.83 ± 0.57	−41.69 ± 0.88	−22.11 ± 0.64
ΔE_{elec}	−1.76 ± 0.73	−12.72 ± 1.47	−214.56 ± 2.04	−230.34 ± 1.41
ΔG_{polar}	20.02 ± 0.63	31.41 ± 1.15	160.47 ± 1.24	150.15 ± 0.99
$\Delta G_{nonpolar}$	−9.63 ± 0.12	−10.25 ± 0.07	−9.51 ± 0.10	−6.031 ± 0.05
ΔG_{total}	−49.63 ± 1.18	−54.43 ± 0.99	−105.36 ± 1.27	−108.22 ± 0.76

[a]All energies are in kJ/mol.

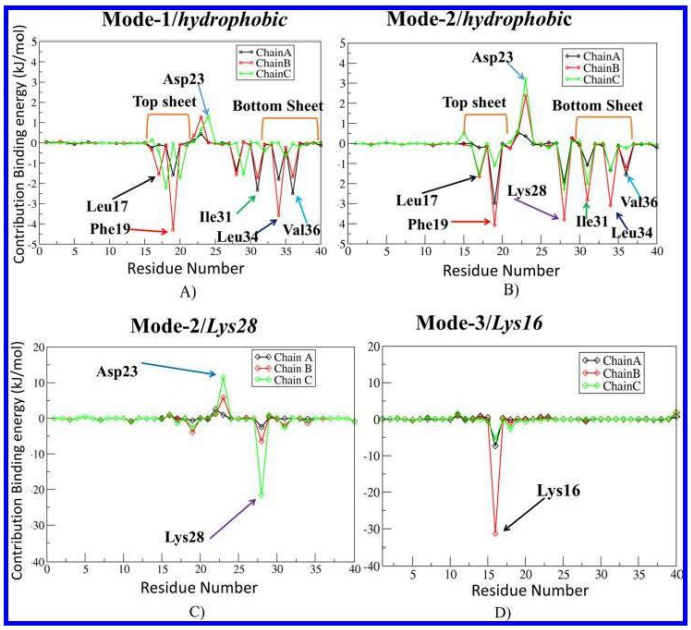

Figure 8. (A) Residue contributions to binding energy in mode-1/*hydrophobic* (U-shaped structure opening). (B) Residue contributions to binding energy in mode-2/*hydrophobic* (tug of war). (C) Residue contributions to binding energy of mode-2/*Lys28* (tug of war). (D) Residue contributions to binding energy of mode-3/*Lys16*.

that 12-crown-4 shifted back to the hydrophobic core. (1) There are a greater number of residues in the hyrophobic core, so 12-crown-4 has a greater opporunity to interact. (2) There is competition between Asp23 (salt-bridge) and 12-crown-4 for binding to Lys28. (3) There is greater competition of Lys28 with water molecules than that of the hydrophobic residues. In order to bind to Lys28, 12-crown-4 must displace ordered water molecules that are hydrogen bonded to the $-NH_3^+$ group (on average a reduction of 1.50 water molecules in the first solvation shell, see Table: 1S). The number of water molecules that are displaced is far fewer for the hyrophobic resdues; for example, on average there is a reduction of 0.04 and 0.19 water molecules, respectively, upon binding to the central chain (chain B) Phe19 and Leu34 residues.

Interaction with Lys16. Various studies have shown that Lys16 and Glu22, with their opposite positive and negative charges, form electrostatic interactions and this favors the Aβ fibrils arrangement in-register antiparallel alignment.[19] An interaction of 12-crown-4, with either Lys16 or Glu22, should therefore, hinder such alignment, decreasing the extent of amyloid fibril formation; 12-crown-4 interaction with Lys16 was, in fact, observed in four simulations.

Figure 7A shows the Lys28−12-crown-4 distance and Figure 7B shows the interaction energy between Lys 28 and 12-crown-4 ($\Delta E_{Lys16-crown}$). 12-Crown-4 binds to Lys16 at ∼22 ns and remains bound until ∼76 ns (for ∼45 ns). The $\Delta E_{Lys16-crown}$ value was ∼−230 kJ/mol during the binding, which is similar to that of $\Delta E_{Lys28-crown}$.

To bind to Lys16, 12-crown-4 needs to displace, on average, 2.7 water molecules from the first solvation shell (Supporting Table 1S). The number of water molecules that get displaced is greater for Lys16 than for Lys28 because, in the absence of 12-crown-4 interaction, there are more water molecules available to interact with Lys16 (4.62 water molecules) than for Lys28

DOI: 10.1021/acschemneuro.6b00185
ACS Chem. Neurosci. 2016, 7, 1433−1441

(3.27) (Figures 4S, 5S); this is because part of the coordination of Lys28 is taken up by the salt-bridge between Asp23 but Lys16 is not engaged in a salt-bridge. The amount of structured water molecules around $-NH_3^+$ after coordination with 12-crown-4 is comparable for Lys16 and Lys28 (approximately 1.8 water molecules on average) since the 12-crown-4 causes a break in the Asp23-Lys28 salt-bridge.

Binding Free Energy and Energetic Contribution. The binding free energy of 12-crown-4 with Aβ40 fibril (ΔG_{total}) was evaluated by the MM-PBSA method (see the Methods Section for more details), during the time of 12-crown-4 binding with Aβ40 fibril for all three binding modes (Table 1). The contribution to ΔG_{total} from van der Waals and electrostatic interactions is denoted by ΔE_{vdw} and ΔE_{elec}. Polar and nonpolar contributions to ΔG_{total} have been denoted by ΔG_{polar} and $\Delta G_{nonpolar}$, respectively. As expected, mode-3 and mode-2/*Lys28* have greater overall binding than mode-2/*hydrophobic* and mode-1. Since, in mode-1 and mode-2/*hydrophobic*, the binding contains hydrophobic residues, the van der Waals energy is the most favorable contributor; however, the electrostatic energy is the most favorable contributor in mode-2/*Lys28* and mode-3/*Lys16*. The ΔG_{polar} value, which is always unfavorable for the 12-crown-4-Aβ40 fibril complexes, is less unfavorable in case of the hydrophobic core binding sites compared to Lys binding sites. For the latter case, the total gain in intermolecular electrostatic interaction compensates an increase in polar solvation energy.

To gain even more detailed thermodynamic insight into the total binding energy, the binding energies were further decomposed into individual residue contributions and are shown in Figure 8. The decomposition of binding energy per residue constitutes ΔE_{vdw}, ΔE_{elec}, ΔE_{polar}, and $\Delta E_{nonpolar}$. It is revealed that, in mode-1 and mode-2/*hydrophobic*, the binding energy contribution is distributed among several residues of the core region (Phe19, Leu17, Lys28, Lue34, Val36); in the case of mode-2/*Lys28* and mode-3/*Lys16*, however, the only significant binders are Lys28 and Lys16. In mode-1, Asp23, Val24, and mode-2 (*hydrophobic* and *Lys28*) the negatively charged Asp23 has unfavorable contributions to the binding energy.

Perspective and Concluding Remarks. Similar binding modes were observed, experimentally and theoretically, for 18-crown-6 with several proteins (but not Aβ fibrils).[10] The crown ether specially interacts with hydrophobic patches forming van der Waals interactions with aromatic or aliphatic residues. Moreover, binding between the crown ether and a single Lys or Lys in the vicinity of hydrophobic residues was observed. Our data also supports the hypothesis by Tian et al.[9] that 12-crown-4 can form hydrogen bonds with positively charged residues, especially with Lys16 and Lys28, and destabilizes the salt-bridges formed by these residues.

Various studies have shown that the salt-bridge between Asp23−Lys28 plays a crucial role in structure stability and cytotoxicity.[20−22] Other experimentally known, structurally distinct inhibitor molecules, such as Congo red, Naproxen, Ibuprofen, and Curcumin are shown to bind to Lys28 using docking and MD simulations studies.[23,24] The salt-bridge formed between Lys16−Glu22 plays an important role in stabilizing the structure of Aβ fibrils in antiparallel arrangement. If the 12-crown-4 binds to Lys16, it could destabilize such antiparallel Aβ fibrils.

Many studies have shown that side-chain interlocking of hydrophobic residues in the core region play a crucial role in the U-shaped structure stability.[25−27] In particular, Chandrakesan et al.[12] showed that contact between Phe19 and Leu34 is crucial for Aβ fibrils formation and suggested that Phe19 and Lue34 provide considerable stabilization for aggregation; the authors proposed that disrupting the contact between Phe19 and Leu34 is expected to have a very strong effect on the aggregation of Aβ fibrils. A study by Das et al. showed that contact between Phe19 and Leu34 plays an important role in Aβ40 oligomer cytotoxicity.[11] Control simulation data in the present study (Aβ40 fibril trimer in absence of 12-crown-4) revealed that the Aβ40 fibril trimer maintained hydrophobic side-chain contact in the core region in all simulation trajectories; this helped it to retain its U-shaped topology. A MD simulation study by Buchete et al.[28] suggested that hydrophobic interactions, stabilizing the C-terminal β-sheet, play a crucial role in the elongation of Aβ fibril. A study by Horn et al.[29] revealed that the Aβ trimer is the smallest unit that can maintain the U-shaped structure and is a potential seed for fibril elongation. It should, therefore, be considered that a disruption of these hydrophobic interactions and the U-shaped structure, as observed in the present study, could indeed affect elongation. Taken together all these data, we propose that 12-crown-4 binding to hydrophobic core residues (Phe19, Leu34) and positively charged Lys16, Lys28 could significantly reduce the cytotoxicity, structure stability and the elongation process.

Studies on oral toxicity of 12-crown-4 in mice and rats showed that 12-crown-4 had median lethal dose (LD_{50}) values of 3.15 g/kg and 2.8 g/kg, respectively.[30,31] A further dermal toxicity study in rabbits revealed that the LD_{50} value was 4.5 g/kg.[32] Due to the limited studies and different organisms being used in testing the toxicity, it would be difficult to generalize 12-crown-4 toxicity without further studies. The present study, however, has shown the chemical features that could be required to design an effective Aβ fibril inhibitor; that is, 12-crown-4 contains both hydrophilic oxygen atoms and hydrophobic hydrocarbon groups.

In summary, we have studied the effect of 12-crown-4 on Aβ40 fibril trimer by performing simulations in the presence and absence of 12-crown-4; we observed three possible binding modes of 12-crown-4 on Aβ40 fibril. First, the 12-crown-4 can enter into the hydrophobic core and interact with hydrophobic residues by van der Waals interactions; when this occurs there is a disruption of the hydrophobic interactions between two β-sheets and this leads to the opening of the U-shaped structure and drastic conversion of β-sheet into random coil and α-helix. The second mode involves a "tug of war", where the 12-crown-4 enters into the hydrophobic core but instead of causing an opening event, it subsequently moves toward the Asp23−Lys28 salt bridge, causing it to break. Lastly, there is significant binding of 12-crown-4 with Lys16, which is implicated in stabilizing the structure of Aβ fibrils in antiparallel arrangement. The present study deepens our knowledge of how a candidate molecule can remodel Aβ40 fibril and provides information that can be used in the design of new, potential drugs; therefore, provides new avenues for Aβ40 fibril inhibition.

■ METHODS

12-Crown-4 Ether Structure and Force Field. The 12-crown-4 is a cyclic ether molecule and the coordinate for 12-crown-4 ether was taken from PubChem compound library (CID: 9269).[33] The force field parameters of 12-crown-4 ether molecule were derived from the Charmm Additive and Classical Drude Polarizable Force Fields for Linear and Cyclic Ethers (ACDPFF).[34] Parameters for 12-crown-4 cyclic ether are provided in Table 2S).

DOI: 10.1021/acschemneuro.6b00185
ACS Chem. Neurosci. 2016, 7, 1433−1441

Simulation Protocol. All simulations were performed using the GROMACS 4.6.3[35] molecular dynamics program. The Charmm36 force field[36] was used for the Aβ40 fibril trimer, which were solvated using the TIP3P water model.[37] Systems of Aβ40 fibril with 12-crown-4 contain 22518 water molecules and systems of the Aβ40 fibril, in the absence of 12-crown-4, contain 18347 water molecules. Nine Na^+ counterions were added to neutralize the systems. All systems were energy minimized using 5000 steepest descent steps.[38] The systems were then equilibrated for 100 ps using the cononical (NVT) ensemble, followed by a further 100 ps of equilibration simulation with the isobaric-isothermic (NPT) ensemble. The production run for all systems were performed in the NPT ensemble. The LINCS[39] algorithm was used to constrain the hydrogen bond lengths of the Aβ40 fibril and 12-crown-4 molecule. Water molecule bond lengths were constrained with the SETTLE[40] algorithm, which allowed an integration time step of 2 fs. Long-range electrostatic interactions were calculated using the particle mesh Ewald (PME)[41] method with a real space cutoff of 1.2 nm. The van der Waals (vdW) interactions were calculated using a cut off of 1.2 nm. The Aβ40 fibril was separately coupled to the external temperature and pressure baths and the nonprotein components, 12-crown-4, water, and ions were together, coupled to the external temperature and pressure baths using velocity-rescale[42] and Parrinello−Rahman[43] methods. All MD simulations were performed at a temperature of 310 K and a pressure of 1 bar. The coupling times of the temperature and pressure were 0.1 and 1.0 ps, respectively.

Set I: Control Aβ40 Trimer Simulations. To explore the inherent conformational changes, and to check the stability of the U-shaped topology in the absence of 12-crown-4, two sets of control simulations were performed, three long (500 ns) and five short simulations (100 ns) using random initial velocities.

Set II: Aβ40 Trimer with 12-Crown-4. The 12-crown-4 and Aβ40 fibril systems consist of an Aβ40 fibril trimer and six 12-crown-4 molecules randomly placed at a minimum distance of 12 Å from the trimer (Figure 1C). The systems were prepared as described previously and an additional six 12-crown-4 molecules were added before solvating the system. Fifteen simulations were performed with random initial velocities and the simulation time was different for all trajectories. In our simulations we did not apply any restraints or prior contact between Aβ40 fibril and 12-crown-4 molecule.

Analysis Details. Interaction and binding energies between the Aβ40 fibril and the 12-crown-4 were calculated using Molecular Mechanics−Poisson−Boltzmann surface area (MM-PBSA), implemented in g_mmpbsa package.[44] The structural stability of the trimer was measured by root-mean-square deviation (RMSD) of the backbone atoms, of residues 11−40, with respect to the energy minimized structure. "Opening" of the U-shaped topology was defined by the center of mass (COM) distance between residue 16−20 (top β-sheet) and residue 33−40 (bottom β-sheet) of all three peptides (Figure 9A). Entering of 12-crown-4 inside the core region is defined by COM distance between 12-crown-4 and residues 16−36 (Figure: 9B). Secondary structure analysis was performed using the dictionary secondary structure of protein (DSSP).[45]

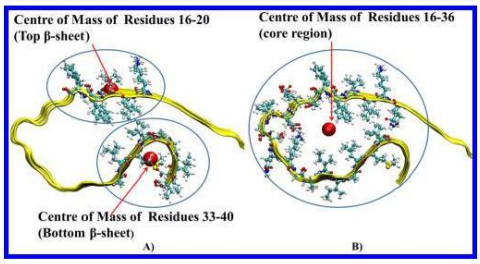

Figure 9. (A) Center of mass (COM) of residues 16−20 and COM of residues 33−40. (B) COM of residues 16−36.

■ ASSOCIATED CONTENT

Supporting Information

The Supporting Information is available free of charge on the ACS Publications website at DOI: 10.1021/acschemneuro.6b00185.

Results for control simulations (500 ns), entering and opening of two other trajectories, displacement of water molecules upon binding, and force field parameters for 12-crown-4 (PDF)

Two simulation movies: (1) entering and opening and (2) "Tug of war" (ZIP)

■ AUTHOR INFORMATION

Corresponding Author

*Skelton@ukzn.ac.za.

Notes

The authors declare no competing financial interest.

■ ACKNOWLEDGMENTS

We are indebted to Centre for High Performance Computing (CHPC) in Cape Town, South Africa and UKZN "hippo" super computer facility, Durban, South Africa for computational resources. We would like to thank college of Health Sciences at UKZN for funding and N.A. is in debt to National Research Foundation, South Africa for funding the project (grant number: 101323). N.A. is an "innovation doctoral scholarship" fellow funded by National Research Foundation, South Africa.

■ REFERENCES

(1) Braun, U., Muldoon, S. F., and Bassett, D. S. (2015) On human brain networks in health and disease. *eLS.*, 1.

(2) Alzheimer's Association. 2016 Alzheimer's disease facts and figures. *Alzheimer's Dementia* 2016, *12*, pp 459−509 10.1016/j.jalz.2016.03.001.

(3) Selkoe, D. J., and Hardy, J. (2016) The amyloid hypothesis of Alzheimer's disease at 25 years. *EMBO Mol. Med. 8*, 595−608.

(4) Nelson, A. R., Sweeney, M. D., Sagare, A. P., and Zlokovic, B. V. (2016) Neurovascular dysfunction and neurodegeneration in dementia and Alzheimer's disease. *Biochim. Biophys. Acta, Mol. Basis Dis. 1862*, 887−900.

(5) Petkova, A. T., Leapman, R. D., Guo, Z., Yau, W.-M., Mattson, M. P., and Tycko, R. (2005) Self-propagating, molecular-level polymorphism in Alzheimer's ß-amyloid fibrils. *Science 307*, 262−265.

(6) Swidan, A., and Macdonald, C. L. (2016) Polyether complexes of groups 13 and 14. *Chem. Soc. Rev. 45*, 3883.

(7) Paul, D., Suzumura, A., Sugimoto, H., Teraoka, J., Shinoda, S., and Tsukube, H. (2003) Chemical activation of cytochrome c proteins via crown ether complexation: cold-active synzymes for enantiomer-selective sulfoxide oxidation in methanol. *J. Am. Chem. Soc. 125*, 11478−11479.

(8) Mistarz, U. H., Brown, J. M., Haselmann, K. F., and Rand, K. D. (2016) Probing the Binding Interfaces of Protein Complexes Using Gas-Phase H/D Exchange Mass Spectrometry. *Structure 24*, 310−318.

(9) Tian, Y., Zhang, X., Li, Y., Shoup, T. M., Teng, X., Elmaleh, D. R., Moore, A., and Ran, C. (2014) Crown ethers attenuate aggregation of amyloid beta of Alzheimer's disease. *Chem. Commun. 50*, 15792−15795.

(10) Lee, C. C., Maestre-Reyna, M., Hsu, K. C., Wang, H. C., Liu, C. I., Jeng, W. Y., Lin, L. L., Wood, R., Chou, C. C., Yang, J. M., and Wang, A. H. -J. (2014) Crowning proteins: modulating the protein surface properties using crown ethers. *Angew. Chem., Int. Ed. 53*, 13054−13058.

DOI: 10.1021/acschemneuro.6b00185
ACS Chem. Neurosci. 2016, *7*, 1433−1441

(11) Das, A. K., Rawat, A., Bhowmik, D., Pandit, R., Huster, D., and Maiti, S. (2015) An early folding contact between Phe19 and Leu34 is critical for amyloid-β oligomer toxicity. *ACS Chem. Neurosci. 6*, 1290−1295.
(12) Chandrakesan, M., Bhowmik, D., Sarkar, B., Abhyankar, R., Singh, H., Kallianpur, M., Dandekar, S. P., Madhu, P. K., Maiti, S., and Mithu, V. S. (2015) Steric Crowding of the Turn Region Alters the Tertiary Fold of Amyloid-β18−35 and Makes It Soluble. *J. Biol. Chem. 290*, 30099−30107.
(13) Lu, J.-X., Qiang, W., Yau, W.-M., Schwieters, C. D., Meredith, S. C., and Tycko, R. (2013) Molecular structure of β-amyloid fibrils in Alzheimer's disease brain tissue. *Cell 154*, 1257−1268.
(14) Petkova, A. T., Ishii, Y., Balbach, J. J., Antzutkin, O. N., Leapman, R. D., Delaglio, F., and Tycko, R. (2002) A structural model for Alzheimer's β-amyloid fibrils based on experimental constraints from solid state NMR. *Proc. Natl. Acad. Sci. U. S. A. 99*, 16742−16747.
(15) Lemkul, J. A., and Bevan, D. R. (2010) Destabilizing Alzheimer's Aβ42 protofibrils with Morin: mechanistic insights from molecular dynamics simulations. *Biochemistry 49*, 3935−3946.
(16) Kai, T., Zhang, L., Wang, X., Jing, A., Zhao, B., Yu, X., Zheng, J., and Zhou, F. (2015) Tabersonine inhibits amyloid fibril formation and cytotoxicity of Aβ (1−42). *ACS Chem. Neurosci. 6*, 879−888.
(17) Viet, M. H., Ngo, S. T., Lam, N. S., and Li, M. S. (2011) Inhibition of aggregation of amyloid peptides by beta-sheet breaker peptides and their binding affinity. *J. Phys. Chem. B 115*, 7433−7446.
(18) Zhao, L. N., Chiu, S.-W., Benoit, J. r. m., Chew, L. Y., and Mu, Y. (2012) The effect of curcumin on the stability of Aβ dimers. *J. Phys. Chem. B 116*, 7428−7435.
(19) Klimov, D. K., and Thirumalai, D. (2003) Dissecting the assembly of Aβ 16−22 amyloid peptides into antiparallel β sheets. *Structure 11*, 295−307.
(20) Schledorn, M., Meier, B. H., and Böckmann, A. (2015) Alternative salt bridge formation in Aβ—a hallmark of early-onset Alzheimer's disease? *Frontiers in Molecular Biosciences 2*, 1−6.
(21) Tarus, B., Straub, J. E., and Thirumalai, D. (2006) Dynamics of Asp23-Lys28 salt-bridge formation in Aβ10−35 monomers. *J. Am. Chem. Soc. 128*, 16159−16168.
(22) Ma, B., and Nussinov, R. (2002) Stabilities and conformations of Alzheimer's β-amyloid peptide oligomers (Aβ16−22, Aβ16−35, and Aβ10−35): sequence effects. *Proc. Natl. Acad. Sci. U. S. A. 99*, 14126−14131.
(23) Ngo, S. T., and Li, M. S. (2012) Curcumin binds to Aβ1−40 peptides and fibrils stronger than ibuprofen and naproxen. *J. Phys. Chem. B 116*, 10165−10175.
(24) Keshet, B., Gray, J. J., and Good, T. A. (2010) Structurally distinct toxicity inhibitors bind at common loci on β-amyloid fibril. *Protein Sci. 19*, 2291−2304.
(25) Bitan, G., Kirkitadze, M. D., Lomakin, A., Vollers, S. S., Benedek, G. B., and Teplow, D. B. (2003) Amyloid β-protein (Aβ) assembly: Aβ40 and Aβ42 oligomerize through distinct pathways. *Proc. Natl. Acad. Sci. U. S. A. 100*, 330−335.
(26) Kreutzer, A. G., Hamza, I. L., Spencer, R. K., and Nowick, J. S. (2016) X-ray Crystallographic Structures of a Trimer, Dodecamer, and Annular Pore Formed by an Aβ17−36 β-Hairpin. *J. Am. Chem. Soc. 138*, 4634−4642.
(27) Ahmed, M., Davis, J., Aucoin, D., Sato, T., Ahuja, S., Aimoto, S., Elliott, J. I., Van Nostrand, W. E., and Smith, S. O. (2010) Structural conversion of neurotoxic amyloid-[beta] 1−42 oligomers to fibrils. *Nat. Struct. Mol. Biol. 17*, 561−567.
(28) Buchete, N.-V., and Hummer, G. (2007) Structure and dynamics of parallel β-sheets, hydrophobic core, and loops in Alzheimer's Aβ fibrils. *Biophys. J. 92*, 3032−3039.
(29) Horn, A. H., and Sticht, H. (2010) Amyloid-β42 oligomer structures from fibrils: a systematic molecular dynamics study. *J. Phys. Chem. B 114*, 2219−2226.
(30) Hendrixson, R. R., Mack, M. P., Palmer, R. A., Ottolenghi, A., and Ghirardelli, R. G. (1978) Oral toxicity of the cyclic polyethers—12-crown-4, 15-crown-5, and 18-crown-6—in mice. *Toxicol. Appl. Pharmacol. 44*, 263−268.
(31) Gad, S., Conroy, W., McKelvey, J., and Turney, K. (1978) Behavioral and Neuropuarmacological Toxicology of the Macrocyclic Ether 18-Ckown-6. *Drug Chem. Toxicol. 1*, 339−353.
(32) Gad, S., Reilly, C., Siino, K., Gavigan, F., and Witz, G. (1985) Thirteen Cationic Ionophores: Their Acute Toxicity, Neurobehavioral and Membrane Effects. *Drug Chem. Toxicol. 8*, 451−468.
(33) Wang, Y., Xiao, J., Suzek, T. O., Zhang, J., Wang, J., and Bryant, S. H. (2009) PubChem: a public information system for analyzing bioactivities of small molecules. *Nucleic Acids Res. 37*, W623−W633.
(34) Vorobyov, I., Anisimov, V. M., Greene, S., Venable, R. M., Moser, A., Pastor, R. W., and MacKerell, A. D. (2007) Additive and classical drude polarizable force fields for linear and cyclic ethers. *J. Chem. Theory Comput. 3*, 1120−1133.
(35) Van Der Spoel, D., Lindahl, E., Hess, B., Groenhof, G., Mark, A. E., and Berendsen, H. J. (2005) GROMACS: fast, flexible, and free. *J. Comput. Chem. 26*, 1701−1718.
(36) Huang, J., and MacKerell, A. D. (2013) CHARMM36 all-atom additive protein force field: Validation based on comparison to NMR data. *J. Comput. Chem. 34*, 2135−2145.
(37) Jorgensen, W. L., Chandrasekhar, J., Madura, J. D., Impey, R. W., and Klein, M. L. (1983) Comparison of simple potential functions for simulating liquid water. *J. Chem. Phys. 79*, 926−935.
(38) Bixon, M., and Lifson, S. (1967) Potential functions and conformations in cycloalkanes. *Tetrahedron 23*, 769−784.
(39) Hess, B., Bekker, H., Berendsen, H. J., and Fraaije, J. G. (1997) LINCS: a linear constraint solver for molecular simulations. *J. Comput. Chem. 18*, 1463−1472.
(40) Miyamoto, S., and Kollman, P. A. (1992) SETTLE: an analytical version of the SHAKE and RATTLE algorithm for rigid water models. *J. Comput. Chem. 13*, 952−962.
(41) Darden, T., York, D., and Pedersen, L. (1993) Particle mesh Ewald: An N· log (N) method for Ewald sums in large systems. *J. Chem. Phys. 98*, 10089−10092.
(42) Bussi, G., Donadio, D., and Parrinello, M. (2007) Canonical sampling through velocity rescaling. *J. Chem. Phys. 126*, 014101.
(43) Parrinello, M., and Rahman, A. (1981) Polymorphic transitions in single crystals: A new molecular dynamics method. *J. Appl. Phys. 52*, 7182−7190.
(44) Kumari, R., Kumar, R., and Lynn, A. (2014) g_mmpbsa A GROMACS Tool for High-Throughput MM-PBSA Calculations. *J. Chem. Inf. Model. 54*, 1951−1962.
(45) Frishman, D., and Argos, P. (1997) Seventy-five percent accuracy in protein secondary structure prediction. *Proteins: Struct., Funct., Genet. 27*, 329−335.

DOI: 10.1021/acschemneuro.6b00185
ACS Chem. Neurosci. 2016, 7, 1433−1441